Author/s:
Heckmann, Denise Annette

Title:
Understanding the molecular mechanisms of AML development and treatment using phosphoproteomics

Date:
2020

Persistent Link:
https://hdl.handle.net/11343/241732

Understanding the molecular mechanisms of AML development and treatment using phosphoproteomics

Denise Annette Heckmann

ORCID ID # 0000-0001-7523-0749

Submitted in total fulfillment of the requirements of the degree of Doctor of Philosophy

February 2020

Walter and Eliza Hall Institute of Medical Research
Department of Medical Biology
University of Melbourne

Abstract

AML (Acute Myeloid Leukemia) is a rapidly progressing cancer of the blood and bone marrow where the accumulation of abnormal myeloid cells crowds out healthy blood cells. Despite the improvements in understanding the biology of AML, these advancements are not reflected in the trajectory of the survival rate. One reason for the poor translation of research results into novel therapies, is the genetic and epigenetic heterogeneity of the disease, which hampers the development of reliable AML models. Mouse models of AML are designed to mimic human disease by expressing known oncogenes in the hematopoietic system of mice. Although the oncogene-specific disease pathology appears to reflect what is observed in human patients, the translation of novel treatments into the clinic has often been unsuccessful.

Expression of the hematopoietic transcription factor EVI1 has been identified as a marker for poor prognosis in human AML patients. In this thesis, I aimed to develop a mouse model, that recapitulates a particularly aggressive and treatment-resistant form of AML by overexpressing EVI1 together with the fusion-oncogene MLL-AF9. Although I successfully generated EVI-expressing AMLs, the presence of the transcription factor did not affect disease features such as latency, disease pathology, morphology and immunophenotype of leukemic cells. However, when cultured *in vitro*, leukemic cells expressing EVI1 were more resistant to Smac mimetic combination treatments and the chemotherapeutic agent Ara-C, therefore reflecting the treatment resistance observed in human patients.

Although some targeted treatments are now available, chemotherapy remains the standard of care therapy for AML. Therefore, to improve disease outcome, novel treatments are

desperately needed. The IAPs (Inhibitor of Apoptosis Proteins) have been identified as an attractive therapeutic target in a number of cancers including AML. Smac mimetics, a class of drugs that specifically inhibit IAPs, have been found to selectively induce cell death in leukemic cells when combined with an inhibitor of the MAP kinase p38 both *in vivo* and *in vitro.* To understand the molecular mechanisms behind this synergistic killing, I studied the phosphoproteome of treated cells using mass spectrometry and revealed that the PI3K/Akt/mTOR survival pathway was activated following Smac mimetic treatment. Upon p38 inhibition, this survival signaling did not occur. Furthermore, CSF1R was identified as a potential regulator of the PI3K/Akt/mTOR pathway. In support of this finding, the combination of a Smac mimetic and CSF1R inhibitor, resulted in synergistic cell killing *in vitro*.

To study proteins, gene tagging provides a valuable tool for a range of applications including real-time monitoring of target protein activities, modifications of proteins and protein-protein interactions. The CRISPR/Cas9 technology is a powerful tool for modifying any DNA of interest and enables the tagging of endogenous genes. However, the targeted insertion of foreign DNA into cell lines is challenging. I aimed to generate endogenously FLAG-tagged proteins in cell lines by targeting components of the TNF pathway using the CRISPR-Cas9 knock-in technology. Although ssDNA containing the FLAG sequence was inserted into the genome of mouse dermal fibroblasts (MDFs) at the correct site, next generation sequencing revealed that this process was both inefficient and error-prone and resulted in the introduction of mutations. Nonetheless, I was able to enrich for tagged RIPK1 following FLAG pull-down, which was detectable via both immunohistochemistry and mass spectrometry.

Declaration

This is to certify that,

i. this thesis comprises only my original work toward the degree of PhD except where indicated in the preface,

ii. due acknowledgment has been made in the text to all other material used,

iii. the thesis is fewer than 100,000 words in length exclusive of tables, maps, bibliographies and appendices.

Denise A. Heckmann

Preface

The work presented in this thesis involved a number of research collaborations as outlined below.

Chapter 3

Flow cytometry data required for **Figure 3.11** was collected with the help of Elise Clayer (Walter and Eliza Hall Institute) while qPCR data in **Figure 3.13** was obtained by Elise Clayer (Walter and Eliza Hall Institute). I performed all other experiments and estimate my contribution to this chapter to be 95%.

Chapter 4

The RIPK1$_{S321A/S336A}$ mutant BMDMs treated in **Figure 4.1** were generated by Najoua Lalaoui (Walter and Eliza Hall Institute). To generate phosphoproteomics data, phosphopeptides of treated BMDMs were enriched with the help of Sean Humphrey (University of Sydney) following the EasyPhos protocol, while mass spectrometry data was acquired by Laura Dagley (Walter and Eliza Hall Institute). Connie Li Wei Suen and Alexandra Garnham (Walter and Eliza Hall Institute) performed the statistical analysis of phosphoproteomics data. **Figures 4.9 & 4.16** were generated with the help of Narelle Keating. I estimate my contribution to this chapter to be 80%.

Chapter 5

Stephen Wilcox (Walter and Eliza Hall institute) performed the Illumina MiSeq sequencing of the CRISPR/Cas9 knock-in MDFs. The RIPK1-FLAG pulldown samples were analysed by

Jarrod Sandow using MaxQuant software (version 1.5.8.3) (Cox *et al.,* 2008) and in-house statistic pipelines (**Figure 5.5**). I estimate my contribution to this chapter to be 90%.

Acknowledgments

Doing a PhD was the hardest journey I have ever undertaken and would not have been possible without the constant love and support from the people around me.

Thanks, Finn, for being my biggest supporter. Thanks for believing I'm the smartest out there, for celebrating all the highs and carrying me through all the lows. Thanks for listening to me practicing my talks and helping me formulating sentences for my thesis without knowing what I'm talking about. I could write a whole thesis about how much you mean to me and how your unconditional love and patience were invaluable for me making it to this point.

I would like to thank John Silke for accepting me into his lab and providing me with constant guidance and advice. I greatly admire your dedication, creativity and your endless wealth of knowledge although I often didn't get your jokes.

To my supervisors Nij, Jarrod and Andrew, thank you believing in me even when I didn't. Thanks for always teaching and supporting me through the toughest times. What I learned from you made me more than just a better PhD student but it impacted my life beyond the lab. Thank you, Jarrod, for introducing me to the best footy club in town. And Nij, thank you for being an amazing role model et ma superviseuse préférée even when our conversations sometimes got lost in translation.

Thank you, Sandra, for being more than just the chair of my committee but a mentor and someone I could always rely on. Your care and constant support greatly contributed to my persistence to finish my PhD.

The support I received outside my division was also of great importance to my success. Thank you, Keely, Marnie and Doug for going out of your way to help and support me. You all make WEHI a great place for students to learn and thrive. Although Doug, your set shot has been a bit of a let-down for the WEHI Wombats.

Thanks to the WEHI Wombats and the student soccer team for making WEHI the best institute not only in science but also in sports. Thanks for giving me the opportunity to kick some goals when I wasn't reaching them in the lab.

I was so fortunate to work along some great friends. Che and Maria, although it was often hard to get work done around you, you made life in the office and lab so much fun. Joggo "8 snags" Bernadini, thank you for being a great friend and for giving me my 5 minutes of complaining a day. Thank you, V-dawg, for being the German voice of complaint that always made me feel like home. Thanks Elise aka. Baguette, for always being right and for being an awesome coffee buddy and a beautiful friend. Thanks Annette, for all the late-night conversations and for never getting tired of listening to me. Linny, thanks for being hilarious and always surprising me. Thanks for being so generous and kind. Dan my man, thanks for all the banter and help. I'm pretty sure I still owe you a soy latte. Cozee, you were such a fun lab and office buddy, although playing soccer against you was always a bit dangerous. Thanks to the rest of the Silke lab – you've been amazing.

Lastly, I want to thank my best friend Gigi who I was lucky enough to meet during my PhD. Having you there in the last year gave me so much strength to persist. Thanks for your endless care, support and love. Thanks for always finding out stuff for me and for reading my thesis. And thanks for trusting my advice. You'll be the most amazing PhD student.

Publications

This thesis contains work that has already been published.

During my PhD, I was financially supported by the **Melbourne International Research Scholarship** (2015 – 2017), **Research Training Program Scholarship** (2017-2019) and the **Edith Moffatt Scholarship** (2019).

Najoua Lalaoui, Kay Hänggi, Gabriela Brumatti, Diep Chau, Nhu-Y.N. Nguyen, Lazaros Vasilikos, Lisanne M. Spilgies, **Denise A. Heckmann**, Chunyan Ma, Margherita Ghisi, Jessica M. Salmon, Geoffrey M. Matthews, Elisha de Valle, Donia M. Moujalled, Manoj B. Menon, Sukhdeep Kaur Spall, Stefan P. Glaser, Jennifer Richmond, Richard B. Lock, Stephen M. Condon, Raffi Gugasyan, Matthias Gaestel, Mark Guthridge, Ricky W. Johnstone, Lenka Munoz, Andrew Wei, Paul G. Ekert, David L. Vaux, W. Wei-Lynn Wong, John Silke. Targeting p38 or MK2 Enhances the Anti-Leukemic Activity of Smac-Mimetics. *Cancer Cell.* 2016 Feb 8;29(2):145-58. doi: 10.1016/j.ccell.2016.01.006.

Table of Contents

Table of Figures

List of Tables

Abbreviations

ACN	acetonitrile
AML	acute myeloid leukemia
ATF2	activating transcription factor 2
bp	base pairs
Bcl-2	B cell lymphoma-2
BIR	baculovirus inhibitor repeat
BMDM	bone marrow derived macrophages
BSA	bovine serum albumin
CARD	caspase recruitment domain
CD	cluster of differentiation
c-FLIP	cellular FADD-like IL-1β-converting enzyme inhibitory protein
cIAP	cellular inhibitor of apoptosis protein
CRISPR	clustered regularly interspaced short palindromic repeats
CSF1R	colony stimulating factor 1 receptor
DD	death domain
DMEM	Dulbecco's modified Eagles media
DMSO	dimethyl sulfoxide
DNA	deoxyribonucleic acid
DP	differentially phosphorylated
ECL	enhanced luminol-based chemiluminescent substrate
EDTA	ethylenediaminetetraacetic acid
EFS	event-free survival

eIF4B	eukaryotic translation initiation factor 4B
ERK	extracellular signal-regulated kinase
EVI1	Ecotropic virus integration site-1
FACS	fluorescence-activated cell sorting
FADD	Fas-associated protein with death domain
FASP	filter aided samples preparation
FCS	fetal calf serum
g	gram
G-CSF	granulocyte-macrophage colony stimulating factor
GFP	green fluorescent protein
GMP	granulocyte-macrophage progenitor
GO	gene ontology
HCL	hydrochloride
HDR	homologous DNA repair
His	histidin
HRP	horseradish peroxidase
HSC	haematopoietic stem cell
IKK	inhibitor of nuclear factor-κB kinase
IL	interleukin
IMDM	Iscove's Modified Dulbecco's Media
ITAM	immunoreceptor tyrosine-based activation motif
Itpkb	inositol-Trisphosphate 3-Kinase B
ITSM	immunoreceptor tyrosine-based switch motif
i.v.	intravenous

JNK	janus kinase
KEGG	Kyoto Encyclopedia of Genes and Genomes
LPS	liposaccharide
LSK	lineage negative SCA-1+ cKit+ cells
LUBAC	linear ubiquitin chain assembly complex
MAPK	mitogen-activated protein kinase
MDF	mouse dermal fibroblast
MK2	MAPK-activated protein kinase 2
MLKL	mixed lineage kinase-like domain protein
MLL	mixed lineage leukemia
Mg	milligram
μg	microgram
μM	micromolar
mL	millilitre
mM	millimolar
mRNA	messenger ribonucleic acid
mTOR	mammalian target of rapamycin
nM	nanomolar
NFAM1	NFAT activating protein with ITAM motif 1
NF-kB	nuclear factor-κB
Ni-NTA	Nickel-charged nitrilotriacetic acid
NK	natural killer
PBS	phosphate buffered saline

PCR	polymerase chain reaction
PI	propidium iodide
PI3K	phosphoinositide 3-kinase
PRAS40	proline-rich Akt1 substrate 1
PTPRC	protein tyrosine phosphatase receptor type C
RIPK1	receptor interacting protein kinase-1
rpm	revolution per minute
Rps6	ribosomal protein S6
RT	room temperature
SCF	stem cell factor
SDS-PAGE	sodium dodecyl sulphate polyacrylamide gel electrophoresis
SEM	standard error of the mean
sgRNA	single guide ribonucleic acid
shRNA	short hairpin ribonucleic acid
SM	second mitochondria-derived activator of caspases mimetic
ssDNA	single stranded deoxyribonucleic acid
TAK1	TGF-β activated kinase
TCEP	tris(2-carboxyethyl)phosphine
TFA	trifluoroacetic acid
TNF	tumour necrosis factor
TNFR1	TNF receptor 1
TRAF2	TNF receptor-associated protein 2
wt	wild-type

1 Introduction

1.1 Acute Myeloid Leukaemia

Acute myeloid leukaemia (AML) is a cancer of the myeloid line of blood cells and is characterized by the rapid growth of abnormal hematopoietic progenitor cells in the bone marrow. Due to the formation of leukemic blasts in the bone marrow, the production of normal blood cells is disturbed leading to anaemia, neutropenia and thrombocytopenia (De Kouchkovsky *et al.*, 2016). AML is the most common myeloid leukaemia and the most common acute leukaemia in adults. Overall, AML accounts for approximately 0.8% of all cancers (Leukaemia Foundation). With the five-year survival rate only being approximately 24.5% (Cancer Australia), the disease is responsible for about 2% of cancer deaths worldwide (National Cancer Institute). AML is a clinically, morphologically, immunophenotypically and genetically heterogeneous cancer and the prognosis for individual patients can range from low to high risk (Dohner *et al.*, 2008; Estey *et al.*, 2006). The disease outcome is associated with the nature of its genetic and karyotypic abnormalities as well as gene expression patterns and DNA methylation signatures (Dohner *et al.*, 2008).

The genetic complexity of AML greatly hampers the successful translation of research into clinical practice. In AML, more than 100 somatic genetic aberrations that can contribute to leukemogenesis are known to date, while patients can harbor a number of mutations (Shima *et al.*, 2011). An individual AML can even be composed of subclones with distinguishable mutational signatures, making each AML patient genetically unique (David Grimwade *et al.*, 2016). Genetic translocation that generate in-frame chimeric fusion genes often involving hematopoietic transcription factors, epigenetic regulators as well as components of the nuclear

pore complex, are recurrently associated with the development of AML (Speck *et al.*, 2002; Suela *et al.*, 2007). Generated chimeric transcription factors alter the expression of genes critical for hematopoietic development as well as differentiation (Estey *et al.*, 2006). As a consequence, hematopoietic differentiation can be blocked and cells can acquire self-renewal capacities (Suela *et al.*, 2007). One theory about the development of AML that was widely accepted for many years, is the "two-hit hypothesis" that suggests that malignant transformation requires the co-occurrence of two mutations – a founder mutation and a driver mutation – in the same myeloid precursor (Kelly *et al.*, 2002) (**Figure 1.1**). Preleukemic founder mutations (e.g. *DNMT3*, *IDH1* and *TET2*) in hematopoietic stem or progenitor cells confer advantages in self-renewal and proliferation. Since these mutations persist and lead to clonal expansion, additional driver mutations in genes involved in cellular differentiation and survival like *FLT3*, *N-RAS* and *K-RAS*, can accumulate in a pre-leukemic cell (Kelly *et al.*, 2002) leading to the onset of AML.

A class of fusion oncogenes that constitute a founder mutation and that are often associated with poor prognosis in AML patients, involve the Mixed-lineage-leukaemia gene (MLL), which is located on chromosome 11q23. MLL-rearrangements are found in the majority of infant AMLs and about 10% of adult de novo and 33% of therapy-related AMLs (H. Liu *et al.*, 2009). The MLL gene encodes a DNA- binding protein that methylates histone H3 lysine 4 (H3K4), and positively regulates gene expression including multiple homeobox (Hox) genes. Dysregulation of Hox genes contribute to leukemogenesis by supporting the immortalization of cells (Alharbi *et al.*, 2013). Leukemogenic MLL translocations encode MLL fusion proteins that have lost H3K4 methyltransferase activity leading to sustained transcriptional activation of target genes such as Meis1 and Hoxa9 (Zeisig *et al.*, 2004; Zeisig *et al.*, 2003). To date, about

80 MLL fusions have been described in the literature (Meyer *et al.*, 2013). Amongst those, only the chromosomal translocation t(1:11) (q21:q23), which results in the expression of the MLL-AF1Q fusion protein, displays a favourable clinical prognosis (EFS = 0.92) . All other MLL fusions generate intermediate to high risk AMLs (EFS = 0.11-0.50) indicating that these fusion oncoproteins have a great potential at initiating and maintaining the disease (Balgobind *et al.*, 2009). The most common MLL fusion partners are AF4, AF6, AF9 and ENL and their associated median survival rates range from less than one year (ENL) to up to four years (AF9) (Liu *et al.*, 2009).

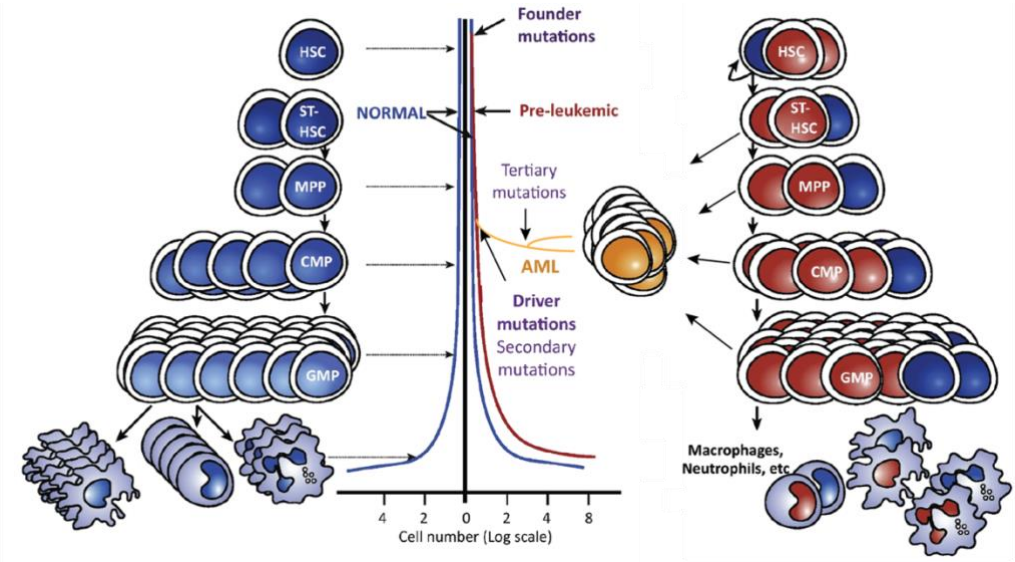

Figure 1.1: Normal Myelopoiesis versus Leukemogenesis in AML

Schematic diagram of myelopoiesis under normal conditions (left) and leukemogenesis in AML (right). Self-renewing hematopoietic stem cells (HSC) generate short-term HSCs (ST-HSCs) which in turn produce multipotent progenitors (MPPs). MPPs then give rise to common myeloid progenitors (CMPs) and granulocyte-monocyte progenitors (GMPs) which finally differentiate into mature myeloid cells including macrophages, monocytes and neutrophils. HSCs can acquire founder mutations leading to generation of pre-leukemic cells. Although pre-leukemic cells are not transformed, their longevity enables the accumulation of driver mutations which lead to the onset of AML. Acquisitions of additional tertiary mutations often occur upon disease progression. These mutations can further enhance AML aggressiveness and resistance to treatment. Driver mutations can develop in pre-leukemic cells at various stages of myelopoiesis as indicated by arrows. Adapted from Brumatti et al. (Trends Mol. Med 2017).

1.2 Mouse models of AML mimic human disease

In order to study disease biology and to develop novel treatments, researchers heavily rely on disease models. Since these models often involve the use of animals, one of the major challenges is to reliably mimic human disease features including disease development, pathology and response to therapy, in animals. Although AML models developed to date partially complement each other, none of the currently available approaches faithfully recapitulate human disease. Consequently, therapeutic progress in AML has been slow, as advancement in research only poorly translated into the clinics (Estey, 2015). Nevertheless, technological improvements in the fields of next generation sequencing and bioengineering continuously promote the development of better disease models.

Genetically altered mouse models enable the study of treatment response in a physiological environment and thereby provide a means to dissect the relationship between complex disease genetics and therapy response in a way that is not possible in humans (Zuber *et al.*, 2009). Mouse models that are currently frequently used, can be placed into one of the following four categories: (1) Spontaneous AML development induced by exposure to carcinogens including chemicals (e.g. 3-methylcholantrene), biologicals (e.g. murine leukemia virus) or radiation, (2) conventional transgenic approach by DNA insertion into the genome via pronuclear microinjection or electroporation, (3) xenotransplantation of leukemic cells or *in vitro* modified HSPCs into immunocompromised mice or (4) adaptive transfer method of *in vitro* modified HSPCs using retroviral transduction with an oncogene followed by tail vein injection into irradiated recipients.

In order to generate mouse models of AMLs driven by specific genetic alterations and combinations thereof, the adaptive transfer method represents a versatile tool to reflect the genetic heterogeneity found in human patients. Using this approach, Zuber et al. developed novel mouse models of common AML genotypes by exploiting the information on genetic lesions that often co-occur in AML patients (Zuber *et al.*, 2009). To induce AML in mice via the adaptive transfer method, fetal liver cells that serve as a source of HSPCs, are retrovirally transduced with one or more oncogenes (**Figure 1.2**). These oncogenes are often made up of a founder mutation in combination with a driver mutation. Transduced fetal liver cells are subsequently transplanted into lethally irradiated recipient mice where the HSPCs reconstitute the hematopoietic system. After a latency that is specific to the oncogene(s), mice develop an AML whose severity and treatment response were found to reflect the oncogene-specific disease pathology and response patterns observed in humans (Zuber et al., 2009). The approach developed by Zuber et al. since served as a valuable tool to study the impact of cancer heterogeneity on therapy response and to explore the molecular mechanisms involved in variable leukemia behaviour.

Although the current AML models have been very informative to date, progress in the treatment of AML is still slow. A major contributor to this lack in advancement is the inability of disease models to faithfully mimic the pathological and biological heterogeneity found in AML patients. Mouse models that represent the complex pathological genetic backgrounds and expression patterns more accurately, are needed to better understand varying therapy responses of AML patients. To develop such models, we should not only aim to replicate genetic mutations that drive AML but also consider aberrantly expressed proteins that may contribute to a disease phenotype. A protein whose correlation with AML has been well

established, is Ecotropic Viral Integration Site 1, or EVI1. The role of EVI1 in disease severity as well as treatment response will be discussed in the following subchapter.

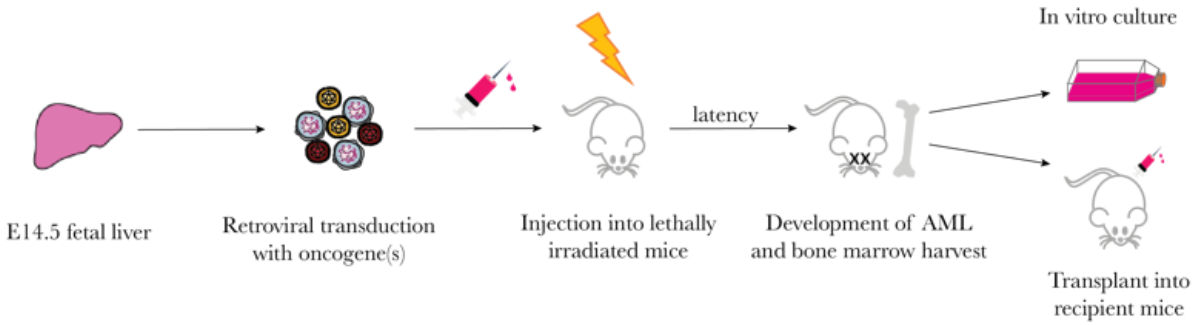

Figure 1.2: Generating AML in mice by expressing oncogenes in the hematopoietic system

Fetal livers are harvested at E14.5 and retrovirally transduced with oncogene(s). Infected cells are then injected into lethally irradiated mice which consequently develop AML after a latency that is specific for the oncogene(s). Bone marrow of deceased mice can be harvested and contained leukemic cells cultured in the presence of IL-3. To induce secondary AML, leukemic cells can be injected into recipient mice.

1.3 EVI1 overexpression is a prognostic marker for poor outcome in MLL-AMLs

The proto-oncogene ecotropic viral integration site 1 (EVI1), located on chromosome 3q26, is a zinc finger transcription factor for cell cycle genes (Morishita *et al.*, 1988). As a transcriptional regulator with stem cell-specific expression, EVI1 is essential for cell fate of HSCs including cell renewal and repopulation capacity. Aberrant expression of EVI1 has been associated with hematopoietic malignancies such as myelodysplastic syndrome (MDS) and AML, as well as several solid epithelial cancers including ovarian and bladder cancer (Brooks *et al.*, 1996; Goyama *et al.*, 2008). When overexpressed, EVI1 can block differentiation and can confer resistance to apoptosis in leukemic cells (Kurokawa *et al.*, 1998; Liu *et al.*, 2006). An association between EVI1 expression and AML has been described on various occasions

(Groschel *et al.*, 2013; Grossmann *et al.*, 2013). In patients bearing 3q26 abnormalities, EVI1 overexpression was detected in virtually all cases of this particularly treatment-resistant AML karyotype, irretrievably linking aberrant EVI1 expression with this genetic subset (Barjesteh van Waalwijk van Doorn-Khosrovani *et al.*, 2003; Lugthart *et al.*, 2010; Lugthart *et al.*, 2008). EVI1 has also been found to be overexpressed in types of adult and paediatric AML that do not harbour 3q26 abnormalities. Overall, EVI1 was shown to be aberrantly expressed in 6-11% of adult AML patients, while in patients with MLL-rearranged AML, overexpression of EVI1 occurred in over 40% of cases (Grossmann e*t al.*, 2013; Lugthart *et al.*, 2010). The exact mechanism that leads to EVI1 overexpression remains unclear. However, the fact that aberrant EVI1 expression is so prevalent in MLL-rearranged AML, supports the notion that EVI1 is directly regulated by the fusion oncoprotein (Bindels *et al.*, 2012). The cell type of origin that acquires the AML-inducing mutations may also be responsible for high EVI1 expression levels, since the MLL-fusion protein MLL-AF9 was not able to induce EVI1 expression upon transformation of GMPs. However, at the same time, transformation of HSCs lead to EVI1 expression to be sustained (Bindels *et al.*, 2012).

When overexpressed in AML patients that harbour an MLL-translocation, EVI1 was associated with a particularly poor prognostic outcome (Groschel *et al.*, 2013). In MLL-AF9 AML, which is generally considered an intermediate risk AML, EVI1 expression divides patients into a favourable and unfavourable subgroup where high EVI1 levels occur in the latter (D. Grimwade *et al.*, 2009). EVI1 expression in these patients correlated with resistance to chemotherapy which might be due to the HSC-specific gene expression profile that has been linked to the overexpression of EVI1 (Valk *et al.*, 2004). In MLL-AF9 AML, high EVI1 levels therefore result in a particularly aggressive subtype of the disease.

The ability of EVI1 to induce MDS and its role in leukemogenesis, have also been demonstrated in mice. In a Hoxa9/Meis1 mouse model, the forced expression of EVI1 accelerated disease onset significantly compared to Hoxa9/Meis1 expression alone, while EVI1 expressed on its own induced MDS (Jin *et al.*, 2007). In another model using a murine MLL-AF9 cell line that has inherently high EVI1 levels, AML was induced by injecting these cells into mice. Upon knock-down of EVI1 by shRNA, disease onset was significantly delayed or even prevented, revealing EVI1 as a driver of the disease (Bindels *et al.*, 2012).

In summary, EVI1 overexpression is a poor prognostic marker in AML and is strongly associated with MLL-translocations. Here, high levels of EVI1 is an indicator of disease severity, treatment resistance and an increased risk of relapse. Since its role in leukemogenesis could also be demonstrated in mice, overexpressing EVI1 in murine AML could lead to the development of an AML mouse model that faithfully reflects a particularly aggressive human disease phenotype.

1.4 Inhibitor of apoptosis proteins as targets in the treatment of AML

Although some targeted drugs have been made available for the treatment of AML, disease management still heavily relies on intensive chemotherapy and allogenic hematopoietic stem cell transplantation. To improve survival rates and to reduce treatment toxicities, novel AML therapies are urgently needed. A promising therapeutic target for the treatment of AML that has been identified are the inhibitor of apoptosis proteins (IAPs), which are recurrently found to be upregulated in AML (Fulda *et al.*, 2012).

The IAPs are characterised by the presence of one or more copies of a domain called baculoviral IAP repeat (BIR), which is comprised of approximately 70 amino acids (**Figure 1.3**). The IAP family members whose role in apoptosis have been described extensively, are XIAP (X-linked inhibitor of apoptosis), cIAP1 and cIAP2 (cellular inhibitor of apoptosis 1 and 2). The three N-terminal BIR domains of XIAP, cIAP1 and cIAP2 have been demonstrated to be crucial for their interaction with other proteins (Hinds *et al.*, 1999; Silke *et al.*, 2014). In all three IAP family members, adjacent to BIR3 is a ubiquitin-associated domain (UBA) which promotes engagement with ubiquitin chains (Gyrd-Hansen *et al.*, 2008). Unique to the cIAPs is the caspase recruitment domain CARD which is located at the C-terminal end of the UBA and whose function in these proteins remains unknown (Silke *et al.*, 2013). The carboxy terminus of XIAP and cIAP1/2 harbour a RING (really interesting new gene) finger domain, which confers E3-ligase activity to the proteins (Y. Yang *et al.*, 2000).

XIAP and cIAP1/2 inhibit apoptosis through different mechanisms. Through its BIR2 and BIR3 domains, XIAP is able to bind activated caspases 3 and 9 thereby inhibiting these caspases and preventing apoptosis (Deveraux *et al.*, 1997; Sun *et al.*, 2000; Takahashi *et al.*, 1998). In contrast, cIAP1 and cIAP2 are not able to prevent cell death by antagonizing caspase function, since their inhibitory activity on caspases is 100- to 1000-fold lower (Eckelman *et al.*, 2006; Roy *et al.*, 1997). In contrast to XIAP, cIAP1 and cIAP2 prevent apoptosis by facilitating the constitutive ubiquitylation of RIPK1 which leads to the formation of the cell death-inducing complex II being blocked (Bertrand *et al.*, 2008; Feoktistova *et al.*, 2011).

In the presence of an apoptotic stimulus, Smac (second mitochondria-derived activator of caspases) or DIABLO (direct mitochondria-derived activator of caspases) is released from the

mitochondria into the cytosol where it relieves the inhibited caspases by competitively binding to the BIR2 and 3 domains of XIAP (Chai *et al.*, 2000; Wu *et al.*, 2000). In contrast, binding of Smac/DIABLO to the BIR3 domain of cIAP1 and cIAP2 induces rapid auto-ubiquitylation and degradation of the cIAPs via the proteasome (Yang *et al.*, 2004). Smac/DIABLO therefore exhibits its pro-apoptotic effect by releasing activated caspases through antagonizing the IAPs. Since IAPs are commonly upregulated in a number of solid and haematological cancers, Smac mimetics, a class of small molecule inhibitors, have been developed for the targeted inhibition of IAPs with the aim of selectively inducing cell death in cancer cells (Fulda *et al.*, 2006; Fulda *et al.*, 2012; Nachmias *et al.*, 2004; Reed, 2003). Importantly, overexpression of IAPs in AML was found to be an indicator of particularly poor prognosis (Fulda *et al.*, 2012).

Since their development, Smac mimetics have been trialled in various cancers and infectious diseases (Bai *et al.*, 2014; Fulda, 2015), (https://clinicaltrials.gov). However, in AML, Smac mimetics failed to efficiently kill leukemic cells as a single agent (Fulda *et al.*, 2012). The observed Smac mimetic resistances could be partially overcome when the smac mimetic BV6 was combined with the chemotherapeutic cytarabine (Chromik *et al.*, 2014).

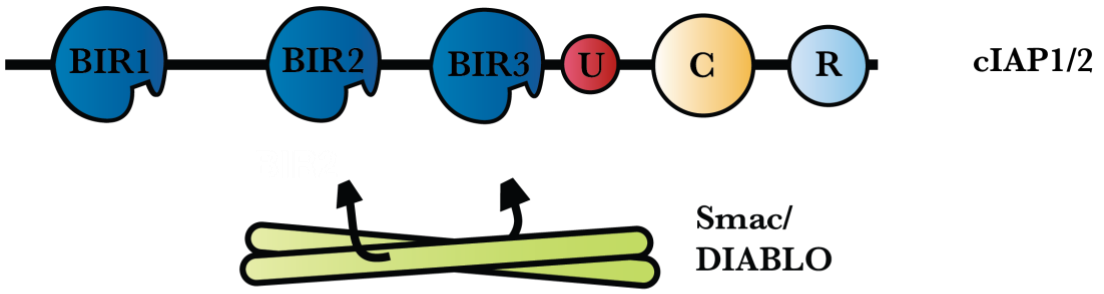

BIR = baculoviral inhibitor of apoptosis protein repeat
U = UBA, ubiquitin associated domain
C = CARD, caspase activation and recruitment domain
R = RING, really interesting new gene domain

Figure 1.3: Smac/DIABLO drives apoptosis by antagonizing cIAPs

Following an apoptotic stimulus, mitochondria release Smac/DIABLO which binds to the BIR3 domain of cIAP1 and cIAP2 inducing auto-ubiquitylation and degradation to drive apoptosis. A UBA promotes engagement with ubiquitin chains while the function of the CARD domain is unclear. The carboxy-terminal RING finger domain provides E3-ligase activity.

1.5 Smac-mimetic killing is dependent on the TNF pathway

Smac mimetic-induced cell death has been found to be dependent on TNF (tumour necrosis factor) signalling (Li *et al.*, 2004; Silke *et al.*, 2014) (**Figure 1.4**). TNF is a master regulator of inflammation and cell death. As such, signalling downstream of TNFR1 has been extensively studied. Upon binding of TNF to TNFR1, the receptor trimerizes which activates a downstream signalling cascade leading to the assemblance of the signalling complex I. This membrane-bound complex consists of the adapter protein TRADD (TNF receptor 1-associated death domain protein) and RIPK1 (receptor interacting kinase 1) who associated via their death domains (DD) and TRAF2 (TNF receptor-associated protein 2) (Inoue *et al.*, 2000; Meylan *et al.*, 2004). The recruitment of cIAP1/2 via TRAF2 enables the ubiquitylation of RIPK1 by the cIAPs, which is essential for the rapid activation of downstream NF-κB and

MAPK (mitogen-activated protein kinase) pathways (Etemadi *et al.*, 2015; Micheau *et al.*, 2003; Samuel *et al.*, 2006). As a transcriptional response, the expression of cytokines and survival proteins such as cIAP1/2 and c-FLIP (cellular FADD-like IL-1β-converting enzyme inhibitory protein) are upregulated (Micheau *et al.*, 2001; Wang *et al.*, 1998). Apart from having a scaffolding function that contributes to the activation of NF-κB and MAP kinases, ubiquitylation of RIPK1 limits the formation of a cytosolic cell death complex II, that has the capacity to induce cell death via apoptosis or necroptosis (Feoktistova *et al.*, 2011; Feoktistova *et al.*, 2012; Zhao *et al.*, 2012). The apoptotic death complex, also referred to as the Ripoptosome, consists of RIPK1, caspase-8 and the adapter proteins FADD and TRADD (Feoktistova *et al.*, 2011; Tenev *et al.*, 2011). The necroptotic death complex on the other hand is devoid of caspase-8 but contains the kinase RIPK3.

Therefore, treatment with the IAP inhibitor called Smac-mimetic enables the formation and activation of complex II. Within this complex, caspase-8 initiates a caspase-dependent apoptotic cell death (Darding *et al.*, 2011). In conditions of reduced caspase-8 activation, RIPK1 induces an alternative caspase-independent cell death pathway called necroptosis (Murphy *et al.*, 2014).

In addition to regulating cell death, cIAP1/2 may limit TNF secretion through the non-canonical NF-κB pathway. Here, cIAP1/2 inhibit the activation of the non-canonical NF-κB pathway by forming a complex with TRAF2 and TRAF3, which leads to the consistent degradation of NIK (NF-κB-inducing kinase) (Vallabhapurapu *et al.*, 2008; Vince *et al.*, 2007). NIK stabilisation is required for the signal integration from a number of TNF receptor family

members and activates the downstream kinase IκB kinase-α (IKKα), which in turn induces p100 phosphorylation and processing to form the p52/RelB complex (Senftleben *et al.*, 2001; Xiao *et al.*, 2001). Translocation of p52/RelB to the nucleus finally activates the transcription of target genes, which include genes involved in cell survival (Roy *et al.*, 2017). Since the basal levels of NIK are actively limited by the TRAF/cIAP complex, degradation of cIAPs by SM results in the accumulatio of NIK and activation of the NF- κB pathway. Although it is believed that TNF production can be regulated through the non-canonical NF- κB pathway, this connection has not been experimentally proven. The inhibition of cIAP1/2 in MEFs and BMDMs for example, did not lead to an observable increase in TNF secretion (Lalaoui *et al.*, 2016). However, when SM was combined with a p38 or MK2 inhibitor in the same cells, TNF secretion was increased dramatically (Lalaoui et al., 2016). The p38/MK2 pathway is therefore able to regulate TNF production when cIAPs are absent.

Although some cancer cells can be killed with Smac mimetics alone, treatment resistances to Smac mimetics as a single agent are commonly observed (Chromik et al., 2014; Fulda et al., 2012; Lalaoui et al., 2016). Consistent with the observation that cells secreting TNF upon treatment are often highly responsive, resistance to Smac mimetics can sometimes be overcome by the addition of exogenous TNF (Lalaoui et al., 2016). This discovery inspired a quest to identify agents that had the potential to increase TNF production in Smac mimetic-treated cells, therefore enhancing cell death and overcoming drug resistance.

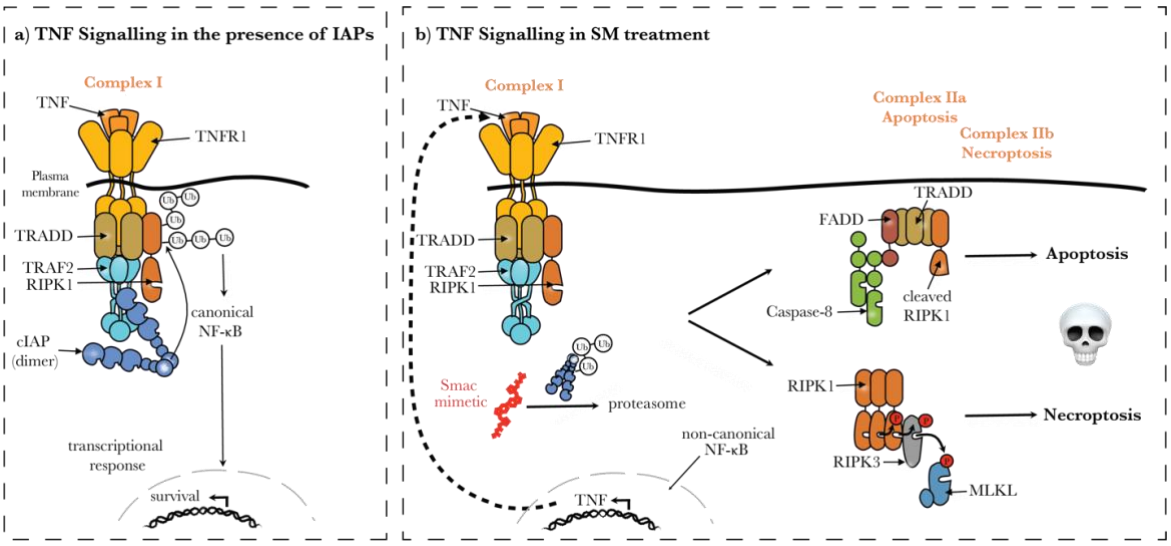

Figure 1.4: Cell death regulation by the TNFR1 signalling complex in the presence and absence of cIAPs

Schematic representation of TNF signalling through TNFR1 and cell death induction by Smac mimetic treatment. A) Binding of TNF induces the formation of complex I, which is composed of TRADD, TRAF2, RIPK1 and cIAP1/2. Ubiquitylation of RIPK1 by cIAPs leads to the downstream activation of the canonical NF-kB pathway which induces the expression of inflammatory and pro-survival proteins. B) Treatment with Smac mimetic causes auto-ubiquitylation of cIAPs and degradation via the proteasome. Non-ubiquitylated RIPK1 can then participate in the formation of cell death-inducing complex II, which also contains Caspase-8, the adapter proteins FADD and TRADD and leads to apoptosis. When Caspase-8 activity is absent, the kinase activities of RIPK1 and RIPK3 allow their stable oligomerization, leading to activation of MLKL whose translocation to the plasma membrane induces necroptosis. Adapted from Lalaoui & Brumatti (Immunol. Cell Biol., 2017).

MLKL = mixed lineage kinase-domain like protein; NF-κB = nuclear factor-κB; P = phosphorylation; RIPK1 = receptor interacting protein kinase 1; RIPK3 = receptor interacting protein kinase 3; TNF = tumor necrosis factor; TNFR1 = TNF receptor 1; TRADD = TNFR1-associated death domain protein; TRAF2 = TNF receptor-associated protein 2; Ub = ubiquitin;

1.6 The mitogen-activated protein kinase p38 can prevent SM-induced cell death

By screening a library of kinase inhibitors for their ability to increase TNF production in Smac mimetic-treated cells, we previously identified that p38 inhibition greatly enhanced Smac mimetic killing efficiency by increasing TNF levels (Lalaoui *et al.*, 2016). When applied to AML mouse models, the combination treatment of the clinical Smac mimetic Birinapant and the p38 inhibitor LY2228820, proved to be a potent killer of leukemic cells both *in vitro* and *in vivo* (Lalaoui et al., 2016). Likewise, when BMDMs were treated with the combination of another Smac mimetic agent, Compound A, and the p38 inhibitor, greater rates of apoptosis were accompanied by increased levels of TNF (Lalaoui *et al.*, 2016). Although the exact mechanisms behind these observations remained unresolved, it was revealed that the combined inhibition of p38 and the IAPs prompted the activation of the MAP kinases ERK1/2 and JNK1/2 (Lalaoui *et al.,* 2016). A possible trigger for the activation of the MAP kinase ERK1/2 may be the induction of TNF secretion caused by the combination of SM/p38i.

Given the central role this cytokine plays in innate immunity and inflammation, TNF is tightly regulated on multiple levels including TNF expression, mRNA transcription, mRNA nuclear export, mRNA stability, translation of pro-TNF and shedding of mature TNF from the cell membrane (Gaestel *et al.*, 2009). Key regulators of these processes include NF-κB and the MAP kinases p38, JNK1/2 and ER1/2 (Das *et al.*, 2009; Gonzalez-Teran *et al.*, 2013; Rutault *et al.*, 2001; Udalova *et al.*, 1998). It has been demonstrated that JNK1/2 is required for the expression of TNF in hematopoietic cells including macrophages (Han *et al.*, 2013), while ERK1/2 regulates the cytokine by both transcriptional and post-transcriptional mechanisms

(Deleault *et al.*, 2008; Rutault *et al.*, 2001). Apart from regulating TNF and stimulating the expression of death receptors, ligands and pro-apoptotic proteins, both JNK1/2 and ERK1/2 can regulate extrinsic apoptosis through additional means. As such, ERK1/2 activity has been described to induce FADD, an adaptor of caspase-8 to the death inducing complex I, while JNK1/2 is able to phosphorylate Bid, triggering the release of Smac/DIABLO (Cagnol *et al.*, 2010; Madesh *et al.*, 2002).

The increased activation of JNK1/2 in cells treated with Smac mimetic and p38 inhibitor, may be a consequence of a negative feedback loop involving p38, whereby the MAP kinase suppresses the activation of TAK1 (transforming growth factor beta-activated kinase 1), a JNK pathway activator, by phosphorylating TAB1 (TAK1-binding protein) (Cheung *et al.*, 2003; Gaestel *et al.*, 2009). However, the inhibition of MK2 (MAP kinase-activated protein kinase 2), a direct p38 substrate, induces the same increase in JNK1/2 phosphorylation and a direct effect of MK2 on the p38-TAB1 interaction has not been described. Neither has MK2 been shown to directly phosphorylate JNK1/2. In support of a feedback effect, inhibition of both p38 and MK2 induced an increase in TAK1 phosphorylation (Lalaoui et al., 2016). Whether MK2 itself is able to participate in this feedback loop or other unknown mediators are involved remains unresolved.

Upon activation by MKK3 and MKK6, p38 activates the kinase MK2 which in turn phosphorylates and thereby inhibits TTP (tristetraprolin), a destabiliser of TNF mRNA (Mahtani *et al.*, 2001). Due to its role in promoting TNF production, the p38 pathway was long considered an attractive target for the therapy of inflammatory diseases leading to the development of clinical p38 inhibitors (Amir *et al.*, 2013). Unfortunately, clinical trials

involving these inhibitors for the treatment of rheumatoid arthritis have failed greatly due to undesirable side effects and lack of efficiency (Duraisamy *et al.*, 2008; Genovese, 2009). In light of its described pro-inflammatory role, the observation that TNF levels increased upon p38 inhibition in the absence of IAPs, was unexpected.

It was not until Jaco et al. discovered that the p38 substrate MK2 can phosphorylate RIPK1, thereby preventing the formation of the death inducing complex II, that we gained a better understanding of how p38 can prevent cell death in Smac mimetic-treated cells (Jaco *et al.*, 2017) (**Figure 1.5**). This study showed that MK2 phosphorylates cytosolic as well as complex I-bound RIPK1 on Ser321, which limited RIPK1 recruitment to complex II, consequently limiting cell death by preventing the formation and activation of complex II. However, RIPK1$_{S321D}$ phospho-mimetic MEFs and BMDMs were only partially protected from Smac mimetic-induced cell death and the additional inhibition of MK2 further sensitized RIPK1$_{S321D}$ mutants (Jaco *et al.*, 2017). Two possibilities can be considered: i) the replacement of the serine by glutamine did not fully mimic the phosphorylation function or ii) there are additional mechanisms through which p38/MK2 can limit TNF-induced cell death. The ability of Smac mimetic to kill cells as a single agent, relies on TNF production and the simultaneous sensitization of cells to the secreted TNF (Varfolomeev *et al.*, 2007; Vince *et al.*, 2007; Wang *et al.*, 2008; Wong *et al.*, 2010). The fact that p38/MK2 inhibition positively effects both aspects of Smac mimetic activity, hints at a close link between TNF production and TNF-induced cell death. Continued efforts into understanding the mechanisms of the combined treatment of Smac mimetic with p38/MK2 inhibitors for the treatment of cancers are therefore justified.

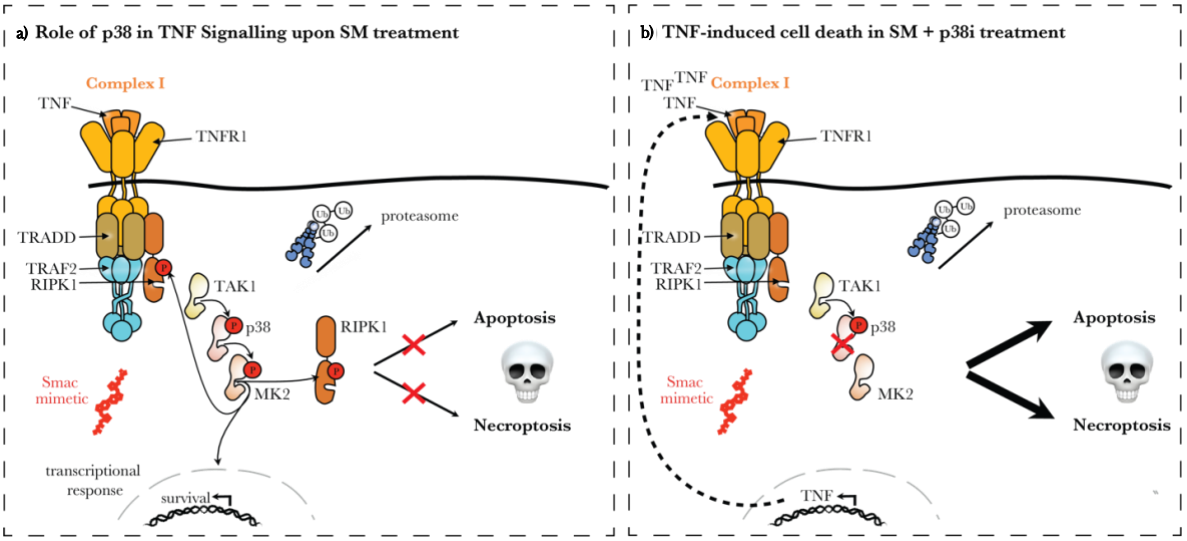

Figure 1.5: The role of p38 in the inhibition of TNF-dependent SM-induced cell death

Schematic representation of the role of p38 in TNF signalling through and cell death induction by Smac mimetic and p38i treatment. A) Upon activation by TAK1, p38 phosphorylates MK2 which in turn phosphorylates RIPK1 to prevent the formation of the cell death-inducing complex II in SM-treated cells. B) Inhibition of p38 prevents the phosphorylation of RIPK1 which can then participate in the formation of complex II. Depending on caspase-8 activity, cell can occur via apoptosis or, when caspase-8 activity is absent, necroptosis. Concurrently, TNF expression is increased amplifying the death signal. Adapted from Lalaoui & Brumatti (Immunol. Cell Biol., 2017).

P = phosphorylation; RIPK1 = receptor interacting protein kinase 1; TAK1 = TGF-β activated kinase 1; TNF = tumor necrosis factor; TNFR1 = TNF receptor 1; TRADD = TNFR1-associated death domain protein; TRAF2 = TNF receptor-associated protein 2.

1.7 TNF Signalling – Some outstanding questions

As discussed previously, TNF is a pleiotropic, inflammatory cytokine that can regulate cell death and survival in a tightly-orchestrated manner. Deregulation of the TNF pathway is associated with a number of autoimmune and inflammatory diseases (Apostolaki *et al.*, 2010). Since the prevalence of such diseases are on the rise, addressing outstanding questions on the TNF pathway is of paramount importance.

In immune cells, TNF-induced cell death plays a critical role in the removal of autoreactive cells to limit unwanted inflammatory responses (Satoh *et al.*, 1989). Deregulation of TNF signalling in these cells leads to autoimmune diseases (McDermott *et al.*, 1999). In fact, TNF is considered a master mediator of the pathogenesis of many autoimmune diseases and chronic inflammation (Yan *et al.*, 2018). With high incidence rates and ever-increasing prevalence, anti-TNF therapies for the treatment of conditions including Crohn's Disease and rheumatoid arthritis, have become the most successful drugs in the overall pharmaceutical industry (marketwatch.com). The involvement of TNF signalling in disease development and treatment has also been described in many cancers, where TNF can have both pro- and anti-tumoral effects (Wajant, 2009).

Even though it has been the subject of intense research for years, many outstanding questions remain, which can be attributed to its extraordinary complexity. A crucial regulator of TNF-induced cell death that has attracted a lot of attention in the last years is RIPK1. Its ability to signal towards both cell death and survival is mediated through different functional domains (**Figure 1.6**). As part of the membrane-bound complex I, ubiquitylated RIPK1 functions as a recruitment platform for TAK1 and IκB kinases (IKK) which promotes the activation of NF-

κB and MAP kinases. In the absence of IAPs, RIPK1 can induce apoptosis in the presence of caspase-8 or necroptosis through phosphorylation of RIPK3, both of which require its kinase activity. At the same time, RIPK1 can also inhibit the formation of the necrosome through mechanisms that remain unclear (Berghe *et al.*, 2015).

Caspase-8 and cFLIP are two further important regulatory players of the TNF pathway who attract great focus. Within the death inducing cytosolic complex II, caspase-8 activity controls apoptotic and necroptotic cell fates. Once activated, caspase-8 inhibits necroptosis by cleaving RIPK1, RIPK3 and CYLD (Feng *et al.*, 2007). Its pro-apoptotic and anti-necroptotic function is regulated by interactions with the pseudo-caspase cFLIP. Caspase-8 homodimers induce apoptosis, however the caspase-8/cFLIP$_L$ heterodimer suppresses both apoptosis and necroptosis (Piao *et al.*, 2012). Binding of cFLIP reduces caspase-8 activity to prevent apoptosis while low levels of enzymatic activity lead to the cleavage of RIPK1 and RIPK3 (Salvesen *et al.*, 2014). It still remains unclear how the different outcomes for the activities of the caspase-8 homodimer and the caspase-8/cFLIP$_L$ heterodimer are regulated. Other important questions that still need to be addressed involve trigger mechanisms by which the receptor-bound complex I is converted to the cytosolic complex II. Is it due to complex internalization, deubiquitylation or other unidentified mechanisms? IAP depletion can trigger the formation of the Ripoptosome independently of TNF-signalling in some cell types (Berghe *et al.*, 2015). It is therefore possible that complex II formation occurs sequentially and not as a direct maturation of complex I. What are the mechanisms by which phosphorylation and (de)ubiquitination events regulate RIPK1 signalling?

Given the complexity of the TNF signalling pathway and the vast number of diseases its dysregulation is associated with, answering these outstanding questions would help us better

understand current treatments and could lay the foundation for the development of novel therapies. Although anti-TNF drugs have been extremely successful in the treatment of autoimmune and inflammatory diseases and significantly improved the lives of millions, serious adverse side effects, emerging drug resistances and limited efficiencies are only a few reasons why continued research into TNF signalling is of paramount importance (Sedger *et al.*, 2014).

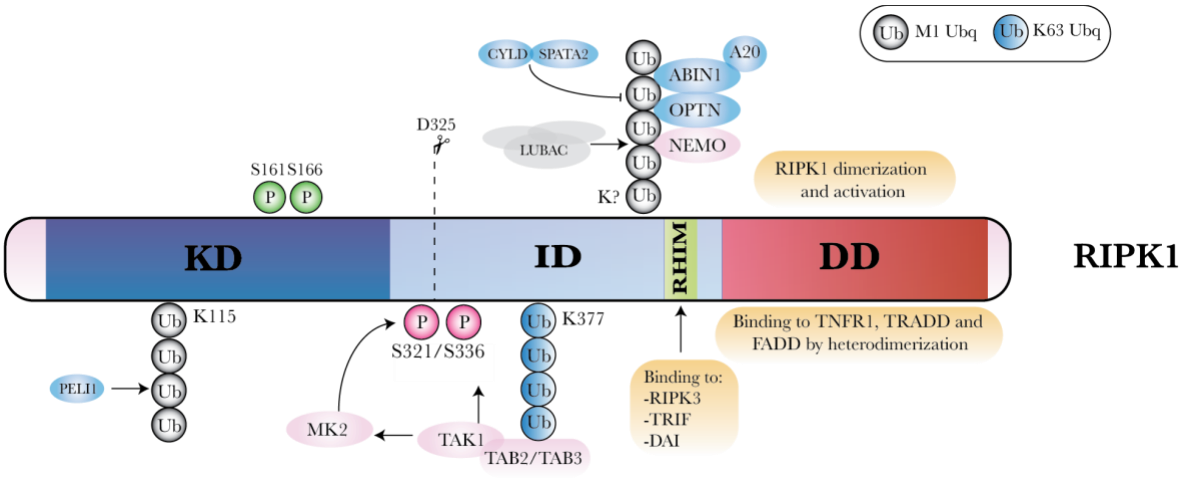

ABIN1 = A20-binding inhibitor of NF-κB; CYLD = cylindromatosis; DAI = DNA-dependent activator of IRFs; LUBAC = linear ubiquitin chain assembly complex; MK2 = MAP kinase-activated protein kinase 2; NEMO = NF-κB essential modulator; OPTN = optineurin; SPATA2 = spermatogenesis associated 2 ; TAB = TAK1-binding protein; TAK1 = TGF-β activated kinase 1; TRADD = TNFR1-associated death domain protein; TRIF = TIR-domain-containing adaptor inducing IFNβ; Ub = ubiquitin.

Figure 1.6: RIPK1 is a master regulator of cell death and survival

Schematic of the domains and post-translational modifications (PTMs) of RIPK1. RIPK1 consists of an N-terminal kinase domain (KD), an intermediate domain (ID) containing a receptor-interacting protein homotypic interaction motif (RHIM) and a C-terminal death domain (DD). Interacting partners are indicated underneath each domain. A number of proteins interact with ubiquitylated Lys377 and possibly other putatively ubiquitylated Lys residues. DD is crucial for the initiation of death receptor signalling and apoptosis. The ID is associated with NF- κB signalling and necroptosis.

1.8 CRISPR/Cas9 mediated knock-in enables the study of endogenous proteins

In order to study the function of a particular protein on an endogenous level, the insertion of a small molecular tag to its N- or C-terminus is a well-established tool. When efficient reagents for the study of a protein of interest are not available, tagging a protein allows one to address a number of questions. A tag permits to pull down the protein of interest with its interactors, enables to study its post-translational modifications and aids with visualizing its location using immunofluorescent imaging techniques. To date, most work involving tagged proteins has been achieved by generating expression constructs of the tagged versions and stably integrating them into cell lines via viral transduction. Often, the applied cell line is lacking the protein of interest either by nature or by genetic deletion. Although widely applied, this technique has various caveats. The expression of a tagged protein can be difficult to accomplish as the deletion itself or the re-introduction of the tagged gene can be lethal to a cell with RIPK1 being a good example for the latter. Physiological expression levels are often difficult to achieve and with protein functions being dosage-dependent, observations based on over-expression systems may not be relevant in a physiological context. Considering the importance of protein levels, we should aim to genetically tag proteins at their endogenous levels. With the CRISPR/Cas9 technology being able to specifically target genetic regions, it is the ideal tool to not only delete sequences but also to introduce foreign sequences into a specific region of the genome of a cell. The CRISPR/Cas9 system relies on RNA-guided sequence-specific endonucleases to induce DNA double-stranded breaks (DSBs) at specific genomic loci (Doudna *et al.*, 2014). Those DSBs can be repaired by the cell's intrinsic DNA repair mechanisms in one of two ways: In the error-prone non-homologous end joining (NHEJ) pathway, the break is repaired by the DNA repair machinery where the ends of the DSB are

rejoined (Doudna *et al.*, 2014). This can result in the generation of random indel mutations leading to frameshifts and the creation of premature stop codons, which ultimately result in genetic knockouts (Ran *et al.*, 2013). Alternatively, when provided with a repair template in form of a plasmid or single stranded DNA (ssDNA), the cell's homologous DNA repair (HDR) pathway can be activated allowing precise editing with high fidelity (Lombardo *et al.*, 2011). It is this HDR pathway that can be exploited to introduce foreign sequences such as molecular tags or mutations into the host's genome.

Nowadays, the application of the CRISPR/Cas9 technology to generate genetic knock-ins in mice is a well-established tool for the study of proteins where it allows researchers to address a vast array of questions (Hille *et al.*, 2018). Although this technique has a high success rate and can be applied to virtually any gene, generating knock-in mice is both cost intensive and time consuming (Doyle *et al.*, 2012). Due to these restrictions and the inability to study human proteins, using the CRISPR/Cas9 knock-in technology in animals is not always a viable option. A more economical and faster approach for the generation of tagged proteins, involves the use of cell lines. Although a number of protocols for the use of CRISPR/Cas9 knock-in in cell lines have been published, these techniques often fail to transfer to other cell lines or target genes (Lino *et al.*, 2018). Reasons for their restricted versatility include our lack of understanding of the molecular mechanisms involved in homologous DNA repair and the fact that in different cell lines, enzymes belonging to the HDR and NHEJ pathway vary in their degree of activity (Liu *et al.*, 2019). The CRISPR/Cas9 technology has revolutionized how we study protein function. Given its immense potential, there is a great drive to gain more insights into what the exact molecular mechanisms of CRISPR/Cas9 are and how we can best harness its ability to precisely edit genes. Ultimately, this will lead to the development of improved,

versatile gene editing tools that can be readily applied to cell lines allowing researchers to study any protein on endogenous levels in a timely and cost-efficient manner.

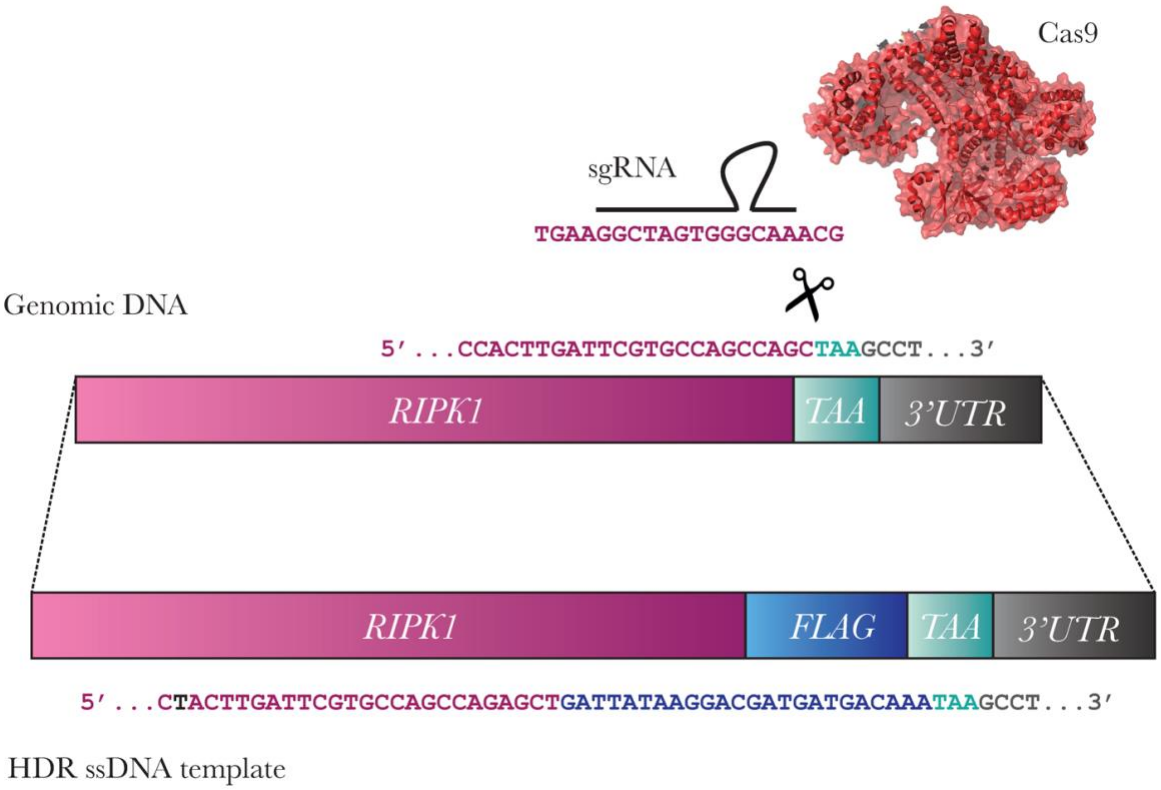

Figure 1.7: CRISPR/Cas9-mediated knock-in to generate FLAG-tagged protein

Schematic representation of CRISPR/Cas9-mediated knock-in of FLAG sequence using ssDNA HDR template. When Cas9 induces a double stranded DNA break (DSB), the presence of a homologous ssDNA template activates the homologous DNA repair (HDR) machinery leading to a correct repair of the break. This mechanism can be hijacked to introduce a foreign sequence such as a FLAG-tag used in this work for the expression of C-terminally tagged FLAG-RIPK1. Pink = RIPK1 exon, blue = FLAG sequence, teal = stop codon, grey = 3' untranslated region.

1.9 Project aims

In this thesis I will present the results from three aims:

(1) Generating a clinically relevant AML mouse model that recapitulates an aggressive, treatment-resistant form of AML by expressing EVI1 with the oncogene MLL-AF9 *in vivo.*

(2) Understanding the role of the MAP kinase p38 in preventing Smac mimetic-induced cell death.

(3) Establishing a protocol that allows the tagging of endogenous proteins of the TNF signalling pathway using the CRISPR/Cas9 knock-in technology.

1.9.1 MLL-AF9 EVI1 mouse model

The translation of novel discoveries into the clinic to treat AML more efficiently, has been hampered by the lack of suitable disease models. The overexpression of the transcription factor EVI1 has been identified as a marker of poor prognosis in AML patients (Groschel *et al.*, 2013). I aimed to generate a mouse model that faithfully reflects a particularly aggressive form of this disease by overexpressing EVI1 in an MLL-driven AML. I hypothesize that the expression of EVI1 gives leukemic cells a proliferative advantage, that may lead to: (A) a more rapid disease onset, (B) a more severe disease phenotype, (C) a more immature immuno-phenotype and (D) greater resistance of leukemic cells to treatment *in vitro*. The results of this work will be presented in Chapter 3 of this thesis.

1.9.2 The role of p38 in inhibiting cell death in IAP-depleted cells

The IAPs have been identified as attractive targets in the treatment of various cancers leading to the development of Smac mimetics. The MAP kinase p38 can prevent Smac mimetic-induced cell death which can be overcome by the addition of p38 inhibitors, revealing a novel role of this protein (Lalaoui et al., 2016). Understanding the mechanisms through which p38

exhibits its inhibitory function was the objective this project. To do so, I studied the phosphoproteome of cells treated with Smac mimetic alone or in combination with a p38 inhibitor to identify pathways that mediate the prevention of cell death. Chapter 4 outlines the results of this work.

1.9.3 Tagging endogenous proteins using CRISPR/Cas9-mediated knock-in

The CRISPR/Cas9 gene editing tool revolutionized that study of proteins by allowing researchers to precisely insert foreign sequences ('knock-in') into the genome of a cell to molecularly tag proteins. This ability enables us to study protein features such as their function, interactors or post-translational modifications on an endogenous level. To date, a number of techniques have been described to efficiently generate knock-in cell lines. While the published approaches vary greatly with regards to cost, labor intensity and versatility, my aim was to establish a protocol that can be applied to a large cohort of cell lines, that is relatively inexpensive and quick and at the same time suited for any gene of interest. To test my approach of choice, I aimed to generate C-terminally tagged FLAG- RIPK1 in mouse dermal fibroblasts (MDFs). The results of this project are discussed in Chapter 5.

2 Materials and Methods

2.1 Antibodies

For Western blotting the following antibodies were used: mouse anti-FLAG (F-3165, Sigma), mouse anti ß-actin (A-1978, Sigma), rabbit anti-phospho JNK (9251, Cell Signaling Technology), rabbit anti-phospho MK2 (3007P, Cell Signaling Technology), rabbit anti-phospho ERK (9102, Cell Signaling Technology), rabbit anti-p38 (9212, Cell Signaling Technology), rabbit anti-phospho p38 (9211, Cell Signaling Technology), rabbit anti-EVI1 (ab28457, Abcam), rabbit anti-GFP (11122, Invitrogen), mouse anti-caspase 8 (sc-789, Santa Cruz Biotechnology).

For immunohistochemistry antibodies used were rat anti-mouse Ly-6G/6C APC-Cy7 (557661, BD Pharmingen), rat anti-mouse F4/80 PE (MCA497GA, AbD Serotec), rat anti-mouse CD11b BV510 (562950, BD Pharmingen), rat anti-mouse CD117 APC (553356, BD Pharmingen), rat anti-mouse Ly6A/E PE (553108, BD Pharmingen), rat anti-mouse NK1.1 FITC (553164, BD Pharmingen), rat anti-mouse B220 PE (12045282, eBioscience), rat anti-mouse Ter119 APC-Alexa Fluor 750 (275921, eBioscience).

2.2 Reagents

Table 2.1 List of reagents

Reagent	Catalogue number	Company
2-Chloroacetamide	C0267	Aldrich
2,2,2-Trifluoroethanol	91683	Sigma-Aldrich
10x T4 ligation buffer	M1801	Promega
Acetonitrile	900667	Sigma-Aldrich

Agarose	BIO-41025	Bioline
Ammonium bicarbonate	09830	Sigma-Aldrich
Ampicillin	ROAMP	Roche
Ara-C	C1768	Sigma-Aldrich
Birinapant	-	TetraLogic
Compound A	-	TetraLogic
Dimethyl sulfoxid	276855	Sigma-Aldrich
ECL	RPN2236	GE Healthcare
EDTA	E9884	Sigma-Aldrich
Effectene	28706	Qiagen
Ethidium bromide	E1510	Sigma
GoTaq green	M712C	Promega
HRP substrate	WBKLS0500	Millipore
L-Broth	P4170	In-house
LY2228820 (p38 inhibitor)	Apex Bio	A5566
Lys-C	90051	Thermo Scientific
Ni-NTA beads	151010	Qiagen
Plasmid purification kit	K20007	Invitrogen
PF-3644022 (MK2 inhibitor)	4279	Tocris Bioscience
Propidium iodide	P4170	Sigma
Ralimetinib	S1494	Selleckchem
Retronectin	-	In-house
Restriction enzymes		NEB

T4 DNA ligase	M1801	Promega
TCEP	20490	Thermo Fisher
Trifluoroacetic acid	T6508	Sigma Aldrich
Trypsin	Xv528x	Promega

2.3 Vector preparation

For the generation of recombinant plasmids, vectors and insert were cut with the appropriate restriction enzyme/s as follows:

Table 2.2: Vector digest reaction

5 µg vector/insert
1 µL restriction enzyme (NEB)
5 µL 10x appropriate enzyme buffer (NEB)
x µL ddH_2O
Σ 50 µL

Cut vector/insert was resolved using a 1.2% (w/v) agarose-TAE (40 mM Tris-acetate pH 8.2, 1 mM EDTA) gel. Bands were excised and DNA purified using the Wizard SV Gel and PCR Clean-Up system (Promega) according to manufacturer's instructions with 50 µL of nuclease free H_2O as the final elution.

2.4 Ligation

The gene of interest was transferred to the target vector by ligating cut vector and insert as followed:

Table 2.3: Ligation reaction

100 ng cut plasmid
300 ng insert
0.8 µL T4 ligase (Promega)
1 µL 10x T4 ligation buffer
x µL nuclease free water
Σ 10 µL

Ligation mixture was incubated at RT overnight.

2.5 Transformation of Stbl4 cells

The amplification of newly generated plasmid was achieved by transformation of 50 µL ice-thawed electrocompetent *Escherichia coli* Stbl4 (in-house) with 2 µL ligation mix. Electroporation was performed in 2 mm electroporation cuvettes (Cell Projects) at 2.5 kV for approximately 5 ms using a MicroPulser electroporator (Bio Rad). Electroporated cells were transferred to LG agar plates (1.5% (w/v) Difco agar, 1% (w/v) tryptone, 0.5% (w/v) yeast extract, 0.5% (w/v) NaCl, 0.2% (w/v) glucose, 10 mM Tris-HCl pH 7.4, 1 mM $MgCl_2$) and were grown in the presence of 100 µL/mL ampicillin for 16 hours at 37 °C.

2.6 Miniprep of plasmid DNA and sequence confirmation

To determine if ampicillin-resistant bacteria have been transformed with the target plasmid, colonies were screened by inoculation in 1.5 mL LB broth (1% peptone (w/v), 0.5% yeast extract (w/v), 0.5% NaCl (w/v)) and incubation with of 100 µL/mL ampicillin for 16 hours at 37 °C. Plasmid DNA was subsequently isolated by resuspending bacterial pellets in resuspension buffer (50 mM Tris-HCl pH 8.0, 10 mM EDTA, 20 mg/mL RNase; Invitrogen) followed by lysis for 1 minute in 200 mM NaOH, 1% (w/v) SDS (Invitrogen) on ice and

precipitation for 5 minutes by the addition of precipitation buffer (Invitrogen). Precipitable material was pelleted and plasmid DNA was retrieved by adding isopropanol to the supernatant at a ratio of 0.7:1. Plasmid DNA was pelleted and washed in 70% ethanol before being dried and resuspended in nuclease free water.

To confirm the sequence of recombinant plasmids, diagnostic digests were performed and promising constructs were finally sent for Sanger sequencing at the Australian Genome Research Facility (AGRF, Melbourne).

2.7 Midiprep of plasmid DNA

Upon confirmation of the sequence, appropriate bacterial clones were inoculated in 50 – 100 mL LB broth and plasmid DNA was isolated using Invitrogen's HiPure plasmid midiprep kit in accordance with the provided instructions. Plasmid DNA pellets were finally resuspended in 50 – 100 µL nuclease free water and DNA concentrations were measured using a spectrophotometer (NanoDrop, Thermo Fisher).

2.8 Cell death assay via flow cytometry

To determine the rate of cell death, the uptake of propidium iodide (PI) was measured via flow cytometry. Cells were harvested and resuspended in PBS at a cell concentration of approximately 1 x 10_5 cells/100 µL. PI solution (10 µg/mL) was added to achieve a final concentration of 100 ng/mL and after incubation on ice in the dark for one minute, PI uptake was measured using a FACSCalibur flow cytometer (BD Biosciences) where it was detected at 660 nm.

2.9 Cell lines and cell culture

Cell lines used were human embryonic kidney cell line (HEK293T), transformed mouse dermal fibroblast (MDFs), primary murine bone marrow-derived macrophages (BMDMs), various AML cell lines (MLL-AF9, MLL-AF9/Nras^{G12D}, MLL-ENL) and fetal liver cells. Cell lines were cultured in Dulbecco's Modified Eagle's Medium (DME, GIBCO) (HEK293Ts, MDFs) or Iscove's Modified Dulbecco's Medium (IMD, GIBCO) (AML cell lines) supplemented with 8% fetal calf serum (FCS, GIBCO) (v/v), 1 mM L-glutamine, 100 units/mL penicillin and 100 μg/mL streptomycin (GIBCO). For the generation of BMDMs, bone marrow from the femur, tibiae and hip of mice was cultured for six days in DME supplemented with 10% FCS (v/v), 20% L929 mouse fibroblast media (in-house) and antibiotics (penicillin and streptomycin). After six days, cells were detached using trypsin-EDTA and a cell scraper and appropriate cell numbers were re-plated in 10 cm and 24-well cell culture plates. Progenitor/stem cells were derived from fetal livers which were isolated from E14 C57BL/6J embryos, resuspended in PBS and cultured in alpha-minimum essential medium (alpha-MEM, GIBCO) supplemented as above but with the addition of 10 mM HEPES, 1mM sodium pyruvate, 10% FCS, 50 μM ß-mercaptoethanol, 100 ng/mL murine stem cell factor (SCF, PeproTech), 10 ng/mL IL-6, 50 ng/mL thrombopoietin and 5 ng/mL FMS-related tyrosine kinase (Flt) 3. All cells were cultured at 37 °C with 10% CO_2 in a humidified incubator.

2.10 Generation of retrovirus and infection

For retroviral infection virus supernatant was produced by co-transfecting HEK293T cells with the 1.5 μg plasmid of interest together with 2.5 μg pUMVC expressing gag and pol and 1 μg pCMV-VSV-G expressing the viral envelope protein in a 10 cm plate using the Effectene

transfection kit (Qiagen). Virus-containing supernatant was harvested after 48 hours and filtered using a 0.45 μm PES filter unit.

2.11 Generation of murine AML

To generate AML in mice, viral supernatants were produced by co-transfecting HEK293T cells with the oncogenic construct and retroviral packaging plasmids. Hematopoietic progenitor/stem cells (HSCs) were infected with the viral supernatant on two consecutive days using the RetroNectin-bound virus method of transduction. Non-tissue culture 24-well plates were initially pre-coated overnight with 30mg/mL RetroNectin at 4 °C and subsequently washed with PBS and blocked with 2% (v/v) BSA for 30 minutes at 37 °C. After the addition of 1mL viral supernatant, plates were spun at 2700rpm for 1 hour at 32 °C and finally seeded with approximately 1 x 10_6 hematopoietic progenitor/stem cells in supplemented alpha-MEM. Before injecting transduced cells into C57BL/6J mice, bone marrow aplasia was induced by total body gamma-irradiation (7.5 Gy). Number of injected cells ranged from 3 x 10_5 to 5 x 10_5 cells per mouse in 200 μL PBS. Injected mice were checked twice daily for signs of leukaemia, which included enlarged spleen, anaemia, hunched posture and lethargy. Upon diagnosis mice were culled and heart bleed as well as harvest of sternum, liver, spleen and bones of the legs were performed. Leukemic cells were then obtained from the bone marrow and were subsequently cultured at 37 °C in IMDM supplemented with 8% FCS and 5 ng/mL IL-3. In order to test their ability to induce AML in secondary recipients, primary leukemic cells were injected into C57BL/6J mice at a cell concentration of 5x10_5 cells/mouse.

2.12 Generation of EVI1 overexpressing murine AML

MLL/AF9-induced AML with EVI1 overexpression was generated using two different approaches. For the first approach, fetal liver derived hematopoietic progenitor/stem cells

were virally transduced with an EVI1 – IRES – GFP construct. Two days after infection, GFP expressing cells were isolated using a fluorescence assisted cell sorter (BD FACSAria Fusion cell sorter) and subsequently infected with the MSCV MLL/AF9 – IRES – mCherry construct. After culturing for two days in supplemented alpha-MEM as described above, infected cells were injected into lethally gamma-irradiated C57BL/6J mice at a concentration of 5 x 10^5 cells/mouse in 200 µL PBS. The second approach made use of a doxycycline (dox)-repressible two vector system developed by J. Zuber et al. (Zuber *et al.*, 2011) where one retroviral vector encodes for MLL/AF9 linked to dsRED under the control of a tetracycline response element (TRE) promoter while a second vector expresses EVI1 linked to the Tet-off transactivator (tTA) and therefore activates TRE expression in a dox-repressible manner. Cells harboring both constructs can be identified by the detection of dsRed expression. EVI1-expressing leukemias were generated by retroviral co-transduction of fetal liver derived HSPCs and injection into lethally irradiated recipient mice.

2.13 SDS PAGE and Western blotting

Protein lysates were prepared by lysing cell pellets either in 2 x SDS lysis buffer (126 mM Tris-HCL pH 8, 20% glycerol (v/v), 4% SDS (w/v), 0.02% Bromophenol blue (w/v), 5% ß-mercaptoethanol (v/v)). Lysates were boiled and sonicated or subjected to repeated freeze/boil cycles. Denatured proteins were separated on a 4 – 15% Criterion TGX precast gel (5671085, Bio Rad) and transferred to a nitrocellulose membrane at 100V for 1 hour at 4°C. Membranes were subsequently blocked in PBST with 5% milk powder (w/v). Probing of the membrane with primary antibody occurred over night at 4°C in PBST with 2% BSA (w/v) and 0.02% NaN_3 (v/v). After washing with PBST, membranes were incubated for an hour in secondary antibody in the presence of 5% milk

and subsequently developed with Millipore ECL (WBKLS0) for analysis with a Chemidoc Gel Imaging System (Bio Rad).

2.14 Blood analysis

Hematological analysis including complete blood count and leukocyte differential count of sick mice was performed on cardiac blood of euthanized mice using an ADVIA Hematology System (Siemens).

2.15 Blood smear

To evaluate cellularity and morphology of leukemic cells present in the peripheral blood, blood smears were prepared on microscope slides by pipetting 7 µL cardiac blood on the slide and spreading the drop using another slide as a spreader. After air-drying blood smears were fixed by placing the slides in a coplin jar containing methanol for one minute. Once dried slides were taken to histology where May-Grünwald Giemsa stain was performed.

2.16 Cytospin

To evaluate cellularity and morphology of leukemic cells present in the bone marrow, fresh bone marrow was diluted to a cell concentration of 1 x 10_5 cells/mL using FCS containing media. 200 µL cell suspension were loaded into the cytospin sample chamber and cells were immobilized onto the attached glass slide by spinning the chamber for 5 minutes at 1000 rpm. Cell suspensions were then allowed to dry at 37 °C before being fixed for one minute in cold methanol. May-Grünwald Giemsa stain was finally performed in our histology laboratory.

2.17 AML *in vitro* treatments

To determine how EVI1 expression affects sensitivity of leukemic cells to treatments *in vitro*, cell death was measured as a response to cells being treated with AraC (125 – 1000 nM) or

Birinapant (125 – 1000 nM) alone or Birinapant (125 – 1000 nM) in combination with Ralimetinib (LY2228820, 1 μM), Idun (5 μM) or Tariquidar (1 μM). Death assays were performed in 96-well plates with cell concentrations of 5 x 10_4 cells/well in 100 μL media and drugs were added in 100 μL at two times the required final concentration. The resulting cell death was determined after 24 hours by the addition of propidium iodine at 1 ug/mL and measuring its uptake via flow cytometry using a CytoFLEX (Beckman Coulter).

2.18 Cell surface marker analysis

Various cell surface markers of leukemic cells were stained for flow cytometry analysis using rat anti-mouse antibodies coupled to a fluorophore. Master stocks of antibody cocktails were prepared in FACS buffer (PBS, 5% (v/v) FCS, 5 mM EDTA) containing rat anti-mouse anti-2.4G2 mAb to prevent unwanted binding to the Fc-region of antibodies. Staining was performed in 96 well plated with approximately 5 x 10_5 per well in 50 μL media. After washing cells in 100 μL FACS buffer, pellets were resuspended in 50 μL antibody cocktail and incubated for 30 minutes on ice in the dark. Following another wash step, cells were resuspended in 150 μL FACS buffer containing propidium iodine and analysed via flow cytometry using an LSRFortessa-X20 analyser (BD). Single stain controls were prepared by incubating one drop anti-rat beads with 1 μL neat antibody for 15 minutes in the dark. Washed beads were resuspended in 150 μL FACS buffer and run on the flow cytometer to determine the required compensations.

2.19 Statistical analysis

Unless stated otherwise, paired parametric t tests were performed for statistical analysis using GraphPad Prism version 7.0d for Mac OS X (GraphPad Software, La Jolla California USA).

2.20 BMDM treatment protocol

BMDMs were seeded in 10 cm plates at a density of 1 x 10_7 cells per plate in 7 mL DME one day prior to treatment. For cell death analysis in a 48 well plate, cells were seeded at 1 x 10_5 cells per well. Per biological sample five different conditions were set up: DMSO control, 1.5 hours Compound A (500 nM), 1.5 hours Compound A (500 nM) and LY2228820 (1 μM), 3 hours Compound A (500 nM) and 3 hours Compound A (500 nM) and LY2228820 (1 μM). Drugs were prepared at 100 times the required final concentration in DME. To terminate treatment, plates were put on ice, media was aspirated and cells were immediately washed three times with ice cold PBS. For enrichment with Fe_{3+}-NTA beads, cell lysis was performed by adding 700 μL hot lysis buffer (5% SDS (w/v), 5 mM TCEP, 10 mM chloroacetamide, 100 mM Tris-HCl pH 7.5, 40 mM NaCl) after which lysates were transferred to tubes and finally boiled for 10 minutes at 95 °C. Per sample, an aliquot of lysate containing 1 mg protein was separated and stored at -80 °C until being processed further. When following the EasyPhos protocol, cells were washed on ice in cold PBS containing a protease inhibitor cocktail (Roche) and subsequently lysed in lysis buffer (1% (w/v) SDS, 100 mM Tris-Cl pH 7.5, 40 mM NaCl). Per sample, an aliquot of lysate equivalent to 0.5 mg protein was separated and stored at -80 °C until being processed further.

2.21 Protein quantification via BCA assay

Protein concentrations were determined using a Pierce BCA protein assay kit (23225, Thermo Fisher). To be compatible with the BCA reagents, cells were lysed in 1% (w/v) SDS. The assay was performed in accordance with the provided instructions and the resulting colour change was measured with a Chameleon V Luminescence Plate Reader (425-159, Hidex).

2.22 On-bead protein digest using Sera-mag speed beads

Thawed lysates were boiled again at 95°C before being subjected to acid hydrolysis by adding 4 – 5 µL neat trifluoroacetic acid (TFA) to bring the final TFA concentration to 1% (v/v). The reaction was quenched with an appropriate volume of 3 M Tris pH 10 to achieve a final concentration of 160 mM Tris and a neutral pH. Lysates were now transferred to a 96-well deep well plate (95040452, Thermo Fisher) with conical bottom. For on-bead digestion 10 µL Sera-mag speed (SP3) beads in water were added to each sample followed by an appropriate volume of acetonitrile to reach a final concentration of 70% (v/v). For incubation, the plate was placed in a ThermoMixer (Eppendorf) and mixed at 1000 rpm for 20 minutes at room temperature. To wash the beads, the plate was placed on a magnetic rack allowing the supernatant to be aspirated without interfering with the magnetic beads. Beads were washed twice with 200 µL 70% (v/v) ethanol and once with 200 µL neat ACN before being lyophilized to remove remaining acetonitrile. In the meantime, the digestion buffer (10% (v/v) 2,2,2-trifluoroethanol (TFE), 100 mM ammonium bicarbonate) containing trypsin and lys-c at an enzyme to substrate ratio of 1:25 was prepared, meaning that for the digest of 1 mg protein, 20 µg of trypsin and lys-c respectively were used. Dried beads were resuspended in 100 µL digestion buffer and sonicated for 2 minutes to ensure substrate accessibility. Digest was performed in the ThermoMixer at 37 °C and 1000 rpm for 1 – 2 hours. To collect the supernatant containing the peptides, the deep well plate was again placed on a magnetic rack and samples were transferred into a 96-well PCR plate. Lastly, 50 µL water were added to each sample before being processed for phospho enrichment.

2.23 EasyPhos - Phospho enrichment using TiO_2 beads

Phospho enrichment was performed following the EasyPhos protocol (Humphrey *et al.*, 2015). In a 2 mL deep well plate, 800 µL acetonitrile were transferred to the digested peptides and mixed in a ThermoMixer for 30 sec at 2000 rpm. To each sample, 150 µL 3.2 M KCl, 55 µL 150 mM KH_2PO_4 and 95 µL TFA were added before being mixed again for 30 sec at 2,000 x g. To clear minor precipitates, the plate was centrifuged for 15 min at 20,000 x g and supernatants were transferred to unused wells on the same plate while carefully avoiding the pellets. To prepare the beads, TiO_2 was resuspended in EP loading buffer (80% (v/v) acetonitrile, 6% (v/v) TFA) at a concentration of 1 mg beads per µL buffer. The amount of TiO_2 beads applied per samples was equivalent to ten times the initial protein concentration (5 mg TiO_2 beads for 0.5 mg protein). Equal amounts of beads were transferred to each sample and the beads/peptides mixtures were subsequently incubated in a ThermoMixer for 5 min at 40 °C and 2,000 x g. Following incubation, the beads were pelleted by centrifugation for 1 min at 2,000 x g and the supernatant containing non-phosphopeptides was aspirated. Beads were resuspended in 500 µL EP wash buffer (60% (v/v) acetonitrile, 1% (v/v) TFA), transferred to new wells that already contained 500 µL EP wash buffer and washed 4 times in 1 mL EP wash buffer. After washing, beads were resuspended in 75 µL EP transfer buffer (80% (v/v) acetonitrile, 0.5% (v/v) acetic acid), mixed in the ThermoMixer for 30 sec at 800 x g and transferred to the top of C8 stage tips. Any remaining beads were captured by washing the wells with an additional 75 µL which were then also transferred to the C8 stage tips. To bind the phosphopeptides, tips were centrifuged to dryness (approximately 5 min) at 1,000 x g and finally eluted twice with 30 µL EP elution buffer (40% (v/v) acetonitrile, 45% (v/v) MilliQ H_2O, 3.75% (v/v) NH_4OH) into 1.5 mL tubes for 3 min at 1,000 x g. Eluates were immediately dried using a vacuum concentrator (SpeedVac, Eppendorf) for 15 min at 45 °C. In the meantime,

SDBRPS stage tips were equilibrated by successive washing with (a) 100 µL acetonitrile, (b) 100 µL 30% (v/v) methanol/1% (v/v) TFA and (c) 100 µL 0.2% (v/v) TFA for 1 min at 1,000 x g. Following vacuum concentration, 10 µL 10% TFA were immediately added to each sample before being transferred to the equilibrated SDBRPS stage tips in 100 µL SDBRPS wash buffer (0.2% (v/v) TFA. Tips were washed twice for 5 min at 1,000 x g and phosphopeptides were finally eluted into clean 1.5 mL tubes using 60 µL SDBRPS elution buffer (80% (v/v) acetonitrile, 15% (v/v) MilliQ H2O, 1.25% (v/v) NH_4OH) by spinning the tips down for 5 min at 1,000 g. Peptides were dried in the vacuum concentrator for 35 min at 45 °C before being resuspended in 6 µL MS loading buffer (2% (v/v) acetonitrile, 1% (v/v) formic acid on Milli-Q water). MS spectra were acquired between a mass range of 200–2000 m/z. Raw files consisting of high-resolution MS/MS spectra were processed with MaxQuant (version 1.5.8.3) (Cox *et al.,* 2008) for feature detection and protein identification using the Andromeda search engine 2. Extracted peak lists were searched against the UniProtKB/Swiss-Prot Homo sapiens (October 2016) and a separate reverse decoy database to empirically assess the false discovery rate (FDR) using strict trypsin specificity allowing up to 2 missed cleavages. The minimum required peptide length was set to 7 amino acids. In the main search, precursor mass tolerance was 0.006 Da and fragment mass tolerance was 40 ppm.

2.24 Statistics of phosphoproteomics analysis

Potential contaminant and reverse entries were removed. The data was reshaped from a long format to a wide one such that each row corresponds to a unique modified sequence and charge combination, and each column to a sample. Duplicate instances of any unique modified sequence and charge combination corresponding to the same sample were aggregated by summing over the respective intensities. Peptides that were detected in at least

6 samples were retained while the rest were filtered out, leaving 5121 peptides for downstream analysis. Quantile normalization was subsequently applied to the data. A linear model incorporating sample quality weights was fitted for each peptide using the lmFit and arrayWeights functions of the limma package (Ritchie, M. E., *et al.*, 2015) in R version 3.6.0 (R Core Team, 2019). Moderated t-statistics were then computed using robust empirical Bayes moderated t-statistics with a trended prior variance (Phipson, B., *et al.*, 2016) to test for differential phosphorylation. P-values were adjusted to control for false discovery rate (FDR) using the Benjamini and Hochberg method. A peptide was classified as differentially phosphorylated if the adjusted p-value was less than 0.1. Volcano plots, mean-difference plots and heatmaps were produced using limma's volcanoplot, plotMD and coolmap functions respectively. Pathway analyses were carried out on differentially phosphorylated peptides in order to test for overrepresentation of biological pathways as defined by Gene Ontology (Ashburner, M., *et al.*, 2000), The Gene Ontology Consortium, 2017), KEGG (Kanehisa, M. and S. Goto, 2000; Kanehisa, M., *et al.*, 2015; Kanehisa, M., *et al.*, 2016)and Reactome (Fabregat, A., *et al.*, 2018) using the goana and kegga functions in limma. Visualizations of KEGG pathways were produced using the pathview package (Luo, W. and C. Brouwer, 2013).

2.25 CSF1R inhibitor treatment of BMDMs

BMDMs were seeded in a 24well plate at a density of 5 x 10_4 cells per plate in 1 mL DME + 10% L929 one day prior to treatment. Cells were treated with Compound A (50, 100 or 500 nM) alone or in combination with LY2228820 (p38i, 1 μM) or AFS-98 (CSF1Ri, 33nM) for 6 or 24 hours. Controls were treated with DME 0.2% (v/v) DMSO. Supernatant and cells were harvested, centrifuged for 5 minutes at 500 g and resuspended in PBS containing PI (100

ng/mL). Cell death was measured via PI uptake using FACSCalibur flow cytometer (BD Biosciences) where it was detected at 660 nm.

2.26 Generation of CRISPR/Cas9 guides and cloning into the CRISPR nuclease vector

2.26.1 Guide sequence and annealing

The sgRNA sequences were generated using the CRISPR.mit.edu guide design tool and overhangs suitable for cloning guides into the lentiCRISPRv2 plasmid were added. The overhang sequences (bold) were:

Oligo 1 → 5' – **CACCG**NNNNNNNNNNNNNNNNNNN – 3'

3' – **C**NNNNNNNNNNNNNNNNNNN**CAAA** – 5' ← Oligo 2

Forward (oligo 1) and reverse (oligo 2) guide sequences were ordered in form of ssDNA oligos from Integrated DNA Technologies. Oligos were annealed as followed:

Table 2.4: Annealing reaction

3 µL	oligo 1 (100 µM)
3 µL	oligo 2 (100 µM)
0.5 µL	NaCl (3 M)
2 µL	$MgCl_2$ (1 M)
2 µL	Tris pH7.5 (1 M)
9.5 µL	ddH_2O
Σ 20 µL	

In a PCR machine, annealing mixture was heated for 5 min at 96 °C followed by incubation at 80 °C for 1 h before being placed on ice.

Table 2.5: List of CRISPR/Cas9 guide RNAs used for knock-in FLAG into NTD or CTD of

Gene	Guide Sequence	Domain
m RIPK1	TCTGGCTGGCACGAATCAAG	CTD
m c-Flip	GGTCCATGGCAGTGGTACGC	NTD
m FADD	GAACAGTGGTGTTTCGTCTA	CTD

2.26.2 Digest and purification of lentiCRISPRv2 plasmid

The lentiCRISPRv2 plasmid encoding Cas9 was digested with BsmBI for 2 h at 37 °C as followed:

Table 2.6: Digest of lentiCRISPRv2

5 µg lentiCRISPRv2
1 µL BsmBI (NEB)
5 µL 10x CutSmart Buffer (NEB)
x µL ddH_2O
Σ 50 µL

Cut vector was resolved using a 1.2% (w/v) agarose-TAE (40 mM Tris-acetate pH 8.2, 1 mM EDTA) gel. Bands were excised and DNA purified using the Wizard SV Gel and PCR Clean-Up system (Promega) according to manufacturer's instructions with 50 µL of nuclease free H_2O as the final elution.

2.26.3 Ligation of lentiCRISPRv2 plasmid with sgRNA guide

Ligation mixtures of lentiCRISPRv2 plasmid and annealed sgRNA sequences contained the following:

Table 2.7: Ligation of lentiCRISPRv2

50 ng cut lentiCRISPRv2

3 µL annealed, diluted oligos (1/1000)
0.8 µL T4 ligase (Promega)
1 µL 10x T4 ligation buffer
x µL ddH_2O
Σ 10 µL

Ligation mixture was incubated at RT overnight. Generated lentiCRISPRv2 plasmid containing Cas9 and sgRNA was amplified by bacterial transformation as described in 2.5. Plasmids were then prepped (2.6) and sequenced (2.7).

2.27 Generating HDR knock-in template

The HDR knock-in templates consisted of ssDNA oligos of approximately 200 bp and were designed for each individual gene where they targeted either the N- or C-terminus. HDR templates contained the FLAG sequence (see figure 2.8) which was flanked by gene-specific homology arms of approximately 80 bp. To prevent Cas9 from cutting the inserted sequence, the PAM sequences in the templates were silently mutated where possible.

Table 2.8: RIPK1 CTD HDR template sequence

Gene	HDR Template Sequence
m RIPK1	gcacttcaccaatgttgcaggatagacctgctgaactacttgattcgtgccagc cagagcgattataaggacgatgatgacaaaTAAgcctgggcaggctctgg cagtgggaagcaaactatttgtctggtgcacaaaccccgtttg

Guide with mutated PAM, FLAG, Stop codon, homology arms

2.28 Generation CRISPR/Cas9 knock-out cell lines

CRISPR/Cas9 guide efficiencies were determined by testing their ability to generate gene knock-outs in MDFs. To do so, cells were virally transduced with the generated

lentiCRISPRv2 plasmids to stably express Cas9 and sgRNA. For lentivirus production, HEK293T cells were transfected with 1 μg pVSV-G (envelope protein expression1.5 ug pCMVΔR8.2 (HIV Pol – reverse transcriptase, Tat – amplifies transcription of viral RNA, Rev – increases transport of viral RNA into cytoplasm, Gag – capsid proteins) and 2.5 μg of the plasmid of interest using an Effectene transfection kit (Qiagen). Media was replaced after 24 h and virus was harvested two days post transfection. Supernatant was filtered and supplemented with polybrene (4 μg/ml). For infection, viral media was added to cells and after two days of incubation, successfully infected cells were selected by addition of puromycin (1 μg/ml).

2.29 CRISPR/Cas9-mediated FLAG knock-in

To generate gene-specific FLAG-knock-in in MDFs, cells were seeded at 2 x 10_5 cells in a 24-well plate. The following day, the appropriate mix of lentiCRISPRv2 plasmid and FLAG-containing ssDNA HDR template were delivered into cells at a ratio of 1:5 via transfection using Lipofectamine 3000. To increase HDR efficiency, cells were also treated with 0.1 μM SCR7 for 2 days. 24 h after transfection, successfully transfected MDFs were selected by the addition of puromycin (1 μg/ml) for 2 days. One-week post transfection, DNA was extracted from a fraction of the cells using a Qiagen DNA extraction kit to test for the presence of the FLAG tag via PCR.

2.30 Detection of FLAG insert via PCR

To determine whether the FLAG-tag was knocked-in successfully a PCR reaction was performed using SYBR Green (ThermoFisher). Genomic DNA was isolated from cells by pelleting 1 x 10_5 cells and digesting them in 100 μL DirectPCR Lysis Reagent (Viagen Biotech) with 0.4 μL Proteinase K (Sigma-Aldrich-Aldrich) at 56°C, with shaking for 3 hours. Proteinase

K was heat inactivated at 85°C for 5 minutes. PCR reactions were done with 1 µL genomic DNA in 10 µL GoTaq Green Master Mix (Promega), with each primer pair at a final concentration of 0.5 µM. Primers were purchased from Integrated DNA Technologies and sequences are listed in **Table 2.9** along with the expected amplicon sizes. Two separate reactions were set up: a control reaction with a forward primer ~50bp upstream of the FLAG-tag and a reverse primer ~900bp downstream and a FLAG-specific reaction with a forward primer that binds directly to the FLAG sequence. PCR products were separated by gel electrophoresis (100 V for 25 min) on a 1.2% agarose gel c containing 0.5 µg/mL ethidium bromide to visualise DNA and were imaged using the ChemiDoc XRS+ machine with ImageLab software (Bio-Rad). For PCR protocol refer to **Table 2.10**.

Table 2.9: Primer sequences to detect FLAG insert

Primer	**Sequence (5' to 3')**	**Expected fragement (bp)**
mRIPK1 control	GAGGCACCAAAGGGGCCAC CCTTAGCACTGTTCCCTGTGCCCAA	1002
mRIPK1 FLAG	CAGGCACTTCACCAATGTTGC TGGTTTCATTGGGTAAGGGGAA	458

Table 2.10: PCR protocol

Temperature	Time	
95 °C	5 min	
95 °C	30 sec	30 cycles
58 °C	30 sec	
72 °C	60 sec	
72 °C	7 min	
15 °C	hold	

2.31 Sanger Sequencing

To confirm the presence of the correct FLAG sequence, Sanger sequencing was performed on the amplicon generated via PCR using the FLAG-specific primer pair. Sequencing was outsourced to the Australian Genome Research Facility, Melbourne by submitting the unpurified PCR product.

2.32 Next Generation Sequencing

To determine the frequencies of FLAG-containing sequences, next generation sequencing was performed using the Illumina Miseq platform. In brief, sequences flanking the FLAG sequence were amplified using primers with specific overhang sequences. Each sample was tested in triplicate. DNA was amplified during 18 cycles with an annealing temperature of 55°C and cleaned up using AMPure beads. A second PCR of 24 cycles was performed using primers complimentary to unique overhangs as indicated in Table 2.11. PCR reactions were set up as outlined in Table 2.12.

Table 2.11: Next generation sequencing primer with unique overhangs (lowercase)

NGS Primer	Sequence (5' to 3')
mRIPK1 fwd	gtgacctatgaactcaggagtcTGGGTGATGAGGGAAGGCATAAAG
mRIPK1 rev	ctgagacttgcacatcgcagcCTTTGCTGCAGATTTCTTTCC

Table 2.12: PCR for next generation sequencing

1 µL DNA (100ng/µL)
10 µL GoTaq Green
0.5 µL fwd primer (10 µM)
0.5 µL rev primer (10 µM)
8 µL ddH_2O
Σ 20 µL

2.33 FLAG pulldown and mass spectrometry analysis

To precipitate FLAG-tagged protein, M2 anti-FLAG conjugated sepharose beads (Sigma) were prepared by washing 30 µL beads per sample (50 % slurry) three times with ddH_2O before being resuspended in DISC DISC (1% TritonX-100, 150 mM NaCl, 20 mM Tris, pH 7.5, 10% glycerol, 2 mM EDTA) lysis buffer to make it 50% slurry. 1 x 10_7 cells were digested in 0.5 mL lysis buffer supplemented with Complete Protease Inhibitor Cocktail (Roche), phosphatase inhibitors and 25 nM NEM for 20 minutes on ice. Lysates were clarified by centrifugation at 17000 g and 4 °C for 15 minutes and subsequently applied to anti-FLAG conjugated beads. Incubation occurred at 4 °C for 2 hours while rotating. Beads were finally washed 3 times in 1 mL lysis buffer for 15 minutes while rotating with the last wash being performed in TBS. Proteins were eluted twice in 50 µL 3x FLAG peptide (500 µg/mL) in TBS pH 7.4 for 5 minutes at RT on a shaker. Eluted proteins were digested with trypsin using filter aided sample preparation (FASP) (Wiśniewski, J. R., *et al.*, 2009). In brief: samples were transferred to 8 M urea, 100 mM Tris-HCl pH 7.4 then reduced using 10 mM TCEP for 20 minutes. Cysteine residues were alkylated using 50 mM iodoacetamine in 8 M urea, 100 mM Tris-HCl pH 7.4 and incubated, protected from light for 20 minutes. Samples were then digested using 1 µg trypsin in 50 mM ammonium bicarbonate solution and incubated for 16 hours at 37°C. Peptides were collected into ammonium bicarbonate and acidified using 1%

formic acid before lyophilisation. Samples were reconstituted in 2% acetonitrile and 1% formic acid in Milli-Q water and analysed by nanoflow reverse-phase LC-MS/MS by Jarrod Sandow at the Walter and Eliza Hall Institute.

3 Generating a clinically relevant AML mouse model by expressing EVI1 with MLL/AF9 *in vivo*

3.1 Generation of the MLL-AF9/EVI1 mouse model

To induce acute myeloid leukemia (AML) in mice, we retrovirally transduced fetal liver cells derived from E14 embryos, which at that stage harbor the hematopoietic system, with the oncogenic fusion protein MLL-AF9. Using the expression system generated by Zuber (Zuber *et al.*, 2009), we were able to track the expression of the oncoprotein by measuring the presence of the fluorescent protein mCherry via flow cytometry (**Figures 3.1 & 3.2**). To generate the MLL-AF9/EVI1 mouse model, we co-infected fetal liver cells with an EVI1 construct that we acquired from the lab of Takahiro Nakamaru at the Cancer Institute in Tokyo, who showed that the co-expression of EVI1 together with the fusion-oncoprotein Hoxa9-Meis1 accelerated the onset of AML from 250 to 150 days (Jin *et al.*, 2007). Using this expression construct allowed us to detect EVI1 by measuring the expression of the fluorescent protein GFP via flow cytometry (**Figure 3.1 B**). Additionally, EVI1 was FLAG-tagged allowing the detection of the protein by western blot since an anti-EVI antibody that was purchased did not generate a specific signal (**Figures 3.3 – 3.6**). Although the presence of a FLAG-tag may alter protein function, this construct has been successfully applied in previous studies, indicating that it expresses a functional version of EVI1. Furthermore, the ability of FLAG-EVI1 to induce MDS-like symptoms was tested during *in vivo* experiments were fetal liver cells were transduced with only FLAG-EVI. These experiments will be able to confirm the proteins functionality.

Transduced fetal liver cells were injected into the tail veins of lethally irradiated C57BL/6 mice where they repopulated the bone marrow and, after a latency of 40-60 days, caused the formation of leukemic blasts. When diseased mice exhibited AML-related symptoms such as

hind limb paralysis, they were euthanized and the leukemic cells were harvested from the bone marrow. To determine if EVI1 was expressed in AMLs, GFP expression was determined via flow cytometry, while MLL-AF9 expression was detectable by measuring mCherry levels (**Figure 3.3 – 3.6**). The disease phenotypes were established by analyzing the infiltration of leukemic cells into the spleen, liver and blood as well as the bone marrow which harbors most of the leukemic blasts (**Figure 3.7**). The morphology of leukemic cells was evaluated by staining blood smears and cytospin slides of the bone marrow with May-Gruenwald Giemsa (**Figure 3.8**). In addition, leukemic cells were collected from the bone marrow of femur and tibia and subsequently cultured in the presence of IL-3. Culturing AML cells *in vitro* allowed us to further characterize the immuno-phenotype of these cells. To do that, a number of hematopoietic surface markers were fluorescently stained using antibodies and their expressions was detected using flow cytometry (**Figure 3.10**). Furthermore, we were able to determine the response of AML cells to various anti-leukemic drugs and drug combinations by measuring via uptake of propidium iodide (**Figure 3.11**).

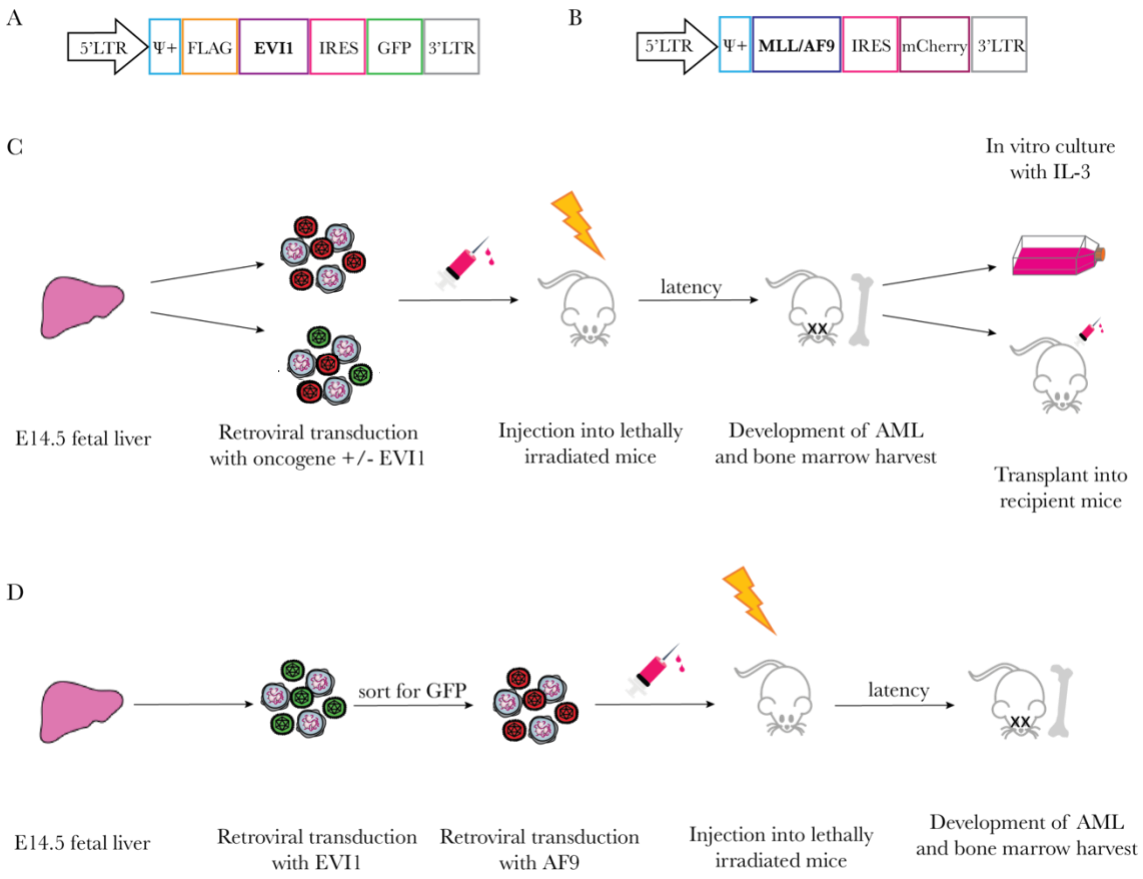

Figure 3.1: Schematic of generating AML mouse models MLL-AF9 and MLL-AF9/EVI1

(A) pMY-FLAG-EVI1-IRES-GFP used to generate EVI1-overexpressing AMLs featured EVI1 with an N-terminal FLAG-tag and IRES-GFP. (B) pMSCV-MLL-AF9-IRES-mCherry used to induce AML featured mCherry as a fluorescent marker. (C) Fetal livers were harvested at E14.5 and retrovirally transduced with either MLL-AF9 alone or in combination with EVI1. Infected cells were injected into lethally irradiated mice which consequently developed AML. Bone marrow of deceased mice was harvested and leukemic cells were cultured in the presence of IL-3. To induce secondary AML, leukemic cells were injected into recipient mice. (D) As an alternative approach, fetal liver cells from E14.5 were first retrovirally transduced with EVI1, sorted for GFP expression and finally infected with the MLL-AF9 construct before being injected into irradiated recipient mice.

In order to generate the MLL-AF9/EVI1 mouse model, fetal liver cells were virally transduced with MLL-AF9 and EVI1 constructs (**Figure 3.1 C**), respectively, and injected into the tail veins of lethally irradiated recipient mice. Per mouse, 5 x 10_5 cells were injected while a portion of the fetal liver cells were kept in culture to determine infection efficiency via flow cytometry

(**Figure 3.2**). For each experiment, three mice were injected with MLL-AF9 infected fetal liver cells while for the combination of MLL-AF9 and EVI1 this number was increased to six after the initial *in vivo* experiment. Furthermore, three mice injected with cells transduced with EVI1 only served as a positive control for the construct, as high EVI1 expression in the hematopoietic system has been demonstrated to induce myelodysplastic syndrome (MDS) or MDS-like symptoms (K. Xu *et al.*, 1999).

3.2 Co-expression of MLL-AF9 and EVI1 was detectable in transduced fetal liver cells *in vitro*

After culturing transduced fetal liver cells in cytokine containing media (SCF, IL-6, TPO and Flt3), an enrichment for mCherry-expressing cells could be observed (**Figure 3.2**). This was expected since the expression of MLL-AF9 transforms cells, conferring a proliferative advantage to those cells. In the first week of culture, GFP (a surrogate for EVI1) expression was only detected in approximately 4% of cells while about 3.5% of those were mCherry/GFP double positives (**Figure 3.2**, bottom panel). While this low number of doubly infected cells may indicate that cells were preferably infected once, it also suggests that EVI expression did not provide a proliferative advantage to MLL-AF9-expressing cells. Cells infected with EVI1 (GFP) only, did not grow in culture, while MLL-AF9 (mCherry) positive cells proliferated. The expansion of a population that expresses very high levels of mCherry, again emphasizes the proliferative advantage MLL-AF9 expression confers to cells. Moreover, after three weeks in culture, only a population of double positive cells that expressed high levels of EVI1 was visible (**Figure 3.2**, bottom panel). This is evident when comparing the FACS results of week 2 where 16% of the cells were positive for both the oncogene and EVI1 while one week later

this population was reduced suggesting that EVI1 did not appear to further increase cell proliferation *in vitro*.

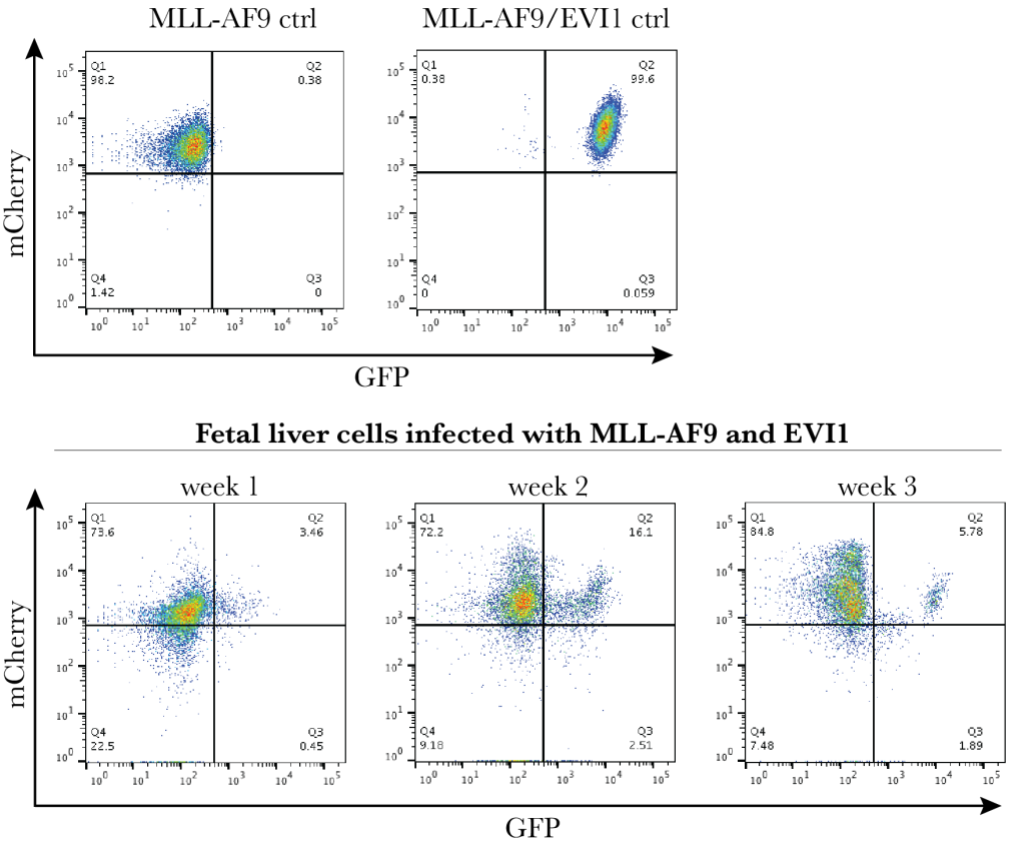

Figure 3.2: FACS of retrovirally transduced HSCs-containing fetal liver cells

Following injection into mice, a proportion of fetal liver cells virally transduced with MLL-AF9 and EVI1 at a ratio of 1:4 were kept in culture in the presence of TPO, SCF, IL-6 and Flt3 to determine infection efficiency via flow cytometry over the course of three weeks. mCherry expression indicated MLL-AF9 levels while GFP reflected EVI1 expression. MLL-AF9 and MLL-AF9/EVI1 leukemic cells derived from mice were used as negative and positive controls, respectively (top panel).

3.3 EVI1-expressing MLL-AF9 AMLs were successfully generated using multiple approaches

As stated previously, in human AML patients, EVI1 expression is a marker for poor prognosis.

We therefore hypothesized, that the co-expression of EVI1 together with the oncogene MLL-

AF9 in mice, may accelerate leukemogenesis leading to a quicker disease onset in mice. Since EVI1 expression should give MLL-AF9-expressing cells an additional proliferative advantage, infecting cells with the two constructs at a 1:1 ratio should be sufficient to generate AMLs that are positive for MLL-AF9 and EVI1. During the initial *in vivo* experiment, fetal liver cells were therefore infected with equal volumes of virus expressing MLL-AF9 or EVI1. Out of the three mice that were injected with cells virally transduced with both constructs, leukemic cells from two mice expressed only mCherry while leukemic cells from the third mouse were positive for both mCherry and GFP (**Figure 3.3 A**). Despite the expression of GFP, EVI1 expression could not be detected neither by through Western blotting (**Figure 3.3 B**) nor by PCR (data not shown). Cells expressing the oncogene MLL-AF9 already have a selection advantage. To increase the chances of generating EVI1 positive leukemias, fetal liver cells would need to be infected with larger amounts of the EVI1-encoding virus compared to virus encoding the oncogene.

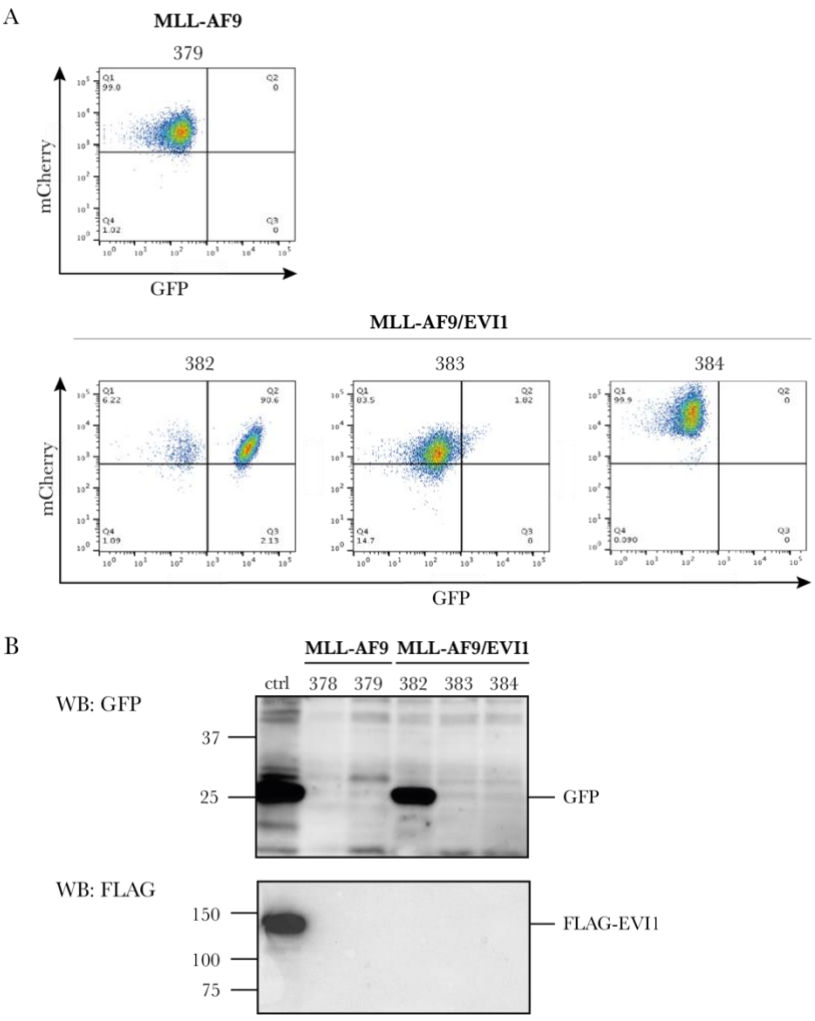

Figure 3.3: EVI1 expression could not be detected in GFP-positive MLL-AF9 AML

(A) Leukemic cells of deceased mice were tested for EVI1 expression by measuring GFP expression via flow cytometry. mCherry expression was measured to determine MLL-AF9 levels. Mice 382-384 were injected with cells infected with MLL-AF9 and EVI1 virus (bottom). Leukemic cells derived from MLL-AF9 AML (379) were used as a negative control. (B) EVI1 expression was also determined via Western blotting by probing for GFP (top) and FLAG (bottom).

For a second *in vivo* experiment, prior transplantation cells were infected with either two or four times the volume of EVI1-expressing virus. All mice (6/6) developed AML, however amongst the mice that received cells transduced with both constructs, only 3/6 mice were double positive for mCherry and GFP (1 received 2 times EV1 virus and 2 received 4 times EV1 virus) (**Table 3.1**, **Figure 3.4 A**). The presence of FLAG-tagged EVI1 could be detected for all three leukemias on a protein level and these levels appeared to correlate with GFP expression levels (**Figure 3.4 B**). It should be noted, that the percentage of double positive cells varied amongst the different mice. Both mouse 618 and 615 had relatively high percentages of double positive cells (81% and 74% respectively) while in mouse 617, only 5% of leukemic cells were double positive.

Given the positive correlation between amount of viral supernatant applied and double positive leukemic cells generated, for a third *in vivo* experiment I again chose the virus ratio of 4:1 (EVI1 to MLL-AF9) and further increased it by infecting fetal liver cells with six times the amount of EVI- encoding virus. Again, three mice were injected with either of the cohorts of infected fetal liver cells while three mice received fetal livers transduced with MLL-AF9 only. Following this approach, all injected mice developed AML, while three of the leukemias expressed GFP to at least some degree as determined via FACS (**Figure 3.5 A**). However, only mouse 907 (virus ratio 6:1) developed a leukemia where the majority of leukemic cells expressed GFP (67%), while for mice 902 (virus ratio 4:1) and 906 (virus ratio 6:1) double positive cells only marginally contributed to the total population with 1% and 10%, respectively.

Since increasing the virus ratio did not lead to the generation of uniform AMLs consisting of 100% double positive leukemic cells, I applied an alternative approach where I transduced

fetal liver cells with the EVI1 construct and subsequently sorted for GFP expression using flow cytometry. Following the sort, cells were infected with MLL-AF9 before being injected into irradiated recipient mice. It should be noted that for this approach an appropriate control i.e. non-infected sorted fetal liver cells did not exist and therefore the comparisons regarding the latency of the disease onset should be interpreted with caution. When infected fetal liver cells were sorted for GFP expression prior to injection, all three mice that developed a disease harbored what appeared to be leukemic cells in their bone marrow that expressed GFP. Notably, for all three mice, the harvested cells were 100% positive for GFP while mCherry levels were barely detectable via FACS (**Figure 3.5 B**, data only shown for mouse 746). It is even more noteworthy that only leukemic cells from mouse 746 could be cultured in IL-3 containing while cells from mice 744 and 748 did not grow under those conditions.

When determining the expression of EVI1 for GFP-positive leukemias generated during approach three (4x and 6x EVI1 virus) and four (sort) on a protein level, the presence of EVI1 was confirmed for all but one of the leukemias (**Figure 3.5 B**). Only cells originating from mouse 902 (4x EVI1 virus) did not express visible levels of EVI1 as determined by Western blotting. However, with the ratio of GFP-expressing cells being only 1%, this result was not unexpected. For all other leukemias, the detected EVI1 protein levels corresponded to the GFP intensities determined via flow cytometry.

In summary, by performing four independent *in vivo* experiments in a total of 21 mice applying varying approaches, I was able to generate six MLL-AF9-induced leukemias where

EVI1 expression was detectable on a protein level and whose cells could be cultured *in vitro* (Table 3.1)

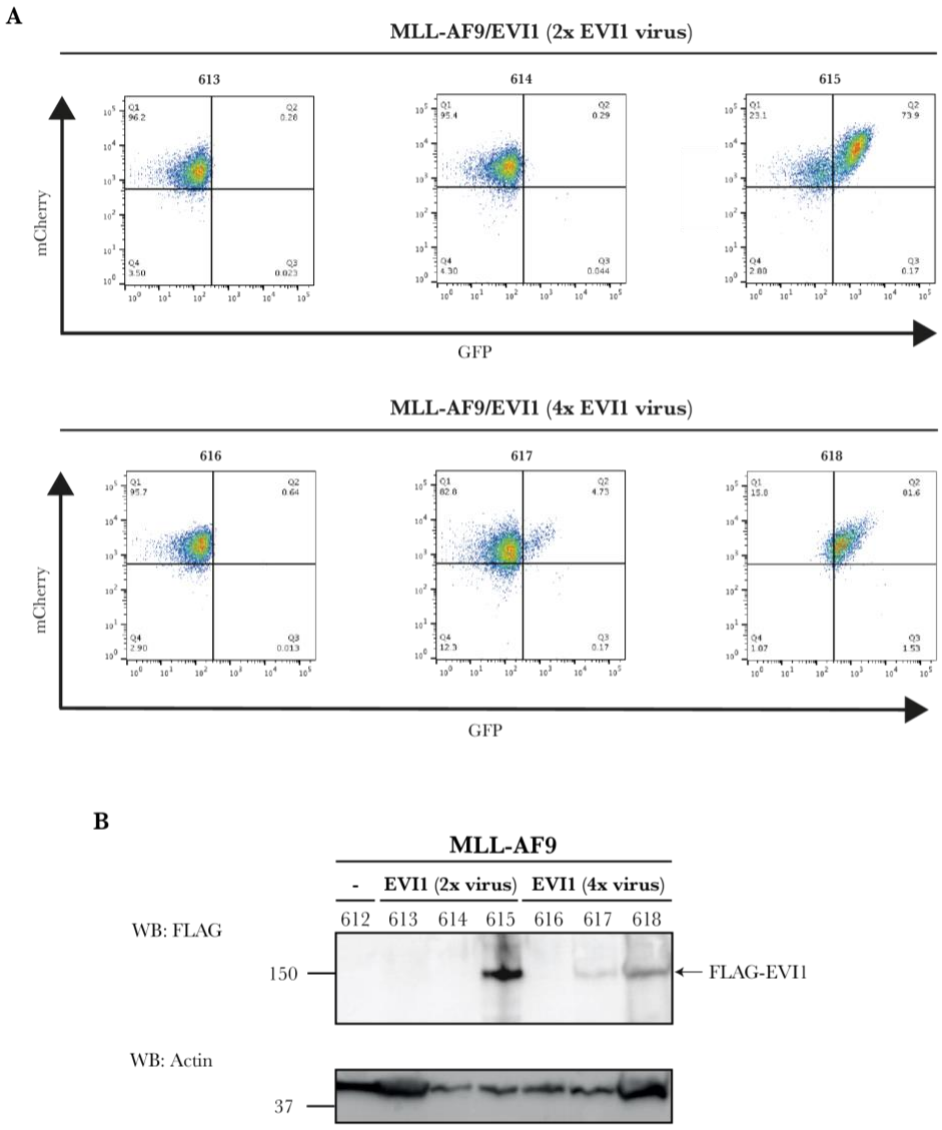

Figure 3.4: EVI1-expressing MLL-AF9 AMLs were successfully generated when using virus ratios of 2:1 or 4:1

(A) Leukemic cells of deceased mice were tested for EVI1 expression by measuring GFP expression via flow cytometry. mCherry expression was measured to determine MLL-AF9 levels. All mice were injected with cells infected with MLL-AF9 and either twice (613-615, top) or four times (616-618, bottom) the amount of EVI1 virus. (B) EVI1 expression was also determined via Western blotting by probing for FLAG. Leukemic cells derived from MLL-AF9 AML (612) were used as a negative control.

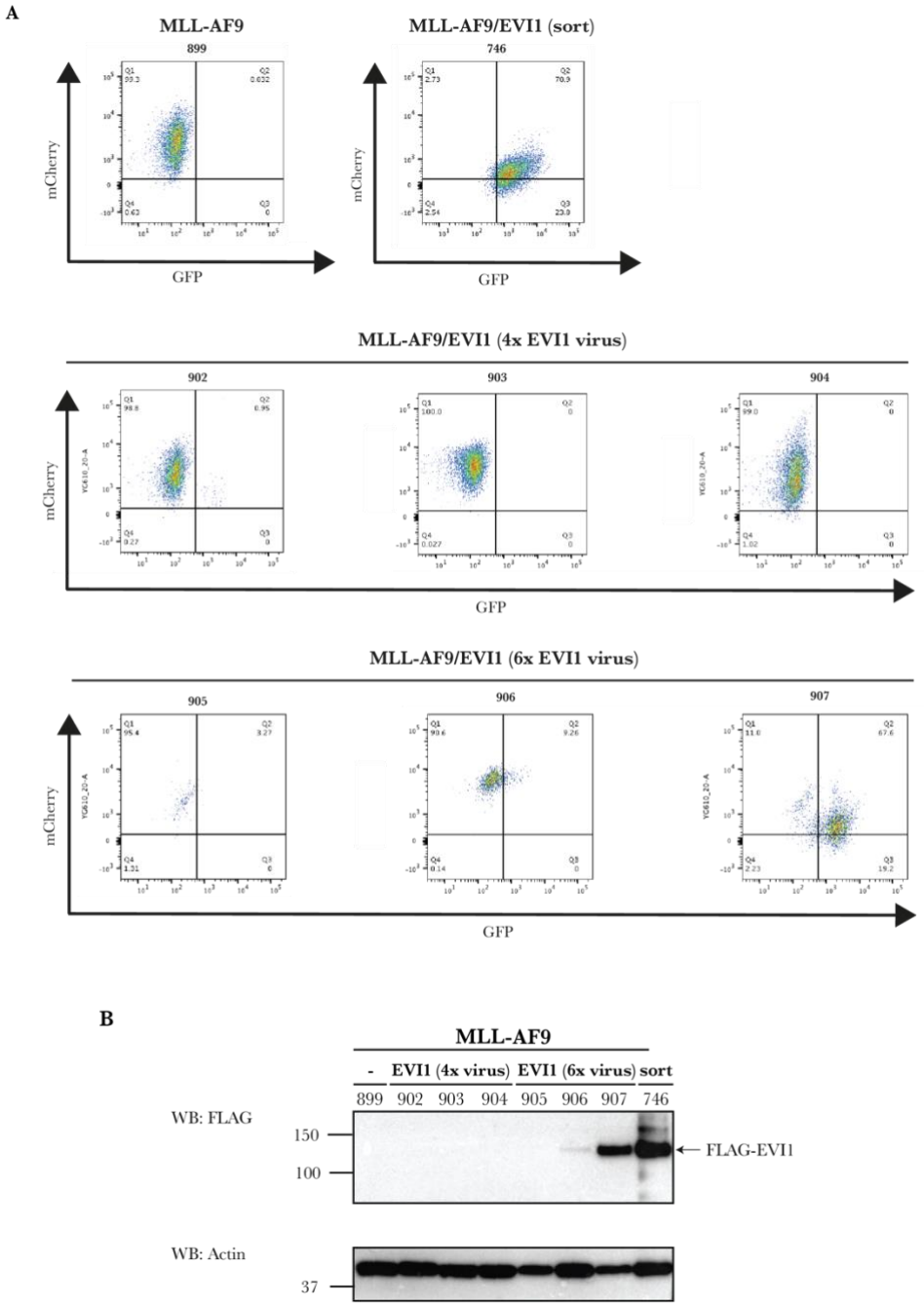

Figure 3.5: EVI1-expressing MLL-AF9 AMLs were successfully generated when using virus ratios of 4:1 or 6:1 and upon prior sorting for GFP

(A) Flow cytometry analysis to test for EVI1 expression in leukemic cells. Mice were injected with fetal liver cells that were simultaneously infected with MLL-AF9 and either four times (902-904) or six times (905-907) the amount of EVI virus. mCherry expression was measured to determine MLL-AF9 levels. (B) EVI1 expression was also determined in leukemic cells via Western blotting and probing for FLAG. Leukemic cells from MLL-AF9 AML (899) served as a negative control.

Table 3.1: Different approaches for the generation of MLL-AF9/EVI1 AMLs

	Virus ratio	*Number mice*	*Number EVI1^{pos} mice*
Approach	**MLL-AF9:EVI1**	**n (total)**	**n (*EVI1^{pos}*)**
Co-infection	1:1	6	0
Co-infection	1:2	3	1
Co-infection	1:4*	6	2
Co-infection	1:6	3	1
Sort	n/a	6	3

* approach 2 and 3 combined

3.4 EVI1-expressing AMLs are fully transformed and can be retransplanted to induce secondary AML

One characteristic of leukemic cells is that their injection into non-irradiated mice causes the development of the disease in the recipients which we refer to as secondary AML. To determine if EVI1-expressing AML can be retransplanted and if the induced secondary AML also expresses EVI1, MLL-AF9/EVI1$_{pos}$ cells 618 (2$_{nd}$ approach, virus ratio 4:1) were injected into three C57BL/6 mice. All recipient mice developed AML within 29 days while GFP expression levels reflected those of the injected, primary AML (**Figures 3.6 A** and **3.7 B**). Furthermore, EVI1 expression was also detectable on a protein level via Western blotting and probing for FLAG (**Figure 3.6 B**). Notably, EVI1 levels for secondary AML 631 were significantly higher than those detected for the primary AML 618 and the secondary AML 632, even when accounting for uneven loading. It is worth mentioning that the levels of EVI1 and GFP levels did not coincide. This might be due to the fact that the lysate for mouse 631 was produced on the day of harvest, while lysates 618 and 632 were generated after several days of *in vitro* culture. The flow cytometry data however, was recorded after all cells had been in culture for various times. Upon harvest of leukemic cells from the bone marrow, EVI1 positive cells generally exhibited higher GFP – and therefore higher EVI1 – expression levels,

which dropped after cells were exposed to *in vitro* culturing conditions. One can only speculate about the reasons behind the sudden reduction in EVI1 expression but it is possible that other cytokines than IL-3 would be required to maintain expression levels that were achieved under physiological conditions. Another possible mechanism is that cells may actively repress EVI1 expression which would also offer an explanation for the difficulties I faced when aiming to generate EVI1-expressing leukemias. Since primary MLL-AF9/EVI1 AML was able to induce secondary AML upon being retransplanted while EVI1 expression was maintained, I concluded that the generated MLL-AF9/EVI1 double positive cells were in fact fully transformed leukemic cells.

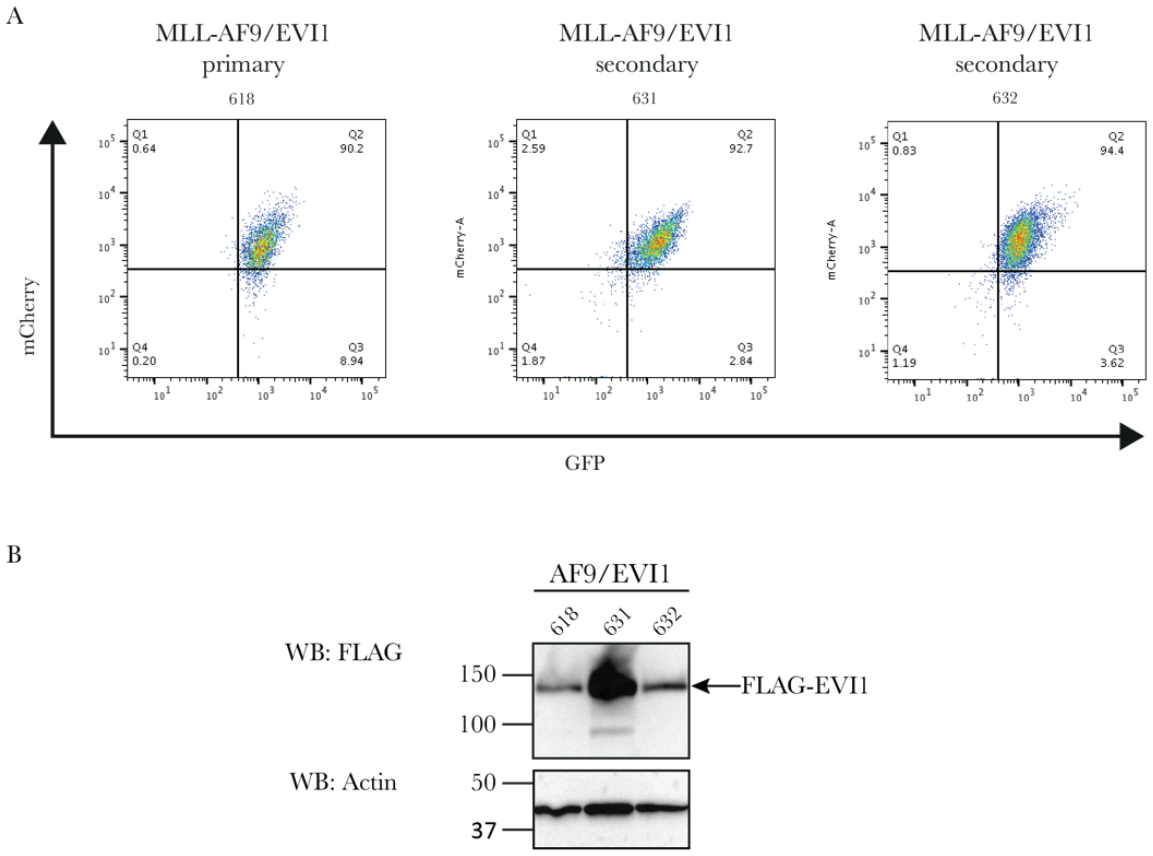

Figure 3.6: EVI1-overexpressing AMLs can be retransplanted and EVI1 expression is sustained in secondary AMLs

MLL-AF9/EVI1 AML leukemic cells (618) were injected into three recipient mice. After developing AML, leukemic cells of mice 631 and 632 were tested for expression of GFP and mCherry using flow cytometry (A) and FLAG-EVI1 expression via Western blot (B). Probing for actin served as a loading control.

3.5 EVI1 overexpression in MLL-AF9 AML does not accelerate disease onset *in vivo*

When injecting fetal liver cells transduced with an oncogene into irradiated mice, the hematopoietic stem and progenitor cells present in that cell population will repopulate the bone marrow of the recipient mouse and after a latency that is characteristic for the oncogene, the development of AML will occur. This latency can be reflective of the severity of the disease

and we therefore hypothesized that if EVI1 expression induces a more severe disease phenotype, the AML onset might be faster in mice injected with fetal liver cells hat express both MLL-AF9 and EVI1. To interpret the data, I adjusted the survival curves for EVI1 expression by separating AMLs where EVI1 infection occurred but was not detected in leukemic cells (MLL-AF9/EVI1$_{neg}$) from AMLs where EVI1 was visibly expressed (MLL-AF9/EVI1$_{pos}$). When summarizing the survival data of all but the sort experiment, EVI1 did not appear to accelerate AML onset when compared to the survival of mice injected with cells that were only infected with MLL-AF9 (**Figure 3.7 A**). For MLL-AF9 AMLs the disease onset ranged from 42 to 81 days while mice injected with cells infected with both MLL-AF9 and EVI1 succumbed to the disease after 43 to 83 days and when adjusting for detected EVI1 expression, AML was developed between 52- and 90-days post injection. This observed latency is in accordance with what is commonly observed in MLL-AF9-induced leukemias (Brumatti *et al.*, 2016). Importantly, consistent with previous reports, when fetal liver cells were infected with EVI1 only, their injection into irradiated recipient mice caused MDS or MDS-like symptoms such as anemia and thrombocytopenia (Jin *et al.*, 2007). All mice injected with EVI-expressing fetal liver cells had to be euthanized after 209 to 251 days post infection due to severe anemia and splenomegaly. This indicated that the construct expressed an EVI1 isoform that was able to conduct a pathophysiological function *in vivo*.

When cells were sorted for GFP expression prior to injection, disease onset was greatly delayed with latencies ranging from 119 to 204 days (**Figure 3.7 B**). Given the lack of an appropriate control group, it can only be guessed that this delay was caused by the sorting process itself rather than the expression of EVI1. An alternative explanation could be that the secondary infection rates with MLL-AF9 were low, which lead to low expression levels of the

oncogene ultimately resulting in increased latencies. Evidence for this can be found in the flow cytometry data, where mCherry levels for AML 746 were low (Figure 3.5 A). When MLL-AF9 and MLL-AF9/EVI1 AML cells (derived from 4x EVI1 virus) were injected into recipient mice for the generation of secondary AML, the expression of EVI1 again did not accelerate disease onset (**Figure 3.7 C**).

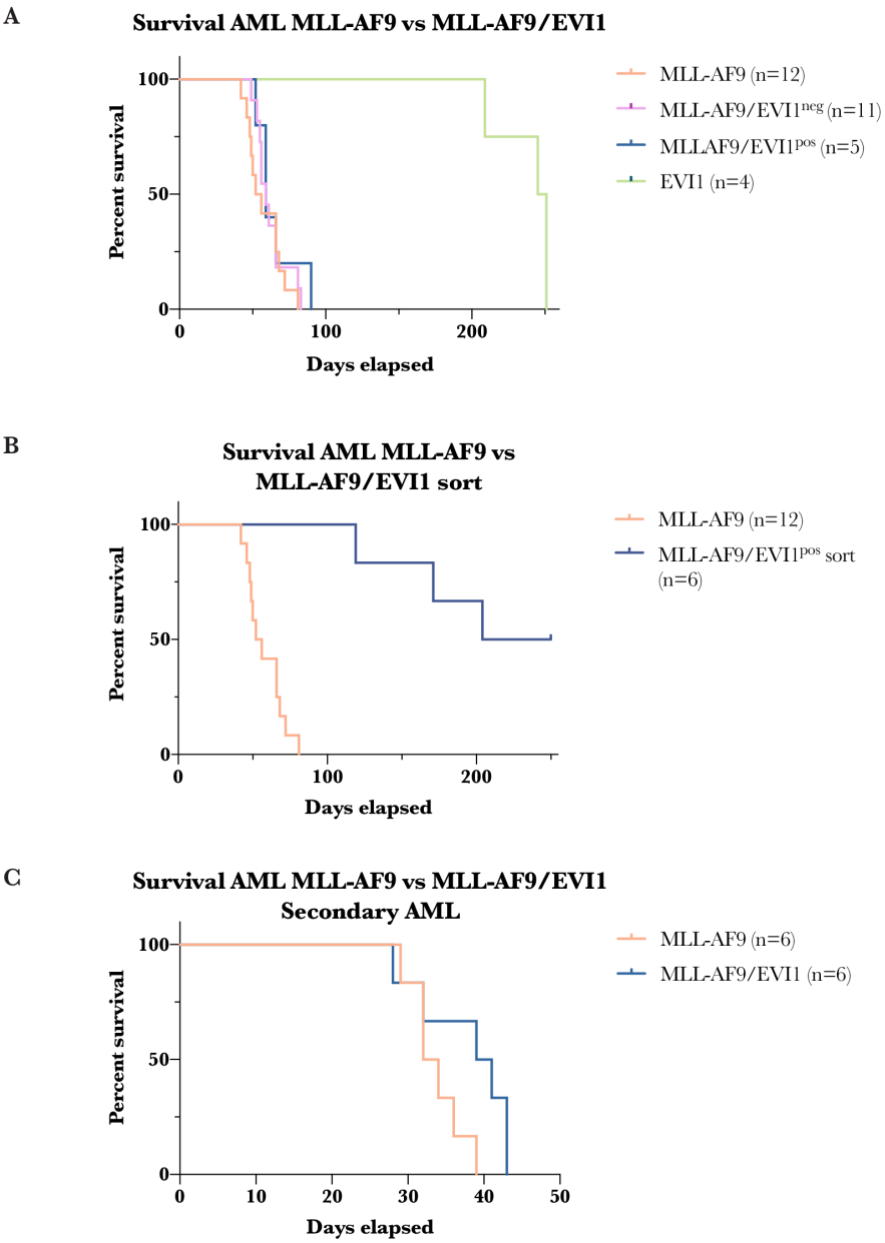

Figure 3.7: EVI1 overexpression in MLL-AF9 AML does not accelerate disease onset in vivo.

(A) Kaplan-Meier survival curve. Irradiated mice were injected with fetal liver cells that were virally transduced with either MLL-AF9 (orange), MLL-AF9 and EVI1 (pink and blue) or EVI1 alone (green). Mice injected with cells that were infected with MLL-AF9 and EVI1 are divided into two groups: mice that developed AML and whose leukemic cells did not express EVI1 (MLL-AF9/EVI1$_{neg}$, pink) and mice whose leukemic cells expressed EVI1 (MLL-AF9/EVI1$_{pos}$, blue). (B) Kaplan-Meier survival curve for MLL-AF9 (orange) and MLL-AF9/EVI1 sort (blue). After infection with EVI1, fetal liver cells were sorted for GFP before being infected with MLL-AF9 and injected into mice. (C) Kaplan-Meier survival curve for secondary AMLs. To generate secondary AMLs, MLL-AF9 (orange) or MLL-AF9/EVI1 (blue) leukemic cells were transplanted into recipient mice.

3.6 EVI1 expression in MLL-AF9 AML does not aggravate pathological features

To further investigate the impact of EV1 expression in the disease severity of MLL-AF9/EVI1 leukemia, I examined the weight of liver and spleen, organs typically infiltrated by leukemic blasts, as well as white blood cell and platelet counts. With progression of the disease, leukemic blasts originating from the bone marrow accumulate in the blood leading to abnormally high white blood cell (WBC) numbers detected in the peripheral blood. The rapid production of abnormal white blood cells in the bone marrow can also lead to reduced platelet numbers due to their impaired production. All mice that developed AML showed signs of splenomegaly and most mice also suffered from hepatomegaly (**Figure 3.8 A, B**). When comparing weights of liver and spleen between the three groups MLL-AF9, MLL-AF9/EVI1$_{neg}$ and MLL-AF9/EVI1$_{pos}$, no significant differences were observed. Mice exhibiting MDS-like symptoms showed no signs of hepatic infiltration while splenomegaly was experienced by three of four mice which is consistent with existing literature (Putz *et al.*, 2006). Most mice that succumbed to AML had elevated white blood cell levels measured in the blood with a healthy level being around 9 x 10_9 cells/µL (**Figure 3.8 C**). Again, no significant differences between the individual groups were observed. It should be noted, that the great variations between WBC levels may be explained with the heterogenicity of AML progression. If leukemic blasts accumulate in the bone marrow rapidly causing the mouse to appear hunched and consequently becomes identified as sick, it might get euthanized before blasts can infiltrate the blood to a great extent. Lastly, most mice with AML showed signs of thrombocytopenia of varying degrees (**Figure 3.8 D**). Mice who developed leukemias positive for EVI1 expression had significantly lower platelet counts than their counterparts. Within the MLL-AF9 cohort the spread between platelet numbers was the greatest ranging from 81 – 777 x 10_9 cells/L while the mean for a healthy female C57BL/6 is 1350 x 10_9 cells/L. Notably, higher platelet numbers in those mice

coincided with lower WBC counts which again could be due to the fact that leukemic blasts accumulated in the bone marrow so quickly, that mice were culled before the blood was fully infiltrated. Given the role of EVI1 as an important transcription factor in hematopoiesis, it is possible that EVI1 expression even in non-transformed, MLL-AF9 negative cells caused an impairment in differentiation leading to thrombocytopenia. In support of that, mice that developed MDS-like symptoms had consistently low platelet counts ranging from 80 – 95 x 10_9 cells/L. It is therefore likely that low platelet numbers observed for EVI-positive AMLs were not indicative of disease severity.

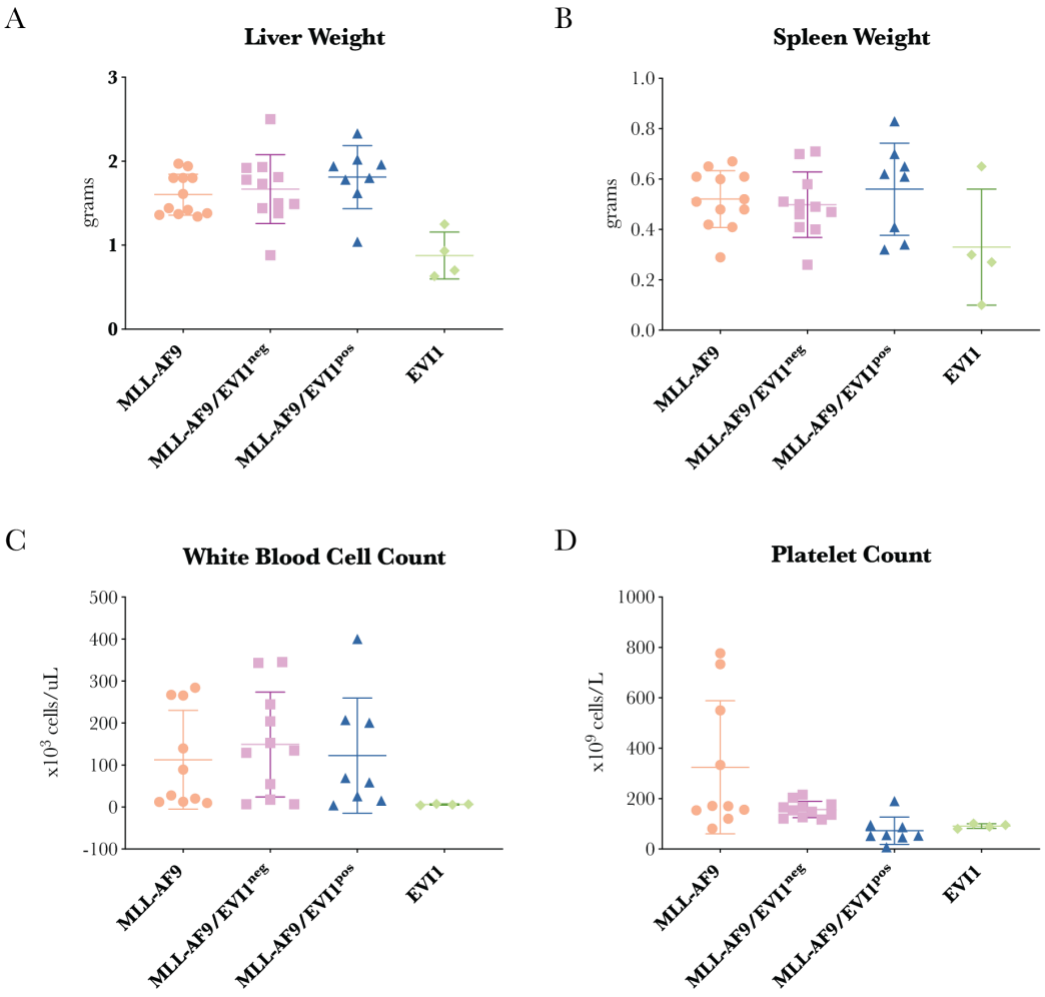

Figure 3.8: EVI1 overexpression in MLL-AF9 AML may lead to reduced platelet numbers in the blood but does not affect other pathological disease features

(A), (B) Liver and spleen weights of mice that developed AML (blue, pink and purple) or MDS (green). AML was induced by injecting mice with fetal liver cells infected with either MLL-AF9 (blue) or MLL-AF9 and EVI1 (pink and purple). Mice were further divided into EVI1 expression being detectable (MLL-AF9/$_{EVI1pos}$, purple) or not detectable (MLL-AF9/EVI$_{neg}$, pink). (C), (D) White blood cell and platelet counts. Heart bleeds were performed on euthanized mice that developed AML (blue, pink and purple) or MDS (green). Blood samples were analysed using an Advia hematology system. Individual values, mean and SEM are shown of two independent experiments. ns = $p>0.05$ as determined by student's t-test (liver $p_1 = 0.15$ (MLL-AF9 vs. MLL-AF9/EVI1$_{pos}$) and $p_2 = 0.45$ (MLL-AF9/EVI1$_{neg}$ vs. MLL-AF9/EVI1$_{pos}$), spleen $p_1 = 0.56$ (MLL-AF9 vs. MLL-AF9/EVI1$_{pos}$) and $p_2 = 0.41$ (MLL-AF9/EVI1$_{neg}$ vs. MLL-AF9/EVI1$_{pos}$), PLT $p_1 = 0.018$ (MLL-AF9 vs. MLL-AF9/EVI1$_{pos}$) and $p_2 = 0.0006$ (MLL-AF9/EVI1$_{neg}$ vs. MLL-AF9/EVI1$_{pos}$), WBC $p_1 = 0.87$ (MLL-AF9 vs. MLL-AF9/EVI1$_{pos}$) and $p_2 = 0.67$ (MLL-AF9/EVI1$_{neg}$ vs. MLL-AF9/EVI1$_{pos}$).

3.7 Morphology of AML blasts is not affected by EVI1 expression

After concluding that EVI1 expression did not induce changes in the pathophysiological features examined, I compared histopathological characteristics by preparing cytological slides of the bone marrow of deceased mice. To do so, I generated cytospin preparations which were subsequently stained using May-Gruenwald-Giemsa staining and imaged at 1000x magnification (**Figure 3.9**). Bone marrow cytospin preparations from six mice per cohort (MLL-AF9 and MLL-AF9/EVI1$_{pos}$) were imaged. At the time of death, the majority of cells present in the bone marrow of mice suffering from AML were leukemic blasts which are easily distinguished from healthy white blood cells by their larger size. For both the MLL-AF9 and MLL-AF9/EVI1-induced AMLs, leukemic blasts exhibited monocytic differentiation which is characterised by nuclear folding, a moderate nuclear-cytoplasmic ratio and light-blue cytoplasm. The observed monocytic morphology indicates that the generated AMLs could be classified as the FAB – M5 subtype which is typically induced by the MLL-AF9 oncogene (Pession *et al.*, 2003). However, in order to confidently diagnose the subtype of AML, a large number of blasts (>100) would have to be scored for each mouse. For the interest of this project however, it was sufficient to compare the morphologies of the leukemic cells and by doing that, I concluded that EVI1 expression did not induce any changes to the morphologies of leukemic cells.

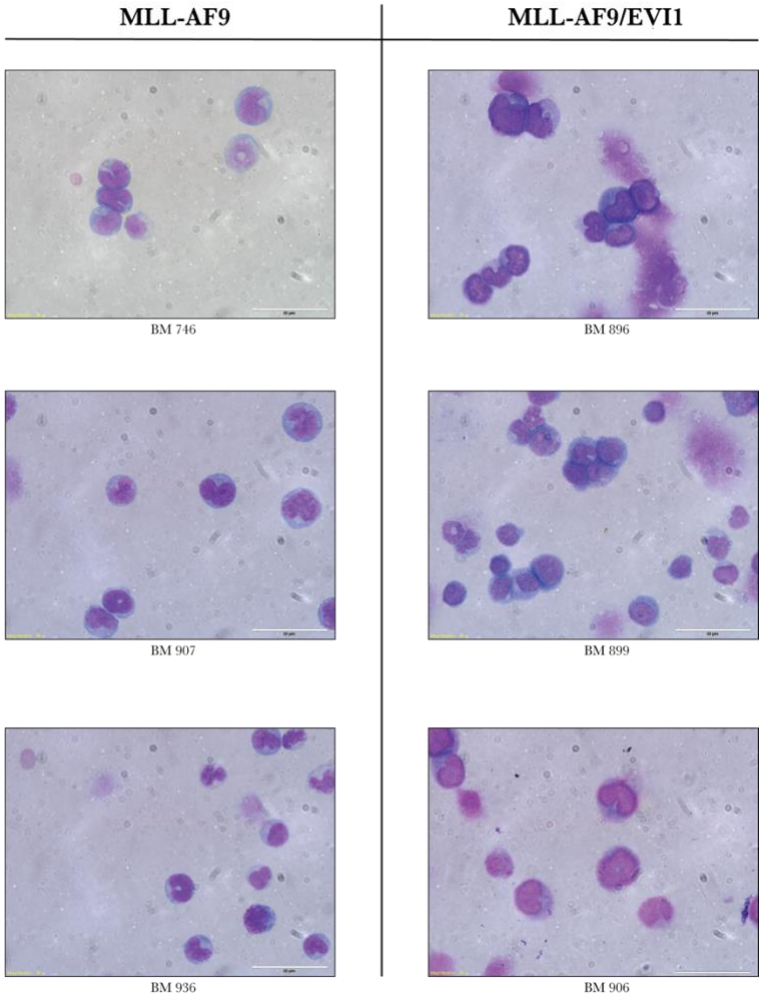

Figure 3.9: EVI1 expression did not induce changes in histopathological features of AML blasts

May-Gruenwald-Giemsa staining of bone marrow from MLL-AF9 (left panel) and MLL-AF9/EVI1 (right panel) AMLs. Bone marrow of euthanized mice that developed AML was harvested and resuspended in FCS-containing media. To generate cytological slides, a total of 40,000 cells were spun onto a microscope slide. Bone marrow-derived cells were visualized with May-Gruenwald-Giemsa staining and imaged at a 1000x magnification using oil immersion. Representative images of three mice are shown.

3.8 EVI expression negatively affects proliferation rates of leukemic cells *in vitro*

When culturing the leukemic cells, I noted that EVI1-expressing cells had lower proliferation rates than their EVI negative counterparts. I therefore performed competitive growth assays by seeding equivalent cell numbers of MLL-AF9 and MLL-AF9/EVI1 AML cells into the same well of a 12-well plate (50% MLL-AF9, 50% MLL-AF9/EVI1$_{pos}$). Their respective growth rates were monitored by measuring the proportion of GFP positive cells via flow cytometry on days zero and two (**Figure 3.10**). MLL-AF9/EVI1$_{pos}$ leukemic cells from three mice were subjected to a competitive assay (746, 907 and 936) with all lines demonstrating a competitive disadvantage compared to the MLL/AF9-EVI$_{neg}$ cells. MLL-AF9/EVI1$_{pos}$ AML cells from mouse 907 (3$_{rd}$ approach, virus ratio 6:1), grew the slowest and after two days in culture, GFP-expressing cells only made up 5% of the total population. It should be noted that at day zero, the GFP populations for the three tested EVI positive leukemias were lower than 50% although equivalent cell numbers were seeded. This result can be explained by the fact that none of the MLL-AF9/EVI1 leukemias were uniform, 100% GFP positive populations.

Figure 3.10: Competitive growth assays revealed that EVI expression reduced the proliferation rate of MLL-AF9 leukemic cells in vitro

MLL-AF9/EVI1 AML cells from mice 746 (top, blue), 907 (middle, pink) and 936 (bottom, green) were each co-cultured with MLL-AF9 cells 896 (purple). Cell compositions of the co-cultures were determined by measuring the percentage of GFP positive cells via flow cytometry on day zero (left) and day two (right) of culture.

3.9 EVI-expressing leukemias demonstrate an unaltered immunophenotype

In the literature, high EVI1 expression in AML patients has often been associated with a less mature disease phenotype since EVI1 expression levels are highest in HSCs (Kataoka *et al.*, 2011; Stavropoulou *et al.*, 2016). Although I was not able to detect obvious differences in histopathological features, it is possible that EVI1 expression induced distinct immunophenotypes. In detail that would mean that EVI1 might affect the differentiation stage of the blasts that make up the majority of leukemic cells. MLL-AF9 has been described to be able to transform both late hematopoietic stem cells (HSCs) and granulocyte/macrophage progenitors (GMPs) (Stavropoulou *et al.*, 2016). Depending on the cell type that gives rise to the leukemia, the severity of the disease can vary considerably (Stavropoulou *et al.*, 2016). Upon transformation, a late HSC for example induces a more aggressive leukemia than a transformed GMP (Basilico *et al.*, 2017). A caveat of our approach of infecting fetal liver cells and relying on hematopoietic stem and/or progenitor cells being infected is that we have no influence on what type of cell is ultimately transformed. Moreover, when presented with the leukemic blasts, we have no means to trace back to the cell type of the leukemia initiating cell (LISC). However, given that the oncogene MLL-AF9 consistently generates AMLs of comparable latency and severity, this caveat is generally neglected. When determining if the expression of EVI1 induces any changes to the immunophenotype due to affecting what cell type is preferentially transformed or by influencing the transformation process itself, analysing the surface marker signature of the leukemic blasts is a valid tool. Cell surface markers that AML cells are commonly tested for include cKit (CD117), Mac-1 (CD11b), Gr-1 and F4/80 (Somervaille *et al.*, 2006). Two MLL-AF9 AMLs and three MLL-AF9/EVI1 AMLs were subjected to surface marker screening using fluorescently labelled antibodies and flow cytometry (**Figure 3.11**). When comparing the immunophenotypes of the two groups no

significant differences were identified. All AMLs expressed high levels of Mac-1, while Gr-1 expression levels ranged from 27% (735, MLL-AF9) to 55% (907, MLL-AF9/EVI1) (**Figure 3.11 A**). This variation however could be observed within each of the groups. The same can be said about F4/80 levels whose expression rates fluctuated between 30% (907, MLL-AF9/EVI1) and 81% (896, MLL-AF9) (**Figure 3.11 B**). However, both high and low F4/80 expression were observed within the two groups. Lastly, cKit$^-$ cells were present in all AMLs while 48% was the largest (907, MLL-AF9/EVI1) and 12% the smallest (735, MLL-AF9) population of cKit$^-$ cells measured within each AML (**Figure 3.11 C**). Again, no significant differences between EVI1 positive and negative AMLs were detectable. This data strongly suggests that all AMLs have a monocytic immunophenotype which is consistent with the results obtained via histopathological analysis. AML 907 (MLL-AF9/EVI1) appeared to possess the least mature immunophenotype exhibiting both the largest population of cKit$^-$ cells and the lowest expression of F4/80. Overall, EVI1 expression did not appear to impact the immunophenotype of leukemic cells.

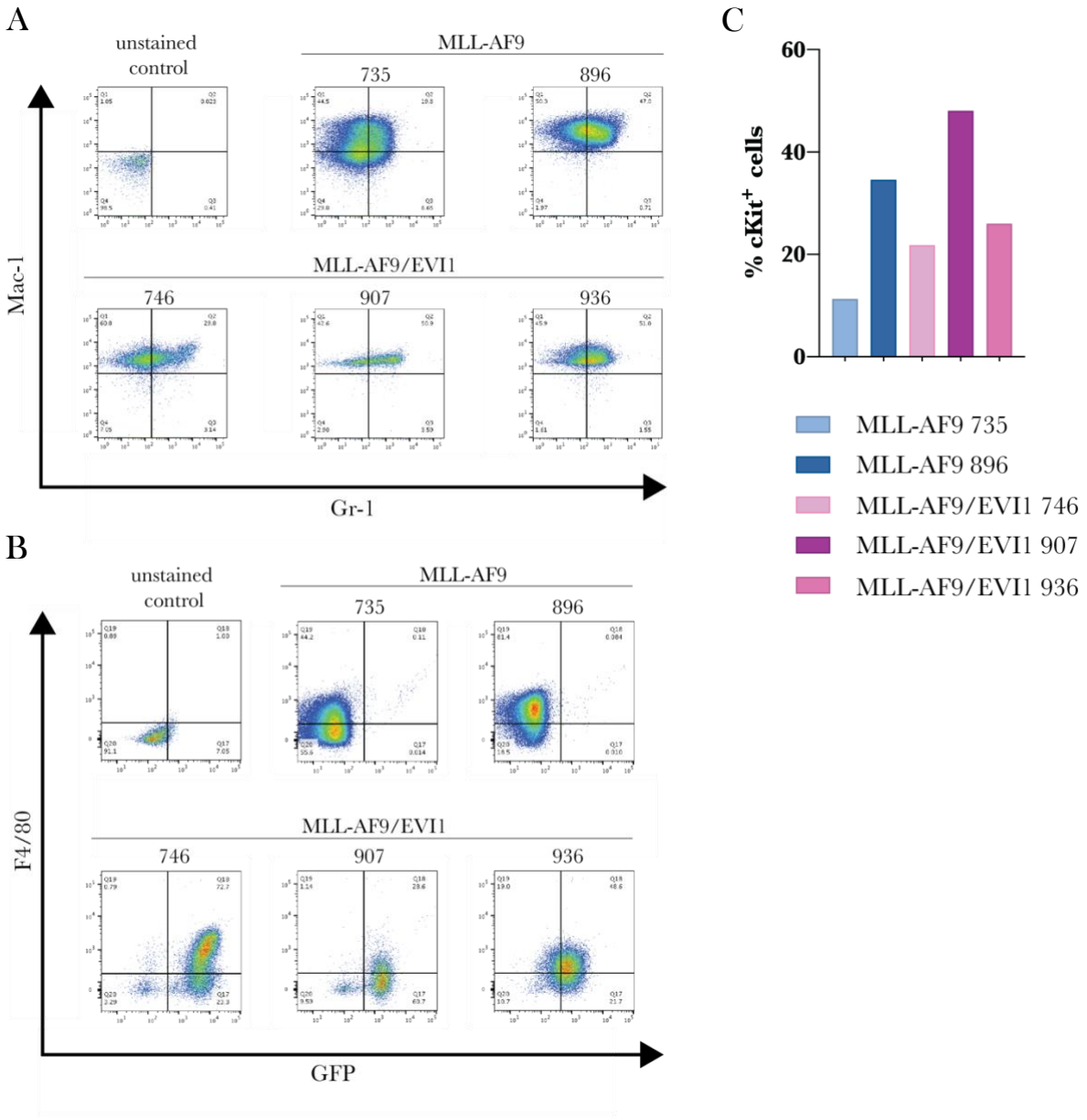

Figure 3.11: EVI1pos MLL-AF9-driven AMLs are immunophenotypically similar to EVI1neg MLL-AF9-driven AMLs

(A), (B) Mice bearing EVI_{pos} or EVI_{neg} MLL-AF9 leukemias were euthanized and bone marrow was harvested and single cell suspensions prepared for analysis. FACS plots of Mac-1 vs. Gr-1 (A) and F4/80 vs. GFP (B) expression on AML cells of MLL-AF9 (735 and 896, top) and MLL-AF9/EVI1 (746, 907 and 936, bottom) leukemias isolated from the bone marrows are shown. An unstained control is shown on the top left. C) Percentage of cKit expressing cells in AMLs driven by MLL-AF9/$EVI1_{neg}$ (735 and 896) or MLL-AF9/$EVI1_{pos}$ (746, 907 and 936).

3.10 Response of EVI1-expressing AMLs to anti-cancer agent

High EVI1 expression is a poor prognostic marker in patients suffering from AML and correlates with resistance to chemotherapy treatment. To determine if EVI1 expression resulted in resistance to chemotherapy *in vitro*, I treated MLL-AF9 and MLL-AF9/EVI1 cells with cell death inducing drugs and drug combinations. Those treatments included the Smac mimetic Birinapant (IAP antagonist), the combination of Birinapant with LY2228820 (p38 inhibitor) which our lab identified as an efficient combination treatment for AML in *vivo* and *in vitro*, and AraC (chemotherapeutic agent). To evaluate dosage dependent treatment responses, Birinapant and AraC concentrations were titrated. To determine cell death rates, the cells' uptake of propidium iodide (PI) was measured via flow cytometry (**Figure 3.12**). Given the consistent treatment responses, I combined PI uptake values for the two tested MLL-AF9 AMLs (897/899). As previously shown (Brumatti et al., 2016; N. Lalaoui *et al.*, 2016), increasing concentrations of Birinapant successfully induced cell death in MLL-AF9 AMLs with the highest observed cell death rate being 80% when treated with 1000 nM of the drug for 24h. Upon addition of the p38 inhibitor LY, this extent of cell death was already achieved at Birinapant's lowest concentration (125 nM) and any increase in Birinapant lead to the killing of close to 100% of cells. The chemotherapeutic agent AraC was also a potent cell death inducer in MLL-AF9 AMLs and a dosage dependent response was also observable.

Interestingly, the three MLL-AF9/EVI1$_{pos}$ AMLs did not respond equally to all treatments which was indicated by large error bars in the cell death bar graph (**Figure 3.12 A**). I therefore separated the cell death rates of the three MLL-AF9/EVI1$_{pos}$ to evaluate the individual treatment responses (**Figure 3.12 B**). MLL-AF9/EVI1$_{pos}$ 936 was already highly sensitive to Birinapant alone after 24h and the addition of LY (p38i) was sufficient to induce complete

killing even at the lowest concentration of Birinapant. When exposed to AraC, MLL-AF9/EVI1$_{pos}$ 936 appeared to be just as sensitive as its EVI1 negative counterparts with cell death rates reaching almost 90% on average for 1000 nM AraC. MLL-AF9/EVI1$_{pos}$ 746 on the other hand was slightly less sensitive to Birinapant alone when comparing its cell death rates to the ones observed for the MLL-AF9 AMLs. When combined with LY (p38i), Birinapant was still efficient at killing leukemic cells derived from MLL-AF9/EVI1$_{pos}$ 746 even at low concentrations. Its response to AraC was the most interesting since here the observed cell death rates did not exceed the background cell death making it completely resistant to the chemotherapeutic. This result is particularly compelling when considering the association of EVI1 expression in AML patients with resistance to chemotherapy. Lastly, MLL-AF9/EVI1$_{pos}$ 907 was unique in its overall treatment response as it appeared to be resistant to any of the drugs or drug combinations. Although the measured cell death rates exceeded background cell death for all treatments, the highest observed rate was below 50% and no significant dosage dependent responses were recorded.

In summary, two of the three tested MLL/AF9-EVI1 AMLs exhibited resistance to the chemotherapeutic agent AraC and while MLL-AF9/EVI1$_{pos}$ 746 was also slightly less responsive to Birinapant, all treatments failed to sufficiently kill MLL-AF9/EVI1 cells derived from MLL-AF9/EVI1$_{pos}$ 907. These observations correlate somewhat with the known role of EVI1 as a predictor for poor treatment response in patients.

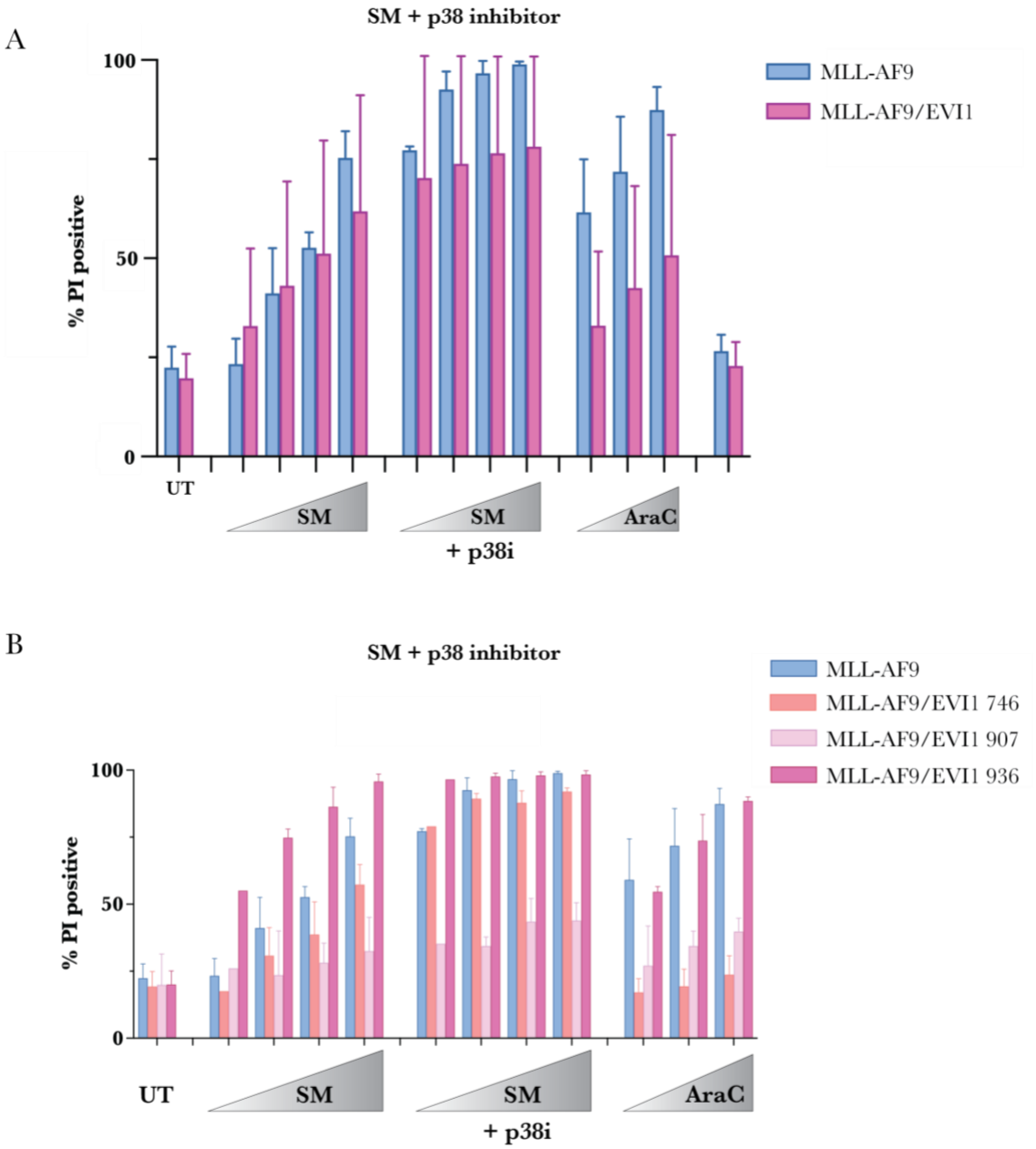

Figure 3.12: The response of EVI1pos MLL-AF9-driven AMLs to various treatments ranges from sensitive to resistant

(A) – (B) Analysis of cell death by propidium iodide uptake and flow cytometry. Leukemic cells expressing MLL-AF9 (897/899, blue) or MLL-AF9/EVI1 (top: dark pink; bottom: 746, orange; 907, light pink; 936, dark pink) were seeded in 96 well plates at 5 x 10_4 cells/well and treated with Birinapant (125-1000 nM), AraC (125-1000 nM) or Birinapant (125-1000 nM) with the p38 inhibitor LY2228820 (LY, 1 µM) for 24 h. Cell death was determined by measuring PI uptake via flow cytometry. DMSO was added to untreated controls at 0.2% (v/v). Individual values, mean and SEM are shown of two independent experiments.

3.11 EVI1 transcript levels varied greatly in MLL-AF9/EVI AMLs

I hypothesized that the increased resistance to all treatments correlated with the level of EVI1 transcript and that more EVI1 would result in AMLs being more resistant to cell death. To test this, I measured EVI1 transcript levels in MLL-AF9/EVI1$_{pos}$ AMLs (746, 907 and 936) and MLL-AF9 AMLs (896 and 899) (**Figure 3.13**). Quantitative PCR revealed that no endogenous EVI1 mRNA was detected in MLL-AF9 while levels in MLL-AF9/EVI1 AMLs varied greatly. As hypothesized, the EVI positive AML that demonstrated the greatest sensitivity to treatment (936) expressed the lowest amounts of EVI1 mRNA with transcript levels only slightly exceeding those of the housekeeping gene (1.15-fold). EVI1 transcript levels detected for MLL-AF9/EVI1$_{pos}$ 746, which appeared to be resistant to the chemotherapeutic agent AraC, were increased by more than 11-fold compared to HPTRC. The most resistant of the MLL-AF9/EVI1 AMLs, 907, revealed the highest EVI1 transcript levels exhibiting a 22-fold increase versus the housekeeping gene. Although the measured transcript levels correlated with the observed treatment responses, further experiments and greater replicate numbers would be needed to confidently link the two. It was however interesting to confirm that the MLL-AF9 AMLs tested, had no detectable levels of EVI1 transcript which is consistent with reports showing that the fusion oncogene MLL-AF9 does not directly induce high EVI1 mRNA expression (Bindels *et al.*, 2012). Instead, the EVI1 transcript levels of the cell that is being initially transformed is the determinant of whether leukemic cells will express high levels of EVI1 or not (Bindels *et al.*, 2012). With EVI1 being predominantly expressed in HSCs and expression decreasing during differentiation (Yuasa *et al.*, 2005), it can be concluded that the more immature the leukemia initiating cell is, the higher EVI1 transcript levels in AML blasts will be. Again, with the number of tested MLL-AF9 AMLs being only two, no confident assumptions can be drawn.

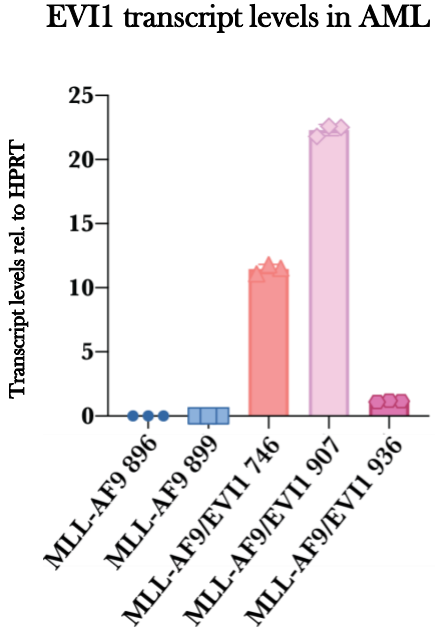

Figure 3.13: EVI1 expression levels varied greatly in MLL-AF9/EVI AMLs while MLL-AF6 and -AF9 -driven AMLs did not express EVI1

Quantitative PCR for EVI1 of MLL-AF9 AMLs 896 (blue circle) and 899 (blue square) and MLL-AF9/EVI1 AMLs 746 (orange), 907 (light pink) and 936 (dark pink). To determine relative transcript levels, SYBR Green based qPCR was performed using primers against EVI1 and HPTRC (housekeeping gene). Individual values, mean and SEM are shown of one experiment however results are representative of two independent experiments.

3.12 Discussion

The aim of this project was to generate a mouse model for an AML that is associated with particularly poor patient outcome and treatment resistance. As a suitable model we chose the co-expression of the chimeric oncogene MLL-AF9 with the hematopoietic transcription factor EVI1. With MLL-AF9 being the oncogenic protein, all AMLs were positive for its expression. However, the generation of leukemias that were positive for both MLL-AF9 and EVI1 was challenging. When applying the same technique of retrovirally transducing fetal liver cells with two constructs, we routinely accelerate disease onset by co-infecting cells with MLL-AF9 and a NRAS mutant whose positive correlation with disease severity in AML is well-established (W. I. Kim *et al.*, 2009). We therefore know that it is possible to infect a fetal liver cell with two constructs leading to the hypothesis that as opposed to NRAS, EVI1 expression is not conferring a proliferative advantage to MLL-AF9 expressing cells. Here it is also noteworthy that a number of AMLs positive for EVI1 only expressed the protein in a subpopulation of its blasts. Although EVI1 levels dropped initially after culturing those cells for multiple weeks, the ratio of EVI1 positive to EVI1 negative cells remained stable. When considering AML as a clonal disease, that is that it originates from one cell being transformed, it appears contradictive that EVI1 positive and negative populations can co-exist in the same leukemia. One possible explanation for this could be that the AMLs we are generating are in fact heterogenous due to the transformation of multiple cells. An alternative theory to this could be that MLL-AF9 positive cells actively aim to suppress EVI1 expression and succeed to do so in only a proportion of cells. Given that in the AMLs where mixed populations were present, ratios between the two populations maintained consistent, we can conclude that EVI1 expression did not impact proliferation rates in those AMLs. It is therefore questionable how downregulating EVI1 expression would be beneficial to leukemic cells *in vitro*. An informative

experiment would involve the injection of AML cells with EVI1 positive and negative populations into recipient mice to investigate whether the secondary AML would be comprised of the same two populations or whether *in vivo*, one of them would be more potent in propagating the disease.

It is likely that EVI1 co-expression does not lead to a proliferative advantage in MLL-AF9 positive cells and the issue of failing to consistently generate double positive AMLs is a technical one. When sorting for EVI1 expression prior to infecting cells with the MLL-AF9 construct, three of six mice did not develop AML at all and the three mice that did get sick after a lengthy latency gave rise to leukemic cells that were 100% EVI1 positive while MLL-AF9 levels were low. It is known that previously infected cells are not as readily transduced in a second round of infection (Walker *et al.*, 1996). This potentially explains why secondary infection of EVI positive cells that were sorted for high GFP expression was of limited success. In addition to being infected multiple times, the process of fluorescence-activated cell sorting itself induced additional stress to the cells which potentially interfered with both the secondary infection as well as the *in vivo* engraftment and disease initiation.

To overcome the described obstacles and to generate double positive AMLs more reliably, fetal liver cells could initially be infected with both constructs at ratios that favor the infection with EVI1 and subsequently be subjected to cell sorting. As my data shows in **Figure 3.2**, when co-infecting fetal liver cells with the MLL-AF9 and EVI1 constructs at a ratio of 4:1, the population of double infected cells several days after infection was about 3.5%. This is opposed to approximately 20% of GFP positive cells achieved through infection with EVI1 alone (data not shown). Therefore, the downside of performing the double infection prior to sorting is the

demand for larger cell numbers that need to be infected. Routinely, we use one fetal liver for the reconstitution of two to three mice depending on the age of the fetal liver cell suspensions to inject 5 x 10_5cells/mouse. When sorting for a population that only makes up about 3.5% of infected fetal liver cells, the number of fetal livers required would increase almost 30-fold. Since mice are lethally irradiated prior to reconstitution, when insufficient cell numbers are injected, mice are likely to succumb to irradiation sickness. Consequently, we are limited with how much we can reduce the amount of fetal liver cells administered to mice. To overcome this, it could be applicable to co-inject non-infected fetal liver or bone marrow-derived support cells to prevent the development of irradiation sickness. However, it is possible that by doing so we would also introduce additional, unpredictable variables. When considering that EVI1 is highly expressed on HSCs, another approach could entail enriching fetal liver cells using immunomagnetic beads. By doing so we would reduce the vector requirements and ensure the expression of pathologically relevant EVI1 isoforms at physiological levels. Furthermore, I believe this approach would have the greatest potential to induce an AML whose disease phenotype realistically recapitulates human AML since in patients with EVI1 positive AML, leukemic blasts exhibit a less mature immunophenotype (Glass *et al.*, 2013). As with the approach discussed above, this method would require large amounts of stem cell containing starting material, i.e. fetal livers or bone marrow since HSCs that are contained in the LSK (lin-Sca+cKit+) population only make up a small percentage of the total cells. Lastly, the enrichment process for HSCs using immunomagnetic beads is inefficient leading to a further increase in required starting material. Alternatively, a single vector construct expressing both MLL-AF9 and EVI1 could be generated. With the size of the MLL-AF9 fusion gene exceeding 11kb, the integration of EVI1 (3kb) would lead to an expression construct whose size is unfavourable for a viral vector. By increasing the size of the viral construct, both the

infection efficiency and copy numbers integrated per cell would decrease. This could be particularly problematic when considering that EVI1 expression levels appeared to positively correlate with treatment resistance of leukemic cells *in vitro*.

When I successfully generated EVI1 positive AMLs, the expression of the transcription factor did not appear to impact the morphology of leukemic blasts as determined via histopathological analysis of bone marrow cytospin preparations. In accordance with that, flow cytometry analysis of various haematological surface markers failed to reveal significant differences in immunophenotypic features between EVI1 positive and negative AMLs. *In vitro*, EVI1 expression lead to a decrease in proliferation rates. The AML culturing media only contained the cytokine Il-3, while under physiological conditions cells are exposed to a variety of cytokines. It is possible that the observed decreased proliferation was related to the culturing conditions and in fact did not reflect any processes that occurred *in vivo*. To test this hypothesis, a range of media compositions consisting of combinations of different cytokines would need to be tested.

Lastly, I addressed the question whether EVI1 mRNA expression lead to MLL-AF9 AMLs being more resistant to treatment-induced cell death. Interestingly, resistance to the chemotherapeutic agent Ara-C was observed in two of three tested MLL-AF9/EVI1 AMLs. While one of them was still sensitive to Birinapant itself and in combination with LY, the other AML was resistant to all treatments that were tested. When measuring EVI1 transcript levels via qPCR, a positive correlation between treatment resistance and EVI1 transcript levels was observed. Those observations are supported by the role of EVI1 as a predictor for poor outcome and treatment resistance in AML patients, while larger replicate numbers and more

experiments would be required to confidently conclude that EVI1 mRNA expression alone was driving this phenotype. The large variations in EVI1 transcript levels represent another obstacle for generating an MLL-AF9/EVI1 mouse model using viral co-infection since it does not allow for controlling integration site or number of copies integrated into the cells' genome. Considering the observed positive correlation between EVI1 transcript levels and treatment resistance *in vitro*, standardization of a model applying the described approach presents a major challenge.

Collectively, the data I have presented delivers a compelling argument for the relevance of a mouse model that reliably reflects treatment-resistant human AML. The applied methods failed at reproducibly generating EVI1 expressing AMLs. Although the proposed changes have the potential to overcome the downfalls of this mouse model, alternative methods that do not rely on the use of viral integration might lead to more success.

4 How does the inhibition of p38 in the absence of IAPs induce cell death?

4.1 p38/MK2 inhibit cell death in Smac mimetic-treated cells by mechanisms other than RIPK1 phosphorylation

Smac mimetics are an attractive drug candidate for the treatment of a number of cancers. However, resistances to treatments with this class of drug have been observed (Brumatti *et al.*, 2016; Najoua Lalaoui *et al.*, 2016). The MAP kinase p38 has been identified to contribute to this resistance, which could be overcome by inhibiting p38 (Najoua Lalaoui *et al.*, 2016). The mechanism through which p38 promotes cell survival upon Smac mimetic treatment involves the activation of its substrate MK2, which in turn phosphorylates RIPK1 at Ser321 (Jaco *et al.*, 2017). This phosphorylation prevents the recruitment of RIPK1 to the cell death-inducing complex II (Jaco *et al.*, 2017). However, phosphorylation of Ser321 is not solely responsible for resistance to Smac mimetic. My host laboratory showed, that $RIPK1_{S321D}$ phospho-mimetic MEFs and BMDMs were only partially protected from Smac mimetic-induced cell death and the additional inhibition of MK2 further sensitized $RIPK1_{S321D}$ mutants (Jaco *et al.*, 2017). Furthermore, two other groups showed that MK2 can also phosphorylate RIPK1 at serine Ser336 (Dondelinger *et al.*, 2017; Menon *et al.*, 2017). To determine whether the inhibitory effect of p38/MK2 on cell death in the absence of the IAPs relies solely on the phosphorylation of RIPK1 at Ser321/Ser336, we generated a $RIPK1_{S321A/S336A}$ mutant knock-in mouse. Since this RIPK1 mutant cannot become phosphorylated by MK2, $RIPK1_{S321A/S336A}$ BMDMs should be sensitized to SM-induced killing. If p38/MK2 are not equipped with an additional function that enables them to prevent cell death upon SM treatment, the combined inhibition of p38 or MK2 and the IAPs should not lead to a further increase in cell death. When performing

this experiment, we observed that RIPK1$_{S321A/S336A}$ BMDMs were in fact sensitized to SM-induced killing, which was particularly apparent at higher SM concentrations (**Figure 4.1**). Interestingly, upon addition of either p38i or MK2i, even at a low concentration of the SM Compound A (5 nM), cell death was significantly increased. This clearly indicates, that there are further, unknown mechanisms by which the p38/MK2 axis can prevent SM-induced killing. Synergistic effects by the addition of p38i or MK2i at larger SM dosages, were probably concealed by the already high rates of cell death induced by SM as a single agent.

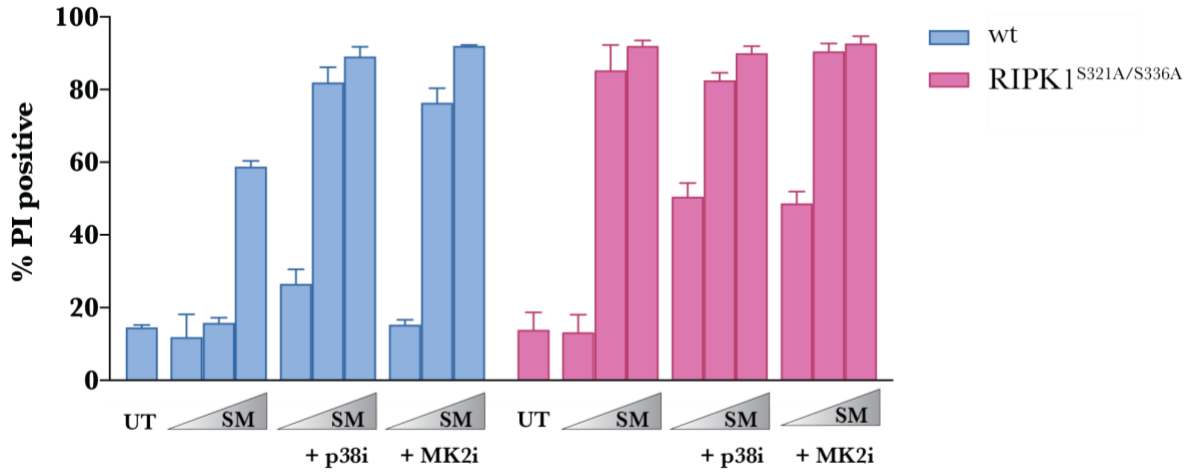

Figure 4.1: Inhibiting p38 or MK2 further increases cell death in RIPK1 phospho-dead mutant
Analysis of cell death by propidium iodide uptake and flow cytometry. Wild-type (blue) and RIPK1$_{S321A/S336A}$ (pink) BMDMs were seeded in 24-well plates at 5 x 10_4 cells/well and treated with Compound A (5, 50, 500 nM) alone or in combination with the p38 inhibitor LY2228820 (1 µM) or the MK2 inhibitor PF3644022 (2 µM). Cell death was determined after 24 hours by measuring PI uptake via flow cytometry. DMSO was added to untreated controls at 0.2% (v/v). Individual values, mean and SEM are shown of two independent experiments.

4.2 Elucidating the mechanism of the Smac mimetic/p38i-induced killing by studying the phospho-proteome by mass spectrometry

After discovering that the MK2-mediated RIPK1 phosphorylation at S321/S336 is not the only mechanism through which p38 inhibits Smac mimetic induced cell death, we decided to

approach the question using a global explorative approach. Since p38 is a kinase and phosphorylation events greatly regulate signaling pathways, studying the phospho-proteome of treated cells via mass spectrometry is an excellent tool to address our question. A number of protocols have been developed to optimize the enrichment of phosphorylated proteins from whole cell lysates for mass spectrometry analysis. I applied the EasyPhos system developed in the laboratory of Matthias Mann (Humphrey *et al.*, 2018). A schematic of the workflow is described in **Figure 4.2**

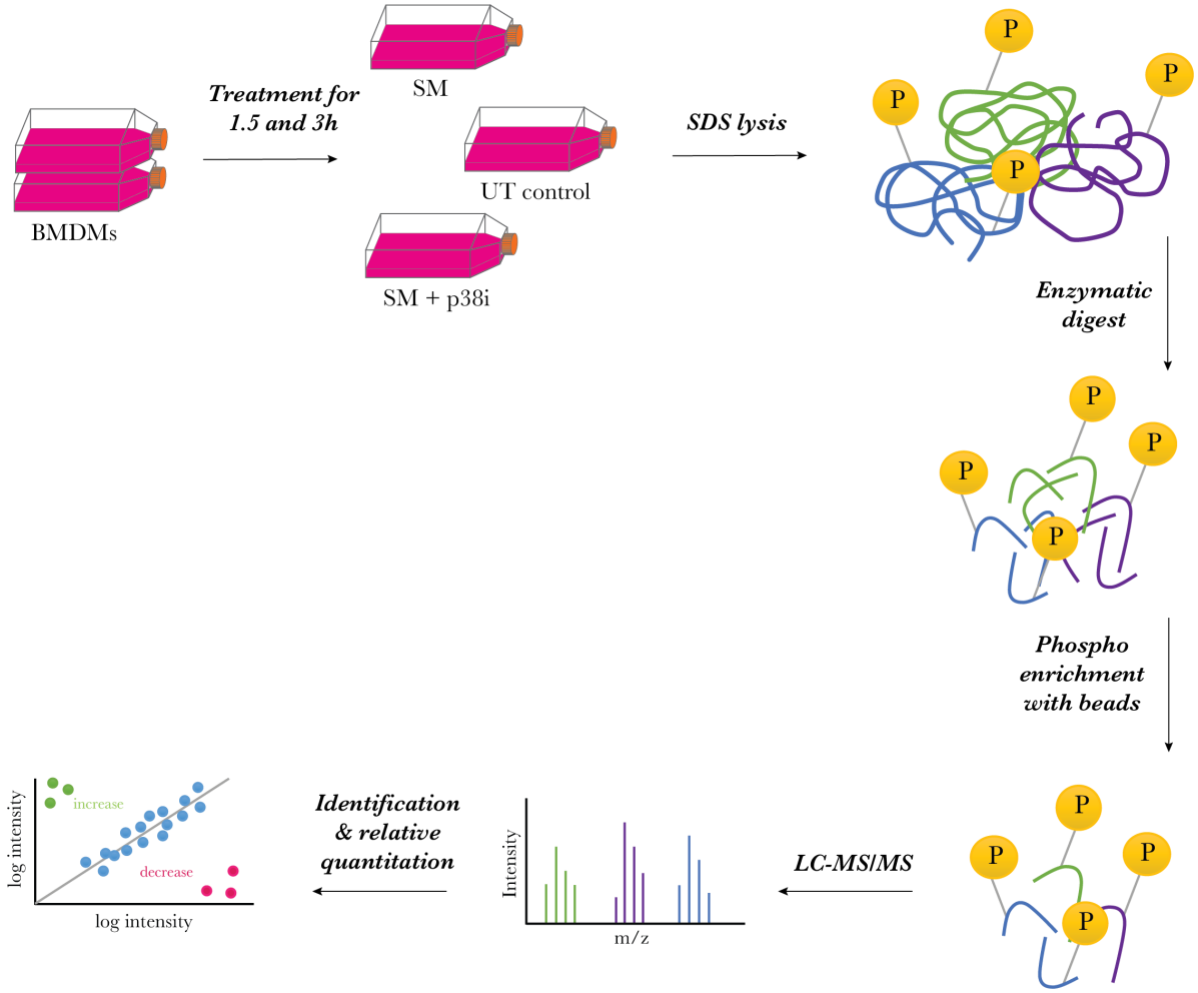

Figure 4.2: Schematic of phospho enrichment and mass spectrometry

BMDMs of six mice were treated with either 1.5 h Compound A (500 nM), 1.5 h Compound A (500 nM) and LY2228820 (1 µM), 3 h Compound A, 3 h Compound A and LY2228820 or DMSO (0.2% (v/v)). Treatment was stopped by washing cell on ice with PBS before lysing cells with SDS-based lysis buffer. Lysates were subjected to on-bead enzymatic digest with trypsin and Lys-C and phospho

peptides were enriched using TiO_2 beads. Isolated phospho peptides were analysed via LC-MS/MS using a Q Exactive hybrid quadrupole-orbitrap.

To ensure that the treatment was performed successfully and cells signaled as intended, I analysed the resulting cell death in BMDMs by measuring the uptake of PI via flow cytometry (**Figure 4.3 A**). Furthermore, I performed Western blot analysis with the lysates and probed for known targets. Apart from replicate 1, the combination treatment induced cell death as expected. Since cell death within 3 hours is minimal, the variations between cell death observed for the 1.5h 911 (Compound A) + LY (p38i) as well as the 3h 911 treatments were not concerning. The 3h combination treatment induced the greatest cell death for all but sample 1 and ranged from 22% to 28%. This indicated that the treatment was performed correctly and cells signaled as expected. This was further supported by the Western blot analysis when I probed for the phosphorylated MAP kinases JNK1/2 and ERK1/2 (**Figure 4.3 B**). It is known that JNK1/2 and ERK1/2 are activated through phosphorylation in their activation loop and hence activated upon the combination treatment, particularly after three hours and that was clearly visible in the Western blot. When inhibited, p38 is not able to phosphorylate its substrates while it can still be phosphorylated itself. We therefore get an accumulation of phospho-p38 which could also be detected via Western blot. MK2 is a well-known p38 target which plays an important role in inhibiting Smac mimetic induced cell death as I have described before. **Figure 4.3 B** shows that MK2 did not get phosphorylated when p38 was inhibited, again indicating that the treatment was successful. Upon the combination

treatment the cell death we observe is known to be induced via apoptosis and we therefore expect to observe cleavage of the caspase 8. These events could also be detected via Western blot (**Figure 4.3 B**) and the occurrence of both correlated with the measured cell death via flow cytometry. Although the cell death detected for replicate 1 did not follow the expected patterns, the signaling events that we observed via Western blot did match the others. It is therefore likely that the cell death assay which was set up on a separate plate on a smaller scale did not induce cell death to the same extent. On the other hand, the lysates used for Western blot analysis were derived from the samples that were later subjected to further processing for mass spectrometry. Hence, I was confident to include this replicate in the following workflow.

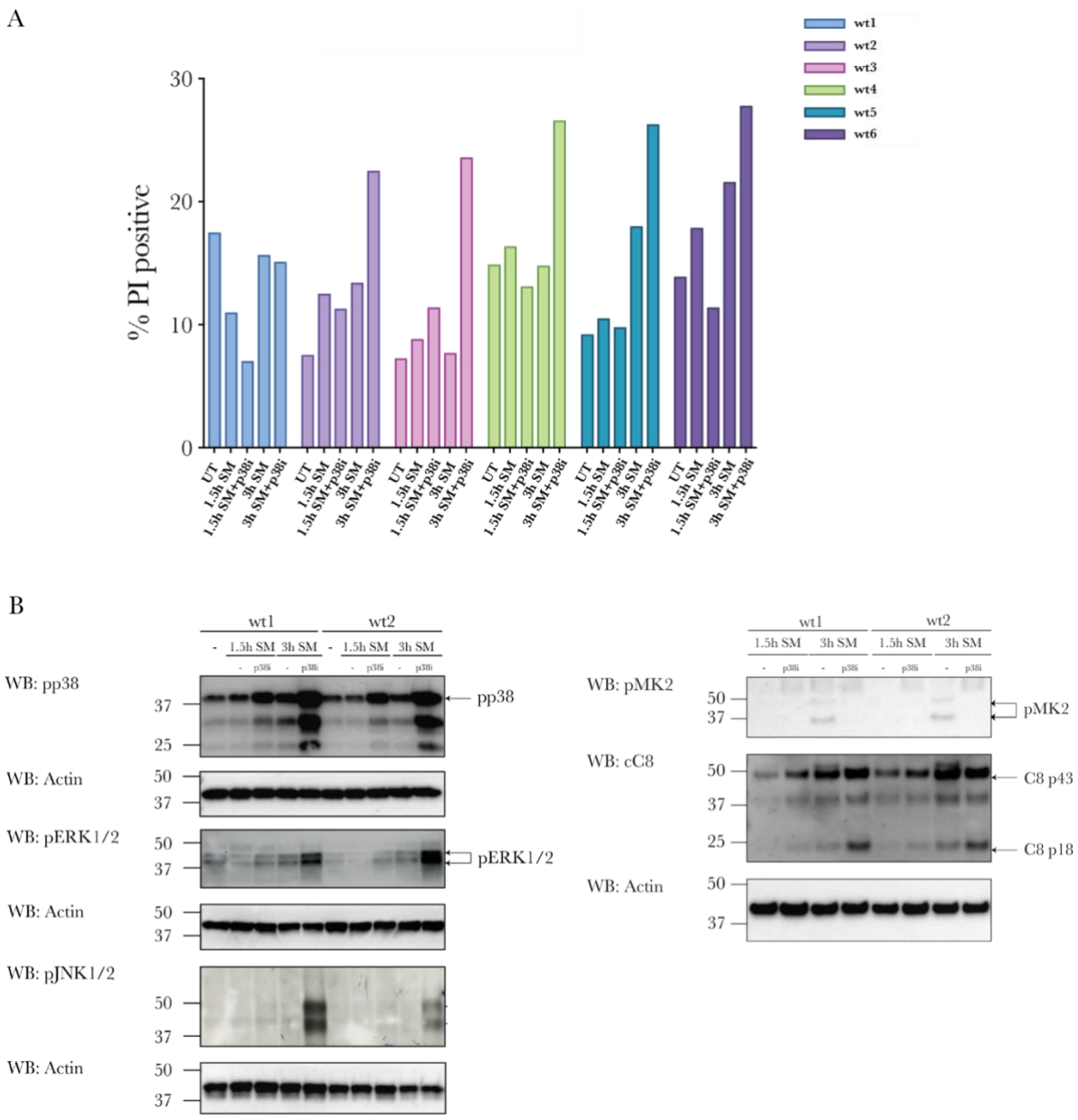

Figure 4.3: Treatment-induced cell death and signalling in BMDMs was confirmed

(A) BMDMs from six mice were treated with DMSO (untreated control), Compound A (500 nM) alone or in the presence of p38 inhibitor LY (1 μM) for 1.5 or 3 hours. Resulting cell death was measured via PI uptake using flow cytometry. (B) Lysates of treated BMDMs were subjected to Western blotting and membranes were probed for phospho-p38, phospho-Erk1/2, phospho-JNK1/2 and phospho-MK2 to confirm that the described treatment induced the expected signaling. Probing for actin served as a loading control.

4.3 Phosphorylated peptides were successfully enriched following the EasyPhos protocol

Enriched phosphorylated peptides were analysed via mass spectrometry and identified during a MaxQuant search. Using R to perform the statistical analysis, proteins that were differentially phosphorylated upon treatment could be ranked according to their significance and fold change. The parameters that were of initial interest were concerning the quality of the performed enrichment. When enzymatically digesting proteins using trypsin and Lys-C, the efficiency of that digest can be measured by determining the proportions of proteins that have no, one or multiple missed cleavages (**Figure 4.4 A**). During this experiment approx. 60% of peptides were completely digested which was reproducible for all replicates. It has been described in the literature that phosphorylation events in proximity to lysine or arginine residues may prevent lysine from cleaving at their carboxyl end increasing the number of missed cleavages (Siepen *et al.*, 2007). Given that the majority of peptides were completely cleaved and that only minor variations across the replicates occurred I was satisfied that the quality of the performed digest was sufficient.

Next, I determined how efficiently I enriched for phosphorylated peptides (**Figure 4.4 B).** Within all replicates, the proportion of unphosphorylated peptides was only around 5% which indicates that the phospho-enrichment was successful. When comparing the numbers of phosphate groups on each peptide, it stood out that dual phosphorylation events were more commonly detected than single phosphorylations (approximately 50% vs. 35%). Although MAP kinases are good examples for proteins that are activated by dual phosphorylation, single phosphorylation is still expected to be the most abundant form observed for this form of post-translational modification. Nonetheless, the low number of non-phosphorylated peptides and

the great reproducibility amongst the replicates we detected proved that the enrichment process was successful.

A

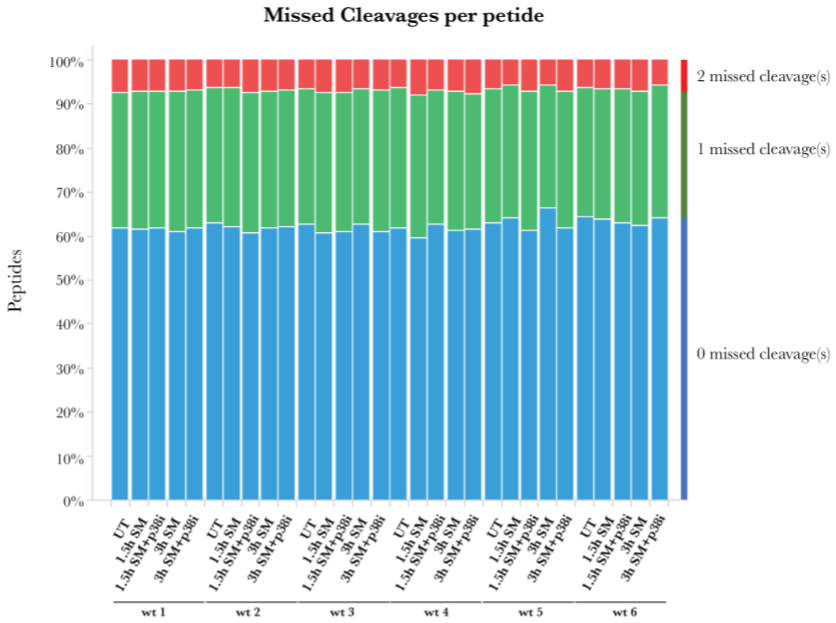

B

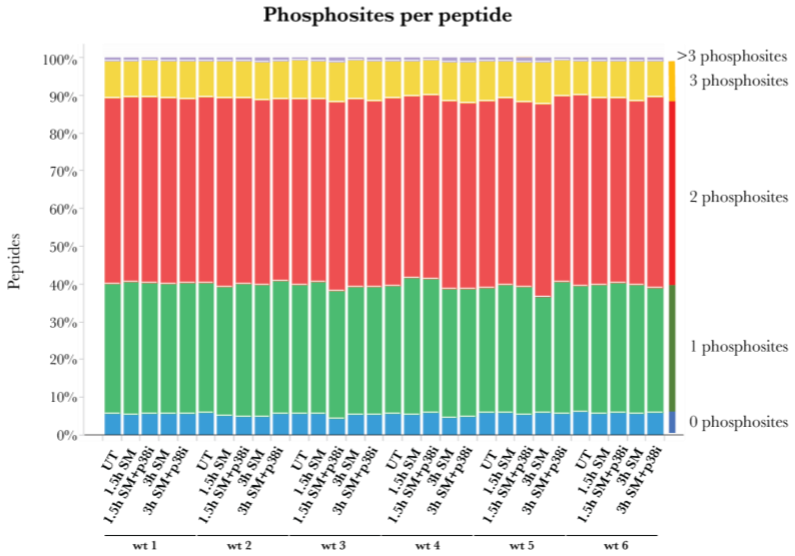

Figure 4.4: QC of mass spectrometry data

(A) Missed cleavage comparison between all samples. Graph shows the proportion of missed cleavages of the peptides detected by LC-MS/MS. Blue indicates the proportion of peptides with no missed cleavages, green and red represent one and two missed cleavages respectively. (B) Number of phosphorylation sites per peptide. Shown are the proportions of peptides with no phosphorylation (blue), single (green), double (red), triple (yellow) or quadruple (purple) serine, threonine or tyrosine phosphorylation(s) detected across all treated BMDM samples.

4.4 Inhibition of p38 induces phosphoproteomic changes with distinct temporal profile

The generated lists of phosphorylated proteins detected for each treatment were now compared to determine the proteins that were differentially phosphorylated between BMDMs treated with Compound A only and BMDMs treated with the combination of Compound A and LY. These comparisons revealed that 178 proteins were significantly differentially phosphorylated between these two groups after 1.5 h of treatment and 220 proteins after 3 h of treatment with a false discovery rate of <0.1 (**Figure 4.5 A, B**; for list of proteins refer to Appendix). Interestingly, after 1.5 h the majority of differentially phosphorylated (DP) proteins were less phosphorylated in the combination treatment. However, after 3 h this tendency vanished and a more evenly balanced relationship between up- and downregulated phosphorylation events was observed. Considering that in p38 we were inhibiting a kinase, it is plausible that as a primary response the combination treatment resulted in fewer proteins being phosphorylated. After 3 h, secondary signaling responses may have led to the initiation of signaling cascades which involved phosphorylation events therefore achieving a balance between up- and downregulated DP proteins. To visualize each DP protein and their phosphorylation patterns across the treatments, heatmaps for both time points were generated (**Figure 4.5 C, D**).

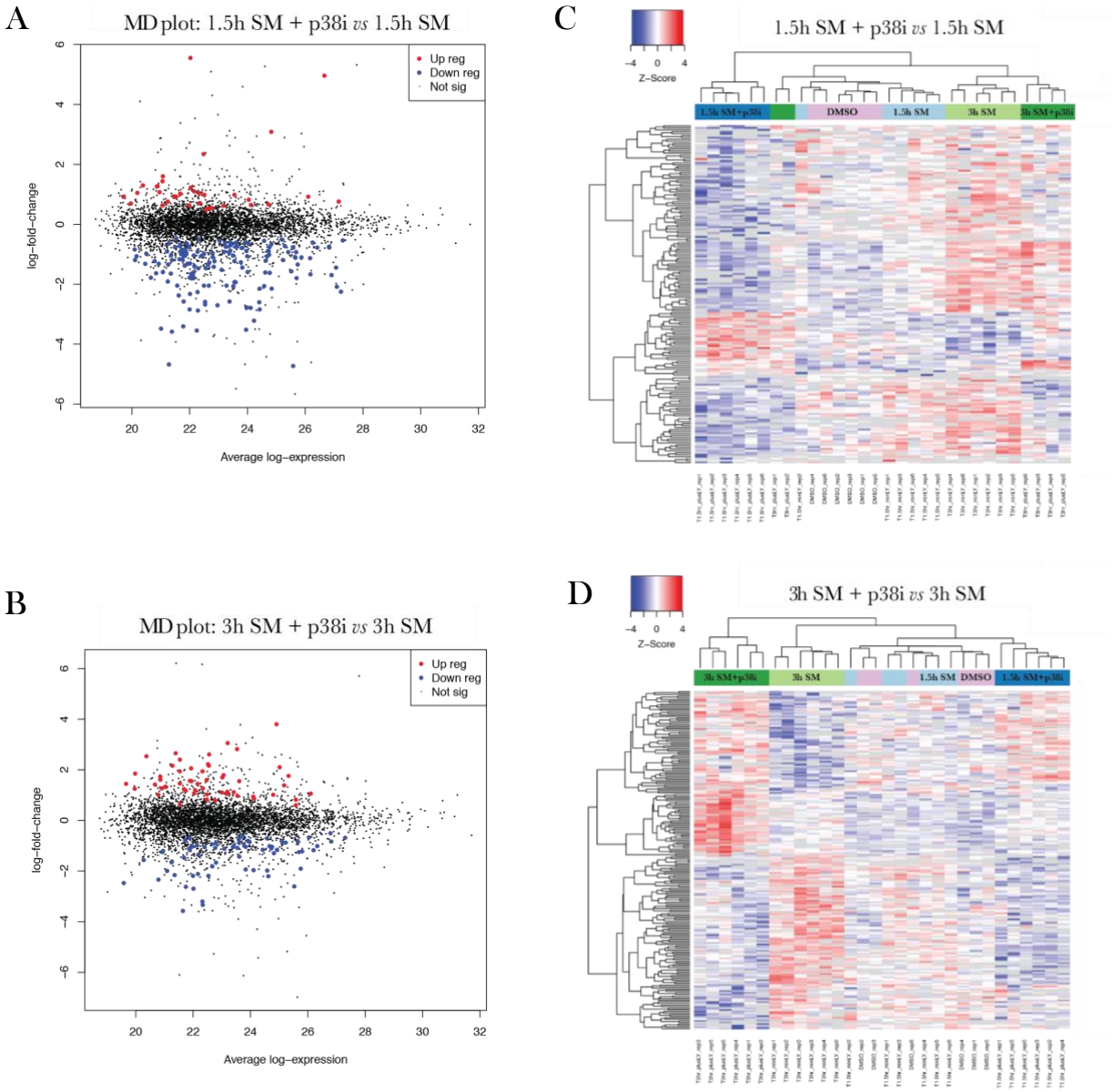

Figure 4.5: Inhibition of p38 induces phosphoproteomic changes with distinct temporal profile

(A), (B) Mean-difference (MD) plot showing all significantly differentially phosphorylated proteins upon treatment for 1.5 hours with Compound A and LY vs. Compound A alone. Proteins in red are more phosphorylated and proteins in blue are less phosphorylated in the combination treatment. Non-significant phosphorylated proteins are in black. For full list of DP proteins refer to Appendix. (C), (D) Heatmap and hierarchical clustering of phosphorylated proteins. Changes in phosphorylation induced by treatment for 1.5 h (C) or 3 h (D) with Compound A (911) in the absence (minLY) and presence (plusLY) of p38 inhibitor (LY) are indicated by the colours red (upregulated in the combination) or blue (downregulated in the combination). Grey bars represent missing values. Z-scores for each replicate in each condition was determined and coloured as shown in the scale bar.

4.5 Detected proteins that were differentially phosphorylated peptides upon treatment with p38i and Smac mimetics included known targets

To test if I generated a robust data set of treatment induced differentially phosphorylated proteins, I searched the detected proteins for known targets that I previously confirmed via Western blotting. Although a number of proteins including MK2 and JNK1/2 could not be found, p38 (MAPK14) and ERK1 (MAPK3) were indeed detected and in both cases the identified phosphorylated peptides represented their dually phosphorylated activation loops (**Figure 4.6**). Not only were we able to enrich for phospho-p38 and phospho-ERK1 but their observed phosphorylation patterns also matched with what I saw in the respective Western blots (**Figure 4.6**).

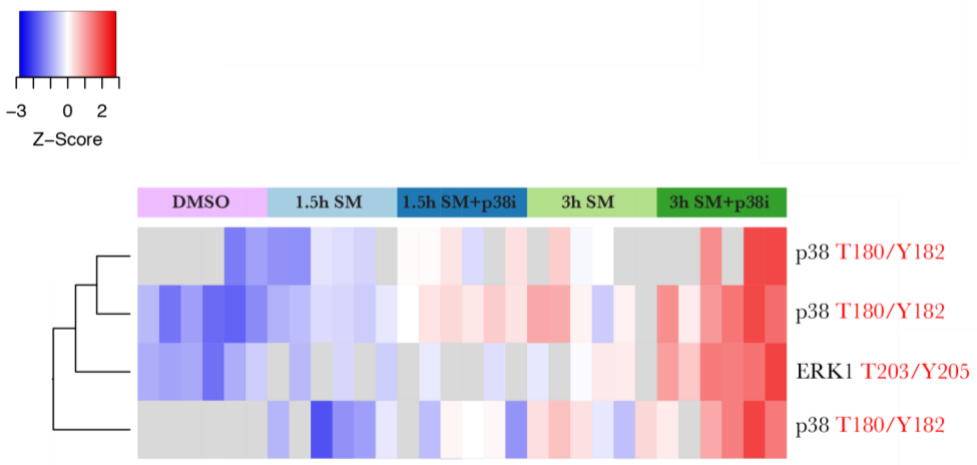

Figure 4.6: Treatment-induced changes in phosphorylation of the known targets p38 and ERK1 were identified during phosphoproteomics analysis

Heatmap and hierarchical clustering of phosphorylated activation loops of p38 and ERK1. Changes in phosphorylation induced by treatment for 1.5h and 3 h with Compound A (911) in the absence (minLY) and presence (plusLY) of p38 inhibitor (LY) are indicated by the colours red (upregulated in the combination) or blue (downregulated in the combination). Grey bars represent missing values. Z-scores for each replicate in each condition was determined and coloured as shown in the scale bar.

After confirming that the generated data set of differentially phosphorylated proteins upon treatment with Smac mimetics and a p38 inhibitor truthfully reflected the behavior of the known targets p38 and ERK1, it was now appropriate to explore the data set for potentially novel mediators. A number of approaches can be pursued in order to strategically analyze such large data sets. One such approach is to rank DP proteins according to their p-value and further investigate proteins with the highest significance. We therefore generated volcano plots of DP proteins detected after 1.5 h and 3 h of treatment where proteins were plotted according to their fold change and p-value and named the 20 proteins with the highest significance (**Figure 4.7**). As observed previously in the generated heatmaps, after 1.5 h the combination treatment preferentially induced a reduction in phosphorylation events with 19 of the top 20 DP proteins being more phosphorylated when treated with Compound A alone. After 3 h however nearly half the DP proteins that were attributed with the highest significance were more phosphorylated following the combination treatment. Notably, ERK1 (MAPK3) was amongst the top hits in the 3 h time point.

To better illustrate the 20 DP proteins whose differences in phosphorylation states were detected with the highest significance, I generated tables summarizing the gene and protein names together with their fold change and adjusted p-value while applying the same color codes as used in the heatmap (**Tables 4.1 and 4.2**).

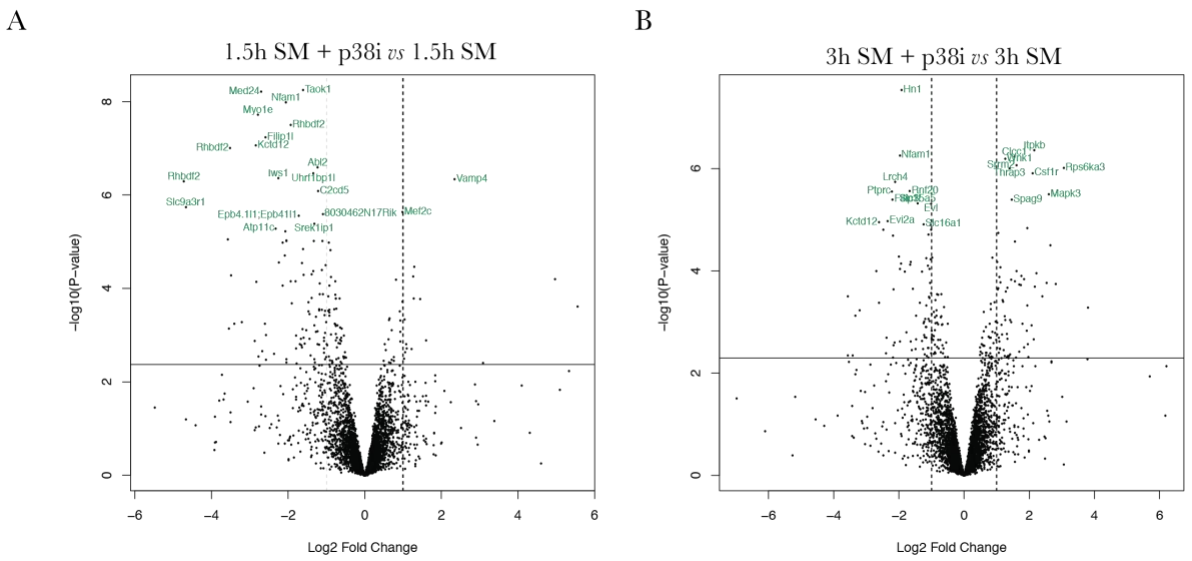

Figure 4.7: Phosphoproteomic profiles of SMAC mimetic treatment versus its combination with the p38 inhibitor LY after 1.5 and 3h treatment in BMDMs

Volcano plot depicting the phosphoproteome of BMDMs treated with Compound A alone or in combination with LY for 1.5 h (A) or 3 h (B). The statistical significance was -$\log_{10}$ transformed (y-axis) and plotted against the fold change. The 20 proteins with the highest significance (lowest p-value) are listed.

Table 4.1: Top 20 DP proteins in BMDMs treated with 1.5h SM vs 1.5h SM + p38i

Gene		logFc	Adj p-value
Taok1	Serine/threonine-protein kinase TAO1	-1.61	1.28E-05
Med24	Mediator of RNA polymerase II transcription subunit 24	-2.70	1.28E-05
Nfam1	NFAT activation molecule 1	-2.05	1.44E-05
Myo1e	Unconventional myosin-Ie	-2.79	2.00E-05
Rhbdf2	Inactive rhomboid protein 2	-1.93	2.65E-05
Filip1l	Filamin A-interacting protein 1-like	-2.59	4.08E-05
Kctd12	BTB/POZ domain-containing protein KCTD12	-2.84	5.17E-05
Rhbdf2	Inactive rhomboid protein 2	-3.51	5.21E-05
Abl2	Non-specific protein-tyrosine kinase;Abelson tyrosine-protein kinase 2	-1.23	1.19E-04
Uhrf1bp1l	UHRF1-binding protein 1-like	-1.34	1.44E-04
Iws1	Protein IWS1 homolog	-2.26	1.60E-04
Vamp4	Vesicle-associated membrane protein 4	2.35	1.60E-04
Rhbdf2	Inactive rhomboid protein 2	-4.72	1.63E-04
C2cd5	C2 domain-containing protein 5	-1.21	2.45E-04
Slc9a3r1	Na(+)/H(+) exchange regulatory cofactor NHE-RF	-4.67	5.06E-04
Mef2c	Myocyte-specific enhancer factor 2C	0.99	6.03E-04
8030462N17Rik	Uncharacterized protein C18orf25 homolog	-1.09	6.25E-04
Epb4.1l1;Epb41l1	Band 4.1-like protein 1	-1.72	6.37E-04
Srek1ip1	Protein SREK1IP1	-1.32	9.07E-04

Table 4.2: Top 20 DP proteins in BMDMs treated with 3h SM vs 3h SM + p38i

Gene		logFc	Adj p-value
Hn1	Hematological and neurological expressed 1 protein	-1.91	1.21E-04
Itpkb	Inositol-triphosphate 3-kinase B	2.15	5.14E-04
Nfam1	NFAT activation molecule 1	-1.97	5.14E-04
Clcc1	Chloride channel CLIC-like protein 1	1.54	5.14E-04
Wnk1	Serine/threonine-protein kinase WNK1	1.25	5.14E-04
Srrm2	Serine/arginine repetitive matrix protein 2	1.60	5.14E-04
Rps6ka3	Ribosomal protein S6 kinase alpha-3	3.05	5.14E-04
Thrap3	Thyroid hormone receptor-associated protein 3	1.38	5.14E-04
Csf1r	Macrophage colony-stimulating factor 1 receptor	2.10	5.67E-04
Lrch4	Leucine-rich repeat and calponin homology domain-containing protein 4	-2.11	7.63E-04
Rnf20	E3 ubiquitin-protein ligase BRE1A	-1.66	9.66E-04
Ptprc	Protein-tyrosine-phosphatase	-2.20	9.66E-04
Mapk3	Mitogen-activated protein kinase 3	2.60	1.01E-03
Filip1l	Filamin A-interacting protein 1-like	-2.19	1.13E-03
Spag9	C-Jun-amino-terminal kinase-interacting protein 4	1.45	1.13E-03
Slc35a5	Probable UDP-sugar transporter protein SLC35A5	-1.42	1.19E-03
Evl	Ena/VASP-like protein	-1.01	1.19E-03
Evi2a	Protein EVI2A	-2.34	2.43E-03
Kctd12	BTB/POZ domain-containing protein KCTD12	-2.61	2.45E-03

To investigate mediator(s) of signaling transduction and initiation events, we screened for the enrichment of proteins that represent certain biological processes or signaling pathways using gene ontology (GO) enrichment analysis and KEGG pathway analysis. We the summarized the 10 biological processes (GO) and 10 pathways (KEGG) that were detected with the highest p-values for each time point (**Tables 4.3 – 4.6**). Notably, "Number of genes/proteins" refers to the number of proteins that belong to a biological process or pathway while "DP" includes the proteins whose phosphorylation states changed significantly across the treatments. Finally, I utilized both the lists of the top 20 DP proteins per timepoint as well as the results generated during GO and KEGG pathway analysis to identify potential mediators of the killing caused by the combination treatment of Compound A and LY. Under the following subheadings I will expand on a number of detected targets and their involvement in pathways that might contribute to the observed treatment-induced signaling.

Table 4.3: Top 10 biological processes determined via gene ontology enrichment analysis of DP proteins treatment with 1.5h SM vs 1.5h SM + p38i

Gene Ontology Enrichment Analysis			
Biological Process	**Number of genes**	**DP**	**p-value**
Immune system process	266	39	4.99E-04
Auditory receptor cell development	3	3	7.12E-04
Chloride channel regulator activity	3	3	7.12E-04
Membrane raft distribution	3	3	7.12E-04
Membrane raft localization	3	3	7.12E-04
Membrane organization	92	18	8.50E-04
Neuroepithelial cell differentiation	7	4	1.77E-03
Hair cell differentiation	4	3	2.66E-03
Negative regulation of sodium ion transport	4	3	2.66E-03
Regulation of cell killing	8	4	3.29E-03

Table 4.4: Top 10 biological processes determined via gene ontology enrichment analysis of DP proteins after treatment with 3h SM vs 3h SM + p38i

Gene Ontology Enrichment Analysis			
Biological Process	**Number of genes**	**DP**	**p-value**
Ion transport	103	24	3.60E-04
Regulation of cell morphogenesis	78	19	8.72E-04
Anion transmembrane transporter activity	16	7	1.15E-03
Regulation of anatomical structure morphogenesis	125	26	1.33E-03
Transporter activity	53	14	1.88E-03
Localization	616	89	2.25E-03
Cytoskeletal protein binding	157	30	2.38E-03
Secretion	117	24	2.55E-03
Cell morphogenesis	144	28	2.58E-03
Positive regulation of tumor necrosis factor production	15	6	4.54E-03

Table 4.5: Top 10 pathways determined via KEGG pathway analysis of DP proteins after treatment with 1.5h SM vs 1.5h SM + p38i

KEGG Pathway Analysis			
Pathway	**Number of proteins**	**DP proteins**	**p-value**
MAPK signaling pathway	31	9	0.0011
Parathyroid hormone synthesis, secretion and action	17	6	0.0026
Apelin signaling pathway	20	6	0.0066
Fc gamma R-mediated phagocytosis	24	6	0.0169
Thermogenesis	24	6	0.0169
Progesterone-mediated oocyte maturation	12	4	0.0180
mTOR signaling pathway	26	6	0.0248
Rap1 signaling pathway	27	6	0.0230
GnRH signaling pathway	14	4	0.0314
PI3K-Akt signaling pathway	39	7	0.0561

Table 4.6: Top 10 pathways determined via KEGG pathway analysis of DP proteins after treatment with 3h SM vs 3h SM + p38i

KEGG Pathway Analysis			
Pathway	**Number of proteins**	**DP proteins**	**p-value**
MAPK signaling pathway	31	9	0.0066
IL-17 signaling pathway	9	4	0.0140
Toxoplasmosis	9	4	0.0140
Fc gamma R-mediated phagocytosis	24	6	0.0515
Viral protein interaction with cytokine/cytokine receptor	4	2	0.0692
HIF-1 signaling pathway	14	4	0.0670
TNF signaling pathway	14	4	0.0700
PI3K-Akt signaling pathway	39	8	0.0747
EGFR tyrosine kinase inhibitor resistance	10	3	0.1008
Toll-like receptor signaling pathway	10	3	0.1008

4.6 Targeted analysis of differentially phosphorylated proteins reveals potential novel mediators of treatment-induced cell death

To identify proteins and pathways that may contribute to the treatment responses observed in BMDMs, that is the prevention (SM) or occurrence of cell death (SM + p38i) and the increase in TNF production (SM + p38i), I performed a targeted analysis of the biological processes and KEGG pathways that were found to be enriched in Tables 4.3 - 4.6. During this analysis,

I searched for differentially phosphorylated proteins that are associated with (A) the induction or prevention of cell death, (B) cell survival signaling or (C) the regulation of TNF expression. Proteins that were identified as potential mediators of the cell death induced by the combination treatment of SM and p38i are discussed in the following.

4.6.1 Inhibition of Apoptosis

4.6.1.1 The pro-apoptotic protein Bim was preferentially phosphorylated in BMDMs treated with Compound A

Treatment with Compound A alone fails to induce cell death in BMDMs. I therefore searched the phosphoproteomic dataset for DP proteins that might have prevented apoptosis when IAPs were inhibited. By doing so, I identified that Bim, a pro-apoptotic member of the Bcl-2 protein family, was preferentially phosphorylated in BMDMs treated with smac mimetic alone. The role of Bim in the intrinsic apoptotic pathway has been well described. Bim, a BH3-only protein, is required for activation of BAX leading to the initiation of mitochondrial apoptosis (H. Kim *et al.*, 2009). Bim activity itself is regulated via phosphorylation by a number of kinases. MEK/ERK-mediated phosphorylation affects the binding of Bim to pro-survival Bcl-2 family members as well as its turnover (R. Ley *et al.*, 2005; Rebecca Ley *et al.*, 2004). Upon exposure to apoptotic stimuli, BimEL levels, Bim's most abundant isoform, become strongly elevated in B and T lymphoid cells while in mitogenically stimulated cells, BimEL is rapidly phosphorylated leading to its levels to decline (O'Reilly *et al.*, 2009). MEK/ERK mediated BimEL phosphorylation which inhibits Bim activation by inducing its degradation via the proteasome, has been identified to target Ser65 (Hübner *et al.*, 2008). Bim activity can furthermore be regulated by the Src family kinase Lyn which can phosphorylate the Bcl-2 protein family member on tyrosine residues 92 and 161 resulting in the inhibition of its pro-

apoptotic function (Aira *et al.*, 2018). Unlike phosphorylation by MEK/ERK which leads to Bim's degradation, modification by Lyn increases Bim's interaction with anti-apoptotic proteins including Bcl-xL. As a consequence, permeabilization of the mitochondrial outer membrane is strongly reduced which ultimately limits apoptosis (Aira *et al.*, 2018).

In BMDMs treated with Compound A for 1.5 h, phosphorylated Bim was enriched by 1.7-fold compared to cells exposed to the combination treatment (**Table 4.7**). The detected phosphopeptide contained the modified residues Ser82 and Ser86 which are both located in the EL domain and are in close proximity to the Ser92 whose phosphorylation by Lyn inhibits Bim activity (**Figure 4.8 A**). To date, Ser82, which is conserved in humans and rats, has not been demonstrated to become phosphorylated. While Ser86 has been reported as a phosphosite in mice during large scale phosphoproteomic explorations, it has not been associated with a function yet (X. Wu *et al.*, 2012). Interestingly, in humans Ser87 which corresponds to Ser83 in mouse BimEL, is believed to become phosphorylated by Akt leading to the inhibition of its pro-apoptotic function (Qi *et al.*, 2006). The ability of Akt to phosphorylate BimEL has been demonstrated using an *in vitro* kinase assay (Qi *et al.*, 2006). Additionally, inhibiting PI3K in cells reduced BimEL phosphorylation (Qi *et al.*, 2006). Although the collective data is indicative of Akt phosphorylating human BimEL on Ser87, and potentially mouse BimEL on Ser83, it was compelling to notice that the sequence containing this residue perfectly matched the MK2 substrate motif. This motif is made up of a large hydrophobic residue, followed by a random amino acid, Arginine, another random residue and serine which becomes phosphorylated (Hyd-X-R-X-S). In BimEL, this motif is represented by the sequence F-V-R-R-S· where S· corresponds to Ser82. Since the activity of MK2 was inhibited upon the combination treatment and activated in smac mimetic-treated

BMDMs, it is plausible to suggest, that MK2 can phosphorylate BimEL on Ser82. Another observation that supports the notion, that the pro-apoptotic function of BimEL played a role in the synergistic cell death induced by the combined inhibition of IAPs and p38, was that Caspase 9, an initiator caspase for intrinsic apoptosis, was cleaved upon this treatment as can be seen via Western blot (**Figure 4.8 B**). Cleavage of Caspase 9 yields the two large subunits p35 and p37. Immunoblotting for cleaved Caspase 9 revealed that a band that corresponded to approximately 37 kDa only appeared in BMDMs treated with the combination of Compound A and LY for 3 h. Since intrinsic apoptosis is always accompanied by Caspase 9 cleavage and given that Bim is required for Bax activation, this result is highly indicative of BimEL being active upon the combination treatment and inactive when cells were only treated with smac mimetic. The identified phosphosite Ser83 might therefore play an important regulatory role in preventing cell death when the IAPs are inhibited. However, the extent of the contribution to the overall cell death by this pathway is questionable, since we know that the cell death induced by the combination treatment is TNF dependent. Nonetheless, the presented data suggests that Bim phosphorylation at Ser83 played a role in preventing cell death upon smac mimetic treatment and that Akt or MK2 could be the kinase that mediated this modification. Experiments involving the generation of phosphomimetic and/or phospho-silent BimEL mutants could further address these observations. It should be noted that cleavage of Caspase 9 can also occur downstream of TNFRII signaling. The role of intrinsic apoptosis in the observed cell death therefore requires further investigation.

Table 4.7: Phosphorylation status of BimEL after treatment with SM + p38i

Protein	Residue(s)	Timepoint	logFc	Rank
BimEL	**S82/S86**	1.5h	**-0.7**	**112**

A

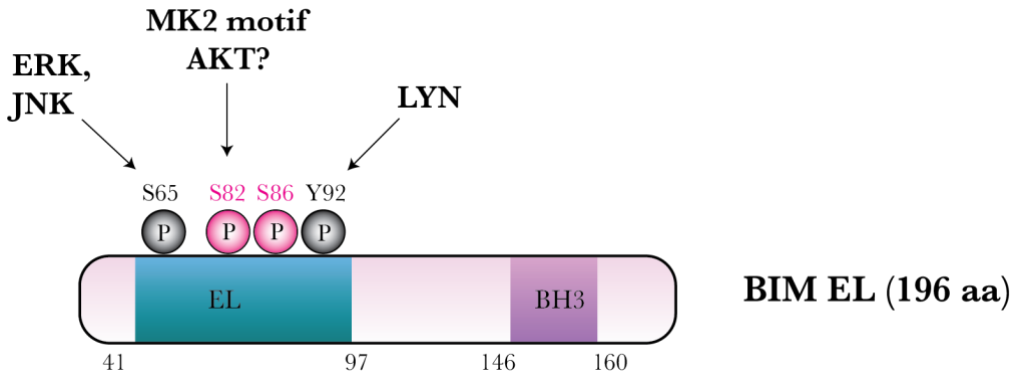

B

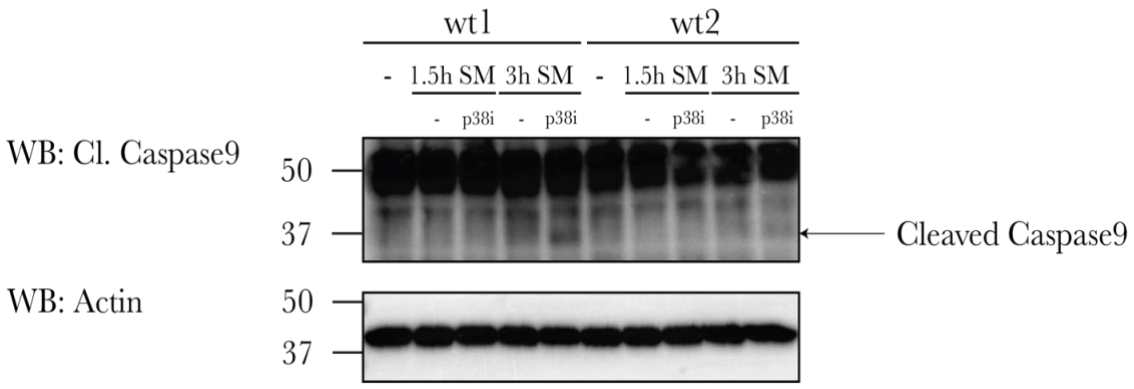

Figure 4.8: The pro-apoptotic protein Bim is less phosphorylated in BMDMs treated with SM + p38i where intrinsic apoptosis occurs

(A) Schematic representation of BimEL. The numbers refer to amino acids flanking the functional domains. Residues in pink represent phosphorylated amino acids identified in BMDMs treated with Compound A, while grey/black residues are known phosphosites that were not detected. Phosphosite S82 contains the MK2 motif while the corresponding residue in humans has been observed to become phosphorylated by Akt. BimEL can be phosphorylated at S65 by ERK which causes to its degradation, or by JNK which activates Bim (O'Reilly *et al.*, 2009; Putcha *et al.*, 2003). Phosphorylation of Y92 by LYN inhibits the pro-apoptotic function of Bim. EL = domain unique to BimEL isoform; BH3 = Bcl-2 homology 3 domain. (B) BMDMs from six mice were treated with DMSO (untreated control), Compound A (SM, 500 nM) alone or in the presence of p38 inhibitor LY (1 μM) for 1.5 h or 3 h. Lysates of treated BMDMs were subjected to Western blotting and membranes were probed for cleaved Caspase 9 to test for evidence of Bim activity leading to cell death via intrinsic apoptosis . Probing for actin served as a loading control. The blot is representative of six biological replicates.

4.6.2 TNF expression pathways

Smac mimetic induced apoptosis is dependent on the expression of the cytokine TNF and in cells treated with the combination of Compound A and the p38 inhibitor LY2228022 we observed an increase in TNF production as described previously. In support of its crucial role in inducing cell death, "positive regulation of TNF production" was listed in the top 10 most significant biological processes enriched in treated BMDMs according to GO analysis (**Table 4.3**). In the following, I will elaborate on four DP proteins whose phosphorylation signatures upon treatment might reveal how TNF production in regulated in treated BMDMs. A summary including their role in TNF regulation is shown in **Table 4.14**.

4.6.2.1 PTPRC, a negative regulator for TNF production, is less phosphorylated upon the combined inhibition of IAPs and p38

PTPRC (Protein Tyrosine Phosphatase Receptor Type C, CD45) is an abundant transmembrane glycoprotein expressed in all nucleated hematopoietic cells (Hermiston *et al.*, 2003). As a tyrosine phosphatase, CD45 plays an important role in regulating immune responses (Shenoi *et al.*, 1999). In T- and B-cells, CD45 phosphatase activity is critical for receptor signal transduction where the Src family kinases Lyn, Fyn and Lck have been identified as its primary targets (D'Oro *et al.*, 1999; Katagiri *et al.*, 1999; Mustelin *et al.*, 1992). By dephosphorylating tyrosine residues that exhibit inhibitory functions, CD45 both positively and negatively regulates these Src family proteins (Shrivastava *et al.*, 2004).

Apart from its role in antigen receptor signal transduction, CD45 has been shown to modulate the initial triggering of cytokine production through a number of other receptors (Huntington *et al.*, 2005). One of the cytokines whose expression is negatively regulated by CD45 is TNF

(Piercy *et al.*, 2006). In BMDMs and DCs lacking CD45, TLR7 stimulation lead to increased TNF- α and IL-6 production as well as enhanced NF-κB activity (Piercy *et al.*, 2006). Furthermore, CD45 was not only shown to negatively regulate TNF- α and IL-6 production via TLRs, but also reduced the response to cytokines such as IFN- α (Piercy *et al.*, 2006). Structural analysis of the receptor revealed that upon dimerization, CD45 activity is inhibited (Hermiston *et al.*, 2003). Dimerization is believed to be regulated via binding of CD45-AP (CD45 associated protein) as well as modifications of the extracellular domain including sialylation and O-glycosylation (Z. Xu *et al.*, 2002). Furthermore, CD45 phosphatase activity is regulated by phosphorylation of its phosphatase II domain at residues Ser990, Ser993, Ser994 and Ser998 where phosphorylation by CK2 induces enzyme activity (Y. Wang *et al.*, 1999).

In BMDMs treated with Compound A, phosphorylated CD45 was enriched by 3-fold (1.5 h) and 4.6-fold (3 h) compared to cells treated with the combination of Compound A and p38i (**Table 4.8**). For both timepoints, differentially phosphorylated CD45 was ranked in the top 30 of the most significant DP proteins. The detected phosphopeptide harbored the modified residues Thr1267 and Ser1286 which both have been described to become phosphorylated during large scale phosphoproteomic studies (**Figure 4.9**). However, their functional roles have not been determined yet. A number of observations support the notion that CD45 is in fact inhibited in the combination treatment but active when cells are treated with SM alone.

As described above, CD45 positively regulates Src family kinases including Lyn and Fyn. Although I was not able to detect phosphorylated Lyn and Fyn via mass spectrometry, phosphorylated Fyb (Fyn binding protein), which has also been indicated to interact with

CD45 (Linhua Zhang, 2005 unpublished), was strongly enriched in Compound A treated BMDMs (**Table 4.9**). Two phosphosites that were identified following using mass spectrometry, Tyr559 and Ser561, are located within the C-terminal region of Fyb (**Figure 4.10**). Both residues are conserved across mouse, rat and human FYB. Phosphorylation by Fyn of Tyr584 and Tyr687 is required for binding of the SH2 domain-containing leukocyte phosphoprotein of 76 kDa (SLP-76) (Geng *et al.*, 1999; Veale *et al.*, 1999). Although phosphorylation of neither of these residues were observed, the close proximity of Tyr559 and Ser561 to the residue Tyr584 is again indicative of the detected phosphorylation being of functional importance. According to phosphosite.org, phosphorylation of CD45 on Tyr559 is the most cited modification, although it has predominantly been observed in T cells.

As mentioned above, activation of Fyb via tyrosine phosphorylation can be induced by Fyn (Veale *et al.*, 1999). Searching the phosphorylated peptide sequence that contained the modified residue Tyr559 for kinase motifs using the tool PhosphoMotif Finder, revealed that this phosphorylation could be catalyzed by a Src kinase family member. Although Tyr559 has not been described as a Fyn target in the literature, it is possible that this Src kinase family member in fact is responsible for the modification of this residue.

The notion that CD45 activity induced the activation of Src family kinases in BMDMs treated with Compound A is further supported by the detection of phosphorylated EVL in the same samples (**Table 4.10 & Figure 4.11**). EVL (En1/VASP-like protein) is an actin associated, cytoskeletal effector protein that, upon activation, associates with Fyb and SLP-76 downstream of Fyn (Krause *et al.*, 2000). Phosphorylated EVL (Ser329) was enriched in Compound A treated BMDMs by 2-fold in both timepoints while in the 3 h time point it was the 18$_{th}$ most

significant DP protein. Although phosphorylation of Ser329 has been frequently observed, it has not been assigned with a function yet. However, it is noteworthy that this modification has been identified in association with Akt and mTOR signaling (Minard *et al.*, 2016; Reinhard *et al.*, 1997; Y. Yu *et al.*, 2011). When searching the sequence of the phosphorylated peptide for a kinase motif, it was revealed that the phosphosite matches the motif of PKA. Interestingly, PKA is known for its ability to phosphorylate EVL leading to its activation and complex formation (Lambrechts *et al.*, 2000) further indicating that modification of Ser329 is activating the protein.

In summary, the presented evidence suggests that the treatment induced phosphorylation signature of CD45 reflects its activation status with the phosphatase being active when cells were treated with Smac mimetic alone. In these BMDMs, CD45 activity might suppress TNF-α production which is required for the induction of apoptosis in the absence of IAPs. However, more evidence is required to confidently attribute a role in the prevention of cell death in Smac mimetic-treated BMDMs to the receptor CD45. Experiments, where CD45 and IAPs are simultaneously inhibited would provide a powerful insight into the receptor's role in TNF- α production in those cells.

Table 4.8: Phosphorylation status of CD45 after treatment with SM + p38i

Protein	Residue(s)	Timepoint	logFc	Rank
CD45	**T1267/S1286**	1.5h	**-1.6**	**30**
CD45	**T1267/S1286**	3h	**-2.2**	**13**

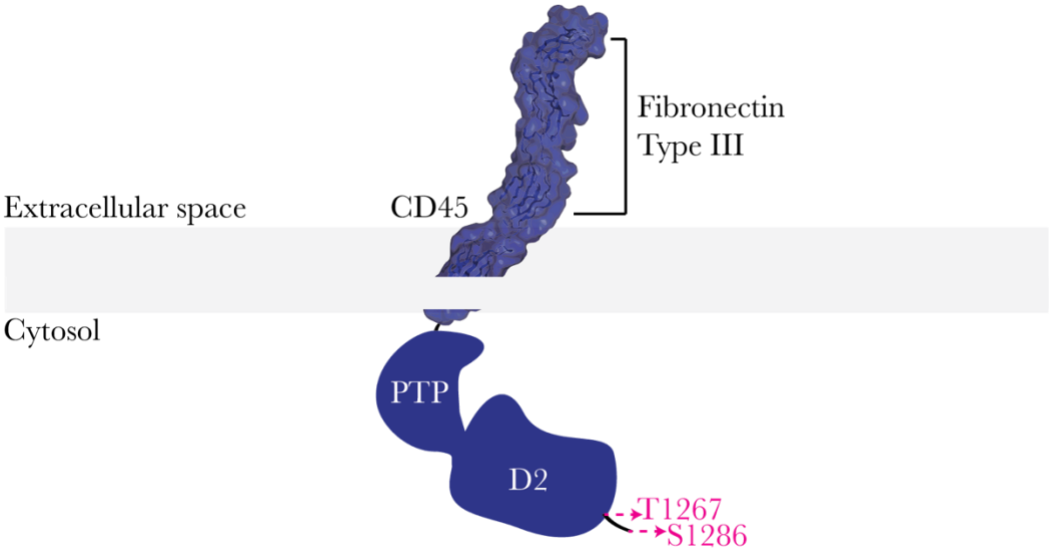

Figure 4.9: The phosphatase CD45 is a negative regulator of TNF production and is less phosphorylated in BMDMs treated with SM + p38i

Structural representation of CD45. The extracellular region contains a serine-threonine-rich domain followed by fibronectin type III-like repeats. The first membrane proximal domain has PTPase activity, while the second domain (D2) is lacking PTPase activity. However, the D2-domain is critical for proper folding and substrate recruitment. Residues shown in pink represent amino acids that have been identified to be phosphorylated in BMDMs treated with Compound A.

Table 4.9: Phosphorylation status of FYB after treatment with SM + p38i

Protein	Residue(s)	Timepoint	logFc	Rank
FYB	**S222**	1.5h	**-0.5**	**109**
FYB	**S89**	1.5h	**-2.7**	**142**
FYB	**Y559/S561**	3h	**-0.6**	**84**

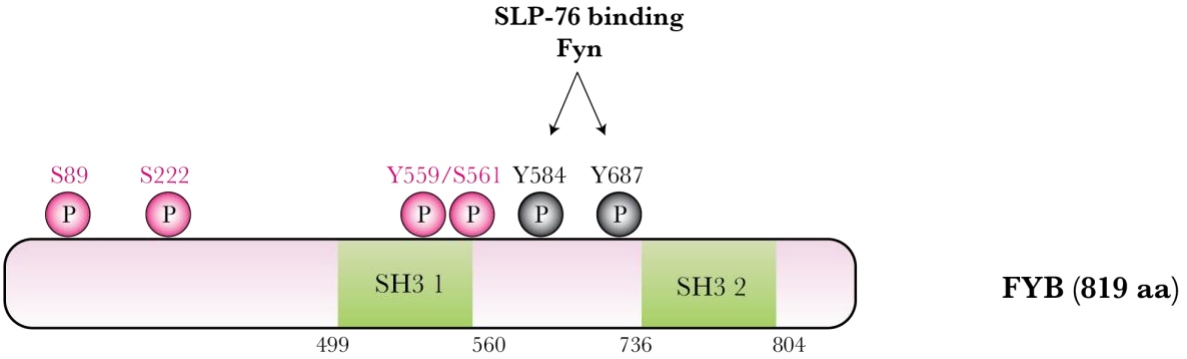

Figure 4.10: Fyn-binding protein (FYB) is a known interactor of CD45 and is less phosphorylated in BMDMs treated with SM + p38i

Schematic representation of Fyn-binding protein (FYB). The numbers refer to amino acids flanking the functional domains. Residues in pink represent phosphorylated amino acids identified in BMDMs treated with Compound A, while grey/black residues are known phosphosites that were not detected. Phosphorylation by Fyn of Y584 and Y687 is required for binding of the SH2 domain-containing leukocyte phosphoprotein of 76 kDa (SLP-76) (Geng *et al.*, 1999; Veale *et al.*, 1999). SH3 = Src homology 3 domain.

Table 4.10: Phosphorylation status of EVL after treatment with SM + p38i

Protein	Residue(s)	Timepoint	logFc	Rank
EVL	**S329**	1.5h	**-0.6**	**96**
EVL	**S329**	3h	**-1.0**	**18**
EVL	**S329**	3h	**-1.0**	**73**

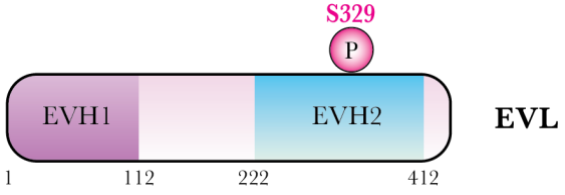

Figure 4.11: En1/VASP-like protein (EVL) is an interactor of FYB and is less phosphorylated in BMDMs treated with SM + p38i

Schematic representation of En1/VASP-like protein (EVL). The numbers refer to amino acids flanking the functional domains. Residue in pink represents the phosphorylated amino acid identified in BMDMs treated with Compound A. The EVH2 domain is required for binding of actin and oligomerisation. EVH1 = Ena/Vasp like homology domain 1; EVH2 = Ena/Vasp like homology domain 2.

4.6.2.2 CD84 phosphorylation upon the combined inhibition of IAPs and p38 might contribute to the activation of MAP kinases and NF-κB

CD84 is a self-ligand receptor and member of the signaling lymphocyte activation molecule (SLAM) protein family which is expressed in a variety of immune cells, including monocytes and macrophages (Sintes *et al.*, 2010). Using siRNA knockdown of CD84 in macrophages, it was revealed that the receptor plays a role in modulating LPS-induced production of inflammatory cytokines including TNF (Sintes *et al.*, 2010). When overexpressed in RAW-264.6 macrophages, CD84 induced MAP kinase phosphorylation and NF-κB activation which was accompanied by an escalation in TNF secretion (Sintes *et al.*, 2010). Within its cytoplasmic tail, CD84 has two conserved intracellular tyrosine-based switch motifs (ITSM) (**TVY**265AVV and **TIY**300SSV) whose involvement in the mediation of cytokine production has been described (Sintes *et al.*, 2010). Interestingly, the dually phosphorylated peptide that was enriched in BMDMs treated with the combination of Compound A and p38i by 2-fold after 3 h contained two modified residues, Ser260 and Thr263, that are either in close proximity (Ser260) or within the first ITSM (Thr263) (**Table 4.11 & Figure 4.12**). This ITSM is indispensable for the recruitment of SAP (SH2 domain-containing cytoplasmic adaptor

protein SLAM-associated protein) which occurs upon TLR signaling and is followed by MAPK phosphorylation and NF- κB activation. Although SAP binding can be initiated by tyrosine phosphorylation of Tyr265, modification of this residue is not required for their association (Tangye *et al.*, 2003). As described previously, in BMDMs treated with Smac mimetic and a p38 inhibitor, we observe strong activation of the MAP kinases ERK1/2 and JNK1/2 which is accompanied by an increase in TNF secretion. We can therefore speculate that ITSM phosphorylation of CD84 may lead to the recruitment of SAP and the activation of the MAP kinase pathways ERK1/2 and JNK1/2, contributing to the increased phosphorylation of these kinases and the subsequent rise in TNF secretion. How the self-ligand receptor CD84 became phosphorylated and potentially activated, remains unclear. To confirm, that CD84 phosphorylation plays a significant role in the activation of the MAP kinases ERK1/2 and JNK1/2 and the subsequent induction of TNF secretion, further experiments involving the inhibition of CD84 and the generation of CD84 phospho mutants are required.

Table 4.11: Phosphorylation status of CD84 after treatment with SM + p38i

Protein	Residue(s)	Timepoint	logFc	Rank
CD84	S260/T263	3h	1.1	188

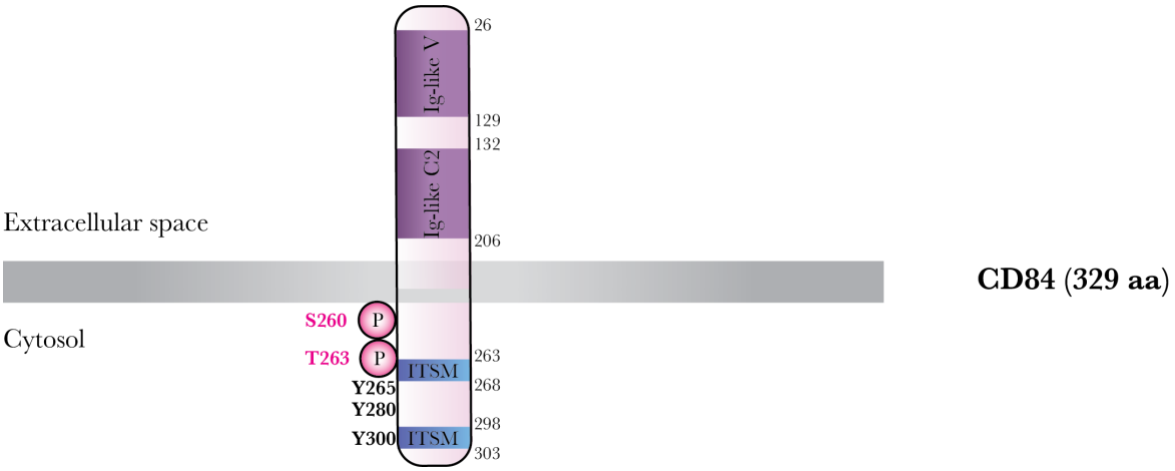

Figure 4.12: The receptor CD84 can induce TNF secretion through activating MAP kinases and is phosphorylated in BMDMs treated with SM + p38i

Schematic representation of CD84. The numbers refer to amino acids flanking the functional domains. Residues in pink represent phosphorylated amino acids identified in BMDMs treated with Compound A, while black residues are known phosphosites that were not detected. ITSM is indispensable for CD84 activity and subsequent MAPK phosphorylation and NF-κB activation which also requires phosphorylation of Y300 (Sintes *et al.*, 2010). ITSM = immunoreceptor tyrosine-based switch motifs.

4.6.2.3 NFAM1 was preferentially phosphorylated in BMDMs treated with Compound A, potentially leading to its inactivation and the suppression of TNF-α promoter transcription

NFAM1 (NFAT1 activation molecule 1) is an immunoreceptor tyrosine-based activation motif (ITAM)-bearing cell surface molecule belonging to the Ig superfamily which is predominantly expressed in B- and T-cells as well as macrophages and neutrophils (Ohtsuka *et al.*, 2004). Upon phosphorylation of two tyrosine residues within the ITAM by Src family kinases, ZAP-70/Syk is recruited to phospho-ITAM (Ohtsuka *et al.*, 2004). Binding and subsequent activation of ZAP-70/Syk in turn transduces a downstream signaling cascade by phosphorylating a number of effector molecules leading to Ca_{2^+}-influx and the activation of the

calcium-dependent phosphatase calcineurin (Sambandam *et al.*, 2017). Upon activation, calcineurin dephosphorylates NFAT (nuclear factor of activated T cells) causing it to translocate to the nucleus where NFAT shows increased transcriptional function (Kiani *et al.*, 2000; Macian *et al.*, 2001).

When first identified, NFAM1 was characterized as a protein whose expression activated the transcription of TNF-α promoters, which was mediated through the calcineurin/NFAT-signaling pathway (J. Yang *et al.*, 2003). As described above, to activate NFAM1, phosphorylation of two tyrosine residues within the ITAM, Tyr215 and Tyr226, is required to initiate its activation and to subsequently induce the expression of TNF-α promoters. Phosphorylated NFAM1 appeared in the top 4 most significant DP proteins for both time points upon treatment and was found to be enriched 4-fold in BMDMs treated with Compound A (**Table 4.12**). The modified residues were identified as Ser235 and Ser241 which, interestingly, are located in close proximity to the ITAM (**Figure 4.13**). Although both phosphosites have been previously reported, no functional association has been made to date. If phosphorylation of Ser235 and Ser241 lead to NFAM1 activation, we would expect to detect activated calcineurin/NFAT-signaling characterized by Ca_{2+} influx and increased TNF-α expression. However, indications for the occurrence of these events were found in BMDMs treated with the combination of Compound A and p38i, where phospho-NFAM1 was detected at lower rates. Suggestive of increased Ca_{2+} influx in cells exposed to the combination treatment was the observation of phosphorylated CLCC1 (Chloride channel CLIC-like protein 1) which was significantly enriched by 4.6-fold in these samples. Although CLCC1 is a chloride channel, it has also been suggested to be calcium sensitive and interactions with calreticulin, a major calcium binding protein, have been recently reported (Li *et al.*, 2018). The detected

cytoplasmic phosphosites Ser429-p and Ser433-p are both conserved across mice, humans and rats and although their functions remain unknown, the modified residues are the two most commonly reported CLCC1phosphosites (Phosphosite.org)

Another indicator for enhanced Ca_{2+} influx in BMDMs treated with Compound A and p38i was the detection of CaMKK2 (Calcium/calmodulin-dependent protein kinase 2) being preferentially phosphorylated in these cells. Here, phospho-CaMKK2 was enriched by 2-fold. The identified phosphosite Ser495-p is located within CaMKK2's calmodulin binding site, while the amino acid sequence surrounding this residue matches the calmodulin-dependent protein kinase II substrate motif (**Figure 4.13**). CaMKK2 activity is stimulated in response to Ca_{2+} signals and isoforms lacking the calmodulin-binding domain are inactive (L. S. Hsu *et al.*, 2001). In light of this information, it is possible that phosphorylation of the calmodulin binding motif at Ser495 reflected activated CaMKK2 which in turn would be indicative of increased Ca_{2+} influx in BMDMs treated with the Compound A/p38i combination.

If Ca_{2+} influx was in fact increased upon combination treatment, it would be plausible that phosphorylated NFAM1 detected in BMDMs treated with only Compound A represented the inactive form of this ITAM-bearing receptor. Given the close proximity of the modified residues Ser235-p and Ser241-p to the ITAM, whose phosphorylation leads to NFAM1 activation, it appears reasonable to suggest that the identified phosphosites contribute to the inhibition of the protein. Consequently, if NFAM1 activation was prevented in smac mimetic treated cells, NFAT-induced transcription of TNF-α promoters would also fail to occur. Although the correlations I have presented here are highly speculative and require further research, the fact that phospho-NFAM1 was ranked in the top 4 most significant DP proteins

for both timepoints, strongly suggests a role for this receptor in the treatment responses observed for BMDMs.

Table 4.12: Phosphorylation status of NFAM1 after treatment with SM + p38i

Protein	Residue(s)	Timepoint	logFc	Rank
NFAM1	**S235/S241**	1.5h	**-2.1**	**4**
NFAM1	**S241**	1.5h	**-1.0**	**56**
NFAM1	**S235/S241**	3h	**-2.0**	**4**
NFAM1	**S241**	3h	**-0.8**	**149**

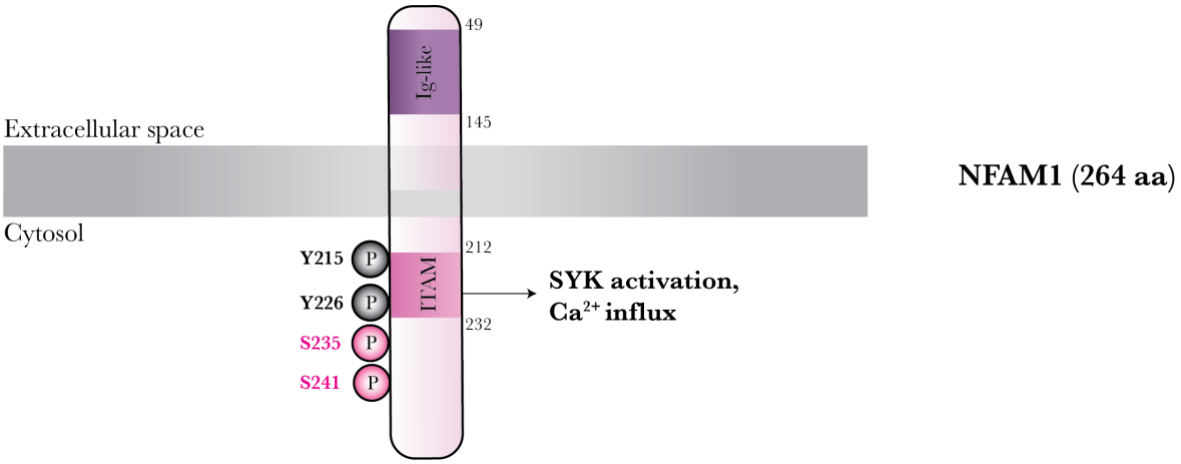

Figure 4.13: NFAT activation molecule 1 (NFAM1) becomes phosphorylated within its ITAM in BMDMs treated with SM

Schematic representation of NFAT activation molecule 1 (NFAM1). The numbers refer to amino acids flanking the functional domains. Residues in pink represent phosphorylated amino acids identified in BMDMs treated with Compound A, while grey/black residues are known phosphosites that were not detected. Phosphorylation of Y215 and Y226 is required for protein activity leading to activation of downstream targets and Ca_{2+} influx. ITAM = immunoreceptor tyrosine-based activation motif.

4.6.2.4 The transcription factor ATF2 was preferentially activated upon the combined treatment of Compound A and p38i possibly inducing TNF expression

Activating transcription factor 2 (ATF2) belongs to the ATF/cAMP-response element-binding protein family of basic region-leucine zipper proteins, where it plays an important role in the cellular stress response (Livingstone *et al.*, 1995; Maekawa *et al.*, 1989; van Dam *et al.*, 1995). Target genes of ATF2 include TNF-α, TGF- β, cyclin and c-jun all of which are genes that are known to be involved in stress response, cell growth and differentiation, immune response and cell death (S. J. Kim *et al.*, 1992; Shimizu *et al.*, 1998; Tsai *et al.*, 1996; van Dam *et al.*, 1993). Its importance for TNF-α production has been convincingly demonstrated when the genetic deletion of ATF2 lead to the suppression of TNF-α expression (T. Yu *et al.*, 2014).

ATF2 transcriptional activity is induced by the dual phosphorylation of Thr51 and Thr53 by MAP kinases. Here, JNK1/2 and p38 have been described to phosphorylate Thr51, while phosphorylation of Thr53 is predominantly mediated by ERK1/2 (Ouwens *et al.*, 2002).

In BMDMs treated with Compound A and p38i, phospho-ATF2 was enriched by 2-fold in both timepoints while total ATF2 levels were consistent across all samples (**Table 4.13; Figure 4.14 B**). Interestingly, the detected phosphopeptide harbored the described modified residues Thr51 and Thr53 indicating that the transcription factor was activated upon the combination treatment (**Figure 4.14 A**). Since both ERK1/2 and JNK1/2 are also strongly activated under these conditions, this observation was in line with our current knowledge of treatment induced signaling. Activated ATF2 could therefore have contributed to the increased expression of TNF in these BMDMs.

Table 4.13: Phosphorylation status of ATF2 after treatment with SM + p38i

Protein	Residue(s)	Timepoint	logFc	Rank
ATF2	**T51/T53**	1.5h	**0.8**	**151**
ATF2	**T51/T53**	3h	**0.5**	**183**

Figure 4.14: Activating transcription factor 2 (ATF2) is important for TNF-α production and is phosphorylated in BMDMs treated with SM + p38i while total ATF2 levels are consistent across all treatments

(A) Schematic representation of activating transcription factor 2 (ATF2). The numbers refer to amino

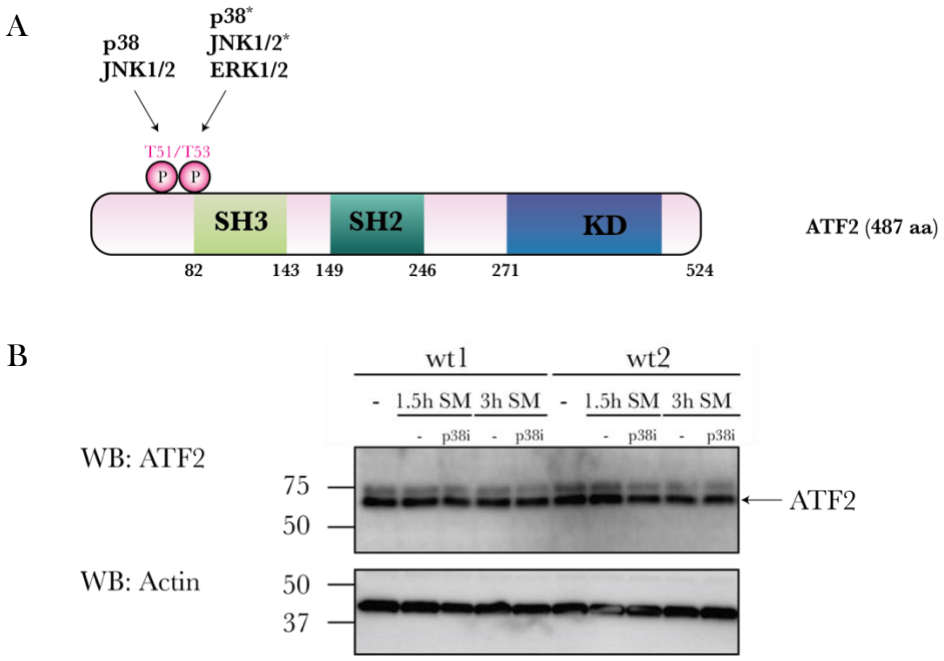

acids flanking the functional domains. Residues in pink represent phosphorylated amino acids identified in BMDMs treated with Compound A and p38i. ATF2 transcriptional activity is induced by the dual phosphorylation of Thr51 (JNK1/2, p38) and Thr53 (predominantly ERK1/2, less: JNK1/2 and p38). SH2/SH3 = Src homology 2/3 domain; KD = kinase domain. (B) BMDMs from six mice were treated with DMSO (untreated control), Compound A (SM, 500 nM) alone or in the presence of p38 inhibitor LY (1 μM) for 1.5 h or 3 h. Lysates of treated BMDMs were subjected to Western blotting and membranes were probed for ATF2 to determine if differential phosphorylation was caused by varying ATF2 expression levels. Probing for actin served as a loading control. The blot is representative of six biological replicates.

Table 4.14: Differentially phosphorylated regulators of TNF production in BMDMs treated with SM

Protein	Regulator of TNF	Timepoint	logFc
CD45	negative	1.5h	-1.6
CD45	negative	3h	-2.2
CD84	positive	1h	1.1
NFAM1	positive	1.5h	-2.1
NFAM1	positive	1.5h	-1.0
NFAM1	positive	3h	-2.0
NFAM1	positive	3h	-0.8
ATF2	positive	1.5h	0.8
ATF2	positive	3h	0.5

4.6.3 Cell survival pathways

4.6.3.1 Novel phosphorylation sites in CSF1R might facilitate treatment-induced cell death by inhibiting the activation of PI3K/Akt

One of the most compelling hits identified during the phosphoproteomics screen was the macrophage colony-stimulating factor 1 receptor (CSF1R) since it is involved in a number of pathways that were strongly enriched upon KEGG pathway analysis (MAPK, Rap1, PI3K-Akt and Ras signalling pathways). Of the four detected phosphoserines on CSF1R, two have never been reported before (S731, S734) while the two that have been described in the literature (S711, S714) have no known function. The four serines appeared to be preferentially phosphorylated upon treatment with the combination of Compound A and p38i for 3 h (**Figure 4.15 & Figure 4.16; Table 4.14**) with the median increase in phosphorylation compared to the single agent treatment being approximately 4-fold (logFc = 2.1).

CSF1R is a tyrosine-protein kinase which acts as a cell surface receptor for the cytokines CSF1 and IL-34 is primarily expressed on monocytes and macrophages (Nakamichi *et al.*, 2013;

Sasmono *et al.*, 2003). In those cell types, CSF1R-mediated signalling plays an essential role in survival, proliferation and differentiation (Chang *et al.*, 2009; Kelley *et al.*, 1999; Murray *et al.*, 2000; Tushinski *et al.*, 1983). A number of phosphorylation sites and their contribution to signalling through this receptor have been well described in the literature (**Figure 4.16**). When projecting the detected phosphoserines onto the sequence of activated CSF1R, their proximity to Tyr721, a tyrosine residue that can be phosphorylated via autophosphorylation and that is essential for the interaction with PI3K, was striking (Stanley *et al.*, 2014). The four serine residues flank Tyr721 in pairs with the maximal distance between a phosphoserine and Tyr721 being only 13 amino acids (Ser734). I hypothesised that the simultaneous phosphorylation of Ser711, Ser714, Ser731 and Ser734 could negatively impact the phosphorylation of Tyr721 by inhibiting autophosphorylation of that residue, preventing the interaction of CSF1R with PI3K. Since this interaction is required for the phosphorylation and activation of Akt, I further hypothesized that phosphorylation of the four serines could negatively regulate Akt activation.

Table 4.15: Phosphorylation status of CSF1R after treatment with SM + p38i

Protein	Residue(s)	Timepoint	logFc	Rank
CSF1R	S731/S734	3h	2.1	10
CSF1R	S711/S714	3h	1.8	49
CSF1R	S711/S714	3h	1.7	58
CSF1R	S711/S714	3h	1.2	181
CSF1R	S731/S734	3h	1.3	211

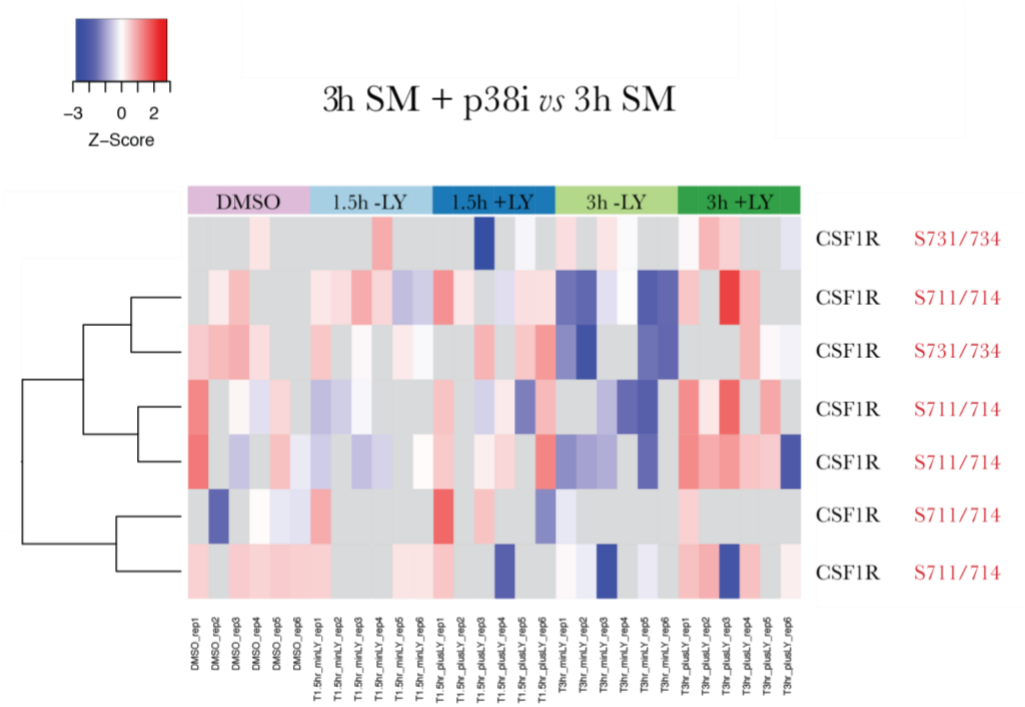

Figure 4.15: CSF1R was preferentially phosphorylated upon 3 h treatment with Compound A and p38i

Heatmap and hierarchical clustering of phosphorylated CSF1R. Changes in phosphorylation induced by treatment for 1.5 h and 3 h with Compound A (911) in the absence (minLY) and presence (plusLY) of p38 inhibitor (LY) are indicated by the colours red (upregulated in the combination) or blue (downregulated in the combination). Grey bars represent missing values. Z-scores for each replicate in each condition was determined and coloured as shown in the scale bar.

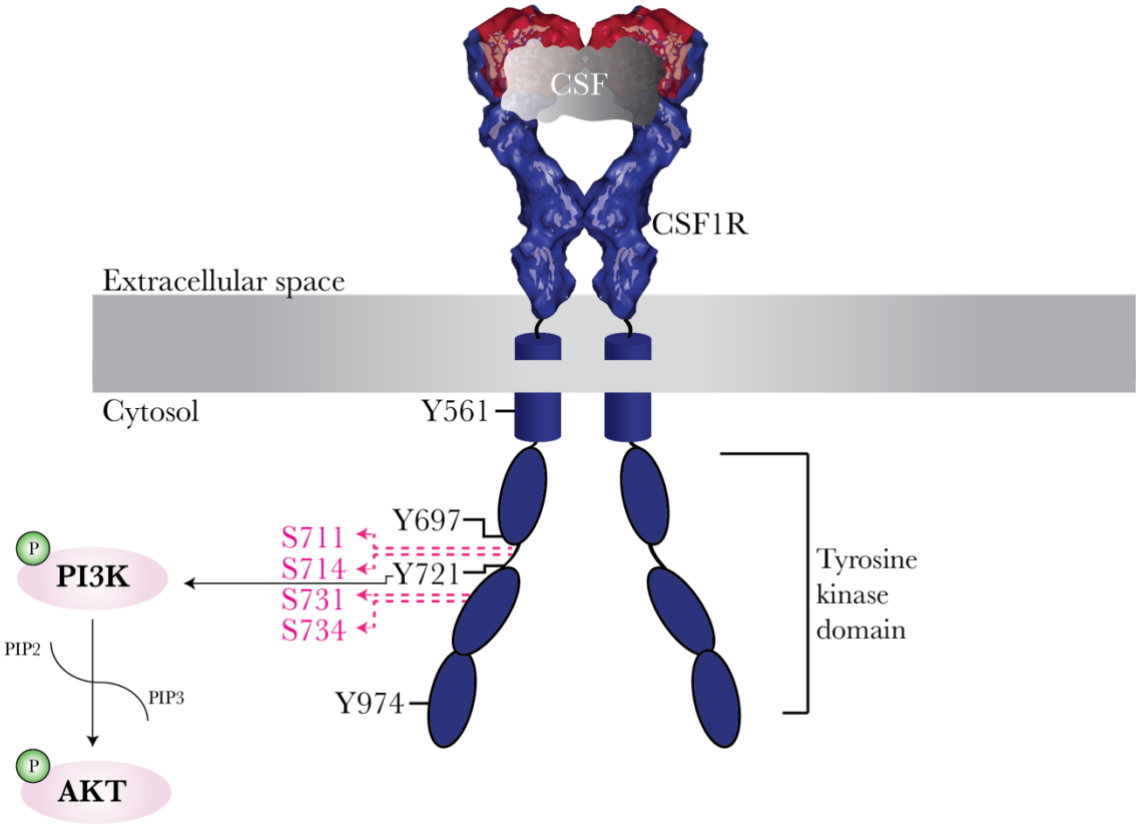

Figure 4.16: The structure of the CSF1 receptor

Schematic representation of the receptor for macrophage colony-stimulating factor (M-CSF) showing subunits, structural elements and phospho-sites of known function (black) as well as treatment-induced phosphorylated residues identified during phosphoproteomics analysis. CSF1R is a homodimeric type III receptor tyrosine kinase (Hamilton, 2008). Phospho-Y721 is required for the phosphorylation and activation of phosphoinositide-3-kinase (PI3K) which in turn phosphorylates phosphatidylinositol (4,5)-bisphosphate (PIP2) leading to the activation of Akt. Residues S711, S714, S731 and S734 (pink) flank Y721 and are preferentially phosphorylated when BMDMs are treated with Compound A and p38i which might prevent the phosphorylation of Y721 reducing CSF1R activity.

To investigate the role of the four CSF1R serine residues that are preferentially phosphorylated upon combination treatment after 3 h, I first sought to verify if all serines are conserved across various species. An alignment of mouse, rat and human CSF1R sequences of the region containing these residues, revealed that in fact mouse Ser711, Ser714, Ser731

and Ser734 are conserved in human and rat CSF1R (**Figure 4.17**). This finding supported the hypothesis, that phosphorylation of the four serines might be functionally relevant for CSF1R signal transduction.

To identify the role these phosphorylation sites could play in the interaction of CSF1R and PI3K and the subsequent activation of Akt, I next determined the levels of phospho-Akt (Ser473) in the lysates of treated BMDMs (**Figure 4.18**). When analysing the Western blots for phospho- and total Akt, it became apparent that while Akt levels remained unchanged across all samples, the combined inhibition of IAPs and p38 lead to a decrease in Akt phosphorylation at Ser473 after 1.5 h and 3h of treatment. Notably, Akt appeared to be phosphorylated and therefore activated in untreated BMDMs and its activation did not increase upon addition of Compound A. A time dependent activation of Akt however could be observed with phosphorylation levels being increased in both treatments after 3 h. Since phospho-Akt levels were decreased in the combination treatment compared to the untreated samples, it is likely that the addition of p38i lead to the active suppression of Akt activation. This conclusion supports the hypothesis that the phosphorylation sites in CSF1R enriched in the combination treatment, have an inhibitory function. It should be stated, however, that the signalling kinetics observed for Akt phosphorylation via Western blotting and CSF1R modification by mass spectrometry did not support the assumption that CSF1R acted as an upstream mediator of Akt. According to the phosphoproteomics data, CSF1R phosphorylation was significantly increased in the combination treatment after 3h while a reduction of Akt phosphorylation as observed via Western blotting was most prominent in BMDMs treated with Compound A and p38i for 1.5 h. It is possible that CSF1R is in fact not a primary mediator of Akt activity and its phosphorylation is rather a secondary event induced

by the increased activity of another kinase that is also regulating PI3K signalling. Another explanation for the observed discrepancies in signalling kinetics could be that CSF1R is already being phosphorylated at an earlier time point but variations in levels of total CSF1R masked these events. If CSF1R was more abundant in the 3 h samples compared to the 1.5 h, phosphorylated peptides could have been detected at higher intensities as a consequence. It is noteworthy that in BMDMs treated with Compound A for 1.5 h, we observed the most missing values for phosphorylated CSF1R-derived peptides as can be seen in the heatmap in **Figure 4.15**. Missing values indicate that a peptide was not detectable in the respective sample, likely caused by a low abundancy of the peptide. When performing statistical analysis however, these missing values can lead to a decrease in significance of observed differences or they can even prevent the evaluation of such when no peptide is detected for any of the six replicates. To investigate whether the increase in CSF1R phosphorylation after 3 h compared to the 1.5 h timepoint was caused by an increase of CSF1R expression, total CSF1R levels needed to be determined either via Western blotting or by analysing the total proteome using mass spectrometry. Time constraints and the lack of an antibody suitable for the immunohistochemical detection of CSF1R prevented me from doing either. I was therefore unable to address the observed discrepancies in signalling kinetics.

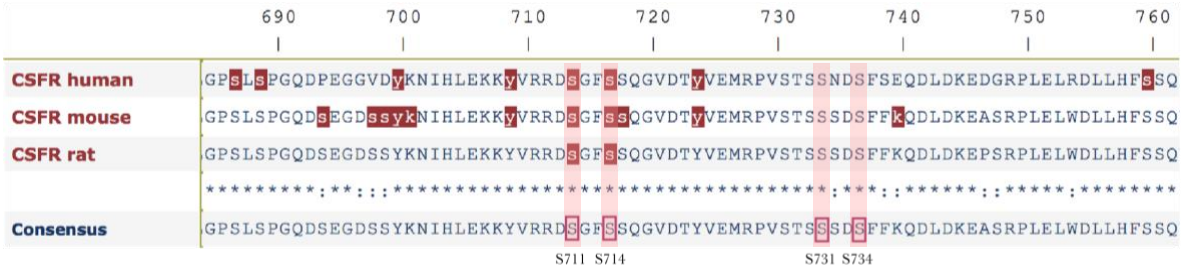

Figure 4.17: The four detected phosphoserines S711, S714, S731 and S734 are conserved across human, mouse and rat CSF1R

Sequence alignment of human, mouse and rat CSF1R using Clustal Omega (Phosphosite.org). Phosphorylated residues are boxed in dark red. Treatment-induced differentially phosphorylated

residues are boxed in light red. All four detected residues are conserved across the three analysed species. S711 and S714 are known phosphosites while phosphorylation of S731 and S734 is a novel observation. Conservation and consensus were calculated using von Neumann entropy from PFAAT.

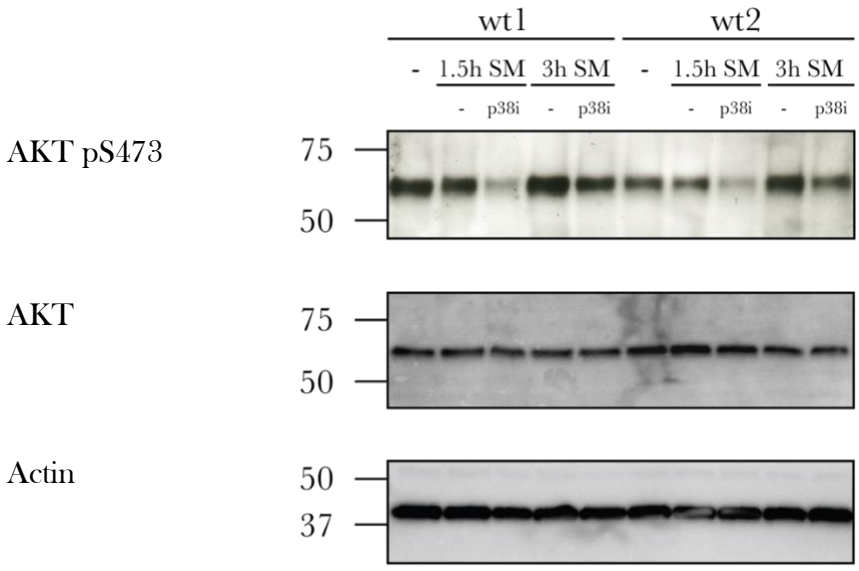

Figure 4.18: Akt is less phosphorylated at S473 in BMDMs treated with the combination of Compound A and p38i

BMDMs from six mice were treated with DMSO (untreated control), Compound A (SM, 500 nM) alone or in the presence of p38 inhibitor LY (1 μM) for 1.5 h or 3 h. Lysates of treated BMDMs were subjected to Western blotting and membranes were probed for phospho-Akt (p-Ser473) and Akt to determine if the combination treatment of SM and p38i prevents the activation/phosphorylation of Akt. Probing for actin served as a loading control. The blot is representative of two independent experiments.

Nonetheless, I further investigated the role of CSF1R in the synergistic killing of SM and p38 inhibition. To do so, I treated BMDMs with a combination of Compound A and AFS-98, a monoclonal antibody commonly applied to inhibit CSF1R *in vivo* and *in vitro* (Sudo *et al.*, 1995), for 6 and 24 h and subsequently measured occurring cell death via PI uptake and flow cytometry (**Figure 4.19**). Firstly, at a concentration of 33 nM AFS-98 did not kill on its own. However, when combined with Compound A, CSF1R inhibition induced synergistic cell death which was most apparent after 24h. After 6h, when the combination of 500 nM Compound

A and LY causes a cell death rate of almost 70%, cell death induced by the same concentration of the smac mimetic and the addition of AFS-98 was determined to be only approximately 45%. A stronger synergistic effect occurred after 24 h treatment when the simultaneous inhibition of CSF1R and the IAPs with 500 nM Compound A resulted in the killing of over 90% of cells, the same as for the combination of Compound A and p38i. At lower concentrations however, the combination of Compound A and AFS-98 was less effective than Compound A with p38i. Nonetheless, the measured cell death for the AFS-98/Compound A combination was consistently higher than for the treatment with Compound A as a single agent. With AFS-98 failing to induce killing on its own, it can be concluded that the inhibition of CSF1R and the IAPs results in synergistic cell death in BMDMs. This data strongly suggests a role for CSF1R in preventing smac mimetic-induced killing and supports the hypothesis, that the identified phosphorylation sites have an inhibitory effect on CSF1R signalling.

To investigate if activation of the cell survival pathway PI3K/Akt is responsible for the prevention of cell death in smac mimetic-treated cells, I screened the phosphoproteomics data for further evidence such as activated downstream targets.

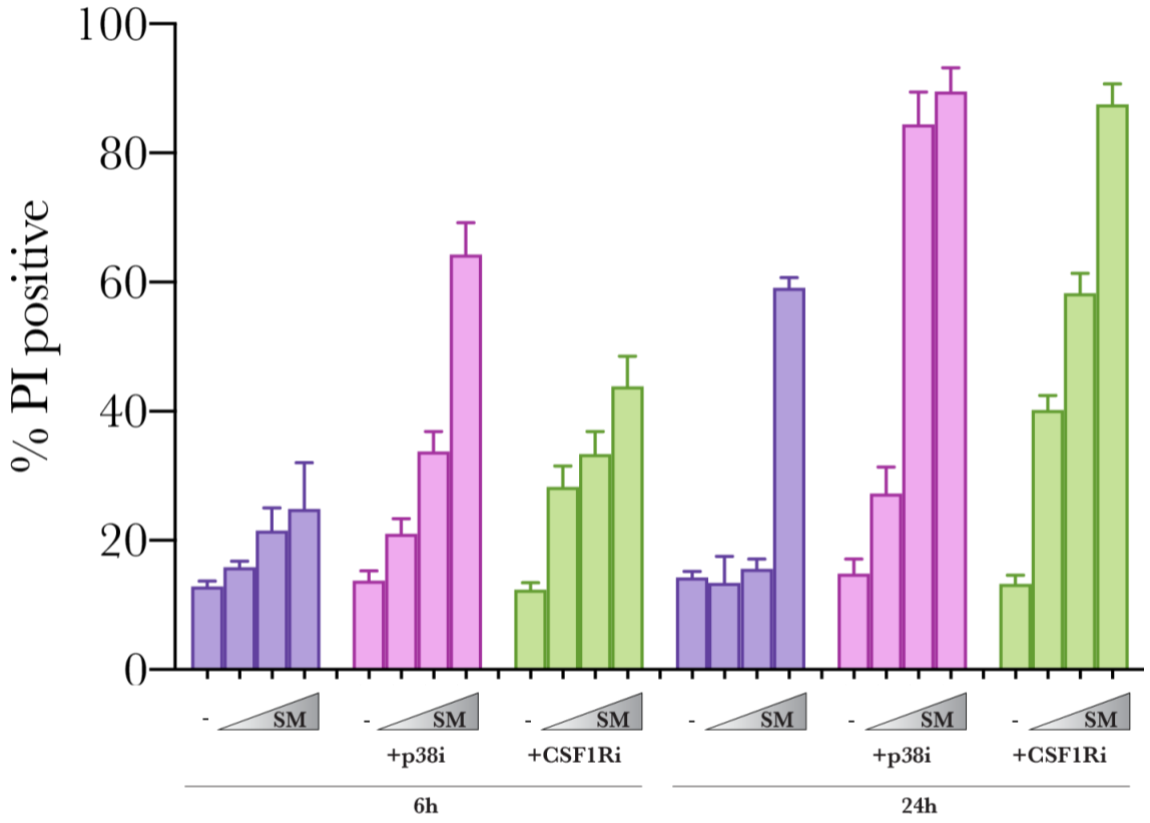

Figure 4.19: Combination of Compound A with CSF1R inhibitor AFS-98 induces cell death in BMDMs

Analysis of cell death by propidium iodide uptake and flow cytometry. Wild-type BMDMs were seeded in 24-well plates at 5 x 10_4 cells/well and treated with Compound A (SM, 50-500 nM) alone or in combination with LY2228820 (p38i, 1 μM) or AFS-98 (CSF1Ri, 33nM) for 6 or 24 hours. Resulting cell death was measured via PI uptake using flow cytometry. DMSO was added to untreated controls at 0.2% (v/v). Individual values, mean and SEM are shown of two independent experiments.

4.6.3.2 The PI3K/Akt/mTOR pathway promotes cell survival

Stimulated by receptor tyrosine kinase (RTK) signaling, the PI3K/Akt/mTOR pathway promotes survival upon cellular stress by activating translation initiation factors and ribosomal proteins that induce the expression of proliferative and pro-survival proteins (Datta *et al.*, 1999). The inappropriate activation of this pathway has been observed in many cancers where it leads to a profound disturbance of cell growth and survival which can amongst other things

contribute to therapy resistance (Porta *et al.*, 2014). Thus, the PI3K/Akt/mTOR pathway represents an attractive therapeutic target for the development of novel cancer treatments (Y. L. Chen *et al.*, 2005; Hennessy *et al.*, 2005).

The KEGG pathway analysis on proteins that were differentially phosphorylated in BMDMs treated with SM alone or in combination with p38i, revealed an enrichment of proteins that participate in the PI3K/Akt and mTOR pathways (**Table 4.15**). **Figure 4.20** illustrates how CSF1R activation can induce the PI3K/Akt/mTOR pathway leading to cell survival signaling through a succession of phosphorylations involving the mTORC1.

Table 4.16: Treatment-induced DP Proteins of the PI3K/Akt and mTOR pathways in BMDMs

Pathway	Proteins	Timepoint	Rank
PI3K/AKT	Atf2,Bcl2l11,Csf1r,Eif4b,Hsp90aa1,Rps6,Spp1	1.5h	10
PI3K/AKT	Atf2,Csf1r,Eif4b,Eif4ebp1,Mapk3,Ppp2r5d,Rps6,Spp1	3h	8
mTOR	Akt1s1,Clip1,Eif4b,Rps6,Rps6ka3,Ulk1	1.5h	8
mTOR	Eif4b,Eif4ebp1,Mapk3,Rps6,Rps6ka3	3h	25

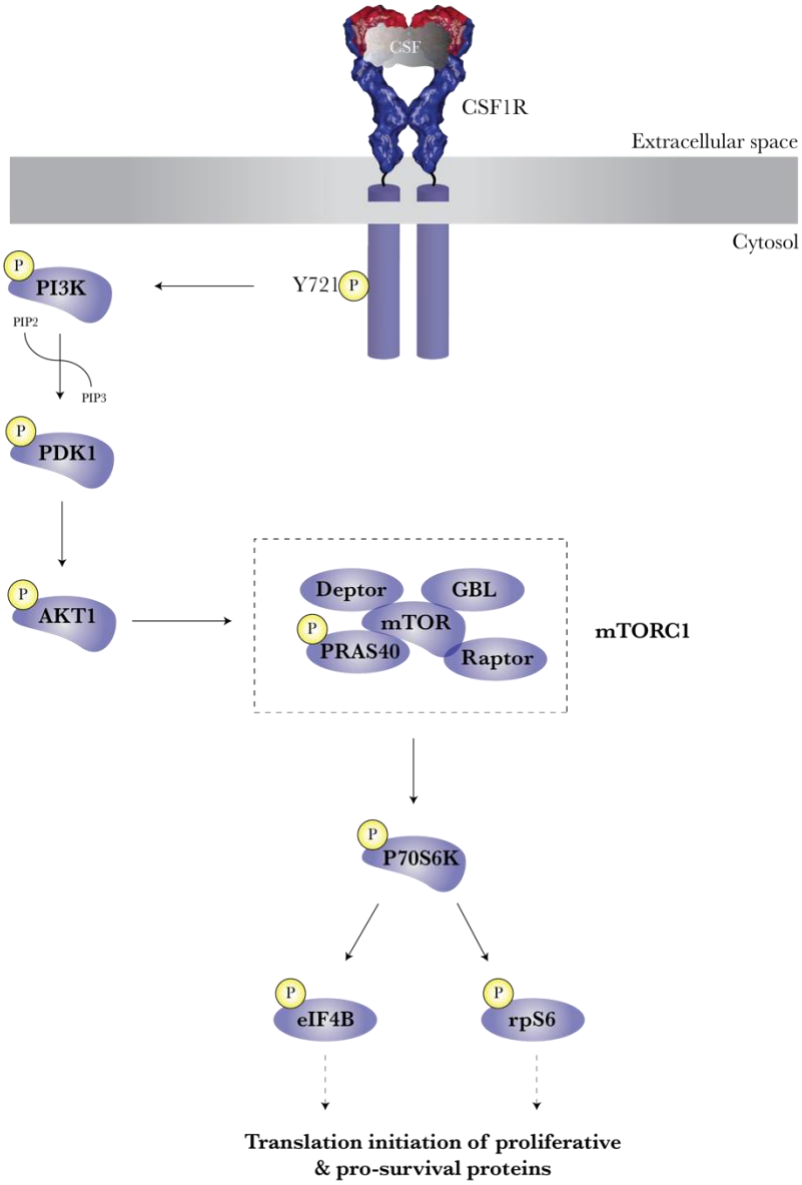

Figure 4.20: The PI3K/Akt/mTor pathway can be activated by binding of CSF to its receptor CSF1

Overview of the PI3K/Akt/mTor pathway. Binding of CSF to CSF1R induces receptor dimerization, autophosphorylation of Y721 and activation of PI3K. Phospho-PI3K in turn phosphorylates PIP2 leading to the phosphorylation of PDK1 and subsequent activation of Akt. Phospho-Akt stimulates mTORC1 through phosphorylation of PRAS40, a negative regulator of mTOR (Dan *et al.*, 2014). Activation of mTORC1 leads to the phosphorylation of its substrate p70S6K which finally activates the translation initiation factors eIF4B and the ribosomal protein rpS6 leading to the translation of proliferative and pro-survival proteins.

4.6.3.3 PI3K/Akt/mTOR targets are preferentially phosphorylated in Smac mimetic treated BMDMs

When screening the phosphoproteomics data for downstream targets of PI3K/Akt/mTOR signaling, a number of hits including direct Akt substrates were found to be predominantly enriched in BMDMs treated with Compound A for both time points. This further supported the hypothesis that these pathways may play a critical role in cell survival in BMDMs treated with Smac mimetics. In the following I will discuss the most significant DP proteins that have been associated with PI3K/Akt/mTOR signaling.

4.6.3.4 Phosphorylation of PRAS40, an Akt substrate, leads to activation of mTORC1

Proline-rich Akt1 substrate 1 (PRAS40) is a subunit of mTORC1 which amongst other things regulates cell survival in response to hormonal and nutrient signals (L. Wang *et al.*, 2007). Within mTORC1, PRAS40 plays an inhibitory role by binding to regulatory-associated protein of mTOR (raptor) (L. Wang *et al.*, 2007). Phosphorylation at T247 by Akt releases PRAS40 from raptor and facilitates its binding to 14-3-3, allowing mTORC1 signaling to be activated (Nascimento *et al.*, 2010). When exploring the phosphoproteome of treated BMDMs, I discovered phospho-PRAS40 to be significantly enriched 2-fold in cells treated with Compound A for 1.5 h (**Table 4.14; Figure 4.21**). The detected phosphosite is T247 making Akt the likely kinase that generated this modification. Consequently, the enrichment of this PRAS40 phosphopeptide following treatment with Compound A further supports that PI3K/Akt/mTOR signaling promotes cell survival in these cells.

Table 4.17: Phosphorylation status of PRAS40 after treatment with SM + p38i

Protein	Residue	Timepoint	logFc	Rank
PRAS40	T247	1.5h	-1.0	152

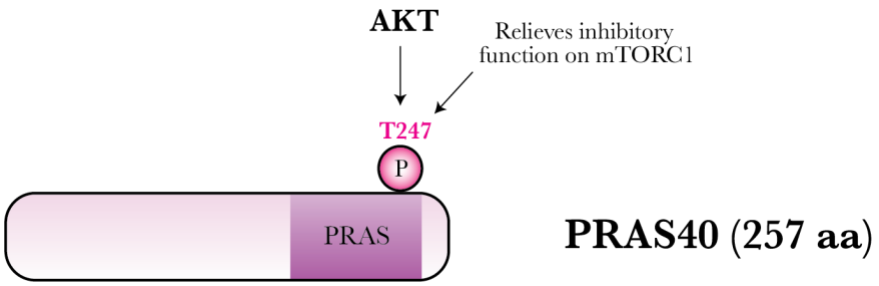

Figure 4.21: Phosphorylation of PRAS40 at T247 allows activation of mTORC1

Schematic representation of PRAS40, a negative regulator of mTOR. Phosphorylation of PRAS40 by Akt within its PRAS domain at T247 is known to relieve the inhibitory function of PRAS40 on mTOR enabling mTORC1 to become active. Phospho-PRAS40 (p-T247) was observed in BMDMs treated with Compound A.

4.6.3.5 RpS6, a downstream target of mTOR, is phosphorylated in BMDMs upon treatment with Smac mimetics

The 40 S ribosomal protein S6 (RpS6) is a component of the 40S subunit and is the major substrate of protein kinases in the ribosome (Nygard *et al.*, 1990). As a downstream target of mTOR, rpS6 is phosphorylated upon a vast number of stimuli which include mitogens, growth factors and tumor-promoting agents (Meyuhas, 2008; Roux *et al.*, 2007; Volarevic *et al.*, 2000). Regulated through phosphorylation, rpS6 impacts cell size, survival and migration by controlling the translation of 5'TOP (5′ terminal oligopyrimidine tract) mRNAs (Pende *et al.*, 2004). The translation of these mRNAs is selectively activated when resting cells are induced to grow or to proliferate (Tang *et al.*, 2001). Since rpS6 is regulated through phosphorylation,

selective inhibition of its phosphorylation has been shown to correlate with inhibition of cell proliferation (Lu *et al.*, 2019). Two families of kinases are known to phosphorylate and hence activate rpS6: p70 S6 kinases (RPS6Kbeta) and p90 ribosomal S6 kinases (RPS6Kalpha). Within these families, the kinases I will be referring to in the following are RPS6Kb1 (S6K1) which is a downstream target of mTORC1 and RPS6Ka3 (RSK2) which is activated as a result of ERK signaling. There are five clustered rpS6 phosphorylation sites that have been mapped to the residues Ser235, Ser236, Ser240, Ser244 and Ser247 and all of them are conserved from Drosophila to mammals (Ruvinsky *et al.*, 2006).

Upon treatment of BMDMs with Compound A, the five phosphorylated serines were identified to be enriched by 4.5-fold (1.5 h) or 6.5-fold (3 h) when compared to the combination treatment (**Table 4.15**). According to the literature, phosphorylation of Ser240 and Ser244 requires S6k1/2 activity while persistent phosphorylation of Ser235 and Ser236 is still observed upon genetic deletion of these kinases (Hutchinson *et al.*, 2011). Phosphorylation of Ser235 and Ser236 was found to be ERK-dependent with the kinases RSK1/2 being responsible for this type of rpS6 modification. In line with the described activation pathways of S6K1 and RSK2 through mTOR and ERK signaling respectively, phospho-S6K1 was enriched in BMDMs treated with Compound A alone for 1.5 h, while phospho-RSK2 was preferentially phosphorylated in the combination treatment in both timepoints (**Figure 4.22**). The detected S6K1-derived phosphopeptides revealed three phosphosites which consisted of Ser441, Thr444 and Ser447. All three phosphorylated residues are located within the autoinhibitory domain of S6K1 and have been described in the literature (Weng *et al.*, 1998). When generating phosphomimetic mutants by simultaneously replacing those serine and threonine residues with glutamic acid (S240E/T244E/S247E),

phosphorylation of Thr252 by PDK1 was facilitated leading to activation of the kinase (Keshwani *et al.*, 2011). Based on these observations and given that the detected Ser240/Ser244 rpS6 phosphorylation sites are known substrates of this kinase, the S6K1 phosphorylation events that preferentially occurred upon Smac mimetic treatment likely reflected its activated state. The RSK2 phosphopeptide harboring the phosphorylated residues Thr365/Ser369/Ser375 was strongly enriched in both timepoints of the combination treatment, where its detection was 3-fold (1.5 h) or 8-fold (3 h) increased compared to the single agent treatment (**Table 4.15**). Interestingly, these residues are located within the RSK2 AGC kinase domain (**Figure 4.22**). As mentioned above, RSK2 activation requires ERK signaling which is strongly enhanced upon combination treatment. Even more strikingly, the detected phosphorylations of T365 and S369 are known to be catalyzed by ERK1/2 leading to RSK2 activation (Vaidyanathan *et al.*, 2007). In contrast, phosphorylation of Ser715 was significantly enriched in BMDMs treated with Compound A alone after 1.5 h. Although its function is unknown, phosphorylated Ser715 has been described to occur upon Akt signaling which again correlates with it being preferentially detected in the Smac mimetic treated BMDMs (Humphrey *et al.*, 2013).

As described above, phosphorylation of rpS6 at residues whose modifications are dependent on either S6K1 (Ser240/Ser244) or RSK2 (Ser235/Ser236) were strongly enriched when cells were treated with Compound A alone. This observation however contradicts the phosphorylation patterns exhibited by its activating kinase RSK2, which is activated upon ERK signaling and hence preferentially phosphorylated in the combination treatment. Notably, phosphorylations of Ser235/Ser236 and Ser240/Ser244 were never detected in isolation but phosphopeptides always contained at least one of the serines known to be modified by the two

kinases. It is possible that this observation occurred due to the enrichment process where peptides with multiple phospho groups were preferentially enriched over those that undergone only a single phosphorylation. Furthermore, the close proximity of the residues prevented the generation of peptides that only covered Ser235/Ser236 or Ser240/Ser244 respectively. Although an arginine residue in position 238 could have led to the generation of peptides containing only one of the two kinase motifs, the presence of the phosphate group(s) may have interfered with the tryptic digest. Another technical explanation for this could be that peptides phosphorylated at residues Ser235/Ser236 only appeared in the combination treatment while being undetectable in BMDMs treated with Smac mimetic alone. The resulting missing values in the single agent treatment would then in turn cause the dismissal of these peptides during the statistical analysis. The contradiction about the co-occurrence of phosphorylations catalyzed by the kinases S6K1 and RSK2 upon treatment with Compound A could be addressed by screening lysates for the phosphorylated residues Ser235/Ser236 and Ser240/Ser244 via Western blotting since commercial antibodies against those sites are available. For the question at hand however, answering this question was not of importance. The relevant findings here were that downstream targets of the mTOR pathway, which signals for cell survival, were found to be activated in BMDMs treated with Smac mimetic while signaling through this pathway was not observed upon the combination treatment.

Table 4.18: Phosphorylation status of rpS6 after treatment with SM + p38i

Protein	Residue(s)	Timepoint	logFc	Rank
rpS6	S236/S240/S244/S247	1.5h	-2.1	28
rpS6	S235/S236/S240	1.5h	-2.1	32
rpS6	S235/S236/S240	1.5h	-2.2	33
rpS6	S236/S240	1.5h	-1.6	98
rpS6	S236/S240/S244	1.5h	-1.8	108
rpS6	S236/S240/S244/S247	1.5h	-1.7	127
rpS6	S236/S244/S247	3h	-2.7	44

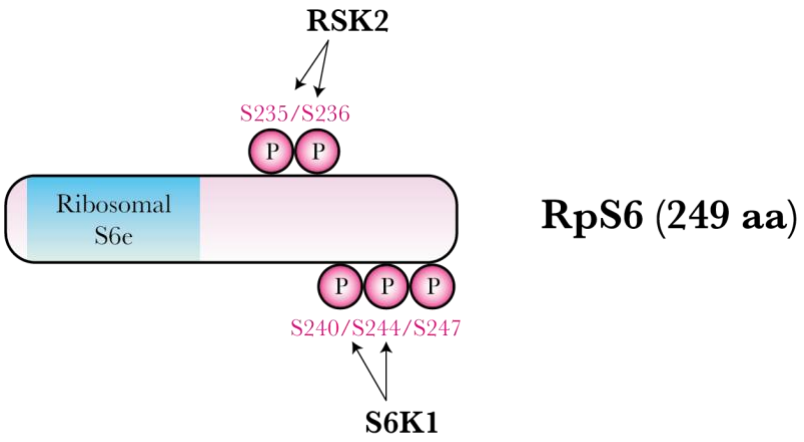

Figure 4.22: RpS6, a downstream target of the mTOR pathway, was preferentially phosphorylated in BMDMs treated with Compound A

Schematic representation of the ribosomal protein RpS6. Shown in pink are the phosphorylated residues p-S235, p-S236, p-S240, p-S244 and p-S247 identified in BMDMs treated with Compound A. Phosphorylation of S235 and S236 require RSK2 activity which is an ERK-dependent kinase. The residues S240 and S244 are substrates of S6K1 and are hence dependent on mTOR activity.

4.6.3.6 The translation initiation factor eIF4B is activated in BMDMs treated with Smac mimetics

As an RNA binding protein, eIF4B is involved in the regulation of the initiation stage of protein synthesis where is it crucial for the recruitment of mRNA to the ribosome. Here, eIF4B supports the unwinding of mRNA secondary structures allowing ribosome scanning by enhancing ATPase and helicase activities of eIF4A. Although a number of eIF4B phosphorylation sites have been identified, only Ser406 and Ser422 have been functionally characterized for their role in proliferating cells (K. Chen *et al.*, 2016; Shahbazian *et al.*, 2010). Activated upon PI3K/Akt/mTOR or MAPK signaling, Ser422 is targeted by both S6K1 (mTOR) and RSK1 (ERK). Phosphorylation of eIF4B at this residue enhances its affinity for the eIF3 complex and hence accelerates translation (Shahbazian *et al.*, 2006). Apart from being regulated via phosphorylation, eIF4B is also a substrate of caspase 3 when activated via the TNF pathway (J.-T. Kim *et al.*, 2013). With its cleavage occurring upon extrinsic apoptosis, eIF4B is believed to play a role in inhibiting cell death (Jeffrey *et al.*, 2002). Deregulated phosphorylation of eIF4B at Ser422 has been observed in many cancers, where it drives not only global translation leading to faster proliferation but also induces the overexpression of oncoproteins such as myc and Bcl2 (J. Yang *et al.*, 2013). Its antiapoptotic function was again confirmed when the introduction of a Ser422E phosphomimetic mutation rendered Abl transformed leukemic cells resistant to the combination of JAK/STAT/Pim and PI3K/Akt/mTOR inhibition while eIF4B wild-type cells were sensitive to this treatment (K. Chen *et al.*, 2016).

Upon treatment with Compound A, phosphorylated eIF4B has been found to be enriched in BMDMs in both timepoints with phospho-Ser422 being one of three detected modified

residues (**Table 4.16**). Since phosphorylation of this site can be catalyzed by the kinase S6K1, which, as described above, was activated in BMDMs treated with Compound A, it is likely that eIF4B phosphorylation occurred as a result of mTOR signaling. The peptide containing the phosphorylation sites S354/S355 were enriched by 2.8-fold (1.5 h) and 4-fold (3 h) in BMDMs treated with Compound A (**Table 4.16**). Although the occurrence of phosphorylation of these residues have been reported in the literature, a functional role has not been ascribed to them. Given their close proximity to the arginine rich motif, it is possible that phosphorylation of Ser354/Ser355 plays a role in eIF4B's RNA binding (**Figure 4.23**). To further investigate their function, eIF4B mutants would have to be generated where the residues Ser354 and Ser355 are replaced by either a small amino acid that cannot get phosphorylated (e.g. alanine), or a phosphomimetic residue (e.g. aspartic acid). Although the role of phosphorylated Ser354/Ser355 remains unknown, the enrichment of phospho-eIF4B Ser422 again supports the notion that in Smac mimetic treated cells, survival is regulated through PI3K/Akt/mTOR signaling.

Table 4.19: Phosphorylation status of eIF4B after treatment with SM + p38i

Protein	Residue(s)	Timepoint	logFc	Rank
eIF4b	**S354/S355**	1.5h	**-1.4**	**78**
eIF4B	**S422**	1.5h	**-0.8**	**91**
eIF4B	**S354/S355**	3h	**-1.9**	**38**

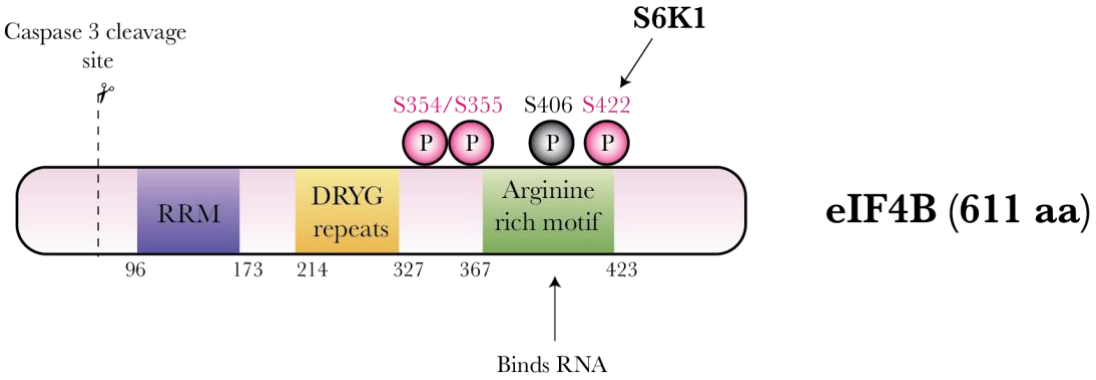

Figure 4.23: The translation initiation factor eIF4B can be activated by S6K1 via phosphorylation at Ser422

Schematic representation of eukaryotic translation initiation factor 4B (eIF4B). The numbers refer to amino acids flanking the functional domains. Residues in pink represent phosphorylated amino acids identified in BMDMs treated with Compound A, while grey/black residues are known phosphosites that were not detected. S422 can be phosphorylated by S6K1 in response to mTOR signaling (Holz *et al.*, 2005). Phosphorylation at S406 is catalyzed by PIM (Cen *et al.*, 2014). Cleavage of eIF4B by caspase-3 after Asp45 occurs during apoptosis (Jeffrey *et al.*, 2002). RRM = RNA recognition motif.

4.6.3.7 Phosphorylation of the kinase Itpkb might lead to its activation and inhibition of the PI3K/Akt/mTOR pathway

Inositol-trisphosphate 3-kinase B (Itpkb) was significantly differentially phosphorylated upon treatment and was identified as the DP protein with the third highest significance in the 3 h timepoint (**Table 4.17**). Its dually phosphorylated form was enriched in the combination

treatment where it was found to be increased by 4-fold compared to the single agent treatment. Interestingly, Itpkb functions as a PI3K/Akt antagonist by phosphorylating IP_3 (inositol-trisphosphate) to produce IP_4 which in turn competes with PIP_3 leading to the inhibition of Akt activation (Siegemund *et al.*, 2015) (**Figure 4.24**). The detected phosphoserines Ser42 and Ser48 have been previously reported in the literature, where they have been identified during large scale phosphoproteomic profiling of mTOR (Humphrey *et al.*, 2013), RIPK3 (X. Wu *et al.*, 2012) and TLR signaling (Weintz *et al.*, 2010) to name a few. However, the function of these phospho sites have not been determined. Both residues are conserved in mouse, human and rat Itpkb indicating that they might be of functional importance. Itpkb has previously been reported to be a substrate of ERK (Hatano *et al.*, 2016). When screening the detected phosphopeptide for potential kinase motifs, it was revealed that the Itpkb peptide sequence contained at least the partial consensus motif of ERK for both phosphoserines (**Figure 4.25**). The minimal ERK phosphorylation consensus motif is SP/TP while the motif LSPG has been found to be enriched in known ERK substrates (Hatano *et al.*, 2016). The preposition that ERK is the kinase responsible for phosphorylating Itpkb at Ser42 and Ser48 is further supported by ERK's treatment induced activation profile. The MAP kinase is strongly activated in BMDMs treated with Compound A and p38i for 3 h which correlates with the enrichment of phosphorylated Itpkb. To confirm a functional role of phospho-Ser42 and -Ser48 in Itpkb activation, mutant Itpkb will need to be generated where the serines are mutated to either a small amino acid that cannot be phosphorylated (e.g. alanine) reflecting non-phosphorylated Itpkb, or to a phosphomimetic (e.g. aspartic acid) to replicate the phosphorylated protein. Furthermore, to establish the role of ERK in Itpkb phosphorylation, and potentially activation, an *in vitro* kinase assay where recombinant ERK and Itpkb are incubated in the presence of ATP could be performed. Using mass spectrometry to sequence

the substrate following the kinase assay would reveal the modified residues. Although it is intriguing to speculate that Itpkb phosphorylation plays a role in the cell death induced by the combination treatment by inhibiting Akt which, when activated, promotes cell survival, testing this hypothesis requires further research. Due to time constraints I was not able to follow up on this observation but I believe the data I have presented justifies future investigations into the role of Itpkb phosphorylation during the combined inhibition of IAPs and p38.

Table 4.20: Phosphorylation status of ITPKB after treatment with SM + p38i

Protein	Residue(s)	Timepoint	logFc	Rank
ITPKB	**S42/S48**	3h	2.2	3

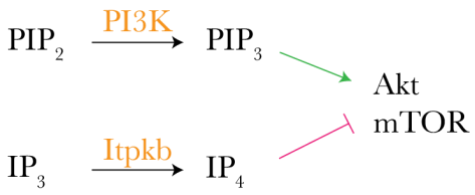

Figure 4.24: Itpkb a PI3K/Akt antagonist

PI3K phosphorylates PIP_2 to generate PIP_3 which in turn can phosphorylate and activate Akt. Upon phosphorylation by Itpkb, IP_3 is converted into IP_4 which prevents Akt phosphorylation by competing with PIP_3 for binding to Akt therefore inhibiting its activation.

Protein	Identified phosphopeptide
Itpkb	AA**LS**(ph)**PG**SVF**S**(ph)**PG**R

Figure 4.25: Identified ITPKB phospho-peptide contains the ERK consensus motif

Sequence alignment of ERK consensus motifs, L[pS/pT]PG (shown in boldface), detected in Itpkb. Phosphorylation sites are highlights in red.

4.7 Discussion

We previously showed, that the combination of a smac mimetic and a p38 inhibitor is an effective treatment for AML *in vivo* (Najoua Lalaoui *et al.*, 2016). Since cell death in BMDMs does not occur upon treatment with SM but is induced when p38 is also inhibited, the MAP kinase prevents cell death in the absence of IAPs. Lalaoui et al. previously discovered, that one mechanism by which p38 inhibits cell death is via the activation of its substrate MK2 which in turn phosphorylates RIPK1 at Ser321 and Ser336 (Jaco *et al.*, 2017, Dondelinger *et al.*, 2017). Phosphorylated RIPK1 is prevented from associating with the death-inducing complex II, subsequently inhibiting cell death (Jaco *et al.*, 2017). To establish whether p38 regulates cell death through additional mechanisms, we generated a $RIPK1_{S321/S336A}$ mutant knock-in mouse which cannot be phosphorylated by MK2. If phosphorylation of RIPK1 by MK2 is the only process by which p38 inhibits cell death, treating $RIPK1_{S321/S336A}$ mutant BMDMs with SM should be sufficient to induce cell death equivalent to that caused by the combination treatment. $RIPK1_{S321/S336A}$ mutant BMDMs were in fact sensitised to SM treatment as shown in **Figure 4.1**. However, when either p38 or MK2 were also inhibited, cell death was further increased, indicating that p38 prevents cell death in the absence of IAPs through additional mechanisms.

To facilitate the identification of proteins and pathways that mediate the treatment-induced cell death and to understand the role of p38 in inhibiting cell death in SM-treated cells, Gene Ontology (GO) and KEGG pathway analyses were performed on treatment-dependent DP proteins. Within these results, I focused on processes and pathways that are likely to be contributing to our observations: cell death and cell survival pathways and regulators of TNF expression.

When searching for mediators of apoptosis, I noticed that Bim, a pro-apoptotic protein required for intrinsic apoptosis, was the sole hit that was significantly differentially phosphorylated upon treatment and was found to be preferentially modified in BMDMs treated with SM (**Table 4.7**; **Figure 4.8 A**). With cell death being inhibited in these cells, I hypothesized that phosphorylation of Bim at Ser82/Ser86 inhibited its activity. This notion was supported by the close proximity of the modified residues to Tyr92, a substrate of LYN whose phosphorylation also prevents Bim activity, and the observation that intrinsic apoptosis occurred in BMDMs when p38 was also inhibited. The latter was demonstrated by the presence of cleaved Caspase 9 in lysates of BMDMs subjected to the combination treatment (**Figure 4.8 B**). Interestingly, phosphorylation of Ser82 has not been reported yet and when searching for kinase motifs, this residue was identified as a potential substrate of MK2 (Hyd-X-R-X-pS). Since this phosphorylation was abolished when p38, and hence MK2, were inhibited, it is possible that Bim is in fact a substrate of MK2 and that by phosphorylating Bim, MK2 negatively regulates its pro-apoptotic activity. This would be in contrast to the role of p38 in inducing apoptosis by directly phosphorylating and activating Bim at Ser65 upon oxidative stress in PC12 cells (Cai *et al.*, 2006). Further experiments including *in vitro* kinase assays to determine if Bim is a substrate of MK2 would be required to confirm our hypothesis. Although these findings were intriguing, the cell death induced by the combination of SM and p38i is Caspase 8-dependent and therefore driven by extrinsic apoptosis (Najoua Lalaoui *et al.*, 2016). Understanding the role of MK2 in regulating intrinsic apoptosis therefore would not address our research question.

As we showed previously, p38 inhibition lead to an increase in TNF production induced by SM which greatly contributed to the increase in cell death (Najoua Lalaoui *et al.*, 2016). This

observation was unexpected since p38 is required for the induction of TNF through Toll-like receptors (Foey *et al.*, 1998). In fact, when p38 was inhibited in BMDMs treated with LPS, we observed a decrease in TNF production (Najoua Lalaoui *et al.*, 2016). Since cell death induced by the combination treatment of SM and p38i is dependent on TNF, identifying regulators of TNF production that contribute to the increased expression of this cytokine, is of great interest. Phosphoproteomic analysis revealed that four potential regulators of TNF production were differentially phosphorylated in treated BMDMs (**Table 4.18**).

CD45, a protein tyrosine phosphatase receptor that is activated by self-dimerization, was found to be dually phosphorylated at its C-terminal domain in BMDMs treated with SM indicating that these modifications were dependent on p38 (**Table 4.8**). CD45 is critical in T- and B-cell signaling, where it associates and regulates intracellular tyrosine kinases of the Src family including LCK, LYN and FYN (Altin *et al.*, 1997). In macrophages and dendritic cells, CD45 has been described to be a negative regulator of TNF expression induced by TLR signaling although the underlying mechanisms are unclear (Piercy *et al.*, 2006). The phosphosites detected in treated BMDMs have been previously reported but their functions remain unknown. With Ser1286 being a conserved residue however, associating it with a functional role is plausible. If CD45 as a negative regulator of TNF expression can in fact be regulated by the detected phosphorylations, it stands to reason that this modified version represented the activate receptor since TNF levels in SM-treated BMDMs were low. Evidence for CD45 activity in these cells were found in the presence of phosphorylated FYB and EVL (**Table 4.9-10**; **Figure 4.10-11**). Both proteins are well-described interactors of FYN, a Src family kinase regulated by CD45.

Although the presented evidence is highly speculative, CD45 was identified as an intriguing target due to its great changes in p38-dependent phosphorylation (3-fold at 1.5h, 4.6-fold at 3h) which were detected at high significance (rank 30 at 1.5h, rank 13 at 3h). Interestingly, in NK cells, CD45 was found to be required for p38 phosphorylation upon ITAM (immunoreceptor tyrosine-based activation motifs) activation (Huntington *et al.*, 2005). Investigating the relationship between p38 and CD45 in macrophages and its impact on the regulation of TNF expression, could revel novel roles of p38 in suppressing TNF.

CD84, a member of the signaling lymphocyte activation molecule (SLAM) immunoglobulin superfamily, was phosphorylated in BMDMs upon combination treatment when p38 was inhibited (**Table 4.11**). It is a self-associating receptor, that is almost ubiquitously expressed within the hematopoietic lineage but still remains poorly understood (Agod *et al.*, 2018). When overexpressed in macrophages, LPS-induced CD84 activation lead to the phosphorylation of MAP kinases which in turn induced the activation of NF-KB followed by an increase in TNF production (Sintes *et al.*, 2010). In line with these observations, knock-down of CD84 in BMDMs decreased TNF expression upon LPS-stimulation (Sintes *et al.*, 2010). Its ability to regulate cytokine production is mediated through two ITSMs (immunoreceptor tyrosine-based switch motif) which can become tyrosine-phosphorylated upon activation, leading to the recruitment of SAP (SLAM associated protein) (Nanda *et al.*, 2005). The phosphosites we detected are within (Thr263) or in close proximity (Ser260) to ITSM1 which also harbors an important regulatory phosphosite (Tyr265) as well as binding site for SAP (Cuenca *et al.*, 2019). Although functional associations for the two detected phosphorylated residues have not been drawn yet, their locations and the fact that both amino

acids are preserved in humans and rats, support that these sites might be involved in regulating receptor activity.

Given that the residues were phosphorylated when p38 was inhibited and where we observe MAP kinase phosphorylation and an increase in TNF production, we can further hypothesize that the observed modifications had a positive regulatory effect. If that relationship was to be confirmed, understanding the role of the simultaneous inhibition of IAPs and p38 on CD84 activation would be of great interest.

CD84 has recently been identified as a potential biomarker and target in the treatment of cancer and autoimmune diseases (Binsky-Ehrenreich *et al.*, 2014; Cui *et al.*, 2013; van den Reek *et al.*, 2017). In chronic lymphocytic leukemia (CLL), significantly elevated CD84 was shown to enhance CLL cell survival by NF-κB activation which results in the upregulation of the pro-survival proteins Bcl-2 and Mcl-1 (Cohen *et al.*, 2012). Due to these observations, CD84 was termed a pro-survival protein (Binsky-Ehrenreich *et al.*, 2014). However, with its potential to increase TNF expression, which, in the absence of IAPs, can induce apoptosis, CD84 upregulation could be a biomarker for treatment response to smac mimetics.

In NFAM1, another receptor belonging to the Ig superfamily was preferentially phosphorylated in BMDMs treated with SM (**Table 4.12**). NFAM1 is activated by dual tyrosine phosphorylation of Tyr215 and Tyr226 within its ITAM (an immunoreceptor tyrosine-based activation motif) which leads to increased transcription of TNF- α promoters mediate through the calcineurin/NFAT-signaling pathway (J. Yang *et al.*, 2003). The phosphosites detected in treated BMDMs, p-Ser235 and p-Ser241, are conserved residues in

human NFAM1 and both have been reported to become phosphorylated. Although the roles of these modifications remain unknown, their close proximity to the regulatory ITAM whose phosphorylation is required for receptor activation, suggests that the observed phosphorylation events are of functional importance. Indicators of active NFAM1 include increased TNF expression and Ca_{2+} influx (Sambandam *et al.*, 2017; J. Yang *et al.*, 2003). While the upregulation of TNF in BMDMs treated with SM and p38i has been directly measured (Najoua Lalaoui *et al.*, 2016), evidence of Ca_{2+} influx is purely speculative. Upon combination treatment, phospho-CLCC1 and phospho-CaMKK2, both of which are Ca_{2+} proteins, were significantly enriched (CLCC1 4.6-fold, rank 4; CaMKK2 2-fold, rank 189). If NFAM1 was in fact active in BMDMs treated with SM and p38i, its phosphorylated form detected in cells treated with SM alone would represent an inhibited version. Since the modifications were dependent on p38 activity, we could then hypothesize that through inhibiting NFAM1, p38 can reduce the transcription of TNF promoters leading to reduced TNF levels. The correlations presented here are partially based on speculation and further research is required to confirm a role of p38 in regulating TNF expression through NFAM1 inhibition. However, the fact that phospho-NFAM1 was ranked in the top 4 most significant DP proteins for both timepoints, strongly suggests a role for this receptor in the treatment responses observed for BMDMs.

ATF2 is a well-characterised transcription factor which, upon phosphorylation and activation, induces the expression of TNF (Tsai *et al.*, 1996). ATF2 is a substrate of a number of MAP kinases and its activation requires successive phosphorylation by p38/JNK1/2 and ERK1/2 (Ouwens *et al.*, 2002). Phosphorylated ATF2 was enriched upon the combination treatment and the detected phosphosites matched the residues known to be modified by p38, JNK1/2

and ERK1/2 (**Table 4.13, Figure 4.14 A**). Since p38 was inhibited and JNK1/2 and ERK1/2 were activated in these cells, the latter two are the likely kinases that phosphorylated and activated ATF2. Although this observation confirms the roles of JNK1/2 and ERK1/2 in inducing TNF expression via ATF2 phosphorylation, its contribution to the overall increase of TNF is unclear since phospho-ATF2 was only enriched by 1.4 - 1.7-fold (**Table 4.13**).

In summary, a number of possible contributors to the increase of TNF upon p38 inhibition have been identified. Further research is required to determine whether one of the described TNF regulators is the main driver of this observation or whether it is caused by a crosstalk between them. Investigating this question could reveal novel protein functions as well as further insights into p38-dependent modes of TNF regulation.

The contribution of the cell survival pathway PI3K/Akt/mTOR to the prevention of smac mimetic-induced killing was convincingly shown. As a possible activator of this survival pathway, I identified CSF1R to be preferentially phosphorylated in BMDMs treated with SM and p38i (**Table 4.14**). Due to their close proximity to Tyr721, whose phosphorylation is required for receptor activity and induction of the PI3K/Akt pathway, I hypothesized that phosphorylated CSF1R detected in the combination treatment represented an inhibited version of the receptor (**Figure 4.16**). Inhibition of CSF1R by phosphorylation at Ser711, Ser714, Ser731 and Ser734 may therefore have prevented activation of PI3K/Akt, allowing cell death to occur. The ability of CSF1R signalling to prevent smac mimetic-induced cell death was confirmed by the use of the CSF1R inhibitor AFS-98. As a single agent, AFS-98 was not toxic to BMDMs but when combined with Compound A, SM-induced cell death was greatly increased (**Figure 4.19**). The combination of SM and CSF1Ri was less potent than

combining SM and p38i and killed cells at a slower rate. This observation however is not surprising when we consider, that p38 prevents cell death in the absence of IAPs through multiple mechanisms, one of which is the phosphorylation of RIPK1 by its substrate MK2. This RIPK1 modification is unlikely to be affected by CSF1R inhibition, although this was not experimentally addressed. It is therefore possible, that the observed discrepancy in cell death caused by the two combinations can be accounted for by the ability of p38/MK2 to regulate RIPK1.

When investigating if the PI3K/Akt pathway is contributing to the observed treatment response, it was revealed via Western blot, that Akt phosphorylation was reduced in BMDMs treated with SM and p38i (**Figure 4.18**). The reduction in phospho-Akt therefore correlated with the detection of phosphorylated CSF1R, supporting the hypothesis that CSF1R upon p38 inhibition failed to activate the PI3K/Akt pathway, consequently enabling cell death. For the treatment with smac mimetic-only, that would mean that cell death might have been prevented by cell survival signalling through PI3K/Akt. A number of targets of the PI3K/Akt/mTOR pathway were also differentially phosphorylated in treated BMDMs in a way that supported our theory (**Table 4.21, Figure 4.26**). At the same time, Itpkb, a PI3K/Akt antagonist, was phosphorylated and potentially activated in the combination treatment. Reduced phosphorylation of Akt could have therefore been facilitated not only by CSF1R inhibition but also Itpkb activation.

In Summary, there is great evidence, that smac mimetic as a single agent failed to induce cell death in BMDMs due to the activity of the cell survival pathway PI3K/Akt/mTOR. This activation was dependent on p38 and may have been induced by CSF1R-mediated signalling

upon binding of CSF1 present in the media. When p38 was inhibited, CSF1R became phosphorylated and inhibited, preventing the activation of the PI3K/Akt/mTOR pathway and enhancing cell death. The mechanism through which p38 might regulate cell survival signalling in smac mimetic-treated cells remains unclear. Since phospho-CSF1R was detected when p38 was inhibited, it is likely that p38 did not directly interact with the receptor but rather negatively regulated an effector upstream of CSF1R. The discussed data suggests a mechanism for resistance to smac mimetic as a single agent, paving the path for the development of novel biomarkers for treatment response.

With this work, I demonstrated that phosphoproteomics is a powerful tool for studying complex signalling events. By applying this technique, we gained a more comprehensive overview of signalling pathways involved in smac mimetic resistance. Additionally, I was able to identify a number of novel phosphorylation sites. A challenge that arises when interpreting phosphoproteomics data, is the lack of information on the function of specific phosphorylation sites. Phosphorylations can impact proteins in various ways. Currently the tools available to determine the function of a phosphorylation site on a protein, either involve overexpression of mutated proteins in knock-out cell lines or the generation of CRISPR/Cas9 knock-in mice which allows studying mutated protein on an endogenous level. Since the large datasets generated during phosphoproteomics often reveal a number of interesting hits with modifications of unknown function, generating knock-in mice is not always an economic option. An attractive tool to study phosphorylation functions on an endogenous level in a quick and economic manner is CRISPR/Cas9 knock-in in cell lines. Developing such a tool was the objective of my next chapter.

Table 4.21: Phosphorylation status of regulators of the PI3K/Akt/mTOR pathway after treatment with SM + p38i

Protein	Regulator of PI3K/AKT/mTOR	Timepoint	logFc
PRAS40	positive	1.5h	**-1.0**
PRAS40	positive	3h	**-**
P70S6K	positive	1.5h	**-1.0**
P70S6K	positive	3h	**-0.6**
eIF4B	positive	1.5h	**-0.8**
eIF4B	positive	3h	**-2.0**
rpS6	positive	1.5h	**-2.3**
rpS6	positive	3h	**-2.7**
ITPKB	negative	1.5h	**-**
ITPKB	negative	3h	**2.2**

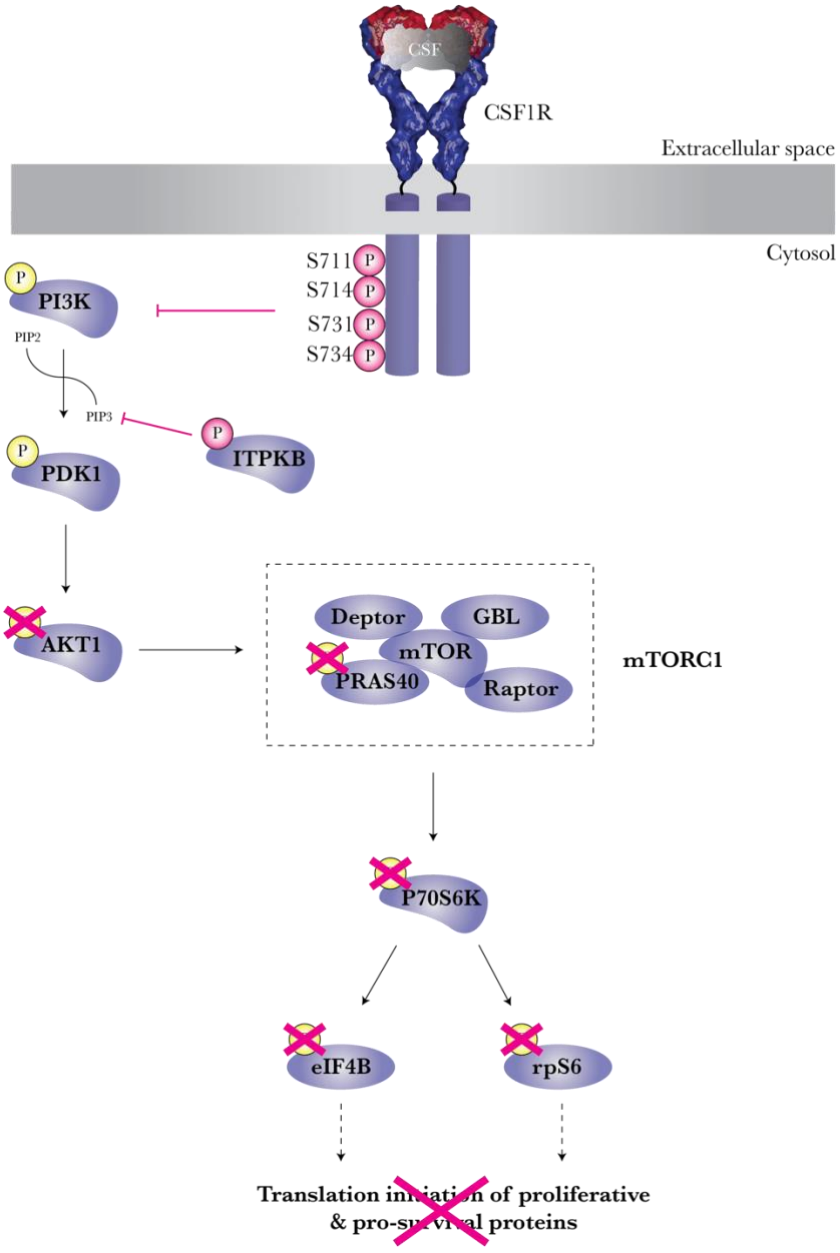

Figure 4.26: The PI3K/Akt/mTor pathway is inactivated in BMDMs treated with SM + p38i

Overview of the Akt/PI3K/mTOR pathway and its activation status in BMDMs treated with SM + p38i. Phosphorylation sites in yellow are required for pathway activation. Phosphorylation sites in pink were identified in BMDMs upon combination treatment. Phosphorylation of CSF1R at S711, S714, S731 and S734 might inhibit PI3K activation. Phosphorylated ITPKB inhibits Akt activation by generating IP_4 which in turn competes with PIP_3. Pink crosses indicate phosphorylation events that are observed in BMDMs treated with SM but prevented upon the addition of p38i. By inhibiting the activation of downstream targets eIF4B and rpS6, cell survival signaling is prevented and cell death can occur.

5 Tagging endogenous proteins of the TNF signaling pathway using the CRISPR/Cas9 knock-in technology

5.1 Using the CRISPR/Cas9 gene editing system to endogenously FLAG-tag RIPK1 – Design of the constructs

Initially developed to purify recombinant proteins, the FLAG-tag is now one of the most commonly used protein tags (Hopp *et al.*, 1988). The FLAG-tag is a hydrophilic polypeptide consisting of eight amino acids (DYKDDDDK). Due to its small size and hydrophilic nature, the function of tagged proteins most often remains unaffected (Hopp *et al.*, 1988). Furthermore, the existence of a high affinity monoclonal anti-FLAG antibody allows us to perform assays that require the recognition by an antibody such as immunofluorescence, immunoprecipitation and Western blotting (Gerace *et al.*, 2015). The potential of a FLAG-tag for immunoprecipitation becomes even more impressive when considering that immunoprecipitated proteins can be eluted competitively by the addition of free FLAG peptide, keeping the antibody intact and reducing the contamination of specifically bound protein with the antibody's chains or non-specifically bound proteins (Gerace *et al.*, 2015). This in turn allows us to use mass spectrometry as a tool to identify novel interacting partners, post-translational modifications or to study signaling dynamics since sample quality is crucial for this versatile high throughput technology. Therefore, development of a robust protocol that enables us to tag proteins endogenously with a FLAG-tag using the CRISPR/Cas9 system would deliver a powerful tool to target any protein in our pathways of interest and address questions regarding protein complex compositions, dynamics and stoichiometries as well as signaling- or treatment- dependent protein modifications.

A number of approaches to endogenously tag proteins using the CRISPR/Cas9 system have been described in the literature (Patrick D. Hsu *et al.*, 2014; Sander *et al.*, 2014). A schematic of the method I have developed is summarized in **Figure 5.1**. Firstly, I chose to use the lentiCRISPR v2 one vector system where Cas9 and sgRNA are expressed by the same vector (Sanjana *et al.*, 2014). This increased the transfection efficiency since only one vector has to be transfected into each cell. It also allowed for the expression of Cas9 to be transient which can reduce off target effects and the risk of the inserted sequence to be cleaved again. Furthermore, in most expression systems Cas9 has a triple FLAG-tag which, if it was stably expressed, would interfere with the detection of the inserted FLAG-tag. The sgRNA targeted the 3' of mouse *RIPK1* and the chosen PAM sequence was less than 10 bp upstream of the stop codon where the 3' FLAG-tag was to be inserted. The donor template containing the FLAG sequence was delivered in the form of a single stranded DNA oligo (ssDNA) of approximately 150 bp (**Figure 5.1**). The FLAG sequence itself was followed by a stop codon and was flanked by two homology arms upstream and downstream of the sgRNA targeted region which were approximately 60 bp each. To prevent Cas9 from cleaving the integrated template, the PAM sequence recognized by the RIPK1 sgRNA was silently mutated.

First, I tested the efficiency of the CRISPR guides in genetically knocking out *RIPK1* in MDFs. Three different guides were designed to increase the chances of finding a suitable guide. In many cell lines the HDR machinery is less active than the NHEJ pathway making a genetic knock-in harder to achieve than its counterpart – the knock-out (Zaboikin *et al.*, 2017). Using a guide that is extremely efficient is therefore important. To test the guides' ability to knock out *RIPK1*, I used an inducible two vector system where the Cas9-expressing construct is stably integrated into the cell's genome and the guide-containing plasmid is delivered into the cells

using viral transduction. GFP is constitutively expressed from the guide plasmid to allow for selection of transduced cells. Following sorting of GFP positive cells via FACS, sgRNA expression was induced by the addition of doxycyclin and several days later the expression of RIPK1 was determined using Western blotting (**Figure 5.2**). One guide was able to knock out *RIPK1* in MDFs. With a knockout efficiency of nearly 100% in a pool of doxycyxlin-treated cells, indicating that this guide was ideal for the CRISPR/Cas9 knock-in approach. As a control, I simultaneously transduced MDFs with guides targeting FADD or cFLIP. RIPK1 levels for these control guides remained unchanged (**Figure 5.3**).

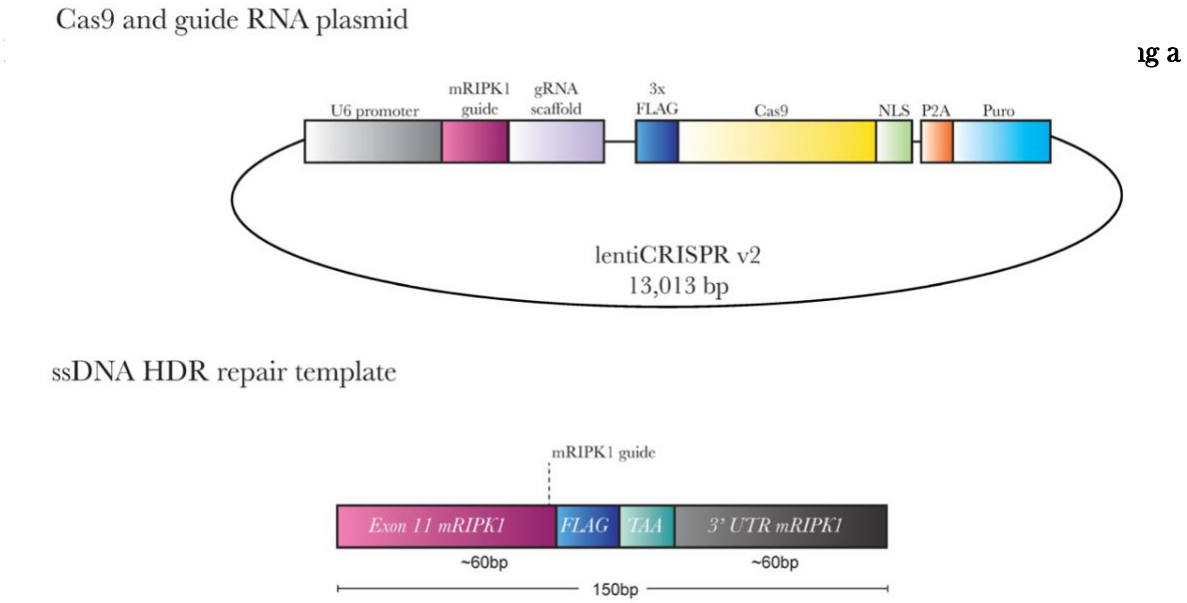

CRISPR/Cas9 guide vector and RIPK1-FLAG HDR ssDNA template. The RIPK1 guide targeting the C-terminus was cloned into the lentiCRISPR v2 construct which also expresses Cas9 and a puromycin resistance cassette. The ssDNA HDR template is 150 bp in length and consists of two homology arms of approx. 60 bp flanking the guide target sequence and the FLAG-tag sequence that itself was followed by a stop codon. Pink = RIPK1 exon, blue = FLAG sequence, teal = stop codon, grey = 3' untranslated region.

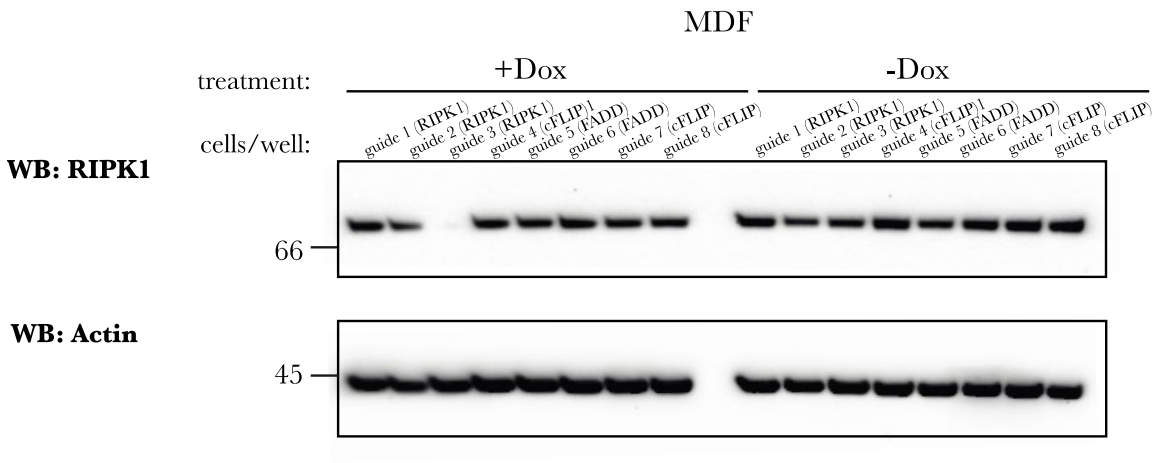

Figure 5.2: CRISPR/Cas9 knockout of *RPK1*

Cas9-expressing MDFs were lentivirally transduced with sgRNA targeting *RIPK1* guides 1-3), *FADD* (guides 5 and 6) or *cFLIP* (guides 4, 7 and 8). Guide expression was induced with doxycyclin and cells were lysed to determine knockout efficiency by Western blotting. Blots were probed for RIPK1 and actin which served as a loading control. Blots for FADD and cFLIP are not shown.

5.2 Transfection of MDFs with Cas9/guide construct and HDR template

After the successful identification of a sgRNA efficiently guiding Cas9 to *RIPK1*, the CRISPR/Cas9 knock-in protocol depicted in **Figure 5.3 A** could now be tested for its ability to introduce a FLAG-tag into the 3' end of the gene. First, wild-type MDFs were transfected with the Cas9/sgRNA dual vector together with the FLAG sequence-containing ssDNA template using the transfection reagent Lipofectamine 3000. To optimize the volume of Lipofectamine 3000 reagent being used, two transfections were set up using either 2 µL or 4 µL of reagent. Transfected cells could be selected for by using puromycin. Since the expression of the Cas9/sgRNA vector was only transient, the puromycin treatment window was crucial. After testing various concentrations and treatment durations, I determined the ideal treatment plan

to be treating transfected cells with 1mg/mL puromycin one day after transfection for two days. The transfection rate was approximately 10-20%.

5.3 Knock-in of the FLAG-tag was confirmed via PCR

To confirm the FLAG-sequence containing the HDR template was successfully knocked-in, PCR reactions were set up for wild-type MDFs transfected with the ssDNA template alone and MDFs transfected with both the RIPK1 sgRNA and the ssDNA template using either 2 µL or 4 µL Lipofectamine 3000 reagent. Two primer pairs were used. For a control PCR, the forward primer targeted a region of the RIPK1 exon 11 while the reverse primer recognized a sequence in the 3'UTR. The presence of the FLAG-tag was confirmed by designing a forward primer whose sequence is complementary to the FLAG sequence while the same reverse primer was used. For both reactions, the size of the resulting amplicon was expected to be approximately 1000 bp. The FLAG-sequence containing HDR template was successfully knocked into the genome of transfected MDFs (**Figure 5.3 B**). Control PCR reactions generated amplicons of the anticipated size for all samples, while the FLAG-specific primer pair was only able to amplify its target sequence in MDFs transfected with the RIPK1 sgRNA and the ssDNA HDR template. This result indicates that the integration of the HDR donor template occurred in the intended region and was guided by the RIPK1 sgRNA.

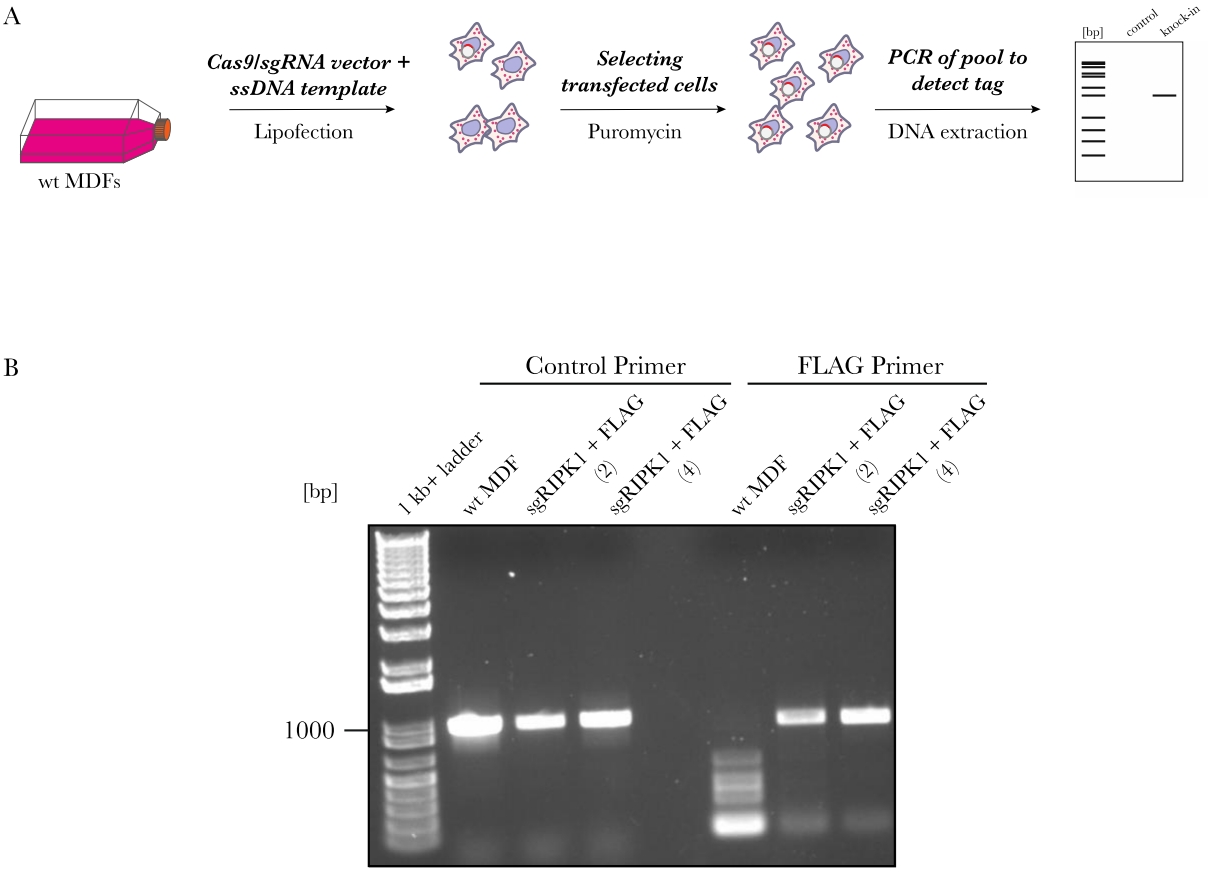

Figure 5.3: CRISPR/Cas9 mediated knock-in was confirmed with PCR

(A) CRISPR/Cas9 knock-in of the FLAG-tag into the *RIPK1* locus was performed by transfecting MDFs with the Cas9/sgRNA construct and the ssDNA HDR template containing the FLAG-tag. Cells were transfected using Lipofectamine 3000. To enrich for positively transfected cells, MDFs were treated with 1ug/mL puromycin 24 h after transfection for two days. One week after treatment, cells were lysed and DNA was extracted. To determine if a knock-in of the HDR template occurred, PCR was performed using either a control forward primer (binds to endogenous *RIPK1* sequence) or a FLAG sequence-specific forward primer and a reverse primer that binds to the 3'UTR of *RIPK1*. (B) PCR of knock-in cell pool. DNA was extracted from wild-type MDFs (wt MDF) and MDFs transfected with RIPK1 sgRNA and ssDNA template containing the FLAG-tag sequence (sgRIPK1 + FLAG). The numbers (2) and (4) indicate the volume of lipofectamine 3000 reagent used for transfection, 2 ul or 4 ul, respectively. Both the control and FLAG-specific PCR reactions generated amplicons of approx. 1kb.

After having confirmed that the knock-in event had occurred in the transfected pool of cells, I now had to isolate clones that expressed the FLAG-tagged RIPK1 protein (**Figure 5.4 A**). Since PCR results do not provide an insight into the efficiency rate at which the knock-in occurred and based on the assumption that the efficiency is low, I decided to seed cells into 96-well plates at concentrations of either one or ten cells per well. The cell sort resulted in the isolation of 32 single cell and 124 cell populations originating from seeding ten cells per well which were then screened for FLAG-tag knock-in using PCR (not shown). In order to generate an amplicon of a distinguishable size, a reverse primer for the FLAG-specific PCR was used that would result in a fragment of approximately 400 bp. Six clones that were identified as positive for the RIP-FLAG sequence in the initial screen were tested again using the same primer pair (**Figure 5.4 B**). All control PCR reactions resulted in products of the correct size. The FLAG-specific primer pair clearly amplified a sequence of the anticipated size for the single cell clone A while only a faint band was visible for C, D and F at that size that all originated from seeding ten cells/well. Since clone A was also the only single cell clone, I proceeded with it and tested whether the expression of FLAG-tagged RIPK1 in clone A could also be confirmed on a protein level.

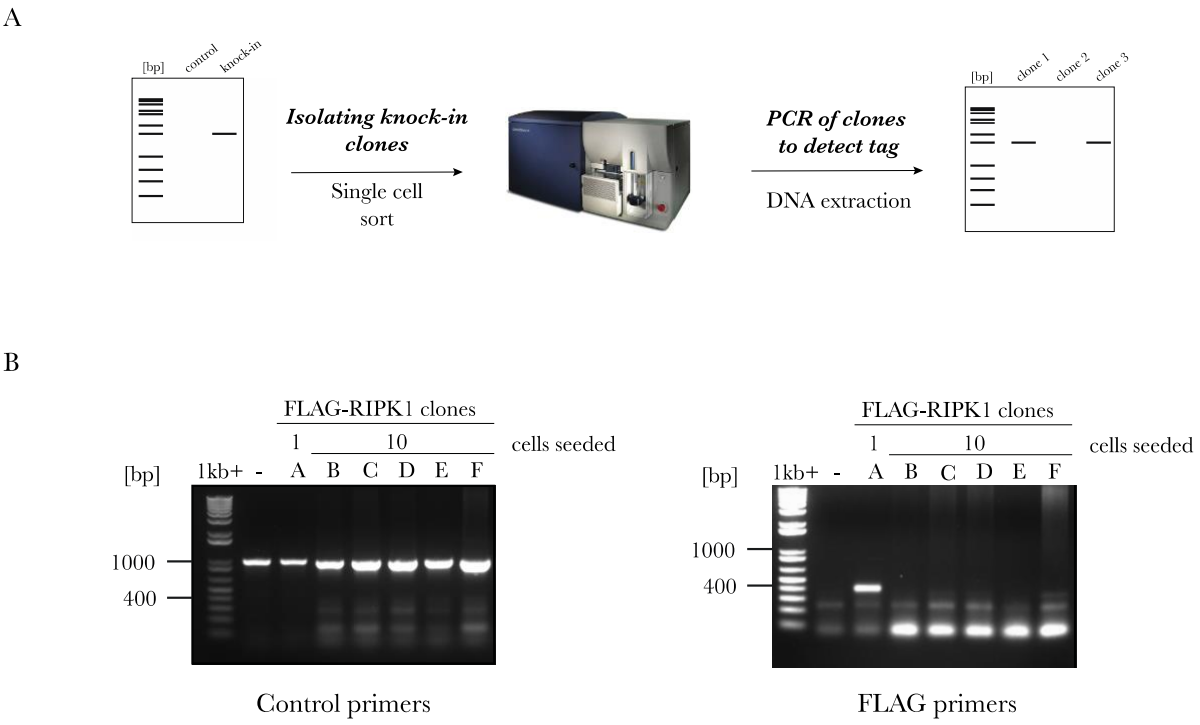

Figure 5.4: CRISPR/Cas9 mediated knock-in was confirmed in a single cell clone

(A) Once the presence of a FLAG-tag was confirmed in the cell pool, FLAG-tagged RIPK1 clones were isolated by sorting either one or ten cells per well into a 96-well plate via flow cytometry. The presence of the FLAG sequence in the clones could then be determined by PCR. (B). Sorted clones were screened by using either a control primer pair resulting in an amplicon of approx. 1kb (left) or a FLAG sequence-specific forward primer and a reverse primer binding to the 3'UTR generating an amplicon of approx. 400 bp (right). DNA extracted from wt MDFs served as negative control (-).

5.4 RIPK1 was successfully immunoprecipitated via its FLAG-tag

After successfully identifying one clone that had the FLAG sequence integrated into its genome, it needed to be confirmed that the FLAG-tagged RIPK1 was expressed correctly on a protein level. I therefore performed immunoprecipitation (IP) with FLAG-antibody-conjugated agarose beads to pull down any endogenously FLAG-tagged protein. After eluting bound protein by boiling the beads in SDS containing buffer, I analysed the samples via Western blotting for RIPK1 and FLAG (**Figure 5.5 A**). I was able to detect RIPK1 in the elution of clone A while

for both the wild-type MDFs and clone B (identified as a negative clone via PCR, **Figure 5.4 B**) RIPK1 did not appear to be pulled down. It should be noted that the size at which RIPK1 (74.8 kDa) appeared, was slightly higher than expected. When probing for FLAG, I was able to observe a band for clone A whose size matched the size at which RIPK1 appeared in the previous blot, while this band was absent in both negative controls. To further increase the certainty that RIPK1 could be pulled down via FLAG IP, I repeated the FLAG enrichment and processed the samples for analysis by mass spectrometry. To induce an increase in RIPK1 expression, cells were treated with TNF (L. Wang *et al.*, 2008). Although TNF treatment did not result in more RIPK1 peptides being detected or the protein coverage being increased, RIPK1 was identified in FLAG IP samples derived from clone A but not in wild-type MDFs (**Figure 5.5 B**). The protein coverage achieved by mass spectrometry was only between 23-26% which were represented by 12-15 unique peptides (**Figure 5.5 C**), none of which contained the FLAG sequence. These peptides were distributed across the RIPK1 protein sequence indicating that the full-length RIPK1 protein was being enriched (**Figure 5.5 D**). When comparing the lists of other proteins being pulled down in the knock-in MDFs with the wild-type sample Tab2, a known RIPK1-interacting protein, stood out as only being detectable in both knock-in samples but not the wild-type (**Figure 5.5 E**) (Yu Wang *et al.*, 2018). Since the IP was only performed with one technical and one biological replicate per sample, statistical analysis could not be applied and the results have therefore to be interpreted with caution. However, given that the wild type control sample was completely devoid of any RIPK1-derived peptides, I was confident that I had successfully generated a clone (clone A) stably expressing a FLAG-tagged version of RIPK1.

A

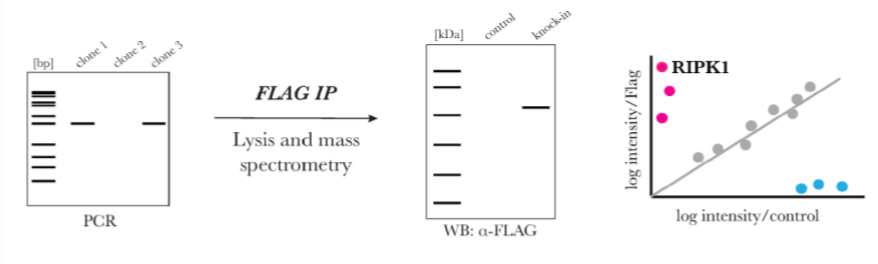
[bp]
clone 1
clone 2
clone 3
PCR
FLAG IP
Lysis and mass spectrometry
[kDa]
control
knock-in
WB: α-FLAG
RIPK1
log intensity/Flag
log intensity/control

B

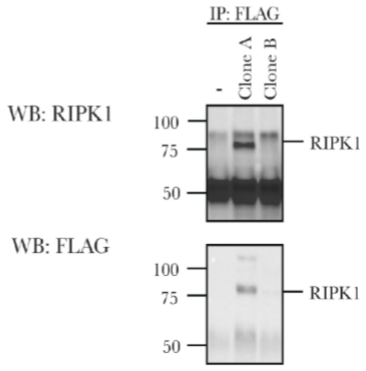
IP: FLAG
-
Clone A
Clone B
WB: RIPK1
100
75
50
RIPK1
WB: FLAG
100
75
50
RIPK1

C

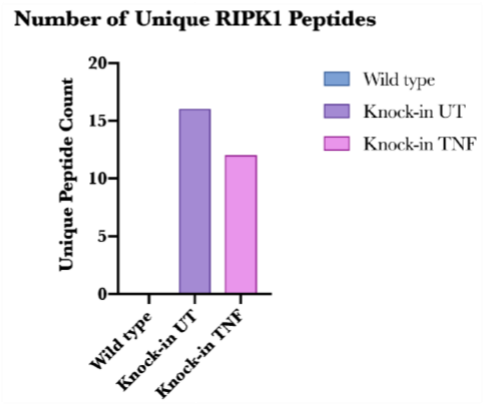
Number of Unique RIPK1 Peptides
Unique Peptide Count
20
15
10
5
0
Wild type
Knock-in UT
Knock-in TNF
Wild type
Knock-in UT
Knock-in TNF

D

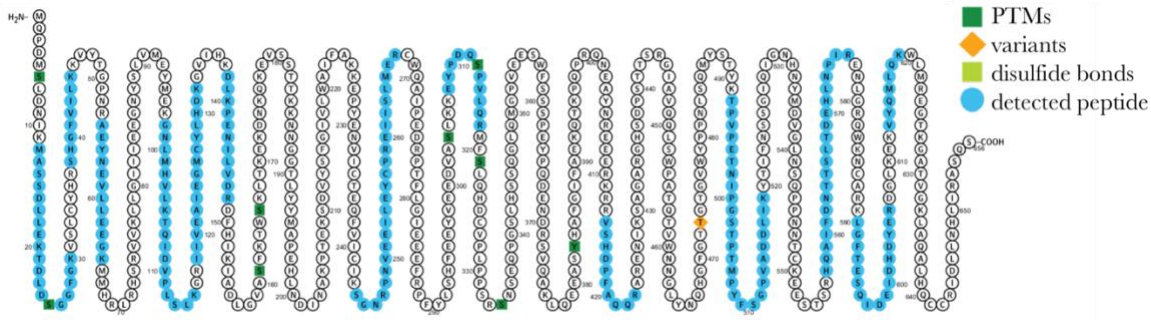
PTMs
variants
disulfide bonds
detected peptide

E

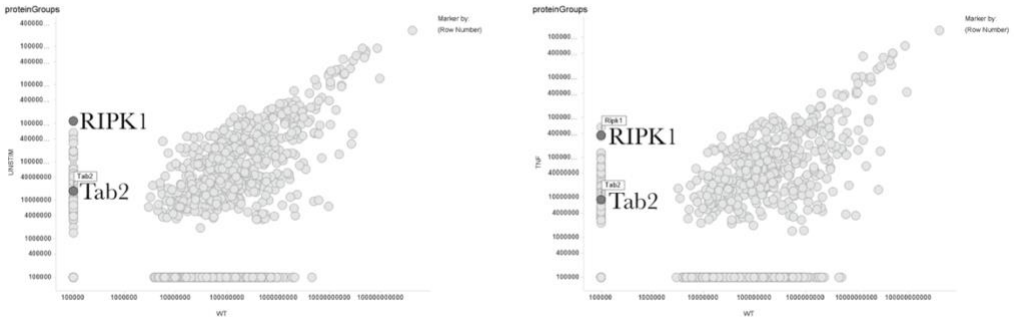
proteinGroups
RIPK1
Tab2
proteinGroups
RIPK1
Tab2

Figure 5.5: FLAG-tagged RIPK1 can be immunoprecipitated using anti-FLAG beads

(A) Workflow schematic. Clones harbouring the FLAG sequence as determined by PCR were subjected to FLAG immunoprecipitation and tagged RIPK1 was identified via Western blot and mass spectrometry. (B) To immunoprecipitate FLAG-tagged RIPK1, lysates of RIPK1 knock-in MDFs and wild-type MDFs (negative control) were incubated with anti-FLAG agarose beads and bound proteins were eluted by boiling the beads in SDS lysis buffer. Eluted proteins were detected via Western blotting and probing for RIPK1 and FLAG. (C) To confirm that RIPK1 could be immunoprecipitated in clone A via its FLAG-tag, wild-type MDFs, untreated knock-in MDFs and knock-in MDFs treated with TNF were lysed and incubated with anti-FLAG-coupled agarose beads overnight. Bound proteins were eluted by the addition of free FLAG peptide and following a tryptic digest, peptides were analysed via mass spectrometry. Numbers of unique RIPK1 peptides achieved for all samples were determined and plotted. (D) The RIPK1-derived peptides detected via mass spectrometry were plotted onto the RIPK1 sequence using the web application Protter (http://wlab.ethz.ch/protter). Detected peptides are highlighted in blue. (E) Spotfire intensity comparison plot showing proteins detected in unstimulated (left) and TNF-treated (right) knock-in samples compared to wild-type. Each protein is represented by a grey sphere. Proteins located along the y-axis were only detected in knock-in samples while proteins along the x-axis could only be found in the wild-type sample. Highlighted are RIPK1 and Tab2, a RIPK1-interacting protein. Data is representative of one experiment.

5.5 Next Generation Sequencing revealed the presence of multiple edited sequences

The fact that only one positive knock-in clone could be identified among the 150 screened clones reflects the low frequency of knock-in events via the HDR pathway compared to NHEJ-induced genetic knockouts. To achieve a quantifiable readout for the knock-in efficiency, I next performed next generation sequencing (NGS) of genomic DNA obtained from the knock-in cell pool. NGS data will not only be an indicator for knock-in efficiency but will also provide a great insight into the sequences generated by the integration of the ssDNA HDR template. NGS primers were designed in a way that wild-type and knock-out sequences could both be amplified by choosing a forward primer approximately 100 bp upstream of the guide's PAM site. When analyzing the NGS data, ten different FLAG sequence-containing sequences were identified, none of which represented the correct knock-in version. Since searching the NGS data set for the FLAG sequence itself, all ten identified sequences contained the correct FLAG insert. It can be assumed, however, that more knock-in sequences existed which harbored errors in the FLAG sequence itself. Within the ten selected sequences a number of deviations from the original template were observed (**Figure 5.6**). Sequence 1 displayed the fewest errors but contained a deletion of 20 nucleotides approximately 20 base pairs upstream of the guide sequence induced a frameshift which resulted in both translation of the FLAG tag and termination of protein translation being incorrect. Sequences 2 - 4 and 6 - 8 were all missing 20 (sequence 7) or 21 nucleotides which partially included the guide sequence. Although a deletion of 21 nucleotides would not induce a frameshift, it cannot be excluded that this mutation altered protein expression or function. Sequence 9 did not have any deletions but insertions of 13 nucleotides within the PAM sequence and four nucleotides right after the FLAG sequence and before the stop codon. Again, those mutations induced frameshifts that were likely to interfere

with protein translation. Given the close proximity of the deletions and insertions to the Cas9 cleavage site, a possible explanation for those mutations is that after the ssDNA HDR template was integrated, the guide was still able to recognize the altered PAM site allowing Cas9 to induce DSBs within the template. It is also likely that DNA repair was not only driven by HDR but also the error-prone NHEJ pathway, leading to non-homologous repair by joining DSB-generated ends. Given that I have been able to isolate a clone where RIPK1 could be pulled down via its FLAG tag, at least one of those sequences is likely to have led to the successful expression of the FLAG-tagged protein. Sequencing of clone A will reveal which of those knock-in sequences, if any, was responsible for that.

By calculating the ratios of reads per sequence and total reads, I determined the highest frequency any FLAG-containing sequence was detected at to be only 0.05% (**Table 5.1**). In other words, I would have to screen 2000 single cell-derived clones to find one clone containing the sequence that occurred at the highest frequency. Taking both the high error rate and the low frequencies of integrations into account, this approach did not seem feasible to be applied as a standard technique for tagging any protein of interest. Nevertheless, in the case of RIPK1 it was still possible that clone A exhibited a useful phenotype. I next aimed to determine the sequence of this clone via Sanger sequencing since in theory only one (homozygous knock-in) or two (heterozygous knock-in) sequences could exist.

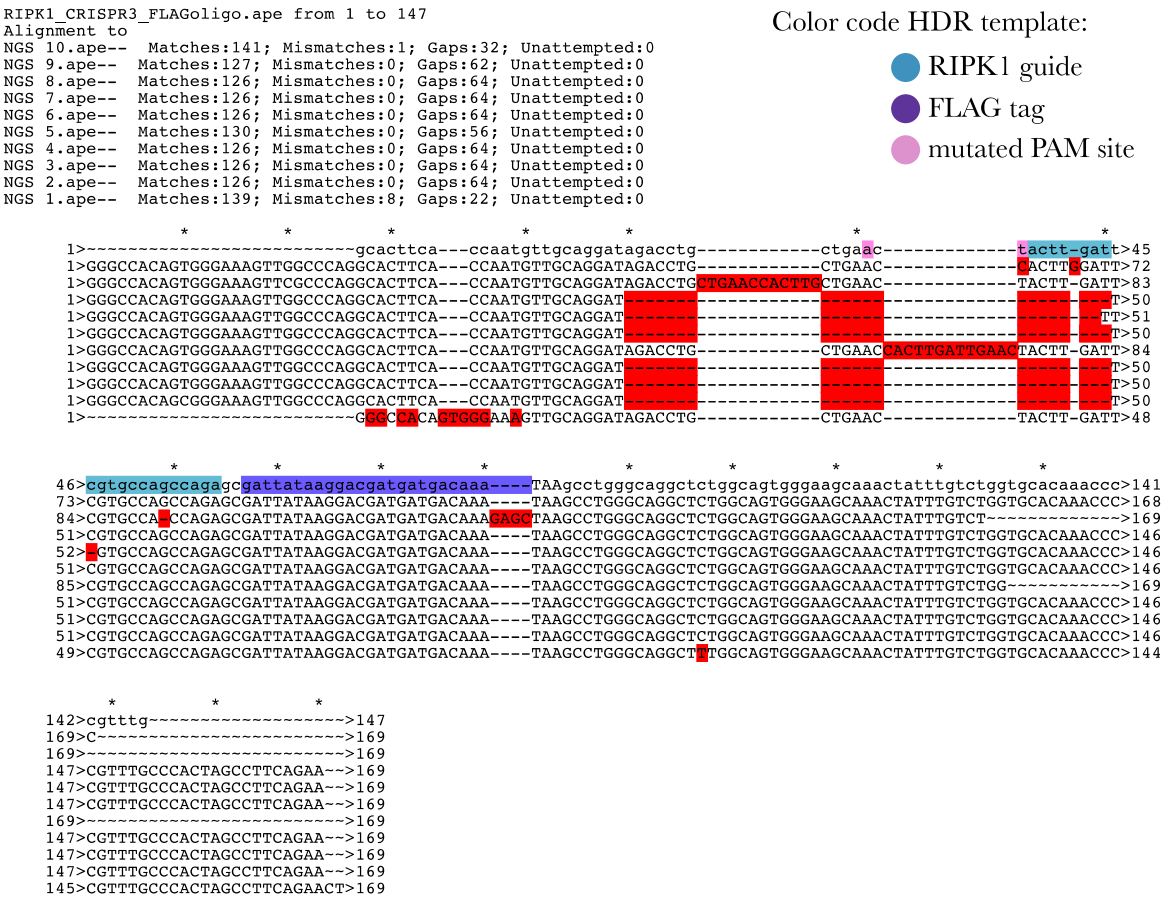

Figure 5.6: Next Generation Sequencing revealed that various knock-in sequences were generated

Multiple sequence alignment of FLAG-tag-containing knock-in sequences with the RIPK1-FLAG HDR template. Next Generation Sequencing of the MDF knock-in pool was performed using Illumina HiSeq. All sequences that contained the correct FLAG-tag sequence were aligned with the RIPK1-FLAG HDR template sequence (top sequence). Mutated PAM site (blue), guide sequence (red) and FLAG sequence (yellow) are highlighted. Gaps and mismatches in the aligned sequences are also marked in red.

Table 5.1: Frequencies of FLAG tag-containing sequences detected by NGS

Sequencing Pool	Total Reads	Sequence #	Frequence
A	219,148	1	**0.03%**
A	219,148	3	**0.03%**
A	219,148	9	**0.03%**
B	276,471	2	**0.008%**
B	276,471	6	**0.03%**
C	208,047	4	**0.05%**
D	149,628	5	**0.03%**
D	149,628	10	**0.03%**
E	98,245	7	**0.04%**
E	98,245	8	**0.04%**

5.6 Sanger sequencing of clone A revealed a high HDR error rate and the presence of multiple FLAG sequences

To reveal the sequence of clone A via Sanger sequencing, I amplified the FLAG sequence-containing region by using a forward primer that was complementary to a sequence approx. 50 bp upstream of the stop codon and a reverse primer that bound to the 3'UTR. To sequence the amplicon from both directions, I used a FLAG-specific forward primer and the PCR reverse primer. Sanger sequencing was performed by AGRF Melbourne and the sequence generated using the reverse primer was used to interpret the results (**Figure 5.7**). The sanger sequencing chromatogram in **Figure 5.7 B** indicated that clone A was heterozygous for the knock-in since at least two sequences co-exist. When multiple sequences are present, Sanger sequencing is not the ideal tool since base calls are made for the nucleotide that was detected with the highest signal intensity. However, when aligning the generated sequence (reverse complement) with the ssDNA HDR template, the sequences aligned perfectly for the stop codon and the adjacent 3'UTR. In support of that, the chromatogram showed high intensities for the leading sequence and only lowly abundant competing sequences. The FLAG sequence matched with clone A's sequence for the first 15 nucleotides and it is here where multiple nucleotide peaks in the same position started to become more prominent in the chromatogram. After the first 15 nucleotides

the FLAG sequences appears to be disrupted. Low intensities and competing nucleotide peaks prevent the interpretation of the sequences present between positions 290-230. Surprisingly, from position 228 the first 15 nucleotides of the FLAG sequence appear again with the exception of position 217 where adenine (A) is being called instead of guanidine (G) (highlighted with #1 in alignment and chromatogram). However, when analyzing the chromatogram in that position it is noticeable that a peak for the nucleotide G coexists whose intensity is only slightly lower than that of the base A which was called. It is therefore likely that this sequence in fact represents a FLAG sequence that was correctly followed by the stop codon. The presence of multiple FLAG sequences indicates that Cas9 was able to cleave the inserted sequence leading to repeated knock-in events. In addition to that, the homologous DNA repair appears to have been error prone or in competition with non-homologous end joining since the additional sequence that is flanked by the two at least partial FLAG sequences cannot be determined. It is however also possible, that that sequence did derive from the template itself and it is due to the low-quality sequence coverage in that area that it cannot be aligned.

Although the full sequence cannot be reliably interpreted, given that I was able to immunoprecipitate RIPK1 via its FLAG-tag it can be assumed that the knock-in did not induce a frameshift and that a functional version of the tag was expressed. The knock-in of approximately 60 additional nucleotides would result in the size of RIPK1 to be increased by more than 2 kDa which in turn could explain why RIPK1's band detected after immunoprecipitation via Western blot was slightly higher than expected. Due to clone A being heterozygous for the knock-in, a functional test was not performed since it wouldn't be possible to attribute its results to either of the alleles. However, given that Tab2, a known interacting partner that binds to ubiquitin chains on RIPK1, was immunoprecipitated with RIPK1 it is likely

that the introduction of the FLAG-tag and the additional sequence did not interfere with at least some of its functions. Since my aim was to develop a CRISPR/Cas9 knock-in protocol that could be used to efficiently generate endogenously tagged proteins in various cell lines in a high throughput manner, I could conclude that the tested approach did not fulfill these criteria.

A

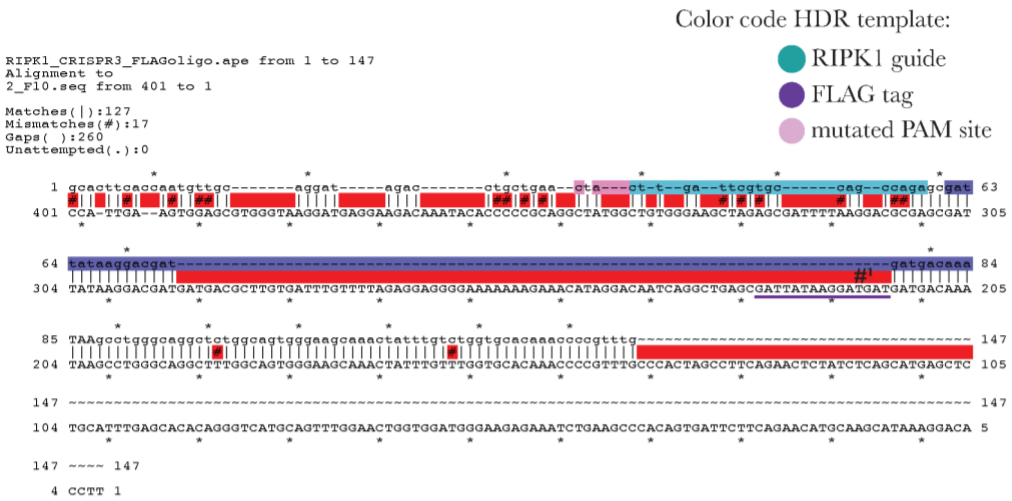

B

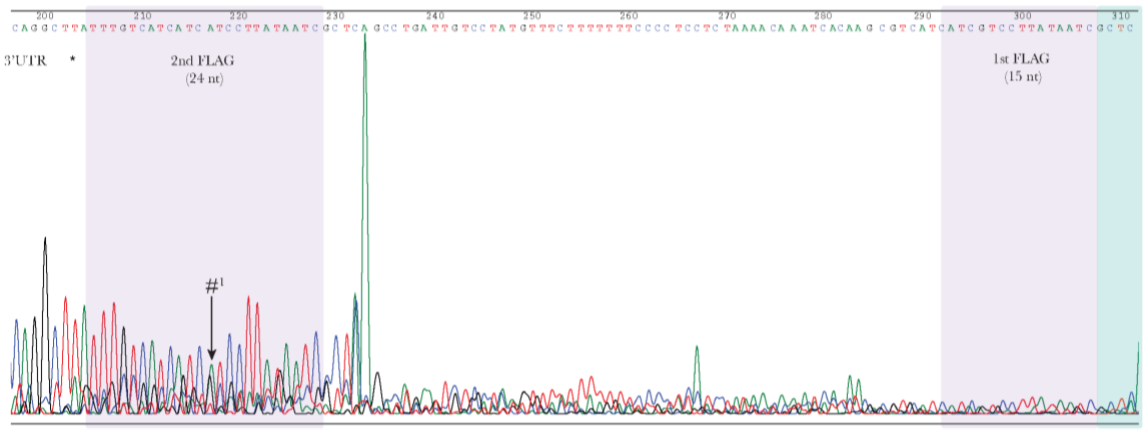

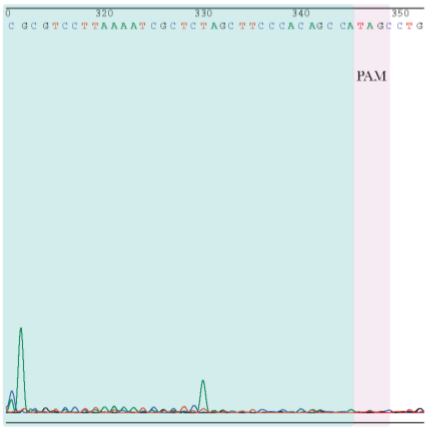

Figure 5.7: The FLAG sequence was not inserted correctly into the genome of clone A

(A) Genomic DNA from clone A was sequenced using a reverse primer binding to the 3'UTR of RIPK1. The generated sequence was then aligned with the ssDNA HDR template using ApE. (B) Sanger sequencing chromatogram of clone A. Highlighted are RIPK1 guide (red), FLAG-tag (yellow) and mutated PAM site (blue).

5.7 Discussion

As mentioned previously, a number of methods have been described that use the CRISPR/Cas9 system to introduce foreign sequences into the host's genome for the generation of tagged proteins. In the approach I applied, the FLAG tag sequence was delivered into the cells via lipofection and in the form of a ssDNA oligomer of only approximately 200 bp. The correct integration of the HDR template relies on ectopically expressed Cas9/sgRNA and the cells' HDR machinery. A high knock-in efficiency is essential to obtain cells harboring the desired foreign sequence. However, with the efficiency for detecting an integrated FLAG sequence being less than 0.1%, large numbers of clones would have to be screened, making the identification of a positive clone a very laborious and time-consuming task. Sequencing of the transfected cell pool also revealed that when a knock-in event occurs, many errors are introduced during the repair process. In fact, I was unable to obtain a sequence where the template was correctly inserted and repaired through the HDR pathway. To improve the applied approach, two factors needed to be considered: the new method would have to lead to a higher knock-in efficiency and the HDR pathway activation would have to be increased to reduce errors during the repair process. The former can be achieved by altering the way of how the guide as well the Cas9 protein are delivered into cell. Rather than transfecting cells with plasmid-borne Cas9 and sgRNA constructs which first have to be transcribed and, in the case of Cas9, translated, both could be delivered in form of Cas9/gRNA ribonucleoproteins (RNPs) (Lin *et al.*, 2014). Rather than relying on the cell to generate functional Cas9-gRNA complexes, Cas9 RNPs are provided to the cell as intact complexes. By skipping the transcription/translation and assembling processes, Cas9 RNPs can increase the efficiency of gene editing by increasing the rate at which it occurs. Since the HDR template does not have to be processed, the induction of DSBs by Cas9 and the activation of the HDR pathway by the

presence of homologous DNA occur as close to the time of transfection as possible. Another advantage the Cas9 RNP has over the plasmid-based method is that the protein complex is getting cleared by the cell rapidly, reducing the amount of time that Cas9 is able to cleave undesired targets or the introduced sequence itself. The downside of this method is that it requires the use of recombinant Cas9 which is costly. Guides have to be either purchased in form of RNA which again is expensive or generated in-house by transcription. Delivering Cas9 RNPs into cells can be achieved by either lipofection or nucleofection with the latter being another costly technique. Another disadvantage of this method is that positively transfected cells cannot be selected for. In MDFs, using lipofection to deliver DNA, only about 10-20% were successfully transfected. Not being able to select for those already increases the screening efforts by a factor of 5 - 10.

Alternatively, instead of increasing the knock-in efficiency, being able to select for positive clones using a selection marker would facilitate the screening process immensely. To accomplish this, an antibiotic resistance or fluorescence marker could be inserted into the genome together with the FLAG tag allowing the selection of positive knock-in clones by treatment with antibiotics or sorting via FACS. In that case, the HDR template would have to be a much larger, plasmid-based construct, decreasing the transfection efficiency. However, since the selection process does not rely on high transfection or gene editing efficiencies, this downside would be neglectable. On the upside, a plasmid-based construct also reduces size restrictions that apply for ssDNA oligomers which limit the length of homology arms. It is possible that homology arms of only approx. 60 bp were insufficient to fully activate the HDR pathway, leading to an error-prone repair. An HDR template plasmid containing the FLAG sequence as well as a selection marker could have much longer homology arms which might increase the accuracy at

which the DNA repair process occurs. The choice of cell type is another factor that needs to be considered when trying to improve gene editing accuracies. A cell's ability to repair Cas9-induced DSBs via the HDR pathway varies greatly (Nambiar *et al.*, 2019). With the CRISPR/Cas9 technology still being in its infancies, particularly when it comes to targeted gene editing, few cell lines have been described with regards to their HDR machineries. One cell line whose application for CRISPR/Cas9 knock-in had been demonstrated and that is frequently used in our lab is the human cell line HeLa (Koch *et al.*, 2018). HeLa cells can be easily cultured, have a high proliferation rate and can be transfected via lipofection at a high efficiency.

Taking all the acquired knowledge together, the subsequent knock-in protocol should include a template in form of a plasmid containing the FLAG sequence followed by a puromycin resistance gene to select for cells where the template has been inserted into the genome correctly with no introduced frameshifts. A schematic of such a plasmid is described in **Figure 5.8**. The depicted plasmid represents an example of how a C-terminal FLAG tag knock-in in human RIPK1 could be generated. However, strategically placed restriction sites would allow the plasmid to be used to target any given gene with a tag of choice. Additionally, the selection marker could also be replaced by an alternative marker such as a fluorescent protein in case antibiotic resistance is not desirable. Since the HDR plasmid is designed specifically for a C-terminal tag where the template is inserted upstream of the stop codon, the tag sequence needs to be followed by a stop codon. In this case, the selection marker would not be transcribed, requiring the presence of an IRES (internal ribosome entry site). If expression of the selection marker was unwanted, loxP sites could flank its sequence so that treatment with Cre recombinase would lead to the deletion of the selection marker. As described earlier, the length of the homology arms is less restricted in a plasmid. The required length for the homology arms

varies depending on the size of the fragment that is to be inserted and generally the longer the insert, the longer the homology arms should be. However, there is no formula to determine the ideal length of the homology arms since that depends on various factors such as the applied cell line and the Cas9 and sgRNA delivery method (Aird *et al.*, 2018). In HeLa cells when using a plasmid-based system for the delivery of both Cas9/sgRNA and the HDR template, homology arms of approx. 800-1000 bp have been shown to be effective at activating the cells' HDR pathway (N. Yan *et al.*, 2020).

Lastly, after more efforts are being applied towards generating endogenously tagged proteins, especially with the generation of knock-in mice being a widely available technique these days, it has been identified that the single FLAG tag can have limitations in its detectability. This is particularly true for immunofluorescent staining or when working with proteins whose expression levels are low. To circumvent this issue, a triple FLAG tag, which consists of 22 amino acids (DYKDHD-G-DYKDHD-I-DYKDDDDK) could replace the single FLAG sequence.

In summary, to improve the tested strategy for performing a CRISPR/Cas9-mediated knock-in of a protein tag, changing to a cell line that is more established for this particular technique might increase chances of success. Additionally, knocking in a selection marker together with the desired tag would allow for bypassing the issues around low efficiency knock-in events. Lastly, delivering the HDR template in form of a plasmid with longer homology arms might activate the HDR pathway more efficiently as well as decrease the error rate during DNA repair. In order to generate a method that would allow us to tag any protein of interest in any desired cell

line we need to better understand how the cells' DNA repair machineries function, how they can be activated or suppressed and how we can harness them more efficiently.

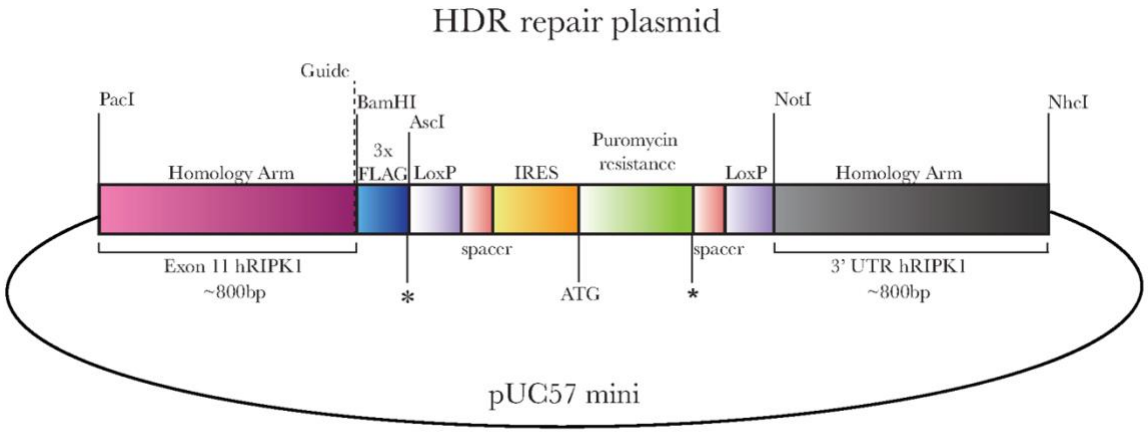

Figure 5.8: Schematic of plasmid-based knock-in approach.

HDR template plasmid for the knock-in of a C-terminal FLAG-tag into hRIPK1. Homology arms flanking the 3XFLAG-tag and the puromycin resistance selection marker are approx. 800 bp long and are homologous to a region in exon 11 of hRIPK1 including the guide sequence and mutated PAM site (left) or the 3'UTR (right). An IRES is placed upstream of the puromycin resistance cassette to ensure its transcription. IRES and puromycin resistance cassettes are flanked by loxP sites and spacers to facilitate cleavage by Cre recombinase. Restrictions sites were placed to enable the replacement of the homology arms (PacI/BamHI and NotI/NheI), the 3XFLAG tag (BamHI/AscI) and the puromycin resistance cassette with its adjacent IRES (AscI/NotI). IRES, internal ribosome entry site.

6 Conclusion and future perspectives

6.1 AML mouse model

In Chapter 3 of this thesis I presented data on the effect of EVI1 overexpression in MLL-AF9 driven AML *in vivo* and *in vitro*. In my study, I aimed to develop a disease model, that faithfully mimics a particular aggressive form of human AML in mice as commonly used AML mouse model currently fail to reflect the molecular complexities observed in patients. Generating EVI1-expressing leukemias consistently was challenging with the majority of mice developing $EVI1_{neg}$ AML. When EVI1 was expressed in leukemic cells, the expression levels varied greatly. Although EVI1 expression did not affect latency, disease pathology or phenotypical features of AML, *in vitro*, $EVI1_{pos}$ AML showed increased resistance to cell death-inducing treatment, where the degree of resistance correlated with EVI1 expression levels. These findings indicate that in MLL-AF9 AML, high levels of EVI1 can reduce the sensitivity of leukemic cells to chemotherapy, at least *in vitro,* which is consistent with what is observed in human patients. This work therefore justifies efforts towards developing a technique that allows the reliable and consistent generation of an MLL-AF9/EVI1 mouse model.

To date, many AML patients are still burdened with a poor prognosis and progression towards improved treatments has been slow. A major barrier for the translation of novel therapies from research into the clinic is the lack of appropriate disease models. AML models often rely on the expression of one oncogene while additional mutations may occur at random during latency. However, AML is a genetically heterogenous disease rather than a homologous collection of malignant cells (Saygin *et al.*, 2019). It exhibits a phenotypic and functional diversity which greatly contributes to treatment resistance and relapse and which is difficult to mimic in AML

models (Meacham *et al.*, 2013). There is strong evidence that within a subclone, the ability of a cell to survive anti-cancer treatment is not determined by genetics but can rather be contributed to epigenetic modifications which lead to the activation of developmental pathways (Visvader *et al.*, 2012). The transcription factor and proto-oncogene EVI1 is commonly over-expressed in AMLs with MLL-translocation, where it is associated with poor prognosis. Evidence suggests, that the transcriptional upregulation of EVI1 in AML is caused by aberrant epigenetic patterns (Vazquez *et al.*, 2011). As discussed earlier (Section 1.3), the role of EVI1 in leukemogenesis in mice has been confirmed and its ability to accelerate disease onset in animal models was in line with observations in human patients, where high EVI1 levels were linked to more aggressive forms of the disease (Gomez-Benito *et al.*, 2010). Generating an MLL-AF9/EVI1 mouse model as a tool to develop novel therapies therefore represents a progression from commonly used models that only rely on the expression of AML-inducing oncogenes. When aiming to develop such a model by injecting fetal liver cells that were retrovirally transduced with constructs encoding for MLL-AF9 and EVI1 into irradiated mice, I faced great challenges that I described in detail in Chapter 3. I hypothesized, that EVI1 expression will provide leukemic cells with an additional proliferative advantage leading to an enrichment of EVI_{pos} cells and hence the development of MLL-AF9/EVI AML. I further hypothesized that the onset of EVI1-expressing AML will be accelerated and exhibit a more severe disease phenotype as well as an increased resistance to treatment. Since the majority of generated leukemias did not express EVI1 and with most EVI_{pos} AMLs only expressing the transcription factor in a population of cells, EVI1 did not appear to provide transformed cells with an additional proliferative advantage. When MLL-AF9/EVI1 AML was successfully generated, latency and severity were unaffected by the expression of EVI1. A role of EVI1 in leukemogenesis was however supported, when EVI_{pos} AMLs demonstrated increased resistance to *in vitro* treatment with a chemotherapeutic agent

or a Smac mimetic combination treatment that otherwise efficiently kills MLL-AF9 cells *in vivo* and *in vitro*. Intriguingly, this resistance positively correlated with EVI1 expression levels.

In summary, I believe that this work delivers a compelling argument for continued efforts into developing an MLL-driven $EVI1_{high}$ AML mouse model. Such a model could faithfully reflect a particularly aggressive and treatment-resistant AML which is of great relevance for the development of novel therapies. Since patients that present at clinical trials have previously undergone unsuccessful conventional therapy, the efficiencies of novel treatments are generally tested in patients that suffer from more aggressive and treatment-resistant forms of AML.

The lack of appropriate mouse models for the overexpression of EVI1 has been discussed in the literature in great detail (Glass *et al.*, 2014). Recently, an EVI1-inducible system was developed by inserting seven Tet operons into the first exon, allowing for the over-expression of all three isoforms of endogenous EVI1 (Ayoub *et al.*, 2018). EVI1 expression was induced by crossing $Evi1^{TO/TO}$ (harbors tet-inducible *Evi1* allele) to $Rosa^{rtTA/rtTA}$ (harbors reverse-tet transactivator). Although this model was used to study the molecular mechanisms of EVI1 in leukemogenesis, it could also be a powerful tool for the efficient generation of EVI1-expressing AML or cancers in general. To do so, fetal livers from $Evi1^{TO/TO}/Rosa^{rtTA/rtTA}$ embryos could be transduced with MLL-AF9 and injected into irradiated mice. Upon administration of Dox, EVI1 expression would be induced in all hematopoietic cells including all leukemic cells that will develop. Therefore, high EVI1 levels would be guaranteed to occur in all AMLs, leading to reduced variability and increased reproducibility. Using this approach could enable us to develop an AML model that can be standardized and that faithfully reflects a particularly

aggressive and treatment-resistant form of AML. Such a model would be a powerful tool for the development of novel therapies.

6.2 The role of p38 in inhibiting Smac mimetic-induced cell death

In Chapter 4 of this thesis I investigated the role of the MAP kinase p38 in inhibiting TNF-dependent death in cells treated with Smac mimetic. To uncover novel functions of p38 in regulating apoptosis in the absence of IAPs, I studied the phosphoproteome of BMDMs treated with Smac mimetic alone or in combination with a p38 inhibitor and identified proteins that were differentially phosphorylated in the two treatments. This work revealed that the cell survival pathway PI3K/Akt/mTOR was activated in Smac mimetic-treated cells and that this activation appeared to be dependent on p38. Additionally, the production of TNF appeared to be negatively regulated by p38, although further research is required to confirm the roles of detected phosphorylation sites on a number of TNF mediators. These findings clearly increase our understanding of treatment resistance to Smac mimetic which greatly limits its application as a single agent. Furthermore, my work presented strong evidence that p38 can inhibit cell death through additional mechanisms to phosphorylation of RIPK1 by MK2 and that these mechanisms involve the activation of cell survival pathways and the suppression of TNF. However, the exact mechanisms by which p38 regulates these processes remain mostly unresolved.

The upregulation of IAPs are commonly detected in different cancers where they can contribute to treatment resistance (Owens *et al.*, 2013). For that reason, the IAPs were identified as an attractive target for anti-cancer therapy which lead to the development of IAP antagonists called

Smac mimetics. Disappointingly, the ability of Smac mimetics to induce cell death in cancer cells as a single agent was limited. However, resistances to Smac mimetic could often be overcome by the addition of exogenous TNF. Today, a number of highly effective combination treatments involving Smac mimetics have been described to selectively and efficiently induce cell death in cancer cells *in vivo* and *in vitro*. One of those treatments that evolved from my lab is the combination of the Smac mimetic Birinapant and a p38 inhibitor (Najoua Lalaoui *et al.*, 2016). Smac mimetics induce cell death that is dependent on TNF and the additional inhibition of p38 has been found to dramatically increase TNF production in treated cells. One mechanism through which p38 inhibits cell death in the absence of IAPs is through the activation of its substrate MK2 which in turn phosphorylates RIPK1 (Jaco *et al.*, 2017). Phosphorylated RIPK1 is unable to participate in the formation of the cell death-inducing complex II, hence inhibiting apoptosis. We have identified that the phosphorylation of RIPK1 is not the only mechanism through which p38 and inhibit cell death, since RIPK1$^{S321A/S226A}$ BMDMs could be further sensitized to Smac mimetic-induced cell death when p38 or MK2 were inhibited (**Figure 4.1**). By studying the phosphoproteome of treated cells, I identified that the cell survival pathway PI3K/Akt/mTOR was activated upon Smac mimetic treatment potentially preventing cell death to occur. As a possible activator of this pathway, I detected novel phosphorylation sites on the receptor tyrosine kinase CSF1R when p38 was additionally inhibited. I hypothesized that four phosphorylated residues detected in the combination treatment, flanked Tyr721, whose phosphorylation is required for CSF1R activity, prevented the activation of the PI3K/Akt/mTOR pathway. As a consequence, inhibition of this cell survival pathway allows cell death to occur. This hypothesis was confirmed, when the inhibition of CSF1R in Smac mimetic-treated cells also induced cell death. Furthermore, I confirmed by Western blot that downstream of PI3K, activation of Akt was reduced in the combination

treatment of Smac mimetic and p38 inhibitor. Whether the ability of p38 to inhibit cell death by activating the cell survival pathway PI3K/Akt/mTOR is independent of MK2-mediated RIPK1 phosphorylation will need to be confirmed. This could be done by assessing the cell death in RIPK1$_{S321A/S226A}$ induced by the combination of Smac mimetic and CSF1Ri. If the inhibition of CSF1R further sensitizes cells to Smac mimetic-induced cell death, it can be assumed that p38 can activate the PI3K/Akt/mTOR pathway independently of RIPK1.

Since the PI3K/Akt/mTOR pathway is commonly upregulated in cancers, my work revealed not only an important resistance mechanism to Smac mimetic treatment but also uncovered a novel role of p38 in the activation of this pathway (Jing Yang *et al.*, 2019). At the same time, the inhibition of p38 effectively prevented PI3K/Akt/mTOR signaling which was potentially mediated by a kinase that is able to inhibit CSF1R activity by phosphorylation. It would be of great interest to identify this kinase which appears to be activated only upon p38 inhibition. Its identification would therefore give us an even greater insight into the complex roles of p38 and its involvement in cell survival and cell death.

Phosphoproteomics represents a powerful tool for studying complex signaling events. During this project, I identified a large number of novel phosphorylation sites and I was able to associate known phosphosites with potential regulatory functions. Although more work is needed to confirm these functions, the amount of information gained from just one experiment is astounding. In order to validate functions of phosphosites in a fast, reliable and economic manner, techniques that allow for the generation of phospho mutants in cell lines need to be improved. One technique that enables us to precisely modify proteins and study their function

in their endogenous environment is CRISPR/Cas9-mediated knock-in. However, the application of this approach in cell lines, remains challenging.

6.3 CRISPR/Cas9-mediated knock-in to generate tagged proteins

In Chapter 6 of this thesis I documented my approach of generating a protocol that allows for the precise insertion of a molecular FLAG-tag into the genome of cells using CRISPR/Cas9-mediated knock-in. By applying this technique, I aimed to tag proteins of the TNF pathway enabling us to address outstanding questions by studying its components on an endogenous level. The use of molecular tags to immunoprecipitate proteins with their interactors or to visualize protein localization in a cell via immunofluorescence, is a well-established tool (Gerace et al., 2015). Traditionally, this involves the generation of a transgenic expression construct which encodes for the gene of interest fused to the FLAG sequence and the stable, random integration of this plasmid into the genome of cell lines via viral transduction (Izmiryan *et al.*, 2011). Often the target cell lines are void of this gene either due to genetic deletion or by nature. This approach however can be flawed since protein expression levels do not replicate endogenous concentrations which can lead to altered protein functions (Moriya, 2015). In some cases, once a gene was deleted in a cell, it cannot be reintroduced as it is the case with mRIPK1. Therefore, the ability to precisely introduce foreign sequences into a cells' genome is a powerful tool that allows researchers to explore proteins in their endogenous environment. Given the complexity of the TNF pathway and the limitations we are facing when using traditional molecular tools, tagging its components using CRISPR/Cas9-mediated knock-in would present us with the opportunity to address questions that we were not able to explore previously. Although a number of protocols that describe methods for applying CRISPR/Cas9-mediated knock-in in cell lines, transferring the approaches to different cell lines and genes often fails.

Generally, the methods differ in the way of how foreign content (DNA, RNA, protein) is delivered into the cell with the two main methods being nucleofection and lipofection. Other deviations involve the format of Cas9 used (recombinant protein vs. DNA expression construct), the format of the guide (RNA vs. DNA expression construct) and the nature of the tag-containing knock-in template (ssDNA vs. plasmid). To develop a protocol that can be routinely used, I chose an approach that is cost-effective and involved the use of a dual expression construct encoding for Cas9 and the sgRNA and an ssDNA HDR knock-in template of maximal 200 bp. All constructs were simultaneously delivered into the cells via lipofection. To test the efficiency of this approach, I aimed to introduce a FLAG-tag into the C-terminus of RIPK1 in MDFs. Although I was able to select for successfully transfected cells due to the presence of a puromycin resistance gene within the Cas9/sgRNA plasmid, extremely low knock-in efficiency required for the screening of hundreds of single cell clones. Unexpectedly, next generation sequencing revealed a high error rate during the homologues DNA repair indicating that the HDR mechanism in MDFs has inferior efficiency and is dwarfed by that of the NHEJ machinery. It is therefore possible, that MDFs are inherently less hospitable to CRISPR/Cas9-mediated knock-in compared to cell types that have been described to exhibit high HDR efficiencies such HEK293T cells (X. Xu *et al.*, 2018).

In summary, two issues needed to be addressed in order to develop a protocol that can be routinely used for tagging any gene of the TNF pathway in cell lines: Firstly, knock-ins needed to occur at higher frequencies to reduce the time required to screen for clones positive for a knock-in and secondly, error rates had to be reduced to generate knock-ins that contained the correct sequences. Since knock-in efficiencies in MDFs were extremely low and errors occurred at a rate that did not even allow for the detection of a correct knock-in sequence even when the

NHEJ inhibitor SCR7 was applied, an alternative cell line needs to be used. A cell line in which CRISPR/Cas9-mediated knock-in has been successfully used in and that is appropriate for the study of the TNF pathway is the human cell line HeLa (Koch *et al.*, 2018). To overcome the necessity of screening a large number of clones, we could simultaneously knock-in a selection marker like an antibiotic resistance gene or a florescent protein. This would allow for the selection of positive clones where the template was inserted into the genome in frame. As described in Chapter 5.7, **Figure 5.8**, I outlined a design of a knock-in construct that would enable the selection of positive clones using puromycin treatment. By applying this approach, we could generate tagged proteins in an efficient, cost-effective and timely manner while overcoming the need of laborious screening processes. The work I have presented here, underlines the challenges we are still facing when trying to harness the ability of the CRISPR/Cas9 technology to precisely insert foreign sequences into the genomes of cell lines. I demonstrated that even when a knock-in occurs, deficiencies in the HDR machinery can lead to a high error rate in the homologous repair of DNA. I believe that by implementing the proposed strategies of choosing a cell line that is equipped with efficient HDR mechanisms and the co-insertion of a resistance marker, tagged proteins could be successfully generated in a timely and cost-effective fashion.

References

Agod, Z., Pazmandi, K., *et al.* (2018). Signaling Lymphocyte Activation Molecule Family 5 Enhances Autophagy and Fine-Tunes Cytokine Response in Monocyte-Derived Dendritic Cells via Stabilization of Interferon Regulatory Factor 8. *Front Immunol, 9*, 62. doi:10.3389/fimmu.2018.00062

Aira, L. E., Villa, E., *et al.* (2018). The oncogenic tyrosine kinase Lyn impairs the pro-apoptotic function of Bim. *Oncogene, 37*(16), 2122-2136. doi:10.1038/s41388-017-0112-0

Aird, E. J., Lovendahl, K. N., *et al.* (2018). Increasing Cas9-mediated homology-directed repair efficiency through covalent tethering of DNA repair template. *Communications Biology, 1*(1), 54. doi:10.1038/s42003-018-0054-2

Alharbi, R. A., Pettengell, R., *et al.* (2013). The role of HOX genes in normal hematopoiesis and acute leukemia. *Leukemia, 27*(5), 1000-1008. doi:10.1038/leu.2012.356

Altin, J. G., & Sloan, E. K. (1997). The role of CD45 and CD45-associated molecules in T cell activation. *Immunol Cell Biol, 75*(5), 430-445. doi:10.1038/icb.1997.68

Amir, M., Somakala, K., *et al.* (2013). p38 MAP kinase inhibitors as anti inflammatory agents. *Mini Rev Med Chem, 13*(14), 2082-2096. doi:10.2174/13895575113136660098

Apostolaki, M., Armaka, M., *et al.* (2010). Cellular mechanisms of TNF function in models of inflammation and autoimmunity. *Curr Dir Autoimmun, 11*, 1-26. doi:10.1159/000289195

Ayoub, E., Wilson, M. P., *et al.* (2018). EVI1 overexpression reprograms hematopoiesis via upregulation of Spi1 transcription. *Nature Communications, 9*(1), 4239. doi:10.1038/s41467-018-06208-y

Bai, L., Smith, D. C., *et al.* (2014). Small-molecule SMAC mimetics as new cancer therapeutics. *Pharmacol Ther, 144*(1), 82-95. doi:10.1016/j.pharmthera.2014.05.007

Balgobind, B. V., Raimondi, S. C., *et al.* (2009). Novel prognostic subgroups in childhood 11q23/MLL-rearranged acute myeloid leukemia: results of an international retrospective study. *Blood, 114*(12), 2489-2496. doi:10.1182/blood-2009-04-215152

Barjesteh van Waalwijk van Doorn-Khosrovani, S., Erpelinck, C., *et al.* (2003). High EVI1 expression predicts poor survival in acute myeloid leukemia: a study of 319 de novo AML patients. *Blood, 101*(3), 837-845. doi:10.1182/blood-2002-05-1459

Basilico, S., & Göttgens, B. (2017). Dysregulation of haematopoietic stem cell regulatory programs in acute myeloid leukaemia. *Journal of molecular medicine (Berlin, Germany), 95*(7), 719-727. doi:10.1007/s00109-017-1535-3

Bertrand, M. J., Milutinovic, S., *et al.* (2008). cIAP1 and cIAP2 facilitate cancer cell survival by functioning as E3 ligases that promote RIP1 ubiquitination. *Mol Cell, 30*(6), 689-700. doi:10.1016/j.molcel.2008.05.014

Bindels, E. M., Havermans, M., *et al.* (2012). EVI1 is critical for the pathogenesis of a subset of MLL-AF9-rearranged AMLs. *Blood, 119*(24), 5838-5849. doi:10.1182/blood-2011-11-393827

Binsky-Ehrenreich, I., Marom, A., *et al.* (2014). CD84 is a survival receptor for CLL cells. *Oncogene, 33*(8), 1006-1016. doi:10.1038/onc.2013.31

Brooks, D. J., Woodward, S., *et al.* (1996). Expression of the zinc finger gene EVI-1 in ovarian and other cancers. *Br J Cancer, 74*(10), 1518-1525. doi:10.1038/bjc.1996.583

Brumatti, G., Ma, C., *et al.* (2016). The caspase-8 inhibitor emricasan combines with the SMAC mimetic birinapant to induce necroptosis and treat acute myeloid leukemia. *Sci Transl Med, 8*(339), 339ra369. doi:10.1126/scitranslmed.aad3099

Cagnol, S., & Chambard, J.-C. (2010). ERK and cell death: Mechanisms of ERK-induced cell death – apoptosis, autophagy and senescence. *The FEBS Journal, 277*(1), 2-21. doi:10.1111/j.1742-4658.2009.07366.x

Cai, B., Chang, S. H., *et al.* (2006). p38 MAP kinase mediates apoptosis through phosphorylation of BimEL at Ser-65. *J Biol Chem, 281*(35), 25215-25222. doi:10.1074/jbc.M512627200

Cen, B., Xiong, Y., *et al.* (2014). The Pim-1 protein kinase is an important regulator of MET receptor tyrosine kinase levels and signaling. *Molecular and cellular biology, 34*(13), 2517-2532. doi:10.1128/MCB.00147-14

Chai, J., Du, C., *et al.* (2000). Structural and biochemical basis of apoptotic activation by Smac/DIABLO. *Nature, 406*(6798), 855-862. doi:10.1038/35022514

Chang, M., Hamilton, J. A., *et al.* (2009). Phosphatidylinostitol-3 kinase and phospholipase C enhance CSF-1-dependent macrophage survival by controlling glucose uptake. *Cell Signal, 21*(9), 1361-1369. doi:10.1016/j.cellsig.2009.04.003

Chen, K., Yang, J., *et al.* (2016). eIF4B is a convergent target and critical effector of oncogenic Pim and PI3K/Akt/mTOR signaling pathways in Abl transformants. *Oncotarget, 7*(9), 10073-10089. doi:10.18632/oncotarget.7164

Chen, Y. L., Law, P. Y., *et al.* (2005). Inhibition of PI3K/Akt signaling: an emerging paradigm for targeted cancer therapy. *Curr Med Chem Anticancer Agents, 5*(6), 575-589. doi:10.2174/156801105774574649

Cheung, P. C., Campbell, D. G., *et al.* (2003). Feedback control of the protein kinase TAK1 by SAPK2a/p38alpha. *Embo j, 22*(21), 5793-5805. doi:10.1093/emboj/cdg552

Chromik, J., Safferthal, C., *et al.* (2014). Smac mimetic primes apoptosis-resistant acute myeloid leukaemia cells for cytarabine-induced cell death by triggering necroptosis. *Cancer Lett, 344*(1), 101-109. doi:10.1016/j.canlet.2013.10.018

Cohen, S., Shoshana, O.-y., *et al.* (2012). The Cytokine Midkine and Its Receptor RPTPζ Regulate B Cell Survival in a Pathway Induced by CD74. *The Journal of Immunology, 188*(1), 259. doi:10.4049/jimmunol.1101468

Cuenca, M., Sintes, J., *et al.* (2019). CD84 cell surface signaling molecule: An emerging biomarker and target for cancer and autoimmune disorders. *Clin Immunol, 204*, 43-49. doi:10.1016/j.clim.2018.10.017

Cui, J., Stahl, E. A., *et al.* (2013). Genome-wide association study and gene expression analysis identifies CD84 as a predictor of response to etanercept therapy in rheumatoid arthritis. *PLoS Genet, 9*(3), e1003394. doi:10.1371/journal.pgen.1003394

D'Oro, U., & Ashwell, J. D. (1999). Cutting Edge: The CD45 Tyrosine Phosphatase Is an Inhibitor of Lck Activity in Thymocytes. *The Journal of Immunology, 162*(4), 1879-1883. doi:doi: 10.4049/jimmunol.178.4.2056

Dan, H. C., Ebbs, A., *et al.* (2014). Akt-dependent activation of mTORC1 complex involves phosphorylation of mTOR (mammalian target of rapamycin) by IkappaB kinase alpha (IKKalpha). *J Biol Chem, 289*(36), 25227-25240. doi:10.1074/jbc.M114.554881

Darding, M., Feltham, R., *et al.* (2011). Molecular determinants of Smac mimetic induced degradation of cIAP1 and cIAP2. *Cell Death Differ, 18*(8), 1376-1386. doi:10.1038/cdd.2011.10

Das, M., Sabio, G., *et al.* (2009). Induction of hepatitis by JNK-mediated expression of TNF-alpha. *Cell, 136*(2), 249-260. doi:10.1016/j.cell.2008.11.017

Datta, S. R., Brunet, A., *et al.* (1999). Cellular survival: a play in three Akts. *Genes Dev, 13*(22), 2905-2927. doi:10.1101/gad.13.22.2905

De Kouchkovsky, I., & Abdul-Hay, M. (2016). 'Acute myeloid leukemia: a comprehensive review and 2016 update'. *Blood cancer journal, 6*(7), e441-e441. doi:10.1038/bcj.2016.50

Deleault, K. M., Skinner, S. J., *et al.* (2008). Tristetraprolin regulates TNF TNF-alpha mRNA stability via a proteasome dependent mechanism involving the combined action of the ERK and p38 pathways. *Mol Immunol, 45*(1), 13-24. doi:10.1016/j.molimm.2007.05.017

Deveraux, Q. L., Takahashi, R., *et al.* (1997). X-linked IAP is a direct inhibitor of cell-death proteases. *Nature, 388*(6639), 300-304. doi:10.1038/40901

Dohner, K., & Dohner, H. (2008). Molecular characterization of acute myeloid leukemia. *Haematologica, 93*(7), 976-982. doi:10.3324/haematol.13345

Dondelinger, Y., Delanghe, T., *et al.* (2017). MK2 phosphorylation of RIPK1 regulates TNF-mediated cell death. *Nat Cell Biol, 19*(10), 1237-1247. doi:10.1038/ncb3608

Doudna, J. A., & Charpentier, E. (2014). The new frontier of genome engineering with CRISPR-Cas9. *Science, 346*(6213), 1258096. doi:10.1126/science.1258096

Doyle, A., McGarry, M. P., *et al.* (2012). The construction of transgenic and gene knockout/knockin mouse models of human disease. *Transgenic research, 21*(2), 327-349. doi:10.1007/s11248-011-9537-3

Duraisamy, S., Bajpai, M., *et al.* (2008). MK2: a novel molecular target for anti-inflammatory therapy. *Expert Opinion on Therapeutic Targets, 12*(8), 921-936. doi:10.1517/14728222.12.8.921

Eckelman, B. P., & Salvesen, G. S. (2006). The human anti-apoptotic proteins cIAP1 and cIAP2 bind but do not inhibit caspases. *J Biol Chem, 281*(6), 3254-3260. doi:10.1074/jbc.M510863200

Estey, E. (2015). Why Is Progress in Acute Myeloid Leukemia So Slow? *Semin Hematol, 52*(3), 243-248. doi:10.1053/j.seminhematol.2015.03.007

Estey, E., & Dohner, H. (2006). Acute myeloid leukaemia. *Lancet, 368*(9550), 1894-1907. doi:10.1016/s0140-6736(06)69780-8

Etemadi, N., Chopin, M., *et al.* (2015). TRAF2 regulates TNF and NF-κB signalling to suppress apoptosis and skin inflammation independently of Sphingosine kinase 1. *eLife, 4*, e10592. doi:10.7554/eLife.10592

Feng, S., Yang, Y., *et al.* (2007). Cleavage of RIP3 inactivates its caspase-independent apoptosis pathway by removal of kinase domain. *Cell Signal, 19*(10), 2056-2067. doi:10.1016/j.cellsig.2007.05.016

Feoktistova, M., Geserick, P., *et al.* (2011). cIAPs Block Ripoptosome Formation, a RIP1/Caspase-8 Containing Intracellular Cell Death Complex Differentially Regulated by cFLIP Isoforms. *Molecular Cell, 43*(3), 449-463. doi:10.1016/j.molcel.2011.06.011

Feoktistova, M., Geserick, P., *et al.* (2012). Pick your poison: the Ripoptosome, a cell death platform regulating apoptosis and necroptosis. *Cell Cycle, 11*(3), 460-467. doi:10.4161/cc.11.3.19060

Foey, A. D., Parry, S. L., *et al.* (1998). Regulation of Monocyte IL-10 Synthesis by Endogenous IL-1 and TNF-α: Role of the p38 and p42/44 Mitogen-Activated Protein Kinases. *The Journal of Immunology, 160*(2), 920.

Fulda, S. (2015). Promises and Challenges of Smac Mimetics as Cancer Therapeutics. *Clin Cancer Res, 21*(22), 5030-5036. doi:10.1158/1078-0432.Ccr-15-0365

Fulda, S., & Debatin, K. M. (2006). Targeting inhibitor of apoptosis proteins (IAPs) for diagnosis and treatment of human diseases. *Recent Pat Anticancer Drug Discov, 1*(1), 81-89.

Fulda, S., & Vucic, D. (2012). Targeting IAP proteins for therapeutic intervention in cancer. *Nat Rev Drug Discov, 11*(2), 109-124. doi:10.1038/nrd3627

Gaestel, M., Kotlyarov, A.*, et al.* (2009). Targeting innate immunity protein kinase signalling in inflammation. *Nat Rev Drug Discov, 8*(6), 480-499. doi:10.1038/nrd2829

Geng, L., Raab, M.*, et al.* (1999). Cutting edge: SLP-76 cooperativity with FYB/FYN-T in the Up-regulation of TCR-driven IL-2 transcription requires SLP-76 binding to FYB at Tyr595 and Tyr651. *J Immunol, 163*(11), 5753-5757.

Genovese, M. C. (2009). Inhibition of p38: Has the fat lady sung? *Arthritis & Rheumatism, 60*(2), 317-320. doi:10.1002/art.24264

Gerace, E., & Moazed, D. (2015). Affinity Pull-Down of Proteins Using Anti-FLAG M2 Agarose Beads. *Methods in enzymology, 559*, 99-110. doi:10.1016/bs.mie.2014.11.010

Glass, C., Wilson, M.*, et al.* (2014). The role of EVI1 in myeloid malignancies. *Blood Cells, Molecules, and Diseases, 53*(1), 67-76. doi:10.1016/j.bcmd.2014.01.002

Glass, C., Wuertzer, C.*, et al.* (2013). Global Identification of EVI1 Target Genes in Acute Myeloid Leukemia. *PloS one, 8*(6), e67134-e67134. doi:10.1371/journal.pone.0067134

Gomez-Benito, M., Conchillo, A.*, et al.* (2010). EVI1 controls proliferation in acute myeloid leukaemia through modulation of miR-1-2. *Br J Cancer, 103*(8), 1292-1296. doi:10.1038/sj.bjc.6605874

Gonzalez-Teran, B., Cortes, J. R.*, et al.* (2013). Eukaryotic elongation factor 2 controls TNF-alpha translation in LPS-induced hepatitis. *J Clin Invest, 123*(1), 164-178. doi:10.1172/jci65124

Goyama, S., Yamamoto, G.*, et al.* (2008). Evi-1 is a critical regulator for hematopoietic stem cells and transformed leukemic cells. *Cell Stem Cell, 3*(2), 207-220. doi:10.1016/j.stem.2008.06.002

Grimwade, D., & Hills, R. K. (2009). Independent prognostic factors for AML outcome. *Hematology Am Soc Hematol Educ Program*, 385-395. doi:10.1182/asheducation-2009.1.385

Grimwade, D., Ivey, A.*, et al.* (2016). Molecular landscape of acute myeloid leukemia in younger adults and its clinical relevance. *Blood, 127*(1), 29-41. doi:10.1182/blood-2015-07-604496

Groschel, S., Schlenk, R. F.*, et al.* (2013). Deregulated expression of EVI1 defines a poor prognostic subset of MLL-rearranged acute myeloid leukemias: a study of the German-Austrian Acute Myeloid Leukemia Study Group and the Dutch-Belgian-Swiss HOVON/SAKK Cooperative Group. *J Clin Oncol, 31*(1), 95-103. doi:10.1200/jco.2011.41.5505

Grossmann, V., Schnittger, S.*, et al.* (2013). High incidence of RAS signalling pathway mutations in MLL-rearranged acute myeloid leukemia. *Leukemia, 27*(9), 1933-1936. doi:10.1038/leu.2013.90

Gyrd-Hansen, M., Darding, M.*, et al.* (2008). IAPs contain an evolutionarily conserved ubiquitin-binding domain that regulates NF-kappaB as well as cell survival and oncogenesis. *Nat Cell Biol, 10*(11), 1309-1317. doi:10.1038/ncb1789

Hamilton, J. A. (2008). Colony-stimulating factors in inflammation and autoimmunity. *Nat Rev Immunol, 8*(7), 533-544. doi:10.1038/nri2356

Han, M. S., Jung, D. Y., *et al.* (2013). JNK expression by macrophages promotes obesity-induced insulin resistance and inflammation. *Science (New York, N.Y.), 339*(6116), 218-222. doi:10.1126/science.1227568

Hatano, A., Matsumoto, M., *et al.* (2016). Phosphoproteomics analyses show subnetwork systems in T-cell receptor signaling. *Genes to Cells, 21*(10), 1095-1112. doi:10.1111/gtc.12406

Hennessy, B. T., Smith, D. L., *et al.* (2005). Exploiting the PI3K/AKT pathway for cancer drug discovery. *Nat Rev Drug Discov, 4*(12), 988-1004. doi:10.1038/nrd1902

Hermiston, M. L., Xu, Z., *et al.* (2003). CD45: a critical regulator of signaling thresholds in immune cells. *Annu Rev Immunol, 21*, 107-137. doi:10.1146/annurev.immunol.21.120601.140946

Hille, F., Richter, H., *et al.* (2018). The Biology of CRISPR-Cas: Backward and Forward. *Cell, 172*(6), 1239-1259. doi:10.1016/j.cell.2017.11.032

Hinds, M. G., Norton, R. S., *et al.* (1999). Solution structure of a baculoviral inhibitor of apoptosis (IAP) repeat. *Nat Struct Biol, 6*(7), 648-651. doi:10.1038/10701

Holz, M. K., Ballif, B. A., *et al.* (2005). mTOR and S6K1 Mediate Assembly of the Translation Preinitiation Complex through Dynamic Protein Interchange and Ordered Phosphorylation Events. *Cell, 123*(4), 569-580. doi:10.1016/j.cell.2005.10.024

Hopp, T. P., Prickett, K. S., *et al.* (1988). A Short Polypeptide Marker Sequence Useful for Recombinant Protein Identification and Purification. *Bio/Technology, 6*(10), 1204-1210. doi:10.1038/nbt1088-1204

Hsu, L. S., Chen, G. D., *et al.* (2001). Human Ca2+/calmodulin-dependent protein kinase kinase beta gene encodes multiple isoforms that display distinct kinase activity. *J Biol Chem, 276*(33), 31113-31123. doi:10.1074/jbc.M011720200

Hsu, Patrick D., Lander, Eric S., *et al.* (2014). Development and Applications of CRISPR-Cas9 for Genome Engineering. *Cell, 157*(6), 1262-1278. doi:10.1016/j.cell.2014.05.010

Hübner, A., Barrett, T., *et al.* (2008). Multisite phosphorylation regulates Bim stability and apoptotic activity. *Molecular Cell, 30*(4), 415-425. doi:10.1016/j.molcel.2008.03.025

Humphrey, S. J., Karayel, O., *et al.* (2018). High-throughput and high-sensitivity phosphoproteomics with the EasyPhos platform. *Nat Protoc, 13*(9), 1897-1916. doi:10.1038/s41596-018-0014-9

Humphrey, S. J., Yang, G., *et al.* (2013). Dynamic adipocyte phosphoproteome reveals that Akt directly regulates mTORC2. *Cell Metab, 17*(6), 1009-1020. doi:10.1016/j.cmet.2013.04.010

Huntington, N. D., Xu, Y., *et al.* (2005). A requirement for CD45 distinguishes Ly49D-mediated cytokine and chemokine production from killing in primary natural killer cells. *The Journal of experimental medicine, 201*(9), 1421-1433. doi:10.1084/jem.20042294

Hutchinson, J. A., Shanware, N. P., *et al.* (2011). Regulation of ribosomal protein S6 phosphorylation by casein kinase 1 and protein phosphatase 1. *The Journal of biological chemistry, 286*(10), 8688-8696. doi:10.1074/jbc.M110.141754

Inoue, J., Ishida, T., *et al.* (2000). Tumor necrosis factor receptor-associated factor (TRAF) family: adapter proteins that mediate cytokine signaling. *Exp Cell Res, 254*(1), 14-24. doi:10.1006/excr.1999.4733

Izmiryan, A., Basmaciogullari, S., *et al.* (2011). Efficient gene targeting mediated by a lentiviral vector-associated meganuclease. *Nucleic Acids Res, 39*(17), 7610-7619. doi:10.1093/nar/gkr524

Jaco, I., Annibaldi, A., *et al.* (2017). MK2 Phosphorylates RIPK1 to Prevent TNF-Induced Cell Death. *Mol Cell, 66*(5), 698-710.e695. doi:10.1016/j.molcel.2017.05.003

Jeffrey, I. W., Bushell, M., *et al.* (2002). Inhibition of protein synthesis in apoptosis: differential requirements by the tumor necrosis factor alpha family and a DNA-damaging agent for caspases and the double-stranded RNA-dependent protein kinase. *Cancer Res, 62*(8), 2272-2280.

Jin, G., Yamazaki, Y., *et al.* (2007). Trib1 and Evi1 cooperate with Hoxa and Meis1 in myeloid leukemogenesis. *Blood, 109*(9), 3998-4005. doi:10.1182/blood-2006-08-041202

Katagiri, T., Ogimoto, M., *et al.* (1999). CD45 Negatively Regulates Lyn Activity by Dephosphorylating Both Positive and Negative Regulatory Tyrosine Residues in Immature B Cells. *The Journal of Immunology, 163*(3), 1321-1326.

Kataoka, K., Sato, T., *et al.* (2011). Evi1 is essential for hematopoietic stem cell self-renewal, and its expression marks hematopoietic cells with long-term multilineage repopulating activity. *J Exp Med, 208*(12), 2403-2416. doi:10.1084/jem.20110447

Kelley, T. W., Graham, M. M., *et al.* (1999). Macrophage colony-stimulating factor promotes cell survival through Akt/protein kinase B. *J Biol Chem, 274*(37), 26393-26398. doi:10.1074/jbc.274.37.26393

Kelly, L. M., & Gilliland, D. G. (2002). GENETICS OF MYELOID LEUKEMIAS. *Annual Review of Genomics and Human Genetics, 3*(1), 179-198. doi:10.1146/annurev.genom.3.032802.115046

Keshwani, M. M., von Daake, S., *et al.* (2011). Hydrophobic motif phosphorylation is not required for activation loop phosphorylation of p70 ribosomal protein S6 kinase 1 (S6K1). *J Biol Chem, 286*(26), 23552-23558. doi:10.1074/jbc.M111.258004

Kiani, A., Rao, A., *et al.* (2000). Manipulating immune responses with immunosuppressive agents that target NFAT. *Immunity, 12*(4), 359-372. doi:10.1016/s1074-7613(00)80188-0

Kim, H., Tu, H.-C., *et al.* (2009). Stepwise Activation of BAX and BAK by tBID, BIM, and PUMA Initiates Mitochondrial Apoptosis. *Molecular Cell, 36*(3), 487-499. doi:10.1016/j.molcel.2009.09.030

Kim, J.-T., Lee, S.-J., *et al.* (2013). Caspase-mediated cleavage and DNase activity of the translation initiation factor 3, subunit G (eIF3g). *FEBS Letters, 587*(22), 3668-3674. doi:10.1016/j.febslet.2013.09.027

Kim, S. J., Wagner, S., *et al.* (1992). Retinoblastoma gene product activates expression of the human TGF-beta 2 gene through transcription factor ATF-2. *Nature, 358*(6384), 331-334. doi:10.1038/358331a0

Kim, W. I., Matise, I., *et al.* (2009). RAS oncogene suppression induces apoptosis followed by more differentiated and less myelosuppressive disease upon relapse of acute myeloid leukemia. *Blood, 113*(5), 1086-1096. doi:10.1182/blood-2008-01-132316

Koch, B., Nijmeijer, B., *et al.* (2018). Generation and validation of homozygous fluorescent knock-in cells using CRISPR-Cas9 genome editing. *Nat Protoc, 13*(6), 1465-1487. doi:10.1038/nprot.2018.042

Krause, M., Sechi, A. S., *et al.* (2000). Fyn-binding protein (Fyb)/SLP-76-associated protein (SLAP), Ena/vasodilator-stimulated phosphoprotein (VASP) proteins and the Arp2/3

complex link T cell receptor (TCR) signaling to the actin cytoskeleton. *J Cell Biol, 149*(1), 181-194. doi:10.1083/jcb.149.1.181

Kurokawa, M., Mitani, K.*, et al.* (1998). The oncoprotein Evi-1 represses TGF-beta signalling by inhibiting Smad3. *Nature, 394*(6688), 92-96. doi:10.1038/27945

Lalaoui, N., Hänggi, K.*, et al.* (2016). Targeting p38 or MK2 Enhances the Anti-Leukemic Activity of Smac-Mimetics. *Cancer Cell, 29*(2), 145-158. doi:10.1016/j.ccell.2016.01.006

Lalaoui, N. and Brumatti, G. (2017). Relevance of necroptosis in cancer. *Immunology and cell biology, 95* (2), 137-145. doi: 10.1038/icb.2016.120

Lambrechts, A., Kwiatkowski, A. V.*, et al.* (2000). cAMP-dependent protein kinase phosphorylation of EVL, a Mena/VASP relative, regulates its interaction with actin and SH3 domains. *J Biol Chem, 275*(46), 36143-36151. doi:10.1074/jbc.M006274200

Ley, R., Ewings, K. E.*, et al.* (2005). Regulatory phosphorylation of Bim: sorting out the ERK from the JNK. *Cell Death Differ, 12*(8), 1008-1014. doi:10.1038/sj.cdd.4401688

Ley, R., Ewings, K. E.*, et al.* (2004). Extracellular Signal-regulated Kinases 1/2 Are Serum-stimulated "BimEL Kinases" That Bind to the BH3-only Protein BimEL Causing Its Phosphorylation and Turnover. *Journal of Biological Chemistry, 279*(10), 8837-8847. doi:10.1074/jbc.M311578200

Li, L., Jiao, X.*, et al.* (2018). Mutation in the intracellular chloride channel CLCC1 associated with autosomal recessive retinitis pigmentosa. *PLoS Genet, 14*(8), e1007504. doi:10.1371/journal.pgen.1007504

Li, L., Thomas, R. M.*, et al.* (2004). A small molecule Smac mimic potentiates TRAIL- and TNFalpha-mediated cell death. *Science, 305*(5689), 1471-1474. doi:10.1126/science.1098231

Lin, S., Staahl, B. T.*, et al.* (2014). Enhanced homology-directed human genome engineering by controlled timing of CRISPR/Cas9 delivery. *eLife, 3*, e04766. doi:10.7554/eLife.04766

Lino, C. A., Harper, J. C.*, et al.* (2018). Delivering CRISPR: a review of the challenges and approaches. *Drug Deliv, 25*(1), 1234-1257. doi:10.1080/10717544.2018.1474964

Liu, H., Cheng, E. H.*, et al.* (2009). MLL fusions: pathways to leukemia. *Cancer Biol Ther, 8*(13), 1204-1211. doi:10.4161/cbt.8.13.8924

Liu, M., Rehman, S.*, et al.* (2019). Methodologies for Improving HDR Efficiency. *Frontiers in genetics, 9*, 691-691. doi:10.3389/fgene.2018.00691

Liu, Y., Chen, L.*, et al.* (2006). Evi1 is a survival factor which conveys resistance to both TGFβ- and taxol-mediated cell death via PI3K/AKT. *Oncogene, 25*(25), 3565-3575. doi:10.1038/sj.onc.1209403

Livingstone, C., Patel, G.*, et al.* (1995). ATF-2 contains a phosphorylation-dependent transcriptional activation domain. *Embo j, 14*(8), 1785-1797.

Lombardo, A., Cesana, D.*, et al.* (2011). Site-specific integration and tailoring of cassette design for sustainable gene transfer. *Nat Methods, 8*(10), 861-869. doi:10.1038/nmeth.1674

Lu, T., Zhu, Z.*, et al.* (2019). DRAM1 regulates autophagy and cell proliferation via inhibition of the phosphoinositide 3-kinase-Akt-mTOR-ribosomal protein S6 pathway. *Cell communication and signaling : CCS, 17*(1), 28-28. doi:10.1186/s12964-019-0341-7

Lugthart, S., Groschel, S.*, et al.* (2010). Clinical, molecular, and prognostic significance of WHO type inv(3)(q21q26.2)/t(3;3)(q21;q26.2) and various other 3q abnormalities in acute myeloid leukemia. *J Clin Oncol, 28*(24), 3890-3898. doi:10.1200/jco.2010.29.2771

Lugthart, S., van Drunen, E., *et al.* (2008). High EVI1 levels predict adverse outcome in acute myeloid leukemia: prevalence of EVI1 overexpression and chromosome 3q26 abnormalities underestimated. *Blood, 111*(8), 4329-4337. doi:10.1182/blood-2007-10-119230

Macian, F., Lopez-Rodriguez, C., *et al.* (2001). Partners in transcription: NFAT and AP-1. *Oncogene, 20*(19), 2476-2489. doi:10.1038/sj.onc.1204386

Madesh, M., Antonsson, B., *et al.* (2002). Rapid kinetics of tBid-induced cytochrome c and Smac/DIABLO release and mitochondrial depolarization. *J Biol Chem, 277*(7), 5651-5659. doi:10.1074/jbc.M108171200

Maekawa, T., Sakura, H., *et al.* (1989). Leucine zipper structure of the protein CRE-BP1 binding to the cyclic AMP response element in brain. *The EMBO Journal, 8*(7), 2023-2028. doi:10.1002/j.1460-2075.1989.tb03610.x

Mahtani, K. R., Brook, M., *et al.* (2001). Mitogen-activated protein kinase p38 controls the expression and posttranslational modification of tristetraprolin, a regulator of tumor necrosis factor alpha mRNA stability. *Mol Cell Biol, 21*(19), 6461-6469. doi:10.1128/mcb.21.9.6461-6469.2001

McDermott, M. F., Aksentijevich, I., *et al.* (1999). Germline mutations in the extracellular domains of the 55 kDa TNF receptor, TNFR1, define a family of dominantly inherited autoinflammatory syndromes. *Cell, 97*(1), 133-144. doi:10.1016/s0092-8674(00)80721-7

Meacham, C. E., & Morrison, S. J. (2013). Tumour heterogeneity and cancer cell plasticity. *Nature, 501*(7467), 328-337. doi:10.1038/nature12624

Menon, M. B., Gropengiesser, J., *et al.* (2017). p38(MAPK)/MK2-dependent phosphorylation controls cytotoxic RIPK1 signalling in inflammation and infection. *Nat Cell Biol, 19*(10), 1248-1259. doi:10.1038/ncb3614

Meyer, C., Hofmann, J., *et al.* (2013). The MLL recombinome of acute leukemias in 2013. *Leukemia, 27*(11), 2165-2176. doi:10.1038/leu.2013.135

Meylan, E., Burns, K., *et al.* (2004). RIP1 is an essential mediator of Toll-like receptor 3-induced NF-kappa B activation. *Nat Immunol, 5*(5), 503-507. doi:10.1038/ni1061

Meyuhas, O. (2008). Chapter 1 Physiological Roles of Ribosomal Protein S6: One of Its Kind. In *International Review of Cell and Molecular Biology* (Vol. 268, pp. 1-37): Academic Press.

Micheau, O., Lens, S., *et al.* (2001). NF-kappaB signals induce the expression of c-FLIP. *Molecular and cellular biology, 21*(16), 5299-5305. doi:10.1128/MCB.21.16.5299-5305.2001

Micheau, O., & Tschopp, J. (2003). Induction of TNF receptor I-mediated apoptosis via two sequential signaling complexes. *Cell, 114*(2), 181-190. doi:10.1016/s0092-8674(03)00521-x

Minard, A. Y., Tan, S. X., *et al.* (2016). mTORC1 Is a Major Regulatory Node in the FGF21 Signaling Network in Adipocytes. *Cell Rep, 17*(1), 29-36. doi:10.1016/j.celrep.2016.08.086

Morishita, K., Parker, D. S., *et al.* (1988). Retroviral activation of a novel gene encoding a zinc finger protein in IL-3-dependent myeloid leukemia cell lines. *Cell, 54*(6), 831-840. doi:10.1016/s0092-8674(88)91175-0

Moriya, H. (2015). Quantitative nature of overexpression experiments. *Molecular biology of the cell, 26*(22), 3932-3939. doi:10.1091/mbc.E15-07-0512

Murphy, J. M., & Silke, J. (2014). Ars Moriendi; the art of dying well – new insights into the molecular pathways of necroptotic cell death. *EMBO reports, 15*(2), 155-164. doi:10.1002/embr.201337970

Murray, J. T., Craggs, G., *et al.* (2000). Mechanism of phosphatidylinositol 3-kinase-dependent increases in BAC1.2F5 macrophage-like cell density in response to M-CSF: phosphatidylinositol 3-kinase inhibitors increase the rate of apoptosis rather than inhibit DNA synthesis. *Inflamm Res, 49*(11), 610-618. doi:10.1007/s000110050638

Mustelin, T., Pessa-Morikawa, T., *et al.* (1992). Regulation of the p59fyn protein tyrosine kinase by the CD45 phosphotyrosine phosphatase. *Eur J Immunol, 22*(5), 1173-1178. doi:10.1002/eji.1830220510

Nachmias, B., Ashhab, Y., *et al.* (2004). The inhibitor of apoptosis protein family (IAPs): an emerging therapeutic target in cancer. *Semin Cancer Biol, 14*(4), 231-243. doi:10.1016/j.semcancer.2004.04.002

Nakamichi, Y., Udagawa, N., *et al.* (2013). IL-34 and CSF-1: similarities and differences. *J Bone Miner Metab, 31*(5), 486-495. doi:10.1007/s00774-013-0476-3

Nambiar, T. S., Billon, P., *et al.* (2019). Stimulation of CRISPR-mediated homology-directed repair by an engineered RAD18 variant. *Nature Communications, 10*(1), 3395. doi:10.1038/s41467-019-11105-z

Nanda, N., Andre, P., *et al.* (2005). Platelet aggregation induces platelet aggregate stability via SLAM family receptor signaling. *Blood, 106*(9), 3028-3034. doi:10.1182/blood-2005-01-0333

Nascimento, E. B. M., Snel, M., *et al.* (2010). Phosphorylation of PRAS40 on Thr246 by PKB/AKT facilitates efficient phosphorylation of Ser183 by mTORC1. *Cellular Signalling, 22*(6), 961-967. doi:10.1016/j.cellsig.2010.02.002

Nygard, O., & Nilsson, L. (1990). Translational dynamics. Interactions between the translational factors, tRNA and ribosomes during eukaryotic protein synthesis. *Eur J Biochem, 191*(1), 1-17. doi:10.1111/j.1432-1033.1990.tb19087

O'Reilly, L. A., Kruse, E. A., *et al.* (2009). MEK/ERK-mediated phosphorylation of Bim is required to ensure survival of T and B lymphocytes during mitogenic stimulation. *Journal of immunology (Baltimore, Md. : 1950), 183*(1), 261-269. doi:10.4049/jimmunol.0803853

Ohtsuka, M., Arase, H., *et al.* (2004). NFAM1, an immunoreceptor tyrosine-based activation motif-bearing molecule that regulates B cell development and signaling. *Proceedings of the National Academy of Sciences of the United States of America, 101*(21), 8126-8131. doi:10.1073/pnas.0401119101

Ouwens, D. M., de Ruiter, N. D., *et al.* (2002). Growth factors can activate ATF2 via a two-step mechanism: phosphorylation of Thr71 through the Ras-MEK-ERK pathway and of Thr69 through RalGDS-Src-p38. *Embo j, 21*(14), 3782-3793. doi:10.1093/emboj/cdf361

Owens, T. W., Gilmore, A. P., *et al.* (2013). Inhibitor of Apoptosis Proteins: Promising Targets for Cancer Therapy. *Journal of carcinogenesis & mutagenesis, Suppl 14*, S14-004. doi:10.4172/2157-2518.S14-004

Pende, M., Um, S. H., *et al.* (2004). S6K1(-/-)/S6K2(-/-) mice exhibit perinatal lethality and rapamycin-sensitive 5'-terminal oligopyrimidine mRNA translation and reveal a mitogen-activated protein kinase-dependent S6 kinase pathway. *Molecular and cellular biology, 24*(8), 3112-3124. doi:10.1128/mcb.24.8.3112-3124.2004

Pession, A., Martino, V., *et al.* (2003). MLL-AF9 oncogene expression affects cell growth but not terminal differentiation and is downregulated during monocyte-macrophage maturation in AML-M5 THP-1 cells. *Oncogene, 22*(54), 8671-8676. doi:10.1038/sj.onc.1207125

Piao, X., Komazawa-Sakon, S., *et al.* (2012). c-FLIP maintains tissue homeostasis by preventing apoptosis and programmed necrosis. *Sci Signal, 5*(255), ra93. doi:10.1126/scisignal.2003558

Piercy, J., Petrova, S., *et al.* (2006). CD45 negatively regulates tumour necrosis factor and interleukin-6 production in dendritic cells. *Immunology, 118*(2), 250-256. doi:10.1111/j.1365-2567.2006.02363.x

Porta, C., Paglino, C., *et al.* (2014). Targeting PI3K/Akt/mTOR Signaling in Cancer. *Frontiers in Oncology, 4*(64). doi:10.3389/fonc.2014.00064

Putcha, G. V., Le, S., *et al.* (2003). JNK-Mediated BIM Phosphorylation Potentiates BAX-Dependent Apoptosis. *Neuron, 38*(6), 899-914. doi:10.1016/S0896-6273(03)00355-6

Putz, G., Rosner, A., *et al.* (2006). AML1 deletion in adult mice causes splenomegaly and lymphomas. *Oncogene, 25*(6), 929-939. doi:10.1038/sj.onc.1209136

Qi, X. J., Wildey, G. M., *et al.* (2006). Evidence that Ser87 of BimEL is phosphorylated by Akt and regulates BimEL apoptotic function. *J Biol Chem, 281*(2), 813-823. doi:10.1074/jbc.M505546200

Ran, F. A., Hsu, P. D., *et al.* (2013). Genome engineering using the CRISPR-Cas9 system. *Nat Protoc, 8*(11), 2281-2308. doi:10.1038/nprot.2013.143

Reed, J. C. (2003). Apoptosis-targeted therapies for cancer. *Cancer Cell, 3*(1), 17-22. doi:10.1016/s1535-6108(02)00241-6

Reinhard, C., Shamoon, B., *et al.* (1997). Tumor necrosis factor alpha-induced activation of c-jun N-terminal kinase is mediated by TRAF2. *The EMBO Journal, 16*(5), 1080-1092. doi:10.1093/emboj/16.5.1080

Roux, P. P., Shahbazian, D., *et al.* (2007). RAS/ERK signaling promotes site-specific ribosomal protein S6 phosphorylation via RSK and stimulates cap-dependent translation. *J Biol Chem, 282*(19), 14056-14064. doi:10.1074/jbc.M700906200

Roy, N., Deveraux, Q. L., *et al.* (1997). The c-IAP-1 and c-IAP-2 proteins are direct inhibitors of specific caspases. *Embo j, 16*(23), 6914-6925. doi:10.1093/emboj/16.23.6914

Roy, P., Mukherjee, T., *et al.* (2017). Non-canonical NFκB mutations reinforce pro-survival TNF response in multiple myeloma through an autoregulatory RelB:p50 NFκB pathway. *Oncogene, 36*(10), 1417-1429. doi:10.1038/onc.2016.309

Rutault, K., Hazzalin, C. A., *et al.* (2001). Combinations of ERK and p38 MAPK inhibitors ablate tumor necrosis factor-alpha (TNF-alpha) mRNA induction. Evidence for selective destabilization of TNF-alpha transcripts. *J Biol Chem, 276*(9), 6666-6674. doi:10.1074/jbc.M005486200

Ruvinsky, I., & Meyuhas, O. (2006). Ribosomal protein S6 phosphorylation: from protein synthesis to cell size. *Trends Biochem Sci, 31*(6), 342-348. doi:10.1016/j.tibs.2006.04.003

Salvesen, G. S., & Walsh, C. M. (2014). Functions of caspase 8: the identified and the mysterious. *Seminars in immunology, 26*(3), 246-252. doi:10.1016/j.smim.2014.03.005

Sambandam, Y., Sundaram, K., *et al.* (2017). NFAM1 signaling enhances osteoclast formation and bone resorption activity in Paget's disease of bone. *Bone, 101*, 236-244. doi:10.1016/j.bone.2017.05.013

Samuel, T., Welsh, K., *et al.* (2006). Distinct BIR domains of cIAP1 mediate binding to and ubiquitination of tumor necrosis factor receptor-associated factor 2 and second mitochondrial activator of caspases. *J Biol Chem, 281*(2), 1080-1090. doi:10.1074/jbc.M509381200

Sander, J. D., & Joung, J. K. (2014). CRISPR-Cas systems for editing, regulating and targeting genomes. *Nature Biotechnology, 32*(4), 347-355. doi:10.1038/nbt.2842

Sanjana, N. E., Shalem, O., *et al.* (2014). Improved vectors and genome-wide libraries for CRISPR screening. *Nat Methods, 11*(8), 783-784. doi:10.1038/nmeth.3047

Sasmono, R. T., Oceandy, D., *et al.* (2003). A macrophage colony-stimulating factor receptor-green fluorescent protein transgene is expressed throughout the mononuclear phagocyte system of the mouse. *Blood, 101*(3), 1155-1163. doi:10.1182/blood-2002-02-0569

Satoh, J., & et al. (1989). Recombinant human tumor necrosis factor alpha suppresses autoimmune diabetes in nonobese diabetic mice. *J Clin Invest, 84*(4), 1345-1348. doi:10.1172/jci114304

Saygin, C., Matei, D., *et al.* (2019). Targeting Cancer Stemness in the Clinic: From Hype to Hope. *Cell Stem Cell, 24*(1), 25-40. doi:10.1016/j.stem.2018.11.017

Sedger, L. M., & McDermott, M. F. (2014). TNF and TNF-receptors: From mediators of cell death and inflammation to therapeutic giants - past, present and future. *Cytokine Growth Factor Rev, 25*(4), 453-472. doi:10.1016/j.cytogfr.2014.07.016

Senftleben, U., Cao, Y., *et al.* (2001). Activation by IKKalpha of a second, evolutionary conserved, NF-kappa B signaling pathway. *Science, 293*(5534), 1495-1499. doi:10.1126/science.1062677

Shahbazian, D., Parsyan, A., *et al.* (2010). eIF4B controls survival and proliferation and is regulated by proto-oncogenic signaling pathways. *Cell cycle (Georgetown, Tex.), 9*(20), 4106-4109. doi:10.4161/cc.9.20.13630

Shahbazian, D., Roux, P. P., *et al.* (2006). The mTOR/PI3K and MAPK pathways converge on eIF4B to control its phosphorylation and activity. *The EMBO Journal, 25*(12), 2781-2791. doi:10.1038/sj.emboj.7601166

Shenoi, H., Seavitt, J., *et al.* (1999). Regulation of Integrin-Mediated T Cell Adhesion by the Transmembrane Protein Tyrosine Phosphatase CD45. *The Journal of Immunology, 162*(12), 7120-7127.

Shima, Y., & Kitabayashi, I. (2011). Deregulated transcription factors in leukemia. *Int J Hematol, 94*(2), 134-141. doi:10.1007/s12185-011-0905-9

Shimizu, M., Nomura, Y., *et al.* (1998). Activation of the rat cyclin A promoter by ATF2 and Jun family members and its suppression by ATF4. *Exp Cell Res, 239*(1), 93-103. doi:10.1006/excr.1997.3884

Shrivastava, P., Katagiri, T., *et al.* (2004). Dynamic regulation of Src-family kinases by CD45 in B cells. *Blood, 103*(4), 1425-1432. doi:10.1182/blood-2003-03-0716

Siegemund, S., Rigaud, S., *et al.* (2015). IP3 3-kinase B controls hematopoietic stem cell homeostasis and prevents lethal hematopoietic failure in mice. *Blood, 125*(18), 2786-2797. doi:10.1182/blood-2014-06-583187

Siepen, J. A., Keevil, E.-J., *et al.* (2007). Prediction of missed cleavage sites in tryptic peptides aids protein identification in proteomics. *Journal of proteome research, 6*(1), 399-408. doi:10.1021/pr060507u

Silke, J., & Meier, P. (2013). Inhibitor of apoptosis (IAP) proteins-modulators of cell death and inflammation. *Cold Spring Harbor perspectives in biology, 5*(2), a008730. doi:10.1101/cshperspect.a008730

Silke, J., & Vucic, D. (2014). IAP family of cell death and signaling regulators. *Methods Enzymol, 545*, 35-65. doi:10.1016/b978-0-12-801430-1.00002-0

Sintes, J., Romero, X., *et al.* (2010). Mouse CD84 is a pan-leukocyte cell-surface molecule that modulates LPS-induced cytokine secretion by macrophages. *J Leukoc Biol, 88*(4), 687-697. doi:10.1189/jlb.1109756

Somervaille, T. C. P., & Cleary, M. L. (2006). Identification and characterization of leukemia stem cells in murine MLL-AF9 acute myeloid leukemia. *Cancer Cell, 10*(4), 257-268. doi:10.1016/j.ccr.2006.08.020

Speck, N. A., & Gilliland, D. G. (2002). Core-binding factors in haematopoiesis and leukaemia. *Nat Rev Cancer, 2*(7), 502-513. doi:10.1038/nrc840

Stanley, E. R., & Chitu, V. (2014). CSF-1 receptor signaling in myeloid cells. *Cold Spring Harb Perspect Biol, 6*(6). doi:10.1101/cshperspect.a021857

Stavropoulou, V., Kaspar, S., *et al.* (2016). MLL-AF9 Expression in Hematopoietic Stem Cells Drives a Highly Invasive AML Expressing EMT-Related Genes Linked to Poor Outcome. *Cancer Cell, 30*(1), 43-58. doi:10.1016/j.ccell.2016.05.011

Sudo, T., Nishikawa, S., *et al.* (1995). Functional hierarchy of c-kit and c-fms in intramarrow production of CFU-M. *Oncogene, 11*(12), 2469-2476.

Suela, J., Alvarez, S., *et al.* (2007). DNA profiling by arrayCGH in acute myeloid leukemia and myelodysplastic syndromes. *Cytogenet Genome Res, 118*(2-4), 304-309. doi:10.1159/000108314

Sun, C., Cai, M., *et al.* (2000). NMR structure and mutagenesis of the third Bir domain of the inhibitor of apoptosis protein XIAP. *J Biol Chem, 275*(43), 33777-33781. doi:10.1074/jbc.M006226200

Takahashi, R., Deveraux, Q., *et al.* (1998). A single BIR domain of XIAP sufficient for inhibiting caspases. *J Biol Chem, 273*(14), 7787-7790. doi:10.1074/jbc.273.14.7787

Tang, H., Hornstein, E., *et al.* (2001). Amino acid-induced translation of TOP mRNAs is fully dependent on phosphatidylinositol 3-kinase-mediated signaling, is partially inhibited by rapamycin, and is independent of S6K1 and rpS6 phosphorylation. *Mol Cell Biol, 21*(24), 8671-8683. doi:10.1128/mcb.21.24.8671-8683.2001

Tangye, S. G., Nichols, K. E., *et al.* (2003). Functional requirements for interactions between CD84 and Src homology 2 domain-containing proteins and their contribution to human T cell activation. *J Immunol, 171*(5), 2485-2495. doi:10.4049/jimmunol.171.5.2485

Tenev, T., Bianchi, K., *et al.* (2011). The Ripoptosome, a Signaling Platform that Assembles in Response to Genotoxic Stress and Loss of IAPs. *Molecular Cell, 43*(3), 432-448. doi:10.1016/j.molcel.2011.06.006

Tsai, E. Y., Jain, J., *et al.* (1996). Tumor necrosis factor alpha gene regulation in activated T cells involves ATF-2/Jun and NFATp. *Mol Cell Biol, 16*(2), 459-467. doi:10.1128/mcb.16.2.459

Tushinski, R. J., & Stanley, E. R. (1983). The regulation of macrophage protein turnover by a colony stimulating factor (CSF-1). *J Cell Physiol, 116*(1), 67-75. doi:10.1002/jcp.1041160111

Udalova, I. A., Knight, J. C., *et al.* (1998). Complex NF-kappaB interactions at the distal tumor necrosis factor promoter region in human monocytes. *J Biol Chem, 273*(33), 21178-21186. doi:10.1074/jbc.273.33.21178

Vaidyanathan, H., Opoku-Ansah, J., *et al.* (2007). ERK MAP kinase is targeted to RSK2 by the phosphoprotein PEA-15. *Proceedings of the National Academy of Sciences of the United States of America, 104*(50), 19837-19842. doi:10.1073/pnas.0704514104

Valk, P. J., Verhaak, R. G., *et al.* (2004). Prognostically useful gene-expression profiles in acute myeloid leukemia. *N Engl J Med, 350*(16), 1617-1628. doi:10.1056/NEJMoa040465

Vallabhapurapu, S., Matsuzawa, A., *et al.* (2008). Nonredundant and complementary functions of TRAF2 and TRAF3 in a ubiquitination cascade that activates NIK-dependent alternative NF-kappaB signaling. *Nat Immunol, 9*(12), 1364-1370. doi:10.1038/ni.1678

van Dam, H., Duyndam, M., *et al.* (1993). Heterodimer formation of cJun and ATF-2 is responsible for induction of c-jun by the 243 amino acid adenovirus E1A protein. *The EMBO Journal, 12*(2), 479-487. doi:10.1002/j.1460-2075.1993.tb05680.x

van Dam, H., Wilhelm, D., *et al.* (1995). ATF-2 is preferentially activated by stress-activated protein kinases to mediate c-jun induction in response to genotoxic agents. *The EMBO Journal, 14*(8), 1798-1811.

van den Reek, J., Coenen, M. J. H., *et al.* (2017). Polymorphisms in CD84, IL12B and TNFAIP3 are associated with response to biologics in patients with psoriasis. *Br J Dermatol, 176*(5), 1288-1296. doi:10.1111/bjd.15005

Vanden Berghe, T., Kaiser, W. J., *et al.* (2015). Molecular crosstalk between apoptosis, necroptosis, and survival signaling. *Molecular & cellular oncology, 2*(4), e975093-e975093. doi:10.4161/23723556.2014.975093

Varfolomeev, E., Blankenship, J. W., *et al.* (2007). IAP antagonists induce autoubiquitination of c-IAPs, NF-kappaB activation, and TNFalpha-dependent apoptosis. *Cell, 131*(4), 669-681. doi:10.1016/j.cell.2007.10.030

Vazquez, I., Maicas, M., *et al.* (2011). Down-regulation of EVI1 is associated with epigenetic alterations and good prognosis in patients with acute myeloid leukemia. *Haematologica, 96*(10), 1448-1456. doi:10.3324/haematol.2011.040535

Veale, M., Raab, M., *et al.* (1999). Novel isoform of lymphoid adaptor FYN-T-binding protein (FYB-130) interacts with SLP-76 and up-regulates interleukin 2 production. *J Biol Chem, 274*(40), 28427-28435. doi:10.1074/jbc.274.40.28427

Vince, J. E., Wong, W. W., *et al.* (2007). IAP antagonists target cIAP1 to induce TNFalpha-dependent apoptosis. *Cell, 131*(4), 682-693. doi:10.1016/j.cell.2007.10.037

Visvader, J. E., & Lindeman, G. J. (2012). Cancer Stem Cells: Current Status and Evolving Complexities. *Cell Stem Cell, 10*(6), 717-728. doi:10.1016/j.stem.2012.05.007

Volarevic, S., Stewart, M. J., *et al.* (2000). Proliferation, but not growth, blocked by conditional deletion of 40S ribosomal protein S6. *Science, 288*(5473), 2045-2047. doi:10.1126/science.288.5473.2045

Wajant, H. (2009). The role of TNF in cancer. *Results Probl Cell Differ, 49*, 1-15. doi:10.1007/400_2008_26

Walker, P. S., Hengge, U. R., *et al.* (1996). Viral interference during simultaneous transduction with two independent helper-free retroviral vectors. *Hum Gene Ther, 7*(9), 1131-1138. doi:10.1089/hum.1996.7.9-1131

Wang, C. Y., Mayo, M. W., *et al.* (1998). NF-kappaB antiapoptosis: induction of TRAF1 and TRAF2 and c-IAP1 and c-IAP2 to suppress caspase-8 activation. *Science, 281*(5383), 1680-1683. doi:10.1126/science.281.5383.1680

Wang, L., Du, F., *et al.* (2008). TNF-alpha induces two distinct caspase-8 activation pathways. *Cell, 133*(4), 693-703. doi:10.1016/j.cell.2008.03.036

Wang, L., Du, F., *et al.* (2008). TNF-α Induces Two Distinct Caspase-8 Activation Pathways. *Cell, 133*(4), 693-703. doi:10.1016/j.cell.2008.03.036

Wang, L., Harris, T. E., *et al.* (2007). PRAS40 regulates mTORC1 kinase activity by functioning as a direct inhibitor of substrate binding. *J Biol Chem, 282*(27), 20036-20044. doi:10.1074/jbc.M702376200

Wang, Y., Guo, W., *et al.* (1999). Phosphorylation of CD45 by casein kinase 2. Modulation of activity and mutational analysis. *J Biol Chem, 274*(11), 7454-7461. doi:10.1074/jbc.274.11.7454

Wang, Y., Shan, B., *et al.* (2018). Parkin regulates NF-κB by mediating site-specific ubiquitination of RIPK1. *Cell death & disease, 9*(7), 732-732. doi:10.1038/s41419-018-0770-z

Weintz, G., Olsen, J. V., *et al.* (2010). The phosphoproteome of toll-like receptor-activated macrophages. *Mol Syst Biol, 6*, 371. doi:10.1038/msb.2010.29

Weng, Q. P., Kozlowski, M., *et al.* (1998). Regulation of the p70 S6 kinase by phosphorylation in vivo. Analysis using site-specific anti-phosphopeptide antibodies. *J Biol Chem, 273*(26), 16621-16629. doi:10.1074/jbc.273.26.16621

Wong, W. W., Gentle, I. E., *et al.* (2010). RIPK1 is not essential for TNFR1-induced activation of NF-kappaB. *Cell Death Differ, 17*(3), 482-487. doi:10.1038/cdd.2009.178

Wu, G., Chai, J., *et al.* (2000). Structural basis of IAP recognition by Smac/DIABLO. *Nature, 408*(6815), 1008-1012. doi:10.1038/35050012

Wu, X., Tian, L., *et al.* (2012). Investigation of receptor interacting protein (RIP3)-dependent protein phosphorylation by quantitative phosphoproteomics. *Mol Cell Proteomics, 11*(12), 1640-1651. doi:10.1074/mcp.M112.019091

Xiao, G., Harhaj, E. W., *et al.* (2001). NF-kappaB-inducing kinase regulates the processing of NF-kappaB2 p100. *Mol Cell, 7*(2), 401-409. doi:10.1016/s1097-2765(01)00187-3

Xu, K., Wang, L., *et al.* (1999). Evi-1 and MDS1-Evi-1 genes in pathogenesis of myelodysplastic syndromes and post-MDS acute myeloid leukemia. *Chin Med J (Engl), 112*(12), 1112-1118.

Xu, X., Gao, D., *et al.* (2018). Efficient homology-directed gene editing by CRISPR/Cas9 in human stem and primary cells using tube electroporation. *Scientific reports, 8*(1), 11649-11649. doi:10.1038/s41598-018-30227-w

Xu, Z., & Weiss, A. (2002). Negative regulation of CD45 by differential homodimerization of the alternatively spliced isoforms. *Nat Immunol, 3*(8), 764-771. doi:10.1038/ni822

Yan, L., Zheng, D., *et al.* (2018). Critical Role of Tumor Necrosis Factor Signaling in Mesenchymal Stem Cell-Based Therapy for Autoimmune and Inflammatory Diseases. *Frontiers in Immunology, 9*(1658). doi:10.3389/fimmu.2018.01658

Yan, N., Sun, Y., *et al.* (2020). A Universal Surrogate Reporter for Efficient Enrichment of CRISPR/Cas9-Mediated Homology-Directed Repair in Mammalian Cells. *Molecular Therapy - Nucleic Acids, 19*, 775-789. doi:10.1016/j.omtn.2019.12.021

Yang, J., Hu, G., *et al.* (2003). Calcineurin/nuclear factors of activated T cells (NFAT)-activating and immunoreceptor tyrosine-based activation motif (ITAM)-containing protein (CNAIP), a novel ITAM-containing protein that activates the calcineurin/NFAT-signaling pathway. *J Biol Chem, 278*(19), 16797-16801. doi:10.1074/jbc.M211060200

Yang, J., Nie, J., *et al.* (2019). Targeting PI3K in cancer: mechanisms and advances in clinical trials. *Molecular Cancer, 18*(1), 26. doi:10.1186/s12943-019-0954-x

Yang, J., Wang, J., *et al.* (2013). eIF4B phosphorylation by pim kinases plays a critical role in cellular transformation by Abl oncogenes. *Cancer Res, 73*(15), 4898-4908. doi:10.1158/0008-5472.Can-12-4277

Yang, Q. H., & Du, C. (2004). Smac/DIABLO selectively reduces the levels of c-IAP1 and c-IAP2 but not that of XIAP and livin in HeLa cells. *J Biol Chem, 279*(17), 16963-16970. doi:10.1074/jbc.M401253200

Yang, Y., Fang, S., *et al.* (2000). Ubiquitin protein ligase activity of IAPs and their degradation in proteasomes in response to apoptotic stimuli. *Science, 288*(5467), 874-877. doi:10.1126/science.288.5467.874

Yu, T., Li, Y. J., *et al.* (2014). The regulatory role of activating transcription factor 2 in inflammation. *Mediators of inflammation, 2014*, 950472-950472. doi:10.1155/2014/950472

Yu, Y., Yoon, S. O., *et al.* (2011). Phosphoproteomic analysis identifies Grb10 as an mTORC1 substrate that negatively regulates insulin signaling. *Science, 332*(6035), 1322-1326. doi:10.1126/science.1199484

Yuasa, H., Oike, Y., *et al.* (2005). Oncogenic transcription factor Evi1 regulates hematopoietic stem cell proliferation through GATA-2 expression. *The EMBO Journal, 24*(11), 1976-1987. doi:10.1038/sj.emboj.7600679

Zaboikin, M., Zaboikina, T., *et al.* (2017). Non-Homologous End Joining and Homology Directed DNA Repair Frequency of Double-Stranded Breaks Introduced by Genome Editing Reagents. *PloS one, 12*(1), e0169931. doi:10.1371/journal.pone.0169931

Zeisig, B. B., Milne, T., *et al.* (2004). Hoxa9 and Meis1 are key targets for MLL-ENL-mediated cellular immortalization. *Mol Cell Biol, 24*(2), 617-628. doi:10.1128/mcb.24.2.617-628.2004

Zeisig, B. B., Schreiner, S., *et al.* (2003). Transcriptional activation is a key function encoded by MLL fusion partners. *Leukemia, 17*(2), 359-365. doi:10.1038/sj.leu.2402804

Zhao, J., Jitkaew, S., *et al.* (2012). Mixed lineage kinase domain-like is a key receptor interacting protein 3 downstream component of TNF-induced necrosis. *Proceedings of the National Academy of Sciences of the United States of America, 109*(14), 5322-5327. doi:10.1073/pnas.1200012109

Zuber, J., Radtke, I., *et al.* (2009). Mouse models of human AML accurately predict chemotherapy response. *Genes & development, 23*(7), 877-889. doi:10.1101/gad.1771409

Zuber, J., Rappaport, A. R., *et al.* (2011). An integrated approach to dissecting oncogene addiction implicates a Myb-coordinated self-renewal program as essential for leukemia maintenance. *Genes & development, 25*(15), 1628-1640. doi:10.1101/gad.17269211